Mammalian faunal recovery following the Cretaceous-Paleogene mass extinction: a multifaceted investigation

Stephanie M. Smith

A dissertation

submitted in partial fulfillment of the

requirements for the degree of

Doctor of Philosophy

University of Washington

2017

Reading Committee:

Gregory P. Wilson, Chair

Sharlene Santana

Tracy Popowics

Program Authorized to Offer Degree:

Biology

University of Washington

Abstract

Mammalian faunal recovery following the Cretaceous-Paleogene mass extinction: a multifaceted investigation

Stephanie M. Smith

Chair of the Supervisory Committee:
Professor Gregory P. Wilson
Department of Biology

The Cretaceous-Paleogene (K-Pg) mass extinction and subsequent recovery were a turning point for terrestrial ecosystems, signaling a shift from communities dominated by dinosaurs to those dominated by mammals. Mammalian body size and taxonomic diversity increased dramatically after the K-Pg mass extinction, but studies of these trends have generally been on broad spatiotemporal scales, or failed to capture the period of earliest biotic recovery directly following the extinction event. This dissertation seeks to deepen scientific knowledge of the mammalian recovery via high-resolution study of taxonomy, faunal succession, and dietary ecology in earliest Pg mammals, on a restricted spatiotemporal scale in the Hell Creek and Tullock formations of northeastern Montana. My co-authored quantitative study of the morphological differentiation among species in the common K-Pg mammalian genus *Mesodma* reveals that at least one species within this historically problematic genus is invalid, suggesting that the incorporation of quantitative information in taxonomic diagnoses is important for

objective identification of taxonomic affinity in isolated teeth. Further, taxonomic identifications constitute the raw data for faunal analyses, meaning that the quality of faunal analyses is directly related to the accuracy and repeatability of such identifications. In our faunal analyses of mammals from the McGuire Creek area of northeastern Montana, which incorporated the findings of my study of *Mesodma*, my co-authors and I find that mammalian recovery began slowly after the K-Pg mass extinction, with McGuire Creek local faunas showing only the earliest signs of recovery within the first 320 thousand years of the Paleogene. We further find that within the Western Interior of North America, McGuire Creek local faunas and other faunas from the Puercan 1 (Pu1) North American Land Mammal Age (NALMA) interval zone were quite similar, whereas in Pu2 and Pu3, North American faunas began to differentiate into northern and southern types. This suggests the possibility of a vicariance event in the early Pg that likely influenced the course of mammalian faunal recovery. My study of dietary ecomorphology in the early Pg of northeastern Montana further enriches our understanding of the mammalian recovery, with results indicating that following the K-Pg mass extinction, local immigrants to the area fueled replacement of dietary ecologies that were culled in the mass extinction. Mammals in the early Pg also showed a shift away from insectivory, which was the most common diet in the K, to increasing omnivory and frugivory in the early Pg, coincident with increasing fruit size in angiosperms. The methods used here for inferring dietary ecology in extinct mammals require some refinement before they can be confidently applied to carnivory and folivory. Overall, this work pushes forward the resolution of our knowledge of mammalian recovery following the K-Pg mass extinction. My results also add to our understanding of the evolutionary process of biotic recovery, as well as how mammals react to ecological perturbation, which is relevant for understanding and managing modern biodiversity crises

TABLE OF CONTENTS

LIST OF FIGURES iv

LIST OF TABLES viii

CHAPTER 1: INTRODUCTION 1

1.1 References cited 8

CHAPTER 2: SPECIES DISCRIMINATION OF CO-OCCURRING SMALL FOSSIL MAMMALS: A CASE STUDY OF THE CRETACEOUS-PALEOGENE MULTITUBERCULATE GENUS *MESODMA* 14

2.1 Author contributions 14

2.2 Abstract 14

2.3 Introduction 16

2.4 Materials and methods 18

2.5 Results and discussion 21

2.6 Acknowledgements 35

2.7 References cited 36

2.8 Figures 43

2.9 Tables 49

2.10 Appendix: p4 specimens and linear measurements 52

CHAPTER 3: MAMMALIAN RECOVERY FOLLOWING THE END-CRETACEOUS MASS EXTINCTION: A HIGH-RESOLUTION VIEW FROM MCGUIRE CREEK, MONTANA, USA 55

3.1 Author contributions 55

3.2 Abstract 55

3.3 Introduction 57

3.4 Geologic setting 59

3.5 Materials and methods 61

3.6 Results 72

3.7 Discussion 76

3.8 Conclusion 88

3.9 Acknowledgements 90

3.10 References cited 91

3.11 Figures 107

3.12 Tables 116

3.13 Appendix: Mammalian systematics 120

3.13.1 Materials and methods 120

3.13.2 Systematic paleontology 123

3.13.3 References cited 156

3.13.4 Figures 165

3.13.5 Tables 179

CHAPTER 4: MAMMALIAN DENTAL ECOMORPHOLOGY ACROSS THE CRETACEOUS-PALEOGENE BOUNDARY THROUGH THE FIRST 1.2 MILLION YEARS OF THE PALEOGENE 191

4.1 Abstract 191

4.2 Introduction 193

4.3 Materials and methods 195

4.4 Results 203

4.5 Discussion 210

4.6 References cited 226

4.7 Figures 246

4.8 Tables 259

4.9 Appendix 1: Descriptions of unattributed mammalian morphotypes 274

4.10 Appendix 2: MorphoSource specimens 280

4.11 Appendix 3: Raw dental topographic analysis (DTA) data 281

CHAPTER 5: CONCLUDING REMARKS 286

LIST OF FIGURES

CHAPTER 2: SPECIES DISCRIMINATION OF CO-OCCURRING SMALL FOSSIL MAMMALS: A CASE STUDY OF THE CRETACEOUS-PALEOGENE MULTITUBERCULATE GENUS *MESODMA*

Figure 2.1 Counties of origin for fossil specimens included in study 43

Figure 2.2 Linear measurements and geometric morphometric landmarks 44

Figure 2.3 Principal components analysis (PCA) of linear measurements alone..... 45

Figure 2.4 PCA of geometric morphometric data 46

Figure 2.5 PCA of geometric morphometric data, centroid size included 47

Figure 2.6 PCA of geometric morphometric data separated by North American Land Mammal Age (NALMA), centroid size included 48

CHAPTER 3: MAMMALIAN RECOVERY FOLLOWING THE END-CRETACEOUS MASS EXTINCTION: A HIGH-RESOLUTION VIEW FROM MCGUIRE CREEK, MONTANA, USA

Figure 3.1 Map of vertebrate microfossil localities in McGuire Creek area, northeastern Montana..... 107

Figure 3.2 Composite stratigraphic section including vertebrate microfossil localities and coals used in study..... 108

Figure 3.3 Single-crystal $^{40}Ar/^{39}Ar$ results for 2330 tephra [CC15-2] 109

Figure 3.4 Raw, rarefied, and SQS richness for McGuire Creek mammalian assemblages, genus- and species-level..... 110

Figure 3.5 Rarefaction curves with 95% confidence intervals for McGuire Creek mammalian assemblages, genus- and species-level 111

Figure 3.6 Rarefaction curves with 95% confidence intervals for Z-Line assemblage and Worm Coulee 1 assemblage, genus- and species-level 112

Figure 3.7 Evenness and dominance for McGuire Creek mammalian assemblages, genus- and species-level 113

Figure 3.8 Dendrogram of North American Puercan mammalian faunas 114

Figure 3.9 Correspondence of North American Puercan mammalian faunas 115

Figure 3.13.1 Tooth measurements and dental naming conventions used in study .. 165

Figure 3.13.2 *Mesodma thompsoni*, mandible (UCMP 132304) 167

Figure 3.13.3 *Cimexomys gratus,* m1 (RAM 6387) and M1 (RAM 4053) 167

Figure 3.13.4 Alphadontidae genus and species indeterminate, labial MX fragment (UCMP 239349) and m1 (UCMP 239334) 168

Figure 3.13.5 *Thylacodon montanensis,* M4 (UCMP 239350) 169

Figure 3.13.6 ?*Leptalestes cooki,* M1 or M2 (UCMP 239344) 169

Figure 3.13.7 Metatheria indeterminate, M4 (UCMP 239368) and MX fragment (UCMP 239372) 170

Figure 3.13.8 *Procerberus formicarum,* p4 (RAM 4106) 170

Figure 3.13.9 *Procerberus cf. P. grandis*, M2 (UCMP 134570) and m1 (RAM 4042) 171

Figure 3.13.10 ?*Ambilestes cerberoides,* maxillary fragment and P3 (UCMP 145148) 172

Figure 3.13.11 ?*Prodiacodon crustulum,* MX (RAM 6412) 173

Figure 3.13.12 ?*Baioconodon* sp., p3 (RAM 4058) 173

Figure 3.13.13 *Mimatuta morgoth,* maxilla with P4–M3 (UCMP 134571)..... 174

Figure 3.13.14 *Mimatuta minuial,* mandible with p4–m3 (UWBM 99100) 175

Figure 3.13.15 Periptychidae, genus and species indeterminate, MX fragment (RAM 4045)..... 176

Figure 3.13.16 *Purgatorius* cf. *P. coracis,* m3 (RAM 4078) 177

Figure 3.13.17 *Purgatorius* cf. *P. coracis,* M2 (UWBM 106217)..... 178

CHAPTER 4: MAMMALIAN DENTAL ECOMORPHOLOGY ACROSS THE CRETACEOUS-PALEOGENE BOUNDARY THROUGH THE FIRST 1.2 MILLION YEARS OF THE PALEOGENE

Figure 4.1 Tree of extant mammals included in comparative sample..... 246

Figure 4.2 Boxplots of orientation patch count rotated (OPCR), Dirichlet normal energy (DNE), and relief index (RFI) across known dietary groups, extant therian mammals 247

Figure 4.3 Bivariate scatterplots and 3D scatter plot of log-transformed dental topographic analysis (DTA) metrics, extant therian mammals..... 249

Figure 4.4 Bivariate scatterplots and 3D scatter plot of log-transformed dental topographic analysis (DTA) metrics, extinct therian mammals..... 251

Figure 4.5 Bivariate scatterplots and 3D scatter plot of log-transformed dental topographic analysis (DTA) metrics, multituberculate taxa..... 253

Figure 4.6 Least-squares linear regression of multituberculate OPCR from Wilson et al. (2012) on OPCR from this study..... 255

Figure 4.7 Boxplots of raw DTA metrics and ln body mass through NALMA interval zones, extinct therian mammals 256

Figure 4.8 Bivariate scatterplots of lnOPCR versus lnRFI through time, by NALMA interval zone 257

LIST OF TABLES

CHAPTER 2: SPECIES DISCRIMINATION OF CO-OCCURRING SMALL FOSSIL MAMMALS: A CASE STUDY OF THE CRETACEOUS-PALEOGENE MULTITUBERCULATE GENUS *MESODMA*

Table 2.1 Placement of landmarks and semilandmarks on multituberculate lower fourth premolars (p4s) 49

Table 2.2 Ratios of length and height dimensions for all *Mesodma* p4s in study 49

Table 2.3 Results of canonical variate analysis (CVA) on linear measurements and 2D geometric morphometric data 50

Table 2.4 Published size ranges for four species of the genus *Mesodma* 50

Table 2.5 Coefficients of variation of linear measurements of *Mesodma* p4s 51

Table 2.10.1 Locality information and linear measurements for all *Mesodma* p4s included in study 52

CHAPTER 3: MAMMALIAN RECOVERY FOLLOWING THE END-CRETACEOUS MASS EXTINCTION: A HIGH-RESOLUTION VIEW FROM MCGUIRE CREEK, MONTANA, USA

Table 3.1 Relative abundance of mammals present at McGuire Creek vertebrate microfossil localities..... 116

Table 3.2 Genus-level richness for McGuire Creek localities..... 117

Table 3.3 Species-level richness for McGuire Creek localities..... 117

Table 3.4 Genus- and species-level richness for Z Line and Worm Coulee 1 118

Table 3.5 Dissimilarity among McGuire Creek localties 118

Table 3.6 North American Puercan mammalian faunas..... 119

Table 3.13.1 Voucher specimens used for systematic comparisons..... 179

Table 3.13.2 Measurements of isolated molars of *Mesodma hensleighi* from McGuire Creek localities..... 181

Table 3.13.3 Measurements of isolated p4s of *Mesodma formosa* from McGuire Creek localities..... 181

Table 3.13.4 Measurements of isolated teeth of *Mesodma formosa* from McGuire Creek localities..... 182

Table 3.13.5 Measurements of p4s of *Mesodma thompsoni* from McGuire Creek localities..... 184

Table 3.13.6 Measurements of teeth of *Mesodma thompsoni* from McGuire Creek localities..... 185

Table 3.13.7 Measurements of teeth of *Cimexomys gratus* from McGuire Creek localties..... 187

Table 3.13.8 Measurements of teeth of *Thylacodon montanensis* from locality UCMP V84194..... 187

Table 3.13.9 Measurements of teeth of *Procerberus formicarum* from McGuire Creek localties..... 188

Table 3.13.10 Measurements of lower molars of *Protungulatum donnae* from McGuire Creek localities..... 188

Table 3.13.11 Measurements of *Mimatuta morgoth*, UCMP 134571..... 188

Table 3.13.12 Measurements of *Mimatuta minuial*, UWBM 99100..... 189

Table 3.13.13 Measurements of lower molars of *Mimatuta* sp. from McGuire Creek

localities 189

Table 3.13.14 Size comparisons between UWBM 106217 and upper molars of published species of *Purgatorius* 190

CHAPTER 4: MAMMALIAN DENTAL ECOMORPHOLOGY ACROSS THE CRETACEOUS-PALEOGENE BOUNDARY THROUGH THE FIRST 1.2 MILLION YEARS OF THE PALEOGENE

Table 4.1 Extant mammalian comparative sample 259

Table 4.2 Fossil therian mammals included in study 261

Table 4.3 Multituberculate specimens included in study 264

Table 4.4 Phylogenetic correlation in dental topographic analysis (DTA) metrics 265

Table 4.5 Correlations among DTA metrics in extant therian mammals 265

Table 4.6 Posterior probabilities of dietary group membership resulting from discriminant function analysis (DFA) for extant mammalian sample 266

Table 4.7 Posterior probabilities of dietary group membership resulting from discriminant function analysis (DFA) for fossil therian mammalian sample 268

Table 4.8 Diet types present in each NALMA or interval zone as determined by DFA 271

Table 4.9 Disparity measures for therian mammals within each NALMA or interval zone 271

Table 4.10 Correlation among DTA metrics in multituberculate mammals 272

Table 4.11 OPCR values and dietary classifications of multituberculates based on regression with Wilson et al. (2012) 272

Table 4.12 Disparity measures for multituberculate mammals within each NALMA or interval zone 273

Table 4.10.1 Specimens downloaded from MorphoSource.org 280

Table 4.11.1 Raw dental topographic analysis (DTA) results for extant comparative therian mammal sample 281

Table 4.11.2 Raw dental topographic analysis (DTA) results for extinct therian mammal sample 283

Table 4.11.3 Raw dental topographic analysis (DTA) results for extinct multituberculate mammal sample 285

ACKNOWLEDGEMENTS

This work would not have been possible without the contributions of my incredible family members, friends, and colleagues. I would like to thank my advisor Greg Wilson, for his guidance throughout the course of this research and my graduate career. By emphasizing scientific observation, scholarship, and clarity of expression in my work, he has helped me develop as a scientist and writer, and hone the skills necessary to produce high quality research. I would further like to thank my committee members, Sharlene Santana, Tracy Popowics, and Caroline Strömberg, for their support and enthusiasm for my research endeavors, and their indispensible advice regarding not only my work, but also how to build a reputation as a strong woman in science. I am additionally grateful to two people who served as unofficial advisors to me during my time as a graduate student: Bill Clemens, who is an amazing scientist and a knowledgeable, kind mentor and friend, and will always find time to talk to me, especially when the conversation is about teeth; and Joe Ammirati, who took a chance hiring me as his TA when I knew nothing about mycology, and who has grown to be one of my most trusted advisors, has taught me so many things about fungi, teaching, and about how to be a good scientist, and is always there for me with a dry joke and some career advice.

Thank you, Wilson Lab big brothers and sister, Jonathan Calede, Meng Chen, Dave DeMar (Davey), and Lauren DeBey: you taught me how to take constructive criticism, keep a good attitude during hard times, drive off-road in the field, talk to landowners, make new friends at conferences, keep calm before giving a talk, balance teaching and research, and have a good time somewhere in between all those things. Thanks to you too, Wilson Lab little brothers and sisters, Alexandria Brannick, Jordan Claytor, Brody Hovatter, Luke Weaver, and Paige Wilson: you have all become great colleagues, and wonderful friends, and your help with field work,

constructive comments on talks and proposals, engaging discussions that keep me learning new things all the time, and overall sense of fun and enthusiasm have helped me through the last few years.

The UW Biology community has supported my work in innumerable ways. My research would not have been possible without the entire Biology administrative and grants team, particularly Marissa Heringer, Sarah O'Hara, Karen Bergeron, Ron Killman, Dave Hurley, and Ben Wiggins. People at Friday Harbor Labs were also instrumental to my success: thanks to Matt Kolmann and Adam Summers for facilitating my use of the CT scanner and talking to me about fish and animals with weird teeth, and to Katie Dobkowski for fun times in Dorm Q! Many thanks to all the UW biograds and postdocs for moral support and a being such a friendly, accepting, inclusive community. I am especially grateful to the Young Naturalists' Society; Lunch Club! (Hannah Jordt, Jake Cooper, and Itzue Caviedes-Solis); the Santana Lab, who let me crash their fieldwork to snuggle phyllostomids in Costa Rica; and paleo-group current and former students (Chuck Beightol, Will Brightly, Camilla Crifò, Stephanie Crofts, Regan Dunn, Elisha Harris, Adam Huttenlocker, Zoe Kulik, Steven Lautzenheister, Savannah Olroyd, Brandon Peecook, Abby Vander Linden, and Meg Whitney). I would like to extend extra special thanks to Leith Leiser-Miller, for being a constant friend and ally, teaching me about bats, singing songs with me in the jungle, sharing giant cans of kombucha, and inspiring me to be creative. I also want to give extra big thanks to Emily Bain and Jessica Spiewak, for indispensible advice, kind listening ears, many nights of trivia with inappropriate team names, peanut butter pie, Gucci Mane jokes, book recommendations, Euchre times, and boat expeditions.

I am indebted to everyone at the Burke Museum for all of their help through the last several years. Meredith Rivin, Ron Eng, Bruce Crowley, Liz Nesbitt, and Christian Sidor have assisted with all things paleontology, and the Paleolunch group has provided thoughtful lunchtime discussions (and delicious snacks). Thanks to Jeff Bradley and Eugene Makela for fostering my enthusiasm for mammals, providing me with specimens for my research, teaching me about museum and live-mount taxidermy, helping me find shrew testicles, and giving me a chance every week to hang out and talk about animals for a few hours.

My fieldwork was possible because of more people than I can possibly hope to count. Thanks to permitting agencies (Bureau of Land Management, Charles M. Russel Wildlife Refuge, Army Corps of Engineers, and the State of Montana) for allowing our lab to collect fossils; all the grads, undergrads and volunteers who have helped with my fieldwork and the lab's fieldwork, especially people who made the epic trek to Coke's Clemmys and came back carrying hundreds of pounds of sediment; and the people of Jordan, Montana and the surrounding area, for letting a bunch of Bone Diggers share their badlands with them every summer, especially Liz and Richard Meyn and Jane and Dale Tharp. Thanks also to everyone involved with the DIG Field School, all the participants and instructors throughout the five years that I was an instructor, who made the DIG a fresh, exciting, and fun learning experience every year.

Undergrads have been an indispensible part of my graduate experience, and I am grateful to all of my students for showing me, in one way or another, how to be a better teacher. Special thanks to Biol475 students from summer 2015 and 2016, many of whom collected specimens and data for this research, and have subsequently become my good friends. Thanks in particular to Amanda Peng, Natalie Toews, Charlie Omana, Kali Garland, Athena Tse, Kristen Campbell,

and Kevin Cole: teaching, lab work, and fieldwork would have been way less fun without you – you guys are the best. Thanks to Gianni Aranoff for helping me figure out how to be a mentor, helping out with my research at FHL and at the Burke, and for processing endless CT scans without complaining about Mimics crashing.

Additional thanks go to: Ken Rose, for serving as my first mentor, showing me how incredible mammal paleontology is, and facilitating my career from my very first year as an undergraduate; Ken Angielczyk, for sparking my interest in ecomorphology is and acting as a long-distance mentor; Lars Schimtz, for teaching me how to use R and sticking with me thorough six years of code about squirrel skulls; Mark Goodwin and Pat Holroyd, for generously letting me use UCMP collections for my research; Courtney Sprain, for giving me many Quotes of the Day and helping me be better at geology; Don Lofgren, for doing the ground work for my studies in McGuire Creek, answering many questions about notes from thirty years ago, and letting me borrow a lot of Alf Museum specimens; Don Hopkins, who sorted a staggering amount of matrix from the not-especially-productive Coke's Clemmys and Luck O Hutch localities; Francois Gould, for taking me in when I was an extremely enthusiastic undergrad; Abby West and Allison Bronson, for Jokes; Neil Brocklehurst, for discussions of quantitative methods, politics, puppers, and movies; Stephen Sardini, for pictures of potassium permanganate reactions and ten years' worth of inside jokes; Class Mammalia, for having such interesting teeth; and D.M. Caldwell, for helping inspire me to do this work in the first place. This research was made possible by funding from many agencies: UW Biology, Friday Harbor Labs, the American Philosophical Society, the Hell Creek Project III, the Burke Museum of Natural History and Culture, the University of California Museum of Paleontology, the Society of Vertebrate Paleontology, and the American Society of Mammalogists.

I would last like to give many thanks and all my love to my family: Dad, Mom, my sister Kathrine, and my cousin Maggie, for your unwavering love, support, and good humor throughout this very long and stressful endeavor; to Amanda Ball, for being my Soul Mate and appropriately suggesting this dissertation be titled “Crunchy crunch munch: The Munch Crunch”; and to Kory Luedke, for everything.

CHAPTER 1: INTRODUCTION

The Cretaceous-Paleogene (K-Pg) mass extinction 66 million years (Ma) ago and the ensuing biotic recovery represent a turning point for terrestrial ecosystems, signaling a shift from vertebrate communities dominated by dinosaurs to those dominated by mammals. Mammalian body size, ecological disparity, and taxonomic diversity increased dramatically after the K-Pg mass extinction (Lillegraven 1972; Stucky 1990; Maas and Krause 1994; Alroy 1999; Smith et al. 2010; Slater 2013; Wilson 2014; DeBey and Wilson 2015, 2017). Despite the growing body of work investigating mammalian change following the K-Pg mass extinction, the details of the biotic recovery process (e.g., precise timing of taxonomic originations, relationship between taxonomic origination and change in ecology and faunal heterogeneity) remain poorly understood. This dissertation seeks to deepen our knowledge of the mammalian biotic recovery following the K-Pg mass extinction via high-resolution study of taxonomy, faunal succession, and dietary ecology in earliest Paleogene (Pg) mammals, on a restricted spatiotemporal scale within the Hell Creek and Tullock formations of northeastern Montana.

The pattern of change during biotic recovery has been described as having three broad phases: the immediate post-extinction "disaster" or "survival" phase, when local faunas have highly uneven relative abundance structure and consist mostly of ecological generalists (eurytopic taxa), opportunists, and species from refugia (immigrants); the "recovery" phase, which coincides with increasing taxonomic richness, and often includes the appearance of more ecological specialists and a decrease in the relative abundance of generalists and opportunists; and the "fully recovered" phase, when pre-extinction levels of evenness have been reached (Kauffman and Harries 1996; Erwin 1998). Although empirical evidence shows that specific

pattern and rate of biotic recovery depend on taxonomic group, ecology, environment, biogeography, and extinction severity (e.g., Jablonski 1998; Chen and Benton 2012; Zhuravlev 1996; Donovan et al. 2016; Sepúlveda et al. 2009), and the process is likely complicated by trophic interactions among recovering groups (Solé et al. 2010), paleobiologists and neontologists have used investigations of taxonomic composition, richness, heterogeneity, and ecological disparity track recovery in a variety of taxonomic groups throughout evolutionary history (e.g., MacMahon et al. 1989; Del Moral 1998; Sepkoski 1998; Sahney and Benton 2008; Payne et al. 2011; Wilson 2013, 2014; Halliday and Goswami 2016; Hull 2015; Ksepka et al. 2017). The three specific studies presented here use techniques from this body of literature, and incorporate new data and methodologies, to (i) test the validity of taxonomic identification techniques in a common mammalian taxon (*Chapter Two*), (ii) track change in mammalian faunal composition and heterogeneity through the early recovery period (*Chapter Three*), and (iii) assess dietary ecology and diversity through the early recovery period (*Chapter Four*).

Chapter Two of this dissertation concerns the raw data of any study of mammalian faunal dynamics: the taxonomic identification of individual fossils. The K-Pg mammalian fossil record is largely composed of isolated teeth and jaws. For mammalian fossil assemblages composed exclusively of teeth, the repeatability and accuracy of species-level taxonomic identifications is fundamental to the assessment of taxonomic composition, richness, and relative abundance, all of which are central to analyses of faunal change through time. In vertebrate microfossil assemblages with closely related, co-occurring species of mammals, such as those found in K-Pg deposits of northeastern Montana, it can be difficult to assign isolated teeth to species, because morphological differences among them may be slight and based on a single tooth position. As a

case study of this problem, in *Chapter Two*, I investigate utility of the allegedly diagnostic lower fourth premolar (p4) for species-level identification in the K-Pg multituberculate mammal genus *Mesodma*.

Mesodma is the most common mammal genus in many K-Pg vertebrate microfossil localities within the Hell Creek and Tullock formations, frequently representing upwards of 50% of total mammalian specimens (Lofgren 1995; Wilson 2014). The difficulty inherent in identifying specimens of *Mesodma* to species level is well established (Novacek and Clemens 1977; Archibald 1982; Lofgren 1995; Webb 2001; Wilson 2005), and can prevent faunal analyses from being conducted at the species level. The four traditionally recognized species of *Mesodma* present in northeastern Montana (*M. hensleighi*, *M. formosa*, *M. thompsoni*, and *M. garfieldensis*) have been reported to have p4s of distinct size and shape (Clemens 1964; Lillegraven 1969; Novacek and Clemens 1977; Archibald 1982). In *Chapter Two*, my co-author and I use a sample of 86 p4s of the various species of *Mesodma* to investigate the degree to which these four species actually differ in morphology, using both linear and geometric morphometric techniques. Results of this analysis have direct implications for the chapters that follow, allowing for a revised taxonomic scheme and a more informed understanding of morphological variation within *Mesodma* through time.

Chapter Three follows directly from *Chapter Two*, using raw data in the form of collections of mammalian teeth and jaws to track faunal change through time. Mammalian faunal composition, taxonomic diversity, and structure following the K-Pg mass extinction are central to understanding how terrestrial communities recovered from such an intense ecological

perturbation. Previous studies of mammalian faunal change in the Hell Creek and Tullock formations of northeastern Montana (Archibald 1983; Archibald and Lofgren 1990; Clemens 2002; Wilson 2014) have examined intervals of the recovery immediately after the extinction (<70 thousand years [ka] later), ca. 300–600 ka later, and ca 1.2 Ma later. Finer-scale sampling of the recovery pattern has been hindered by a lack of mammal-bearing localities of the appropriate ages. In *Chapter Three,* my co-authors and I begin to fill this gap by analyzing new or expanded samples from four vertebrate microfossil localities in the McGuire Creek area of McCone County, Montana, which represent a temporal sequence of mammalian local faunas from within ca. 320 ka of the K-Pg mass extinction. Within a high-precision chronostratigraphic framework based on $^{40}Ar/^{39}Ar$ tephra ages and magnetostratigraphy, I use quantitative techniques, including relative abundance, rarefaction, and a variety of heterogeneity indices to compare taxonomic composition, heterogeneity, and richness among McGuire Creek mammal faunas, which represent a snapshot of the earliest mammalian biotic recovery in the area. These analyses allow me to assess the degree of recovery in McGuire Creek mammalian faunas in the first ca. 320 ka of the Paleogene, and quantify changes between the oldest local fauna (within ca. 25 ka of the mass extinction) and the two younger local faunas I sampled.

The fine spatiotemporal scale of the McGuire Creek faunal analyses presented in *Chapter Three* reduces the influence of spatial environmental gradients; further, the geochronological framework in which I conduct my analyses enables more precise measurement of timing of changes in mammalian taxonomic richness and faunal structure. Yet the mammalian faunal recovery was also taking place in the larger context of the Western Interior of North America. I incorporate this context using cluster analysis and correspondence analysis. I use these two

analyses to make quantitative comparisons among McGuire Creek local faunas, other local faunas from northeastern Montana, and faunas from across the Western Interior through the earliest-Pg Puercan North American Land Mammal Age (NALMA). Results presented in *Chapter Three* push forward the resolution of our understanding of the post-K-Pg mammalian faunal recovery in a single part of the Western Interior, emphasize the importance of geochronological data in the study of recovery, and highlight issues with describing nuanced temporal phenomena using the current NALMA biochronology system.

Complementing the analyses in *Chapter Three*, *Chapter Four* seeks to track the dietary ecology of mammals in northeastern Montana during the early mammalian faunal recovery, through the first ca. 1.2 Ma of the Paleogene. Diet is a major component of an organism's ecological niche, and can be inferred in fossil mammals using tooth morphology. In *Chapter Four*, I employ dental topographic analyses (DTA) of individual lower cheek teeth to better understand the dietary ecologies of early Paleogene mammals. DTA relates the three-dimensional (3D) morphology of a tooth to the dietary ecology of the mammal it belongs to, via comparison with extant mammals of known diets (Evans et al. 2007; Boyer 2008; Bunn et al. 2011; Evans 2013; Winchester et al 2014).

Previous research has suggested that in the earliest Paleogene, mammalian ecological guilds (as approximated by estimated body size and qualitative assessment of tooth morphology; Archibald 1983) that existed before the mass extinction event were refilled before new guilds were established (Archibald 1983). Additionally, the recovery of dietary diversity in the earliest Paleogene (early Puercan [Pu1]) of northeastern Montana appears to have been initially fueled

by the numerous immigrant taxa that appeared locally rather than by the resident survivors of the mass extinction (Wilson 2013). In *Chapter 4,* I test these existing hypotheses with new data: specifically, dental topographic data from both therian and multituberculate mammals from Lancian, Puercan, and earliest Torrejonian (To1) NALMA interval zones of northeastern Montana. Using an comparative sample of extant mammals with known diets, I am able to make predictions about the dietary preferences of extinct mammalian taxa, and to track, for example, the prevalence of animal-based diets versus plant-based diets in mammals through the Lancian, Puercan, and early Torrejonian, and the relationship between the rise of plant-based diets and the North American floral record (e.g., Wing and Tiffney 1987; Eriksson 2016 and references therein). However, there are also assumptions and caveats associated with the methods used in this study; these are presented with suggestions for future optimization of the use of comparative DTA to predict diet in fossil taxa.

Chapter 5 comprises concluding remarks and a synthesis of the most important findings from each of the three preceding chapters.

As a whole, this dissertation lends several types of important novel high-resolution data to our growing understanding of the mammalian faunal recovery following the K-Pg mass extinction. Although the restricted spatiotemporal scale is an important feature of this work, it nonetheless serves to underline the continuing need for small-scale faunal studies throughout the Western Interior to develop a more holistic view of recovery. Our current capability to make comparisons among mammalian faunas across large geographic distances is sometimes hampered by the quality of the mammalian fossil record and the precision of available dating

techniques; future studies should seek to add high-precision local faunal data to more locations throughout the Western Interior, for a more geographically integrated, high-resolution understanding of the recovery. Ongoing fossil sampling in northeastern Montana will also undoubtedly result in new evidence regarding the mammalian faunal recovery, building on and increasing the robustness of the data presented here to bolster local and regional Montana recovery signals, and further our knowledge of the continental recovery signal across the Western Interior.

REFERENCES CITED

Alroy, J., 1999, The fossil record of North American mammals: evidence for a Paleocene evolutionary radiation: Systematic Biology, v. 48, p. 107–118, doi: 10.1080/106351599260472.

Archibald, J.D., 1982, A study of Mammalia and geology across the Cretaceous-Tertiary boundary in Garfield County, Montana: University of California Publications in Geological Sciences 122, 286 p.

Archibald, J.D., 1983, Structure of the KT mammal radiation in North America: speculations on turnover rates and trophic structure: Acta Palaeontologica Polonica, v. 28, p. 7–17.

Archibald, J.D., and Lofgren, D.L., 1990, Mammalian zonation near the Cretaceous-Tertiary boundary: Geological Society of America Special Papers, v. 243, p. 31–50.

Boyer, D.M., 2008, Relief index of second mandibular molars is a correlate of diet among prosimian primates and other euarchontan mammals: Journal of Human Evolution, v. 55, p. 1118–1137, doi: 10.1016/j.jhevol.2008.08.002.

Bunn, J.M., Boyer, D.M., Lipman, Y., St. Clair, E.M., Jernvall, J., and Daubechies, I., 2011, Comparing Dirichlet normal surface energy of tooth crowns, a new technique of molar shape quantification for dietary inference, with previous methods in isolation and in combination: American Journal of Physical Anthropology, v. 145, p. 247–261, doi: 10.1002/ajpa.21489.

Chen, Z.-Q., and Benton, M.J., 2012, The timing and pattern of biotic recovery following the end-Permian mass extinction: Nature Geoscience, v. 5, p. 375–383, doi: 10.1038/ngeo1475.

Clemens, W.A., 1964, Fossil mammals of the type Lance Formation,Wyoming. Part I. Introduction and Multituberculata: University of California Publications in Geological Sciences, v. 48, p. 1–105.

Clemens, W.A., 2002, Evolution of the mammalian fauna across the Cretaceous-Tertiary boundary in northeastern Montana and other areas of the Western Interior: Geological Society of America Special Paper, v. 361, p. 217–245.

DeBey, L.B., and Wilson, G.P., 2014, Mammalian femora across the Cretaceous–Paleogene boundary in eastern Montana: Cretaceous Research, v. 51, p. 361–385.

DeBey, L.B., and Wilson, G.P., 2017, Mammalian distal humerus fossils from eastern Montana, USA with implications for the Cretaceous-Paleogene mass extinction and the adaptive radiation of placentals: Palaeontologia Electronica, v. 20, p. 1–93.

Del Moral, R., 1998, Early succession on lahars spawned by Mount St. Helens.: American Journal of Botany, v. 85, p. 820–828.

Donovan, M.P., Iglesias, A., Wilf, P., Labandeira, C.C., and Cúneo, N.R., 2016, Rapid recovery of Patagonian plant–insect associations after the end-Cretaceous extinction: Nature Ecology & Evolution, v. 1, p. 12.

Eriksson, O., 2016, Evolution of angiosperm seed disperser mutualisms: The timing of origins and their consequences for coevolutionary interactions between angiosperms and frugivores: Biological Reviews, v. 91, p. 168–186, doi: 10.1111/brv.12164.

Erwin, D.H., 1998, The end and the beginning: Recoveries from mass extinctions: Trends in Ecology and Evolution, v. 13, p. 344–349, doi: 10.1016/S0169-5347(98)01436-0.

Evans, A.R., 2013, Shape descriptors as ecometrics in dental ecology: Hystrix, v. 24, p. 133–140, doi: 10.4404/hystrix-24.1-6363.

Evans, A.R., Wilson, G.P., Fortelius, M., and Jernvall, J., 2007, High-level similarity of dentitions in carnivorans and rodents.: Nature, v. 445, p. 78–81, doi: 10.1038/nature05433.

Halliday, T.J.D., and Goswami, A., 2016, Eutherian morphological disparity across the end-Cretaceous mass extinction: Biological Journal of the Linnean Society, v. 118, p. 152–168, doi: 10.1111/bij.12731.

Hull, P., 2015, Life in the aftermath of mass extinctions: Current Biology, v. 25, p. R941–R952.

Jablonski, D., 1998, Geographic variation in the molluscan recovery from the end-Cretaceous extinction: Science, v. 279, p. 1327–1330.

Kauffman, E.G., and Harries, P.J., 1996, The importance of crisis progenitors in recovery from mass extinction: Geological Society, London, Special Publications, v. 102, p. 15–39.

Ksepka, D.T., Stidham, T.A., and Williamson, T.E., 2017, Early Paleocene landbird supports rapid phylogenetic and morphological diversification of crown birds after the K–Pg mass extinction: Proceedings of the National Academy of Sciences, p. 201700188.

Lillegraven, J.A., 1969, Latest Cretaceous mammals of upper part of Edmonton Formation of Alberta, Canada, and review of marsupial-placental dichotomy in mammalian evolution: The University of Kansas Paleontological Contributions, Article 50 (Vertebrata 12), 122 p.

Lillegraven, J.A., 1972, Ordinal and familial diversity of Cenozoic mammals: Taxon, p. 261–274.

Lofgren, D.L., 1995, The Bug Creek problem and the Cretaceous-Tertiary transition at McGuire Creek, Montana: University of California Press, v. 140.

Maas, M.C., and Krause, D.W., 1994, Mammalian turnover and community structure in the Paleocene of North America: Historical Biology, v. 8, p. 91–128.

MacMahon, J.A., Parmenter, R.R., Johnson, K.A., and Crisafulli, C.M., 1989, Small mammal recolonization on the Mount St. Helens volcano: 1980-1987: American Midland Naturalist, p. 365–387.

Novacek, M., and Clemens, W.A., 1977, Aspects of intrageneric variation and evolution of Mesodma (Multituberculata, Mammalia): Journal of Paleontology, p. 701–717.

Payne, J.L., Summers, M., Rego, B.L., Altiner, D., Wei, J.Y., Yu, M.Y., and Lehrmann, D.J., 2011, Early and Middle Triassic trends in diversity, evenness, and size of foraminifers on a carbonate platform in south China: implications for tempo and mode of biotic recovery

from the end-Permian mass extinction: Paleobiology, v. 37, p. 409–425, doi: 10.1666/08082.1.

Sahney, S., and Benton, M.J., 2008, Recovery from the most profound mass extinction of all time: Proceedings of the Royal Society of London B: Biological Sciences, v. 275, p. 759–765.

Sepkoski, J.J., 1998, Rates of speciation in the fossil record.: Philosophical transactions of the Royal Society of London. Series B, Biological sciences, v. 353, p. 315–326, doi: 10.1098/rstb.1998.0212.

Sepúlveda, J., Wendler, J.E., Summons, R.E., and Hinrichs, K.-U., 2009, Rapid resurgence of marine productivity after the Cretaceous-Paleogene mass extinction: Science, v. 326, p. 129–132.

Slater, G.J., 2013, Phylogenetic evidence for a shift in the mode of mammalian body size evolution at the Cretaceous-Palaeogene boundary: Methods in Ecology and Evolution, v. 4, p. 734–744, doi: 10.1111/2041-210X.12084.

Smith, F.A., Boyer, A.G., Brown, J.H., Costa, D.P., Dayan, T., Ernest, S.K.M., Evans, A.R., Fortelius, M., Gittleman, J.L., and Hamilton, M.J., 2010, The evolution of maximum body size of terrestrial mammals: Science, v. 330, p. 1216–1219.

Solé, R. V., Saldaña, J., Montoya, J.M., and Erwin, D.H., 2010, Simple model of recovery dynamics after mass extinction: Journal of Theoretical Biology, v. 267, p. 193–200, doi: 10.1016/j.jtbi.2010.08.015.

Stucky, R.K., 1990, Evolution of land mammal diversity in North America during the Cenozoic: in H. H. Genoways, ed., Current mammalogy, Vol. 2., p. 375–432.

Webb, M.W., 2001, Fluvial Architecture and Late Cretaceous mammals of the Lance Formation, southwestern Bighorn Basin, Wyoming [Ph.D. thesis]: University of Wyoming.

Wilson, G.P., 2005, Mammalian Faunal Dynamics During the Last 1.8 Million Years of the Cretaceous in Garfield County, Montana: Journal of Mammalian Evolution, v. 12, p. 53–76, doi: 10.1007/s10914-005-6943-4.

Wilson, G.P., 2013, Mammals across the K/Pg boundary in northeastern Montana, U.S.A.: dental morphology and body-size patterns reveal extinction selectivity and immigrant-fueled ecospace filling: Paleobiology, v. 39, p. 429–469, doi: 10.1666/12041.

Wilson, G.P., 2014, Mammalian extinction, survival, and recovery dynamics across the Cretaceous-Paleogene boundary in northeastern Montana, USA: Geological Society of America Special Papers, v. 503, p. 365–392, doi: 10.1130/2014.2503(15).

Winchester, J.M., Boyer, D.M., St. Clair, E.M., Gosselin-Ildari, A.D., Cooke, S.B., and Ledogar, J.A., 2014, Dental topography of platyrrhines and prosimians: Convergence and contrasts: American Journal of Physical Anthropology, v. 153, p. 29–44, doi: 10.1002/ajpa.22398.

Wing, S.L., and Tiffney, B.H., 1987, The reciprocal interaction of angiosperm evolution and tetrapod herbivory: Review of Palaeobotany and Palynology, v. 50, p. 179–210.

Zhuravlev, A.Y., 1996, Reef ecosytem recovery after the Early Cambrian extinction: Geological Society, London, Special Publications, v. 102, p. 79–96.

CHAPTER 2: SPECIES DISCRIMINATION OF CO-OCCURRING SMALL FOSSIL MAMMALS: A CASE STUDY OF THE CRETACEOUS-PALEOGENE MULTITUBERCULATE GENUS *MESODMA*

Smith, S.M., and Wilson, G.P., 2017, Species discrimination of co-occurring small fossil mammals: a case study of the Cretaceous-Paleogene Multituberculate genus *Mesodma*: Journal of Mammalian Evolution, v. 24, p. 147–157. doi: 10.1007/s10914-016-9332-2

2.1 AUTHOR CONTRIBUTIONS

SMS and GPW conceived of the project and collected geometric morphometric data; SMS conducted analyses, made figures, and wrote the main body of the manuscript; GPW took photographs of teeth for geometric morphometric analysis and contributed to the manuscript.

2.2 ABSTRACT

The mammalian fossil record is largely composed of isolated teeth and tooth-bearing elements. In vertebrate microfossil assemblages with closely related, co-occurring species of mammals, it can be difficult to identify isolated teeth to species-level because morphological differences among species can be slight and based on a single tooth position. Here we investigate the utility of the allegedly diagnostic lower fourth premolar (p4) for species-level identification in the genus *Mesodma* (Multituberculata, Neoplagiaulacidae). We conducted linear and geometric morphometrics on 86 p4s representing four Cretaceous-Paleogene (K-Pg) species of *Mesodma* that are common in deposits of the western interior of North America. Although *Mesodma* has

been extensively discussed in the literature, these four species overlap considerably in p4 size and shape, making species-level identifications challenging. Using linear measurements, landmarks, and semilandmarks, we quantified p4 size and shape to understand morphological variation across the genus and uncover practical sources of morphological differentiation among the species represented here. Our results indicate (1) size is more important than shape for identifying p4s of *Mesodma* species; p4 shape varies across the genus, but cannot be used alone to identify isolated p4s to species; (2) *M. garfieldensis* and *M. thompsoni* cannot be distinguished from each other using p4 size or shape; we therefore subsume *M. garfieldensis* within *M. thompsoni*; and (3) *M. formosa* increased in size across the K-Pg boundary. In light of these results, we recommend that taxonomic diagnoses relying on isolated teeth incorporate quantitative analyses of morphology whenever possible to increase the accuracy of species-level identifications and paleofaunal studies that employ them.

2.3 INTRODUCTION

The mammalian fossil record is largely composed of teeth and tooth-bearing elements, whereas articulated skeletons and crania are more rare, particularly in vertebrate microfossil assemblages. Fortunately, the size and shape of mammalian teeth can be diagnostic to a lower-level taxon, often to the species level. Thus, for mammalian fossil assemblages composed exclusively of teeth, the precision and accuracy of a dental diagnosis is fundamental to the assessment of taxonomic composition, richness, and relative abundances, all of which are central to analyses of paleofaunal change through time (e.g., Maas et al. 1995; Clyde and Gingerich 1998; Eberle and Lillegraven 1998; Flynn et al. 2003; Eberle 2003; Wilson 2005, 2014; Chew 2009). When a specimen does not resemble a known taxon, a new genus or species may be erected, diagnosed, and described on the basis of a single tooth or tooth-bearing element. However, it is sometimes unclear what degree of morphological difference is required to place isolated teeth into separate species, or whether teeth belonging to co-occurring, congeneric species can be reliably separated from one another if they are not associated with other dental, cranial, or skeletal material.

To investigate how size and shape variation can be used to effectively discriminate among taxa in samples of isolated teeth, we focused on the diagnostic lower fourth premolar (p4) of the neoplagiaulacid multituberculate genus *Mesodma*. This genus currently comprises eight species of small multituberculates (<170 g; Wilson et al. 2012) that range from Late Cretaceous (Santonian) to late Paleocene in age (84–57 million years ago; Cifelli et al. 2004). During the latest Cretaceous and earliest Paleogene in western North America, *Mesodma* had particularly high relative abundance; in the Hell Creek and Tullock formations of northeastern Montana, *Mesodma* often accounts for upwards of 50% of the total mammalian sample from a vertebrate

microfossil locality (Lofgren 1995; Wilson 2014). Nonetheless, workers have expressed difficulty in assigning these specimens to species (e.g., Lofgren 1995; Webb 2001; Wilson 2004). We chose to study the p4 because workers have commonly relied upon it to distinguish among multituberculate species and because it is more amenable to shape analysis than the molars are. Indeed, in some cases, species-level identifications are only possible when multituberculate molars are associated with a p4 because, as is the case within the genus *Mesodma*, molars of different species are morphologically indistinguishable apart from size differences (Lillegraven 1969). Previous studies found that p4s of several species of *Mesodma* differ in size and shape (e.g., Clemens 1964; Lillegraven 1969; Novacek and Clemens 1977; Archibald 1982), although these species exhibited varying degrees of overlap in these characteristics. Accordingly, rigorous quantitative analysis of size and shape in a large sample of isolated p4s of *Mesodma* should produce discrete groupings that correspond to known species. As a test of this hypothesis, we (1) used linear and geometric morphometric analyses to measure size and shape variation in p4s of four recognized species of *Mesodma* (*M. hensleighi*, *M. formosa*, *M. thompsoni*, *M. garfieldensis)* from the latest Cretaceous-earliest Paleogene (K-Pg) interval, (2) compared this variation to that described in the literature for these taxa, and (3) assessed the utility of this variation in identifying isolated teeth to the species level. We found that, although there is some variation in shape among these species, size is a greater source of interspecific variation and is thus more useful in identifying isolated p4s to the species level. This contrasts with the literature, which has emphasized shape over size in distinguishing among p4s of different species of *Mesodma*. In light of our results, we recommend that taxonomic diagnoses and identifications that rely on isolated fossil teeth should apply statistical analyses of size and shape to large samples, whenever possible, so as to clarify morphological boundaries

among species and to improve the reliability of taxonomic identifications and diversity metrics that form the basis of paleofaunal studies.

2.4 MATERIALS AND METHODS

Specimen selection. Our data set consists of 86 lower p4 specimens from the University of California Museum of Paleontology (UCMP), each of which has previously been assigned to one of four species of the neoplagiaulacid multituberculate genus *Mesodma* (*M. hensleighi*, *M. formosa*, *M. thompsoni*, *M. garfieldensis*). Wilson (2013) used 84 of these specimens in his analysis of mammalian morphological disparity across the K-Pg boundary; we added two type specimens to the data set. Selection of specimens emphasized completeness and preservation of the crown to maximize the accuracy of dental shape analyses. All specimens are from latest Cretaceous- and earliest Paleogene-age (Lancian [La] and early Puercan [Pu1] North American Land Mammal "Ages," respectively) vertebrate microfossil localities in northeastern Montana and eastern Wyoming (Fig. 2.1, Table 2.10.1). Specimens of *M. thompsoni* in our sample are from La localities, although this species has also been reported from the Pu1 of northeastern Montana (Wilson 2014). Specimens of *M. formosa* and *M. hensleighi* are from both La and Pu1 localities, and *M. garfieldensis* is known from only Pu1 localities. We excluded other species of *Mesodma* from other time periods because here we are interested in species discrimination and its implications for understanding the K-Pg mass extinction and recovery. Morphological analysis of the entire genus is beyond the scope of this paper.

Imaging. Digital images of all specimens except UCMP 116621 and UCMP 47217 are from the data set of Wilson (2013). We took digital images of UCMP 116621 with a Canon EOS Digital

Rebel XS according to the protocol in Wilson (2013); i.e., the tooth was oriented so that the entire buccal aspect of the crown was in the same focal plane. Because the holotype of *M. thompsoni* (UCMP 47217) was not available for direct study, we used a published line drawing of the specimen (Clemens 1964: fig. 10) to take measurements and digitize landmarks. To test for possible differences in tooth orientation introduced by using a published line drawing rather than a digital image, we digitized a line drawing (Archibald 1982: fig. 11a) and a digital image of another specimen (UCMP 116622). When we conducted a geometric morphometric analysis that included the shape data from both the digital image and line drawing of UCMP 116622 (see below, Two-dimensional geometric morphometrics), the two data points for this specimen appeared in close proximity to one another in the plots of our principal components analysis (PCA); we concluded that any shape or size error introduced by using published line drawings is minimal. We removed the line drawing of UCMP 116622 from subsequent analyses.

Linear measurements. We took linear measurements following the measurement scheme of Clemens (1964), Novacek and Clemens (1977), and Archibald (1982) (Fig. 2.2a). We took measurements in ImageJ version 1.46r, using a scale bar included in each digital image. We conducted ordinations and statistical analyses of linear measurements in R version 3.2.1 (2015, www.r-project.org), using functions from the package MASS (Venables and Ripley 2002), pgirmess (Giraudoux 2015), and the built-in stats package (R Core Team 2015). For comparisons with the findings of Archibald (1982) and Novacek and Clemens (1977), we calculated the ratio of p4 height to length (H/L, degree of arc in the p4 profile) and the ratio of p4 length-to-apex-of-the-crown to total length (L1/L, symmetry of the crown profile) (Fig. 2.2A). We conducted PCA on linear measurements of L, L1, and H on all *Mesodma* specimens, and tested for significant

differences in mean values using non-parametric tests (Welch's non-parametric t-test, Kruskal-Wallis test, and Kruskal-Wallis multiple comparison test) because not all species showed normal distributions for these values (Shapiro-Wilk test, at an alpha level of 0.05). To assess intraspecific variation, we calculated coefficient of variation on L, H, and L1 (Simpson 1960).

Two-dimensional geometric morphometrics. We used two-dimensional (2D) geometric morphometrics (GM) to collect p4 shape data that might not be accessible through linear measurements alone. Of specific interest to this study was the shape of the apical curve of the p4 because it has commonly been used to diagnose multituberculate species (e.g., Clemens 1964; Archibald 1982). Unlike therian tribosphenic molars, which have primary cusps and cuspids that can be used as homologous landmarks for GM, there are no clear single-point homologies along the curve of multituberculate p4s; however, the apical curve of the p4 as a whole can be considered homologous (Zelditch et al. 2004; Wilson 2013). Our landmark scheme (Fig. 2.2B, Table 2.1) consists of 18 sliding semilandmarks (SLMs) that represent the curve, 19 helper points that assist in the process of superimposition, and two traditional landmarks (LMs) that anchor each end of the curve. It is similar to the scheme used by Wilson (2013: fig. 2C), but we excluded the buccal lobe of the p4 from our shape analyses because of its high intraspecific shape variability and because it has not previously been used to diagnose species of *Mesodma*.

We used tpsDIG2 v.2.17 (Rohlf 2013a) to modify previously digitized curves from Wilson (2013) and to digitize LMs, SLMs, and helper points on the two additional specimens. We first placed the two LMs, and then traced a curve along the top of the crown between the LMs (Fig.

2.2B). We resampled the curve to 39 equally spaced points, including the two LMs, and converted those points to LMs using tpsUtil v.1.60 (Rohlf 2013b).

We conducted all geometric morphometric analyses in R using functions from the package geomorph (Adams and Otárola-Castillo 2013). Specifically, we read the LM configurations into R from a TPS file output from tpsDIG and tpsUtil, and then rotated, scaled, and translated the data with generalized least square (GLS) Procrustes superimposition (Zelditch et al. 2004). We designated sliding SLMs using a "sliders" file as output by the geomorph function define.sliders. Each slider had two adjacent helper points, which were immobile during GLS Procrustes superimposition and defined the length of the curve on which the sliders were allowed to move to minimize Procrustes distance (Sampson et al. 1996; Gunz and Mittenroecker 2013). Following GLS Procrustes superimposition, we removed the helper points to yield a data set of partial warp scores for 18 SLMs and two LMs. To assess similarities in p4 shape and size among our specimens, we conducted PCA on two data sets: partial warp scores with associated centroid size for each specimen (as calculated by the geomorph function gpagen), and partial warp scores without centroid size. For each data set, we also conducted canonical variate analysis (CVA) to determine the utility of the data set for classifying p4s to species level.

2.5 RESULTS AND DISCUSSION

Our primary objective in these analyses was to understand the utility of p4 shape for species-level taxonomic identification in the multituberculate genus *Mesodma*. Differences in p4 shape within the genus have previously been described using ratios of linear measurements (Novacek and Clemens 1977; Archibald 1982). Our PCA of linear measurements (Fig. 2.3) indicates that

shape, as captured by linear measurements, is not as important as size for identifying p4s to species level. PC1 mostly represents size and accounts for 96.0% of the variance. Canonical variate analysis (CVA) was successful at identifying the two smaller species, with 100% of *M. hensleighi* specimens and 94.6% of *M. formosa* specimens classified correctly (Table 2.3). CVA was not as successful at discriminating between the two larger species. Although 88.0% of *M. garfieldensis* specimens were correctly classified, 90.9% of *M. thompsoni* specimens were classified incorrectly as *M. garfieldensis* (Table 2.3).

In our initial 2D GM analysis, we investigated shape exclusively and explored sources of shape variation that could not be detected with linear measurements alone. We considered relative shape differences across the genus by comparing scores of each species along PC1, PC2, and PC3, which represent 42.3%, 20.9%, and 16.6% of the shape variation, respectively. Subsequent PCs represent less than 10% of the shape variation and were not considered significant for understanding shape variation across the genus. Results of GM analyses are shown in Fig. 2.4. PC1 represents variation in the arc of the p4, with higher scores indicating a more domed profile, and lower scores a lower, flatter profile. PC2 represents a change in the shape of the distal aspect of the tooth, with lower scores indicating a convex curved shape, and higher scores a slightly concave shape. PC3 represents variation in the mesial edge of the tooth, with lower scores indicating a more acute angle to the gum line, and higher scores a more obtuse angle to the gum line. There is no obvious clustering of conspecifics in the morphospace (Fig. 2.4), and CVA performed poorly, with only 52.3% of specimens identified correctly, including 0.0% of *M. thompsoni* specimens (Table 2.3).

On the basis of this poor performance of CVA and the absence of p4-shape-based species groupings, we chose to reintroduce size into our analyses. We ran PCA on a data set composed of the Procrustes-aligned shape data and corresponding centroid size for each specimen. Results of this analysis are shown in Fig. 2.5. PC axes are designated sPC1 and sPC2 to indicate the inclusion of centroid size. sPC1 and sPC2 account for 99.9% and 0.01% of variation, respectively. sPC3 and higher were not considered because of the very small amount of variation they represented (all < 0.005%). Variation along sPC1 mostly represents size, which is the overwhelming source of variation in this data set, whereas shape is only a minimal source of variation. CVA of this data set resulted in a high proportion of correctly identified specimens (81.4% correct classification, Table 2.3). This high percentage is driven by *M. hensleighi* (100.0% correct classification) and *M. formosa* (94.6% correct classification). The two largest species were classified correctly less frequently, with 84.0% of *M. garfieldensis* specimens and 9.1% of *M. thompsoni* specimens correctly classified. Misidentified specimens of *M. garfieldensis* were attributed to either *M. thompsoni* (8.0%) or *M. formosa* (8.0%), whereas misidentified specimens of *M. thompsoni* were attributed to either *M. formosa* (9.1%) or *M. garfieldensis* (81.8%).

p4 size, not shape, matters most. The results of these analyses show that we were unable to adequately distinguish among species of *Mesodma* on the basis of p4 profile shape alone. The overlap of species within the PCA morphospaces (without [Fig. 2.4] and with size [Fig. 2.5]) combined with poor classification performance in the CVA (Table 2.3) indicate that the main source of variation among species within this genus is tooth size and, by extension, body size (Gould 1975; Gingerich et al. 1982). Size-based partitioning among sympatric species of

Mesodma makes sense in light of the morphological similarity among them, at least as represented by the p4. Although these congeners likely had similar dietary ecologies (insectivory to animal-dominated omnivory; Wilson 2013), they might have exploited differently sized food resources, thus reducing overlap in their dietary niches (Hutchinson 1959; Mayr 1970). Linear measurements do indicate some detectable differences in p4 crown shape across some species, but they are slight (Table 2.2). Below we present a series of pairwise comparisons of our species of *Mesodma*, each including an assessment, based on our analyses, of the morphological differences (p4 size and shape) between the two species being considered. Following these comparisons, we discuss the validity of these four species, and make suggestions for application of our results in taxonomic practice.

***M. hensleighi* versus *M. formosa*.** *Mesodma hensleighi* is easy to distinguish from its congeners because of its small size. Both published size ranges and size ranges from the present study (Table 2.4, Figs. 2.3 and 2.5) show little overlap with those of *M. formosa*, which is the next smallest species in our sample. Novacek and Clemens (1977) were able to achieve 100% correct classification of specimens of *M. hensleighi* using discriminant analysis on their data set, which included p4 length. We were likewise able to obtain 100% correct classification of *M. hensleighi* with both linear measurements and GM analyses including centroid size (Table 2.2). One specimen that was originally identified as *M. formosa*, UCMP 115931, plots consistently with all specimens of *M. hensleighi* in the PCAs (Figs. 2.3, 2.5), and was identified as such by CVA; this likely represents a misidentification and does not overly complicate the differentiation of *M. hensleighi* from *M. formosa*. If we consider this specimen to be *M. hensleighi* instead of *M. formosa*, p4 size ranges for the two species do not overlap in our sample. As such, we find that

p4 measurements from the literature are sufficient to distinguish these two species from one another (see below, Recommendations and future directions).

M. garfieldensis* versus *M. thompsoni. Size does not adequately differentiate between *M. garfieldensis* and *M. thompsoni.* In the PCA that incorporates centroid size (Fig. 2.5), *M. thompsoni* mostly plots at the large end of the size range (sPC1) for *M. garfieldensis* and has a slightly larger average size, but the latter difference is not significant (Welch's non-parametric t-test, $p > 0.1$; Fig. 2.5, Table 2.4). Although the accuracy of the CVA is higher with the inclusion of size than it is without size (Table 2.3), the percent correct identification is still below 10% for *M. thompsoni*. Nearly all (81.8%) of the misidentified specimens of *M. thompsoni* were identified as *M. garfieldensis*. This is in strong contrast to the very high percentage of correct identifications of specimens of *M. hensleighi* and *M. formosa* (Table 2.3). In light of these results, we carefully inspected the original diagnosis and description of *M. garfieldensis* to understand the quantitative and qualitative morphological characteristics that purportedly separate it from *M. thompsoni*.

The diagnosis of *M. garfieldensis* is based on the size ratios of the molars (relatively longer first molars than other species); average number of cusps on M1/m1 (higher than other species); and shape of the p4 ("greatest height to length ratio of any species of *Mesodma*," Archibald 1982: 47). Here, we consider morphology of the p4 only; molar morphology is discussed in the following section. In Archibald's (1982) discussion of p4 shape in *M. garfieldensis,* he noted a bimodal shape-distribution in the hypodigm, which included 17 complete p4s. Approximately half of the specimens exhibited a lower, flatter profile, and the other half a taller, more domed

profile. He attempted to capture these two morphs in the chosen holotype (UCMP 116622) and paratype (116621), respectively. Using 2D GM, we were unable to detect this bimodal shape-distribution in our sample, which is slightly larger (N = 25) and includes several specimens recovered from the type locality (Table 2.10.1), including the holotype and paratype. In the GM analyses, our sample of *M. garfieldensis* shows a normal (not bimodal) shape-distribution along PC1 (Shapiro-Wilk, $p = 0.3$), PC2 ($p = 0.8$), and PC3 ($p = 0.8$), which together account for 79.9% of variance in the morphospace. Additionally, the paratype (UCMP 116621) consistently plots near specimens of *M. formosa* in the morphospace (Figs. 2.3 and 2.5), and thus, we argue that it is probably a misidentified specimen of *M. formosa*.

Linear measurements of our sample also do not support *M. garfieldensis* as having the highest p4 arc profile (H/L ratio) of any species in the genus; instead, *M. formosa* exhibits the highest mean H/L, followed by *M. hensleighi*; *M. thompsoni* and *M. garfieldensis* are tied for the lowest mean H/L (Table 2.2). Among the three larger species, the only significant differences in H/L are between *M. formosa* and *M. garfieldensis*, and *M. formosa* and *M. thompsoni* (Kruskal-Wallis multiple comparison test, $p < 0.05$).

The strong similarities between *M. garfieldensis* and *M. thompsoni* led us to consider the possibility that they represent a single species. To test this hypothesis, we calculated the coefficient of variation (CV) for each linear measurement: L, L1, and H (Table 2.5). CV has been used to understand the amount of morphological variation that might be expected in a sample containing only one species (e.g., Simpson 1960; Gingerich 1974; Cope 1993). This method has received some criticism due to negative correlation between the arithmetic mean of a

given measurement and its CV (Polly 1998). However, when compared to the data shown by Polly (1998: fig. 1), our data have a considerably smaller range of arithmetic means (2–5 mm vs. 0–15 mm), meaning that any correlation between size and CV is unlikely to have a strong effect on our comparisons across species of *Mesodma*. Here, we focus on p4 length, because it is the least likely to be altered by apical tooth wear or preservation.

As shown in Table 2.5, all four species show similar CVs for p4 length (4.98–5.56), with *M. garfieldensis* having a slightly smaller value than the others (4.98 vs. 5.43–5.56). When we combined the samples of *M. garfieldensis* and *M. thompsoni*, the resulting CV (5.23) is similar to those of the other individual species of *Mesodma*, whereas all other combinations of species (e.g., *M. garfieldensis* + *M. formosa*) yielded considerably higher values (7.5–9.8). In other words, lumping specimens of *M. thompsoni* and *M. garfieldensis* into a single sample yields a CV typical of other species in the genus, and supports other shape- and size-based evidence that these two species might represent a single species.

M. garfieldensis* = *M. thompsoni. Here, we propose that *M. garfieldensis* is a junior synonym of *M. thompsoni.* This taxonomic proposal is based largely on comparisons of the morphology and size of the p4, which is admittedly a very small part of mammalian anatomy. However, we argue that the molars referred to *M. garfieldensis* are also not sufficiently distinct from named species of *Mesodma* to merit assignment to a separate species. The diagnosis of *M. garfieldensis* (Archibald 1982) states that the primary differences between it and the other known species of *Mesodma* are the size ratios of the molars (e.g., m1:m2), with *M. garfieldensis* having proportionally longer first molars than any other species. This diagnosis is based on the average

length of specimens of *Mesodma* from a single vertebrate microfossil locality, UCMP V74111. Large M2/m2s, which were quite rare in Lancian assemblages (Archibald 1982: fig.10), were not present at V74111. This resulted in shorter average M2/m2 lengths, and consequentially a relatively longer average length for M1/m1s, despite the fact that M1/m1s of *M. garfieldensis* fall into the size range of known species of *Mesodma* (*M. formosa* and *M. thompsoni*). The use of molar size ratios in the diagnosis of *M. garfieldensis* is problematic because none of the molars in the hypodigm have been found in association with one another or with a diagnostic p4. As noted by Lillegraven, "Since essentially all materials referable to the genus [*Mesodma*] are isolated teeth, most associations are open to question" (1969: 17). Until samples of dentulous jaws of *M. garfieldensis* are available, the hypothesis that *M. garfieldensis* and other species of *Mesodma* differ in ratios of M1:M2 and m1:m2 length cannot be rigorously tested.

Because we did not recover significant differences in the morphology and size of p4s attributed to *M. thompsoni* and *M. garfieldensis*, and, in light of the information concerning molars presented above, we find no evidence to support separation of *M. garfieldensis* (Archibald 1982) and *M. thompsoni* (Clemens 1964). Thus, we argue that according to ICZN rules of taxonomic priority we should subsume *M. garfieldensis* (Archibald 1982) within *M. thompsoni* (Clemens 1964). We follow this proposal throughout the remainder of this paper; hereafter, references to and analyses of samples of *M. thompsoni* also include specimens previously attributed to *M. garfieldensis.*

M. formosa* versus *M. thompsoni. Clemens (1964) differentiated *M. thompsoni* from *M. formosa* on the basis of (1) size, with *M. thompsoni* being larger than *M. formosa*; (2) robustness

of the mandible, with *M. thompsoni* being more robust; and (3) shape of the p4 profile, with that of *M. thompsoni* being flatter and less symmetrical than that of *M. formosa*. Clemens (1964) did not quantify p4 shape; however, several subsequent studies (Novacek and Clemens 1977; Archibald 1982) did so by using H/L and L1/L as a proxy for height and symmetry of the p4 profile, respectively. Our results are consistent with Clemens' (1964) observations: p4s of *M. formosa* have on average a significantly more domed (larger H/L) and significantly more symmetrical (L1/L closer to 0.5) profile than those of *M. thompsoni* (incl. *M. garfieldensis*) (Table 2.2). Nevertheless, on the basis of our observed ranges for H/L and L1/L, we question whether in this case these ratios are the best way to diagnose taxa most frequently represented by isolated teeth. Although the mean values for specimens assigned to these two species are significantly different at an alpha level of 0.05 (based on Welch's non-parametric t-test for difference in means; $p < 0.01$), a combined distribution of L1/L for both species does not differ significantly from normal (Shapiro-Wilk test, $p > 0.1$), nor does a combined distribution of H/L ($p > 0.5$). Additionally, the ranges of L1/L and H/L values for these two species are nearly identical (Table 2.2). This overlap in ranges means that, despite the significant difference in mean H/L and L1/L, using these metrics alone to refer isolated teeth to these species could be problematic. The published size ranges of *M. formosa* and *M. thompsoni* also exhibit overlap, but to a lesser degree than the ranges of the shape metrics (Table 2.4). In turn, the most effective means of differentiating between these two species is size (see below, Recommendations and future directions). However, the size difference between these two taxa is complicated by apparent changes in *M. formosa* across the K-Pg boundary that are detailed below.

Size change across the K-Pg boundary. Fig. 2.6 shows the sPCA split into La and Pu1 samples. All three species are represented in both samples (but note: Pu1 *M. thompsoni* = formerly *M. garfieldensis*). Because there is only one Pu1 specimen of *M. hensleighi* in our data set, it is not possible to assess intraspecific size differences between La and Pu1 samples of this taxon. La and Pu1 specimens of *M. thompsoni* do not differ significantly in size (Welch's non-parametric t-test of p4 length (L), $p > 0.1$). La specimens of *M. formosa* are smaller than Paleogene specimens of this taxon (Welch's non-parametric t-test of p4 length (L), $p < 3.0e\text{-}08$). In the La plot, the gap between *M. formosa* and *M. thompsoni* along sPC1 is substantial; however, across the K-Pg boundary (Pu1 plot), specimens of *M. formosa* are larger relative to their La counterparts, and, in turn, the size gap between *M. formosa* and *M. thompsoni* is gone. We examined two different explanations for this size change across the K-Pg boundary.

If we accept that Pu1 specimens of *M. formosa* were identified correctly, then one possibility is that *M. formosa* underwent an anagenetic increase in size over the K-Pg boundary. In this case, all three local species of *Mesodma* would have survived the K-Pg mass extinction, and, in turn, we would expect a bimodal size-distribution of *M. formosa* and *M. thompsoni* specimens. Indeed, our Pu1 data show a significantly non-normal size-distribution (Shapiro-Wilk, $p < 0.05$). However, the Pu1 sample shows more overlap in size between *M. formosa* and *M. thompsoni* than between the La samples of *M. formosa* and *M. thompsoni*. Although the CVA distinguishes between these two species (Table 2.3), a more fundamental biological question is whether two groups should be considered separate species if their size ranges abut so closely and their morphologies do not differ enough to be distinguished in the absence of size.

This question lead us to consider to a second possibility that Pu1 specimens of *M. formosa* actually belong to *M. thompsoni* and represent an expansion in the size range of *M. thompsoni* across the K-Pg boundary; this would also imply the extinction of *M. formosa* at the boundary. If this were the case, we might expect our data to resemble those from the Novacek and Clemens (1977) study of *Mesodma* from the Bug Creek Anthills (BCA) assemblage. In a sample of 335 p4s, those authors were unable to detect statistical signs of the presence of multiple species (such as multimodality), and concluded that only one species was represented, as opposed to two (*M. thompsoni* and *M. formosa*, Sloan and Van Valen 1965). However, the BCA is now recognized as a temporally mixed assemblage containing both La and Pu1 specimens (Lofgren 1995), so a Pu1-only pattern might not be detectable, especially in this case where the single hypothesized Pu1 species closely resembles several La species. Nevertheless, Novacek and Clemens (1977) also investigated a small sample (N = 14) of *Mesodma* p4s from the slightly younger (late Puercan, Pu3) Garbani local fauna, and found no evidence of multiple species present in that sample either. Because our current sample of Pu1 p4s exhibits a non-normal, possibly multimodal size-distribution, our data more closely match the scenario in which multiple species (*M. formosa* and *M. thompsoni*) were present in the local fauna. Thus, we argue that all three taxa survived the K-Pg boundary and that *M. formosa* experienced anagenetic size increase across this boundary, potentially resulting from ecological pressures of the K-Pg extinction or from the influx of mammalian immigrants that followed it (Wilson 2014).

Recommendations and future directions. On the basis of our results, we recognize three species of *Mesodma* in our Lancian and Puercan 1 samples. The original description of *M. hensleighi* (Lillegraven 1969) presents a size for only the holotype. Although it does note that *M.*

hensleighi is "significantly smaller" than *M. formosa* (Lillegraven 1969: 17), the description does not include a size cutoff between the two species, perhaps because, in the small available samples, these two species did not approach one another in p4 size (Lillegraven 1969: table 1). In our sample, we also found that these two species do not overlap in size, so we do not offer additional criteria to differentiate these taxa. In contrast, published p4 size ranges of *M. formosa* and *M. thompsoni* overlap (Table 2.4), and, in our study, the ranges of two shape metrics (L1/L and H/L) overlap in these two species to an even greater extent than their size ranges do (Tables 2.2, 2.4). Consequently, a clear cutoff for size and shape metrics cannot be drawn between these two species. Nevertheless, previous studies and our study show that the majority of p4s identified as *M. formosa* are 3.9 mm or less in length, whereas those identified as *M. thompsoni* tend to be greater than 3.9 mm in length. In combination with an examination of shape metrics (L1/L and H/L), this size guideline may help in taxonomic identification of relatively large, isolated p4s of *Mesodma*. Further study of larger samples of p4s of these two species would help to clarify their diagnostic characteristics; analysis of a geographically broader sample of p4s would be especially useful, as it would aid in understanding intraspecific variation in size and shape of *M. thompsoni* and *M. formosa* p4s across space as well as through time.

Difficulties in species-level identifications obscure perceived patterns of extinction, pseudoextinction, and survival of lineages. In his study of Lancian- and Puercan-age mammals from the McGuire Creek area in northeastern Montana, Lofgren (1995) refrained from identifying over 2,200 specimens of isolated and associated teeth of *Mesodma* below the genus level, citing the "difficulties inherent in species identification" (p.78). This was a prudent choice at the time of his study, but it resulted in a loss of taxonomic resolution for analyses of the K-Pg

mass extinction. As another example, the two species of the Puercan eutherian genus *Mimatuta* can be distinguished from each other only when molar specimens are in association with a lower fourth premolar; specifically, the p4 metaconid of *Mimatuta minuial* is "rather strong" compared to that of *Mimatuta morgoth* (Van Valen 1978: 62). Consequently, isolated molars referable to the genus must be left as *Mimatuta* sp., and are either (1) excluded from species-level faunal analyses, or (2) included in faunal analyses that are conducted at the genus level; either case results in a loss of resolution. Anagenesis can also exacerbate identification problems among already morphologically similar species. As stratigraphic sampling increases, gradual changes in morphology and/or size of a species through time can be uncovered, which may close gaps between previously distinct species, and force seemingly arbitrary delimitations along morphological and/or size continua, if organisms are to be grouped into discrete taxa (Rose and Bown 1986). In the case of the genus *Mesodma*, a confluence of anagenetic change and morphological similarity among species has made it very challenging to identify isolated teeth of this genus to the species level.

Although the inherent vagaries of the fossil record (e.g., scant genetic, behavioral, and soft-tissue data) will continue to limit the ability of paleontologists to make lower-level taxonomic identifications, new technologies, approaches, and analytical methods have helped us to extract more morphological data from incomplete fossils and to draw sharper contrasts among them. For example, recent developmental approaches to understanding evolution of mammalian dental morphology have explored the genetic basis for morphogenesis of dental size, cusp number and morphology, and number of teeth (Jernvall et al. 2000; Moustakas et al. 2011; Häärä et al. 2012; Harjunmaa et al. 2012). A better understanding of the underpinnings of dental morphology and

variability within species will help us make better-informed decisions about what characters are the most biologically informative and best to use for species delimitation.

In this study, we applied geometric morphometrics to more precisely describe and compare the p4 morphology of four species of *Mesodma*. Whereas GM did not enhance our ability to discriminate among species, it did highlight a lack of diagnostic p4 shape characters and turned our focus instead to size for identification purposes. More specifically, our results indicate that (1) the main source of variation among the p4s of *Mesodma* species is size, whereas shape provides little assistance in species discrimination; (2) *M. garfieldensis* and *M. thompsoni* likely represent a single species, *M. thompsoni*; and (3) *M. formosa* underwent a significant increase in size across the K-Pg boundary. Although further investigation into the morphological differences between Puercan *M. thompsoni* and *M. formosa* is warranted due to their similarity in size, we have outlined practical suggestions for identifying Lancian and Puercan 1 specimens of *Mesodma* using p4 measurements. Moving forward, we hope to mitigate problems of taxonomic identification using a combination of morphological, developmental, and evolutionary data, which will allow us to make more precise, quantitative, practical, and biologically informative taxonomic diagnoses.

2.6 ACKNOWLEDGEMENTS

Funding for this research was provided by the University of Washington and the Hell Creek Project III. We would like to thank all previous Hell Creek field crews for their hard work and help with acquisition of specimens for this study. Permits to collect vertebrate fossils on state and federal land were provided by the U.S. Bureau of Land Management, Montana Department of Natural Resources, and Charles M. Russell Wildlife Preserve. We thank the University of California Museum of Paleontology (UCMP), especially Patricia Holroyd and Mark Goodwin, for access to specimens, and the UCMP Welles Fund, which enabled SMS to visit UCMP collections for this research. Special thanks to Anne Weil for digital images of UCMP 116621. We are also grateful to W.A. Clemens, members of the Wilson Lab (Alexandria Brannick, Jonathan Calede, Meng Chen, Lauren DeBey, and David DeMar, Jr.,), Ian Browne, and Yue Zhang for helpful comments and discussions concerning this research and manuscript.

2.7 REFERENCES

Adams DC, Otárola-Castillo E (2013) geomorph: an R package for the collection and analysis of geometric morphometric shape data. Meth Ecol Evol 4:393–399

Adams DC, Rohlf FJ, Slice DE (2013) A field comes of age: geometric morphometrics in the 21st century. Hystrix 24:7–14

Archibald JD (1982) A study of Mammalia and geology across the Cretaceous-Tertiary boundary in Garfield County, Montana. Univ Calif Publ Geol Sci 122:1–286

Chew AE (2009) Paleoecology of the early Eocene Willwood mammal fauna from the central Bighorn Basin, Wyoming. Paleobiology 35:13-31. doi: 10.1666/07072.1

Cifelli RL, Eberle JJ, Lofgren DL, Lillegraven JA, Clemens WA (2004) Mammalian biochronology of the latest Cretaceous. In: Woodburne MO (ed) Late Cretaceous and Cenozoic Mammals of North America: Biostratigraphy and Geochronology. Columbia University Press, New York, pp 21–42

Clemens WA (1964) Fossil mammals of the type Lance Formation, Wyoming: Part I. Introduction and Multituberculata. Univ Calif Publ Geol Sci 48:1–105

Clyde WC, Gingerich PD (1998) Mammalian community response to the latest Paleocene thermal maximum: an isotaphonomic study in the northern Bighorn Basin, Wyoming. Geology 26:1011–1014

Cope DA (1993) Measures of dental variation as indicators of multiple taxa in samples of sympatric *Cercopithecus* species. In: Kimbel WH, Martin LB (eds) Species, Species Concepts and Primate Evolution. Springer, New York, pp 211–237

Eberle JJ (2003) Puercan mammalian systematics and biostratigraphy in the Denver Formation, Denver Basin, Colorado. Rocky Mt Geol 38:143–169

Eberle JJ, Lillegraven JA (1998) A new important record of earliest Cenozoic mammalian history: geologic setting, Multituberculata, and Peradectia. Rocky Mt Geol 33:3–47

Flynn JJ, Wyss AR, Croft DA, Charrier R (2003) The Tinguiririca Fauna, Chile: biochronology, paleoecology, biogeography, and a new earliest Oligocene South American Land Mammal 'Age.' Palaeogeogr Palaeoclimatol Palaeoecol 195:229–259. doi: 10.1016/s0031-0182(03)00360-2

Gingerich PD (1974) Size variability of the teeth in living mammals and the diagnosis of closely related sympatric fossil species. J Paleontol 48:895-903

Gingerich PD, Smith BH, Rosenberg K (1982) Allometric scaling in the dentition of primates and prediction of body weight from tooth size in fossils. Am J Phys Anthropol 58:81–100

Giraudoux P (2015) pgirmess: Data Analysis in Ecology. R package version 1.6.2. http://CRAN.R-project.org/package=pgirmess

Gould SJ (1975) On the scaling of tooth size in mammals. Am Zoologist 15:353–362

Gunz P, Mitteroecker P (2013) Semilandmarks: a method for quantifying curves and surfaces. Hystrix 24:103–109

Häärä O, Harjunmaa E, Lindfors PH, Huh SH, Fliniaux I, Åberg T, Jernvall J, Ornitz DM, Mikkola ML, Thesleff I (2012) Ectodysplasin regulates activator-inhibitor balance in murine tooth development through Fgf20 signaling. Development 139:3189–3199. doi: 10.1242/dev.079558

Harjunmaa E, Kallonen A, Voutilainen M, Hamalainen K, Mikkola ML, Jernvall J (2012) On the difficulty of increasing dental complexity. Nature 483:324–327. doi: 10.1038/nature10876

Hutchinson GE (1959) Homage to Santa Rosalia, or, Why are there so many kinds of animals? Am Nat 93:145-159

Jernvall J, Keränen SVE, Thesleff I (2000) Evolutionary modification of development in mammalian teeth: quantifying gene expression patterns and topography. Proc Natl Acad Sci USA 97:14444–14448.

Lillegraven JA (1969) Latest Cretaceous mammals of upper part of Edmonton Formation of Alberta, Canada, and review of marsupial-placental dichotomy in mammalian evolution. Univ Kansas Paleontol Contr 50:1-122

Lofgren DL (1995) The Bug Creek problem and the Cretaceous-Tertiary transition at McGuire Creek, Montana. Univ Calif Publ Geol Sci 140:1–185

Maas MC, Anthony MRL, Gingerich PD, Gunnell GF, Krause DW (1995) Mammalian generic diversity and turnover in the late Paleocene and early Eocene of the Bighorn and Crazy Mountains Basins, Wyoming and Montana (USA). Palaeogeogr Palaeoclimatol Palaeoecol 115:181–207. doi: 10.1016/0031-0182(94)00111-K

Mayr E (1970) Biological properties of species. In: Populations, Species, and Evolution: An Abridgment of Animal Species and Evolution. Harvard University Press, Cambridge, pp 37–54

Moustakas JE, Smith KK, Hlusko LJ (2011) Evolution and development of the mammalian dentition: insights from the marsupial Monodelphis domestica. Devel Dynamics 240:232–239. doi: 10.1002/dvdy.22502

Novacek M, Clemens WA (1977) Aspects of intrageneric variation and evolution of *Mesodma* (Multituberculata, Mammalia). J Paleontol 51:701–717

Polly PD (1998) Variability in mammalian dentitions: size-related bias in the coefficient of variation. Biol J Linn Soc 64:83–99

R Core Team (2015) R: A language and environment for statistical computing. R Foundation for Statistical Computing, Vienna, Austria http://www.R-project.org/

Rohlf FJ (2013a) tpsDig, Version 2.17. Department of Ecology and Evolution, State University of New York, Stony Brook

Rohlf FJ (2013b) tpsUtil, Version 1.60. Department of Ecology and Evolution, State University of New York, Stony Brook

Rose KC, Bown TM (1986) Gradual evolution and species discrimination in the fossil record. Rocky Mt Geol 24:119-130

Sampson PD, Bookstein FL, Sheehan FH, Bolson EL (1996) Eigenshape analysis of left ventricular outlines from contrast ventriculograms. In: **Marcus** LF, **Corti** M, **Loy** A, **Naylor** GJP, **Slice** DE (eds) Advances in Morphometrics. Springer, New York, pp 211–233

Simpson GG (1960) Notes on the measurement of faunal resemblance. Am J Sci 258:300–311

Sloan RE, Van Valen LM (1965) Cretaceous mammals from Montana. Science 148:220–227

Smith AB (1994) Systematics and the Fossil Record: Documenting Evolutionary Patterns. Wiley, New York

Van Valen LM (1978) The beginning of the age of mammals. Evol Theory 4:45–80

Venables WN, Ripley BD (2002) Modern Applied Statistics with S, 4th edn. Springer, New York

Webb MW (2001) Fluvial architecture and Late Cretaceous mammals of the Lance Formation, southwestern Bighorn Basin, Wyoming. Dissertation, University of Wyoming

Wilson GP (2004) A quantitative assessment of mammalian change leading up to and across the Cretaceous-Tertiary boundary in northeastern Montana. Dissertation, University of California, Berkeley

Wilson GP (2005) Mammalian faunal dynamics during the last 1.8 million years of the Cretaceous in Garfield County, Montana. J Mammal Evol 12:53–76

Wilson GP (2013) Mammals across the K/Pg boundary in northeastern Montana, USA: dental morphology and body-size patterns reveal extinction selectivity and immigrant-fueled ecospace

filling. Paleobiology 39:429–469

Wilson GP (2014) Mammalian extinction, survival, and recovery dynamics across the Cretaceous-Paleogene boundary in northeastern Montana, USA. Geol Soc Am Spec Pap 503:365–392

Wilson GP, Evans AR, Corfe IJ, Smits PD, Fortelius M, Jernvall J (2012) Adaptive radiation of multituberculate mammals before the extinction of dinosaurs. Nature 483:457–460. doi: 10.1038/nature10880

Zelditch ML, Swiderski DL, Sheets HD (2004) Geometric Morphometrics for Biologists: A Primer. Elsevier Academic, San Diego

2.8 FIGURES

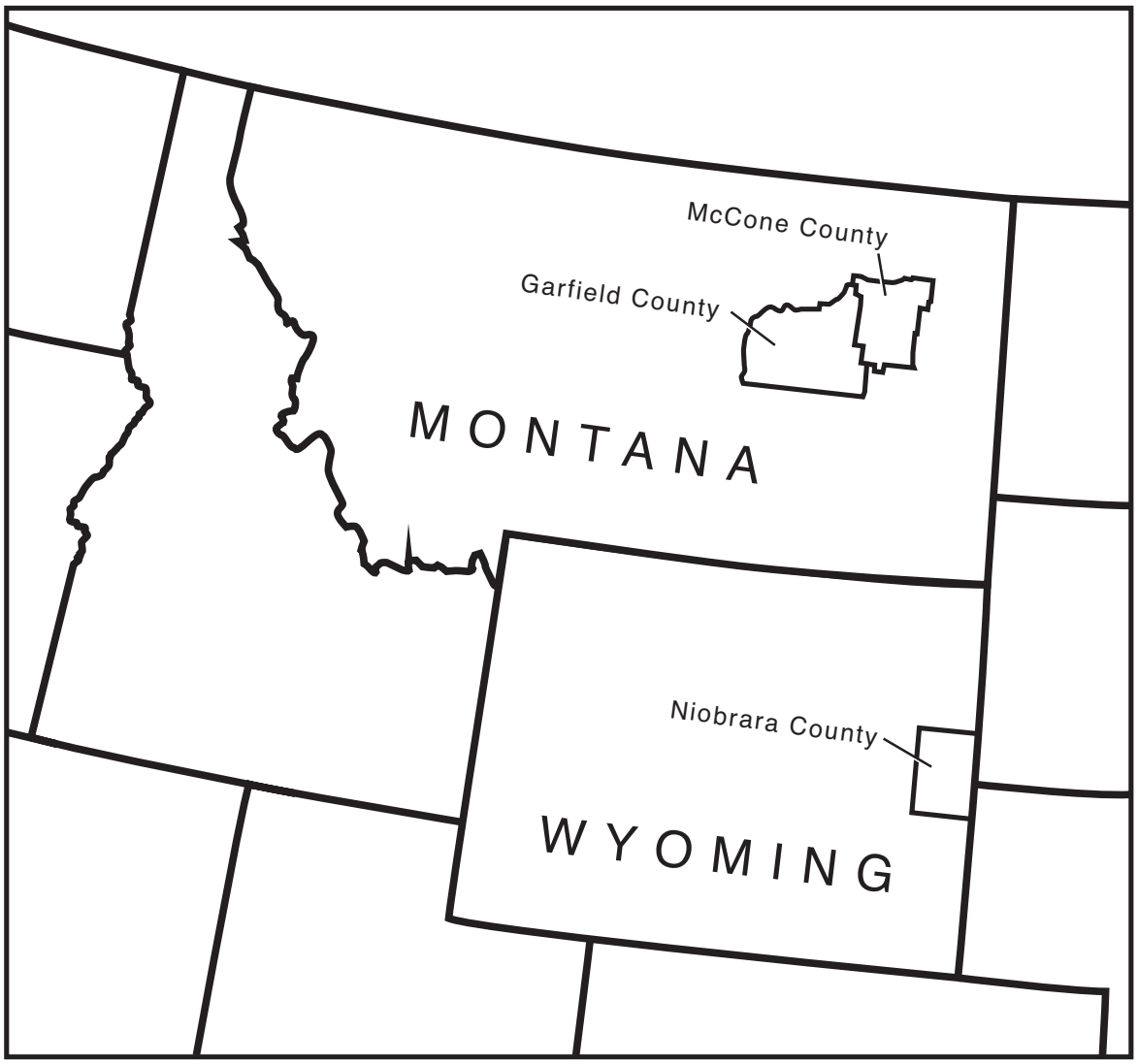

Figure 2.1 Counties of origin for fossil specimens included in this study. Specimens originating from Niobrara County, WY are Cretaceous in age (Lance Formation). Specimens from Garfield and McCone Counties, MT are Cretaceous or Paleogene in age (Hell Creek and Tullock Formations).

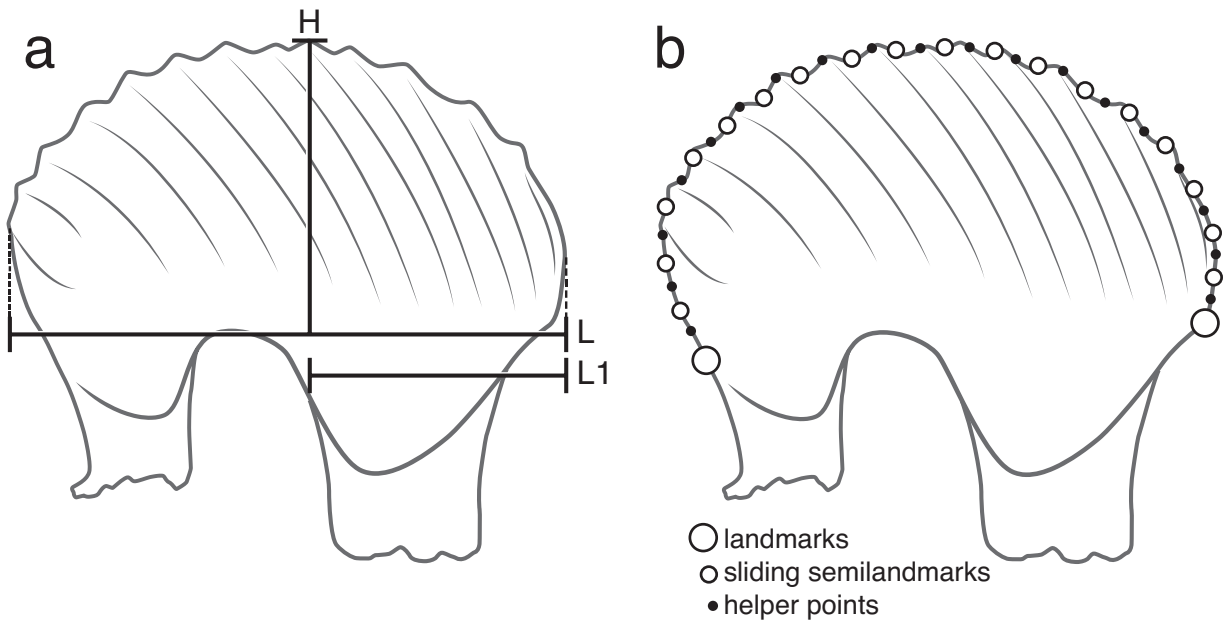

Figure 2.2 Measurements and geometric morphometric landmarks shown on a generalized multituberculate p4 in buccal view, anterior to the right. a, linear measurements, after Novacek and Clemens (1977). L, greatest length from anterior edge of crown to posterior edge, along a baseline tangent to the highest point on the arch of the crown between the roots. H, crown height measured at right angle from the baseline to the highest point on the apical curve of the tooth. L1, length from the anterior edge of the crown to the highest point on the apical curve, parallel to L. b, landmarks, semilandmarks, and helper points used in geometric morphometric analyses. See Table 2.1 for landmark information.

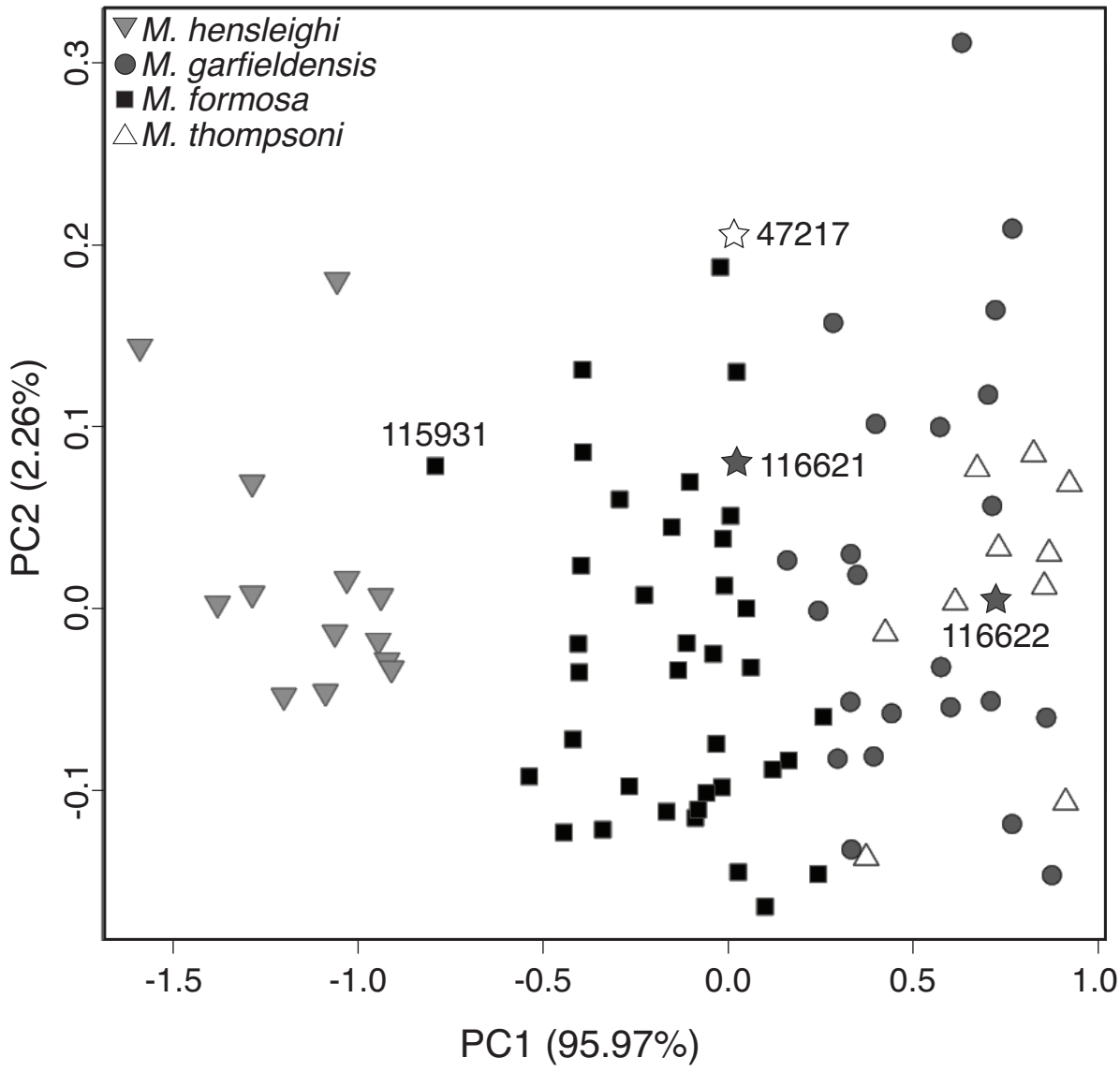

Figure 2.3 Principal components analysis (PCA) of linear measurements alone. Stars represent type specimens: the paratype and holotype of *M. garfieldensis* (UCMP 116621 and 116622, respectively) and the holotype of *M. thompsoni* (UCMP 47217). UCMP 115931 likely represents a misidentified specimen of *M. hensleighi* (see text).

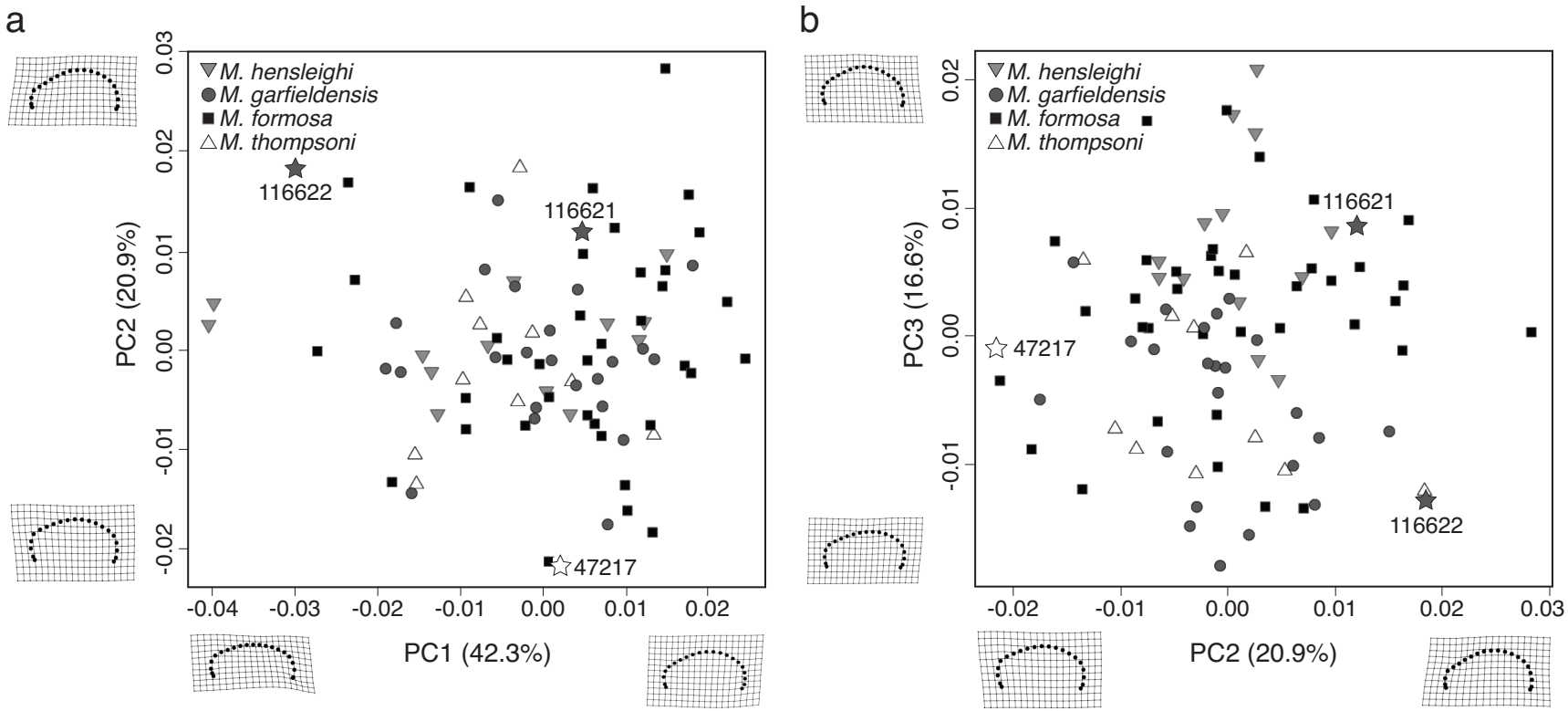

Figure 2.4 PCA of Procrustes-aligned coordinates for four species of *Mesodma*. Partial warps show change from consensus shape to the extremes (positive and negative) of principal component axes 1 and 2 (a) and 2 and 3 (b). Stars represent type specimens: the paratype and holotype of *M. garfieldensis* (UCMP 116621 and 116622, respectively) and the holotype of *M. thompsoni* (UCMP 47217)

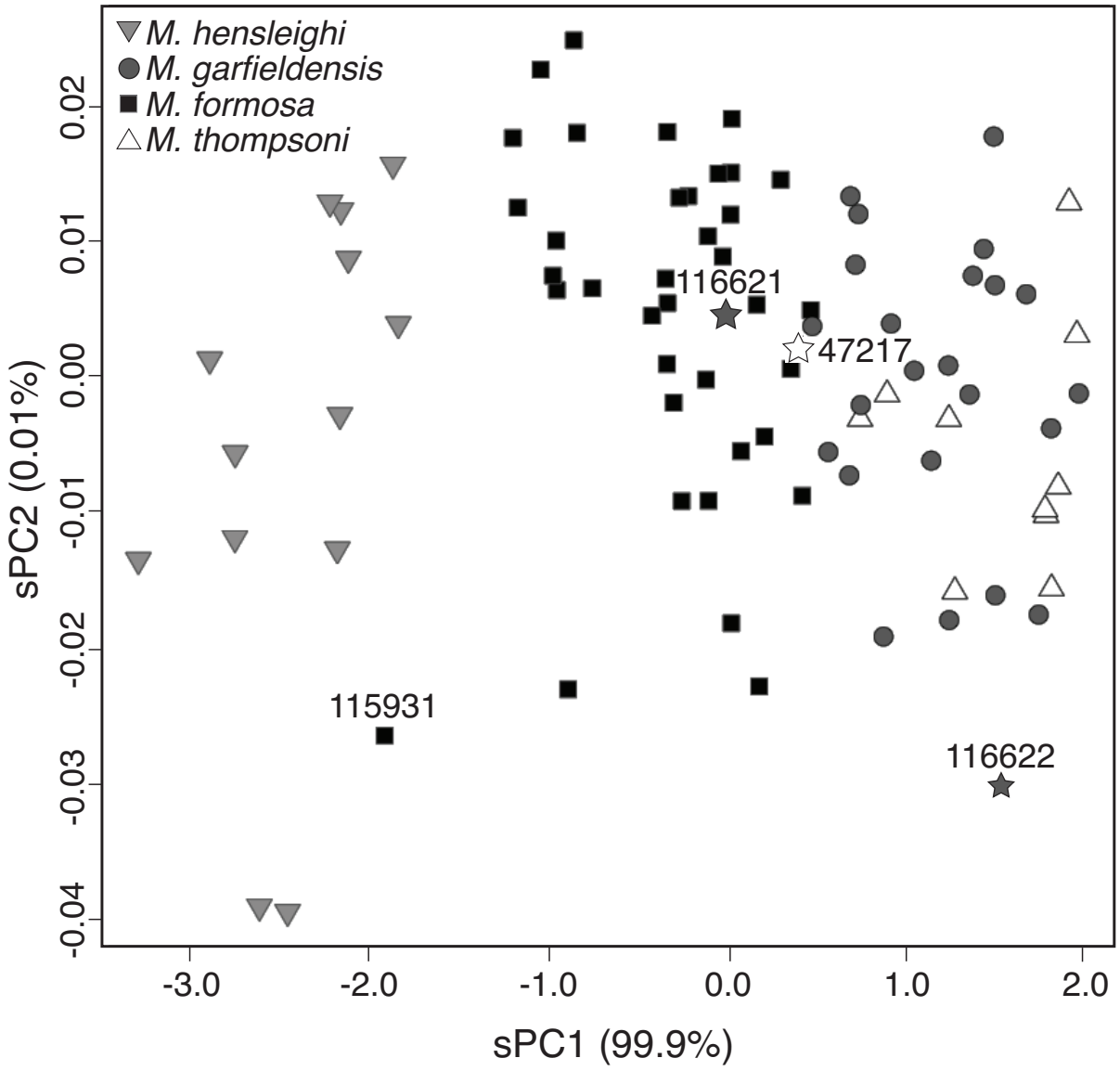

Figure 2.5 PCA of Procrustes-aligned coordinates for four species of *Mesodma*, with the addition of centroid size. Stars represent type specimens: the paratype and holotype of *M. garfieldensis* (UCMP 116621 and 116622, respectively) and the holotype of *M. thompsoni* (UCMP 47217). UCMP 115931 likely represents a misidentified specimen of *M. hensleighi* (see text).

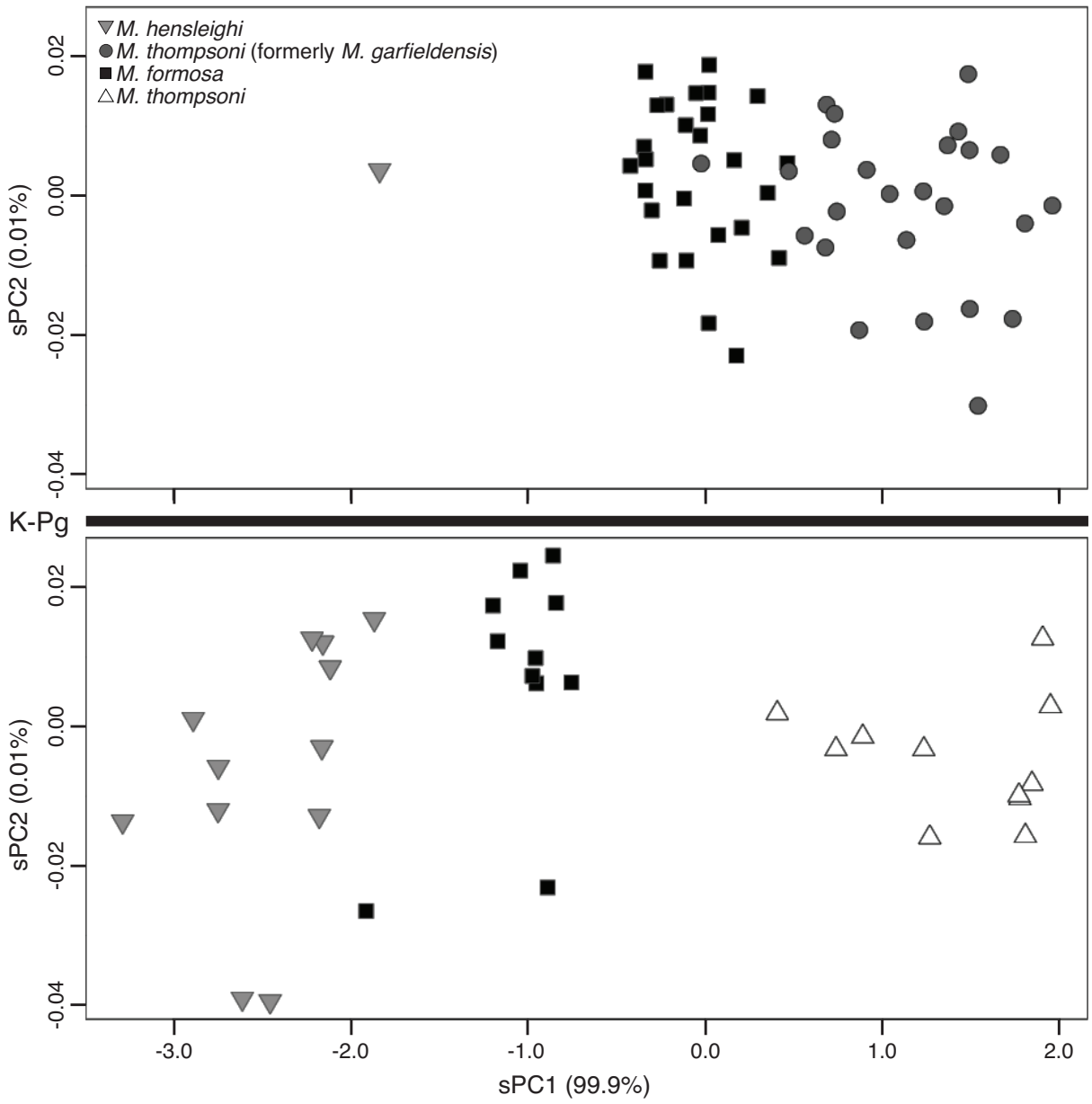

Figure 2.6 PCA morphospaces including centroid size for Lancian (bottom) and Puercan 1 (top) samples. Black line represents K-Pg boundary.

2.9 TABLES

Table 2.1 Placement of landmarks and semilandmarks on multituberculate lower p4s. Landmark configuration modified after Wilson (2013).

Type	Placement
Landmark	
1	Point of maximum curvature between buccal lobe and anterior margin of crown
2	Distalmost point of contact between crown and distal root
Semilandmark	
3–21	Partial outline of crown in buccal view; SLMs are equidistant from one another and from the points defining the beginning (LM 1) and end (LM 2) of the curve they represent.

Table 2.2 Ratios of length and height dimensions for all *Mesodma* p4s in the study. See Fig. 2A for definitions of linear measurements. OR: observed range; SD: standard deviation of the mean.

		M. hensleighi	*M. formosa*	*M. thompsoni*	*M. garfieldensis*
L1/L	$\bar{x}$=	0.46	0.46	0.43	0.43
	OR	0.40–0.48	0.40–0.50	0.39–0.48	0.32–0.48
	SD	±0.02	±0.03	±0.02	±0.03
H/L	$\bar{x}$=	0.47	0.49	0.46	0.46
	OR	0.40–0.52	0.42–0.52	0.43–0.48	0.42–0.51
	SD	±0.01	±0.02	±0.01	±0.02
	N	13	37	11	25

Table 2.3 Results of canonical variate analysis (CVA) on linear measurements and 2D geometric morphometric data.

% correct	*M. hensleighi*	*M. formosa*	*M. thompsoni*	*M. garfieldensis*	TOTAL
Linear meas.	100.0	94.6	9.1	88.0	82.6
GM: no size	38.5	73.0	0.0	52.0	52.3
GM: with size	100.0	94.6	9.1	84.0	81.4
GM: with size, *M. garfieldensis* = *M. thompsoni*	100.0	100.0	94.3	N/A	97.7
N	13	37	11	25	86

Table 2.4 Published ranges for four species of the genus *Mesodma*. All values in mm. Measurements in first three rows are combined ranges including values taken from Clemens (1964), Lillegraven (1969), Novacek and Clemens (1977), and Archibald (1982). Measurements of the sample of *M. formosa* from Clemens (1964) are not included here, because the sample likely contained specimens of *M. hensleighi*, which had not been described at the time of publication.

	M. hensleighi	*M. formosa*	*M. thompsoni*	*M. garfieldensis*
Previous studies				
L	2.66–3.05	2.85–3.95	3.50–4.57	3.66–4.61
L1	1.01–1.39	1.22–1.78	1.36–2.06	1.45–2.31
H	1.03–1.53	1.22–1.74	1.64–2.13	1.53–1.93
This study (N = 86)				
L	2.51–3.01	3.14–4.02	3.89–4.65	3.84–4.55
L1	1.04–1.42	1.36–1.92	1.51–2.11	1.63–2.13
H	1.12–1.53	1.51–1.92	1.80–2.10	1.81–2.20
N	13	37	11	25

Table 2.5 Coefficients of variation of linear measurements of *Mesodma* p4s.

Species or combination of species	N	Length	L1	Height
M. hensleighi	13	5.43	8.72	10.28
M. formosa	37	5.56	7.52	5.73
M. garfieldensis	25	4.98	7.11	5.55
M. thompsoni	11	5.56	7.63	5.93
M. thompsoni + *M. garfieldensis*	36	5.23	7.26	5.67
M. thompsoni + *M. formosa*	48	9.81	9.24	7.93
M. thompsoni + *M. garfieldensis* + *M. formosa*	73	9.76	9.11	7.93
M. garfieldensis + *M. formosa*	62	9.3	8.82	7.63
M. garfieldensis + Paleocene *M. formosa*	51	7.54	7.61	6.4

2.10 APPENDIX: p4 SPECIMENS AND LINEAR MEASUREMENTS

Table 2.10.1 Locality and linear measurement data for specimens included in this study. All specimens are lower fourth premolars (p4s) from the collections of the University of California Museum of Paleontology (UCMP). Locality and specimen numbers are UCMP numbers. Diagram of linear measurements can be found in Fig. 2.2.

Genus	species	NALMA	Spec. #	Loc. #	Formation	County	State	L	L1	H
Mesodma	*formosa*	Lancian	47025	V5620	Lance	Niobrara	WY	3.46	1.59	1.60
Mesodma	*formosa*	Lancian	47011	V5620	Lance	Niobrara	WY	3.43	1.54	1.74
Mesodma	*formosa*	Lancian	45795	V5620	Lance	Niobrara	WY	3.29	1.61	1.63
Mesodma	*formosa*	Lancian	45726	V5620	Lance	Niobrara	WY	3.57	1.71	1.60
Mesodma	*formosa*	Lancian	46407	V5620	Lance	Niobrara	WY	3.45	1.44	1.79
Mesodma	*formosa*	Lancian	45722	V5620	Lance	Niobrara	WY	3.41	1.59	1.72
Mesodma	*formosa*	Lancian	47208	V5620	Lance	Niobrara	WY	3.35	1.66	1.69
Mesodma	*formosa*	Lancian	45724	V5620	Lance	Niobrara	WY	3.38	1.62	1.71
Mesodma	*formosa*	Lancian	115931	V73087	Hell Creek	Garfield	MT	3.14	1.36	1.51
Mesodma	*formosa*	Lancian	187938	V99220	Hell Creek	Garfield	MT	3.47	1.70	1.65
Mesodma	*formosa*	Lancian	187898	V99220	Hell Creek	Garfield	MT	3.43	1.48	1.80
Mesodma	*formosa*	Puercan 1	150117	V65127	Tullock	McCone	MT	3.76	1.79	1.77
Mesodma	*formosa*	Puercan 1	150116	V65127	Tullock	McCone	MT	3.69	1.77	1.82
Mesodma	*formosa*	Puercan 1	150121	V65127	Tullock	McCone	MT	3.71	1.78	1.71
Mesodma	*formosa*	Puercan 1	150120	V65127	Tullock	McCone	MT	3.65	1.67	1.88
Mesodma	*formosa*	Puercan 1	150119	V65127	Tullock	McCone	MT	3.76	1.84	1.82
Mesodma	*formosa*	Puercan 1	150118	V65127	Tullock	McCone	MT	4.02	1.84	1.84
Mesodma	*formosa*	Puercan 1	150124	V65127	Tullock	McCone	MT	3.72	1.70	1.88
Mesodma	*formosa*	Puercan 1	150123	V65127	Tullock	McCone	MT	3.88	1.82	1.81
Mesodma	*formosa*	Puercan 1	150122	V65127	Tullock	McCone	MT	3.78	1.76	1.68
Mesodma	*formosa*	Puercan 1	150111	V71203	Tullock	McCone	MT	3.68	1.59	1.90
Mesodma	*formosa*	Puercan 1	150110	V71203	Tullock	McCone	MT	3.67	1.78	1.79

Mesodma	*formosa*	Puercan 1	150109	V71203	Tullock	McCone	MT	3.61	1.75	1.74
Mesodma	*formosa*	Puercan 1	150108	V71203	Tullock	McCone	MT	3.59	1.62	1.75
Mesodma	*formosa*	Puercan 1	150115	V71203	Tullock	McCone	MT	3.82	1.75	1.87
Mesodma	*formosa*	Puercan 1	150114	V71203	Tullock	McCone	MT	3.62	1.68	1.87
Mesodma	*formosa*	Puercan 1	150113	V71203	Tullock	McCone	MT	3.66	1.60	1.81
Mesodma	*formosa*	Puercan 1	150112	V71203	Tullock	McCone	MT	3.76	1.68	1.87
Mesodma	*formosa*	Puercan 1	150104	V72210	Tullock	Garfield	MT	3.89	1.66	1.62
Mesodma	*formosa*	Puercan 1	150103	V72210	Tullock	Garfield	MT	3.82	1.89	1.85
Mesodma	*formosa*	Puercan 1	150102	V72210	Tullock	Garfield	MT	3.84	1.72	1.81
Mesodma	*formosa*	Puercan 1	116875	V74110	Tullock	Garfield	MT	3.80	1.51	1.92
Mesodma	*formosa*	Puercan 1	150107	V74111	Tullock	Garfield	MT	3.76	1.65	1.90
Mesodma	*formosa*	Puercan 1	150106	V74111	Tullock	Garfield	MT	3.89	1.83	1.91
Mesodma	*formosa*	Puercan 1	116636	V74111	Tullock	Garfield	MT	3.96	1.92	1.88
Mesodma	*formosa*	Puercan 1	116626	V74111	Tullock	Garfield	MT	3.87	1.59	1.80
Mesodma	*formosa*	Puercan 1	187532	V96268	Tullock	Garfield	MT	3.56	1.55	1.70
Mesodma	*garfieldensis*	Puercan 1	150086	V65127	Tullock	McCone	MT	4.43	1.88	2.07
Mesodma	*garfieldensis*	Puercan 1	150085	V65127	Tullock	McCone	MT	4.41	2.07	2.10
Mesodma	*garfieldensis*	Puercan 1	150079	V65127	Tullock	McCone	MT	4.15	1.81	1.81
Mesodma	*garfieldensis*	Puercan 1	150088	V70199	Tullock	McCone	MT	4.11	1.65	1.87
Mesodma	*garfieldensis*	Puercan 1	150087	V70199	Tullock	McCone	MT	3.95	1.73	1.85
Mesodma	*garfieldensis*	Puercan 1	150092	V70201	Tullock	McCone	MT	4.27	1.95	2.08
Mesodma	*garfieldensis*	Puercan 1	150091	V70201	Tullock	McCone	MT	4.02	1.88	1.91
Mesodma	*garfieldensis*	Puercan 1	150090	V70201	Tullock	McCone	MT	4.27	1.92	2.05
Mesodma	*garfieldensis*	Puercan 1	150089	V70201	Tullock	McCone	MT	4.55	2.05	2.03
Mesodma	*garfieldensis*	Puercan 1	150097	V71203	Tullock	McCone	MT	4.16	1.90	1.97
Mesodma	*garfieldensis*	Puercan 1	150096	V71203	Tullock	McCone	MT	4.16	1.91	1.81
Mesodma	*garfieldensis*	Puercan 1	150095	V71203	Tullock	McCone	MT	4.05	1.86	1.95
Mesodma	*garfieldensis*	Puercan 1	150094	V71203	Tullock	McCone	MT	3.97	1.78	1.99
Mesodma	*garfieldensis*	Puercan 1	150093	V71203	Tullock	McCone	MT	4.54	2.13	2.02
Mesodma	*garfieldensis*	Puercan 1	150098	V71203	Tullock	McCone	MT	4.05	1.94	1.89
Mesodma	*garfieldensis*	Puercan 1	116621	V74111	Tullock	Garfield	MT	3.84	1.63	1.81
Mesodma	*garfieldensis*	Puercan 1	150099	V74111	Tullock	Garfield	MT	4.30	1.79	2.08
Mesodma	*garfieldensis*	Puercan 1	150100	V74111	Tullock	Garfield	MT	4.10	1.78	1.92

Mesodma	*garfieldensis*	Puercan 1	116635	V74111	Tullock	Garfield	MT	4.50	1.83	1.93
Mesodma	*garfieldensis*	Puercan 1	116622	V74111	Tullock	Garfield	MT	4.45	1.93	2.00
Mesodma	*garfieldensis*	Puercan 1	150101	V77087	Tullock	Garfield	MT	4.47	1.79	2.10
Mesodma	*garfieldensis*	Puercan 1	187529	V96268	Tullock	Garfield	MT	4.39	1.98	2.07
Mesodma	*garfieldensis*	Puercan 1	187512	V96268	Tullock	Garfield	MT	4.49	1.75	2.20
Mesodma	*garfieldensis*	Puercan 1	186794	V96268	Tullock	Garfield	MT	4.49	1.62	1.95
Mesodma	*garfieldensis*	Puercan 1	186796	V96268	Tullock	Garfield	MT	4.23	1.75	1.81
Mesodma	*hensleighi*	Lancian	51461	V5620	Lance	Niobrara	WY	2.76	1.21	1.20
Mesodma	*hensleighi*	Lancian	47191	V5620	Lance	Niobrara	WY	2.83	1.36	1.14
Mesodma	*hensleighi*	Lancian	51746	V5620	Lance	Niobrara	WY	2.95	1.18	1.41
Mesodma	*hensleighi*	Lancian	51856	V5620	Lance	Niobrara	WY	2.98	1.38	1.47
Mesodma	*hensleighi*	Lancian	45727	V5620	Lance	Niobrara	WY	2.99	1.42	1.47
Mesodma	*hensleighi*	Lancian	51749	V5620	Lance	Niobrara	WY	2.89	1.34	1.46
Mesodma	*hensleighi*	Lancian	47202	V5620	Lance	Niobrara	WY	2.62	1.24	1.25
Mesodma	*hensleighi*	Lancian	185868	V73087	Hell Creek	Garfield	MT	2.89	1.39	1.26
Mesodma	*hensleighi*	Lancian	115930	V73087	Hell Creek	Garfield	MT	2.70	1.27	1.29
Mesodma	*hensleighi*	Lancian	174209	V75162	Hell Creek	Garfield	MT	2.86	1.36	1.43
Mesodma	*hensleighi*	Lancian	153522	V84130	Hell Creek	Garfield	MT	3.01	1.41	1.35
Mesodma	*hensleighi*	Lancian	187723	V99230	Hell Creek	Garfield	MT	2.51	1.04	1.12
Mesodma	*hensleighi*	Puercan 1	150084	V77087	Tullock	Garfield	MT	2.97	1.42	1.53
Mesodma	*thompsoni*	Lancian	47217	V5620	Lance	Niobrara	WY	3.89	1.51	1.80
Mesodma	*thompsoni*	Lancian	108053	V72212	Hell Creek	Garfield	MT	4.53	1.89	2.13
Mesodma	*thompsoni*	Lancian	116604	V73087	Hell Creek	Garfield	MT	4.57	2.11	2.09
Mesodma	*thompsoni*	Lancian	116605	V74116	Hell Creek	Garfield	MT	4.65	1.95	2.07
Mesodma	*thompsoni*	Lancian	174275	V75178	Hell Creek	Garfield	MT	4.16	1.85	1.95
Mesodma	*thompsoni*	Lancian	187559	V75178	Hell Creek	Garfield	MT	4.51	1.97	2.19
Mesodma	*thompsoni*	Lancian	137546	V75178	Hell Creek	Garfield	MT	4.10	1.96	1.86
Mesodma	*thompsoni*	Lancian	153516	V77130	Hell Creek	Garfield	MT	4.45	1.91	2.06
Mesodma	*thompsoni*	Lancian	168712	V77130	Hell Creek	Garfield	MT	4.38	1.91	1.90
Mesodma	*thompsoni*	Lancian	168710	V77130	Hell Creek	Garfield	MT	4.58	1.96	2.08
Mesodma	*thompsoni*	Lancian	156129	V80092	Hell Creek	Garfield	MT	4.43	1.86	2.00

CHAPTER 3: MAMMALIAN RECOVERY FOLLOWING THE END-CRETACEOUS MASS EXTINCTION: A HIGH-RESOLUTION VIEW FROM MCGUIRE CREEK, MONTANA, USA

Smith, S.M., Sprain, C.J., Wilson, G.P., Clemens, W.A., Lofgren, D.L., and Renne, P., In review, Mammalian recovery following the end-Cretaceous mass extinction: A high-resolution view from McGuire Creek, Montana, USA: Geological Society of America Bulletin.

3.1 AUTHOR CONTRIBUTIONS

All authors contributed to study design**.** SMS and CJS executed analyses, wrote the main text body, and made the figures and tables, and incorporated comments and additions from all other authors**.** SMS, GPW, DLL, and WAC made taxonomic identifications of fossil specimens**.** All authors made field collections of fossil specimens, stratigraphic data, and tephras for $^{40}Ar/^{39}Ar$ geochronology.

3.2 ABSTRACT

Changes in mammalian faunal composition and structure following the Cretaceous-Paleogene mass extinction are central to understanding not only how terrestrial communities recovered from this ecological perturbation, but also the evolution of archaic groups leading to extant mammalian clades. Here, we analyzed changes in mammalian local faunas during the earliest Paleogene biotic recovery on a small spatiotemporal scale. We compiled samples of mammals from four localities in the Tullock Member of the Fort Union Formation, in McGuire Creek, McCone County, Montana, and placed these localities into a high-precision chronostratigraphic

framework using $^{40}Ar/^{39}Ar$ tephra ages and magnetostratigraphy. Within this framework, we quantitatively compared faunal composition, heterogeneity, and richness among McGuire Creek local faunas, and made broader comparisons to other earliest Paleogene faunas from throughout the Western Interior of North America. In the first ca. 320 ka of the recovery, mammalian local faunas in McGuire Creek, all of which can be placed in the Puercan 1 North American Land Mammal Age interval zone, underwent modest increases in taxonomic richness and heterogeneity, indicating the beginning of biotic recovery; however, no McGuire Creek fauna reached fully recovered levels of taxonomic richness. Further, appearance of immigrant taxa such as *Purgatorius*, which is otherwise known only from Pu3, in younger McGuire Creek faunas demonstrates important compositional changes within the Pu1 of McGuire Creek. These results highlight the difficulties with describing the nuanced mammalian recovery process using the NALMA system, and emphasize the increasing importance of high-precision dating, especially when comparing faunas across large geographic distances.

3.3 INTRODUCTION

The Cretaceous-Paleogene (K-Pg) mass extinction triggered a distinct shift in terrestrial ecosystems, from vertebrate faunas dominated by dinosaurs to those dominated by mammals. Mammalian extinction levels were as high as 75%–93% of species across the K-Pg boundary (Wilson, 2014; Longrich et al., 2016), but in the aftermath, mammals rapidly increased in their range of body sizes (Alroy, 1999; Smith et al. 2010), taxonomic richness (Lillegraven, 1972; Stucky, 1990; Alroy, 1999; Wilson, 2014), and ecological disparity (Wilson, 2013; Halliday and Goswami, 2015; DeBey and Wilson, 2015; Grossnickle and Newham, 2016). Many modern clades of mammals originated around this time as well (Archibald and Deutschman, 2001; Meredith et al., 2011; O'Leary et al., 2013; dos Reis et al., 2014). This critical episode of mammalian diversification is also intimately connected to the biotic recovery from the K-Pg mass extinction. Thus, study of this event has the potential to shed light on early mammalian evolution and, more broadly, on our understanding of the process of ecosystem rebuilding following environmental devastation of the K-Pg and potentially other extinction events.

Northeastern Montana (Garfield and McCone counties; Fig. 1) is an area particularly well suited for the study of biotic and abiotic patterns before and after the K-Pg mass extinction. Long-term paleontological and geological study of the exposures of the Hell Creek Formation and Tullock Member of the Fort Union Formation (Clemens and Hartman, 2014) have amassed abundant samples of microfossils and a high-resolution chronostratigraphy (Swisher et al., 1993; LeCain et al., 2014; Sprain et al. 2015, in review). Previous studies that have focused on post-K-Pg mammalian faunal change in this study area (Archibald, 1982; Clemens, 2002; Wilson, 2014) have examined only two intervals of the recovery, one immediately after the mass extinction

(<70 ka) and another ca. 300–600 ka later. Finer sampling of the recovery pattern has been hindered by a lack of mammal-bearing localities from intermediate strata.

In this study, we report on three new earliest Paleocene mammalian fossil assemblages from localities in the lower part of the Tullock Member in McCone County. These localities are all located within 2 km^2 of each other in the McGuire Creek area and are temporally constrained by high-precision $^{40}Ar/^{39}Ar$ ages and magnetostratigraphy to the first ca. 320 ka after the K-Pg mass extinction. The restricted spatial scope of this study minimizes the influence of spatial and environmental gradients (e.g., latitudinal temperature gradients) or biogeographic provinciality that could compromise datasets comprising localities separated by tens or hundreds of kilometers. The fine temporal scale enables us to more precisely measure the timing and rate of changes in the mammalian local faunas under study, including changes in both taxonomic richness and faunal structure. However, we also recognize that the local McGuire Creek biotic recovery was taking place in the regional context of NE Montana, and the broader context of the Western Interior of North America as a whole. We therefore make comparisons among local, regional, and continental patterns of mammalian biotic recovery in the earliest Paleocene of North America to more fully understand the significance of McGuire Creek faunal change in relation to the bigger picture of post-KPB biotic recovery. Our results add another piece of the puzzle to our growing understanding of mammalian evolution following the extinction of non-avian dinosaurs, and provide new information about the spatiotemporal variability of the process of biotic recovery within the Western Interior of North America.

Institutional abbreviations

RAM, Raymond M. Alf Museum of Paleontology; **UCMP**, University of California Museum of Paleontology; **UWBM**, University of Washington Burke Museum of Natural History and Culture.

3.4 GEOLOGIC SETTING

The McGuire Creek watershed is located within the northwestern portion of the Williston Basin and is a part of an area that has been extensively studied for changes around the K-Pg mass extinction, known as the Hell Creek region (Fig. 3.1). Outcrops in the McGuire Creek area comprise two formations: the Hell Creek Formation (mostly Cretaceous) and the Tullock Member of the Fort Union Formation (mostly Paleogene). Both formations are broadly fluvial in origin, comprising siltstones, mudstones, lignites, and sandstones, which are common deposits representative of flood plains and channels (Gill and Cobban, 1973; Cherven and Jacobs, 1985; Fastovsky, 1987). The contact between the Hell Creek and Fort Union formations is commonly defined by the first laterally persistent lignite (Brown, 1952), known as the Z coal (Collier and Knetchel, 1939), above the highest remains of unreworked *in situ* non-avian dinosaurs (Calvert, 1912; Brown, 1952; Clemens and Hartman, 2014; Moore et al., 2014; Hartman et al., 2014). The contact is generally characterized by a color change from more somber gray colors of the Hell Creek, to yellower and more variegated sediments in the Tullock Member (Archibald et al., 1982; Fastovsky and Bercovici, 2016). In the Tullock Member, variegated bedding (Fe-stained laminated siltstones), massive channel sandstones, and lignite deposits are also more common (Archibald, 1982; Fastovsky and Bercovici, 2016). All of these differences suggest a change in hydraulic flux and a rise in water table associated with the formational contact (Fastovsky, 1987;

Fastovsky and Bercovici, 2016). In the western portion of the Hell Creek region (central Garfield County), the formational contact is typically coincident or near coincident with the K-Pg boundary (KPB) (Moore et al., 2014; Sprain et al., 2015). There, within or just below the first laterally persistent lignite (~15 cm thick), the horizon associated with the Chicxulub impact, is found within a claystone marked by an anomalously high Ir-concentration, and in some places shocked quartz, and spherules (Alvarez, 1980; Bohor et al., 1984; Moore et al., 2014; Clemens and Hartman, 2014). For this reason, in that area the formational contact coal has been called the Iridium Z, or IrZ, coal (Swisher et al., 1993).

In the eastern portion of the Hell Creek region, where McGuire Creek is located, the Ir-anomaly has not been identified and it has been shown through $^{40}Ar/^{39}Ar$ dating that the Z coal most commonly ascribed to the formational contact is ca. 20 ka younger than the KPB (Sprain et al., 2015). In McGuire Creek, the formational contact as defined by Lofgren (1995) is marked by a thick basal Z coal (~1 m), dubbed the McGuire Creek Z (MCZ; Fig. 3.2) coal for its pervasive outcropping in the McGuire Creek basin. Lofgren (1995) mapped the MCZ coal over an area extending from T22N R43E Section 17 in the northwest to T21N R43E Section 11 in the southeast (~20 sq. km, Lofgren, 1995: plate 1). The color change between more somber greys to more yellow sediments occurs below the MCZ coal and is roughly coincident with a ~10 cm-thick carbonaceous shale layer. This carbonaceous shale layer is also coincident with a negative carbon isotope excursion, which Arens et al. (2014) interpreted as marking the KPB; however, neither an impact claystone nor the Nirvana bentonite (a tephra layer unique to the IrZ coal found in Garfield County; Ickert et al., 2015) is readily apparent. It is therefore possible that the carbonaceous shale layer may be roughly correlative to the IrZ coal.

The MCZ coal has been identified across the Hell Creek region due to the presence of two distinctive tephras (Lerbekmo and McGuire Creek bentonites), both of which have unique chemical and isotopic composition of phenocrysts (Ickert et al., 2015). Dating of the McGuire Creek tephra from within this coal near the Z-Line locality in Sprain et al. (2015) yielded an age of 65.998 ± 0.044/0.061 Ma (1 sigma; the slash separates analytic and systematic uncertainty), consistent with the placement of this coal above the first appearance of Paleocene pollen (Hotton, 2002). Pooling this age with other dates obtained for this tephra from across the Hell Creek region yields an inverse variance weighted mean age of 66.024 ± 0.014/0.044 Ma (compiled in Sprain et al., in review). We consider this pooled age to be the best constraint on the age of the MCZ coal, and will refer to it throughout the rest of the study.

Within the McGuire Creek area, three other coals above the MCZ are shown to be laterally persistent based on mapping conducted by one of us (DLL) in 1996. These coals are referred to by numerical designations, which roughly correspond with their elevation expressed in feet: 2330, 2380, and 2440 (Fig. 3.2).

3.5 MATERIALS AND METHODS

Mammalian fossil localities: geological descriptions

During the summers of 2014, 2015, and 2016, we revisited four vertebrate microfossil localities in the McGuire Creek area of McCone County, northeastern Montana: UCMP V84193/UWBM C2366 (Z-Line Quarry, ZLQ), UCMP V84194/UWBM C2554 (Z-Line Quarry East, ZLE),

UCMP V88036/UWBM C1700 (Luck O Hutch, LOH), and UCMP V88046/UWBM C1908 (Coke's Clemmys, CC) (Figs. 3.1 and 3.2).

The Z-Line localities (ZLQ and ZLE, henceforth, collectively referred to as ZL) are stratigraphically between the carbonaceous shale layer and the MCZ coal. The carbonaceous shale layer here is ~10 cm thick, dark grey in color, and very fissile. It grades laterally into coal and has 1–2 cm thick fine-grained siltstone that is pink in color (5 R 6/2; Munsell color) ~4 cm from the top of the layer. Another 1–2 cm-thick claystone is the lower bound to the carbonaceous shale and it is light grey to pink in color. This claystone does not have any obvious indicators of the impact layer, such as spherules. Approximately 4 m above the carbonaceous shale is the MCZ coal. There the coal is ~70 cm thick and contains both the Lerbekmo and McGuire Creek bentonites. Between the carbonaceous shale and the MCZ coal is the Z-Line channel deposit, containing both ZLQ and ZLE, which are ~12 m laterally apart from each other. Both fossil localities occur near the base of the channel deposit, ~3 m below the MCZ coal. The fossil-bearing horizon at ZLE is a ~12 cm-thick, poorly sorted, brown to tan fine grained sandstone that includes carbonaceous plant hash as well as vertebrate fossils. The fossil-bearing horizon at ZLQ is similar to that at ZLE, in that fossils occur at the base of the sandstone, directly above the carbonaceous shale (Fig. 3.2). Lateral to the Z-Line channel deposit, a series of light-grey to buff mudstones, siltstones, and fine sandstones crop out between the carbonaceous shale layer and the MCZ.

The Luck O Hutch locality (LOH) occurs ~2.3 m above the MCZ coal at the base of a ~9 m-thick channel deposit called Jack's Channel, which comprises a medium-fine grained sandstone

that is grey in color (Fig. 3.2). Large indurated blocks within the channel show bedding planes that are both horizontal and cross bedded. The base of the channel deposit is erosive and locally occurs between 2.0 and 2.7 m above the MCZ. An indurated Fe-stained layer that is laterally variable in thickness occurs at the base of the channel deposit. Vertebrate fossils occur in laterally discontinuous lenses within that layer, although the fossils are not numerous. These lenses include numerous Fe concretions, carbonaceous plant material, and small pieces of coal. Between the MCZ and the base of Jack's Channel is ~2–3 m of a variegated muddy siltstone. Approximately 14.5 m above the top of Jack's Channel, the 2380 coal is exposed. That coal here is ~0.5 m thick and it contains a thin tephra layer (~2 mm) about 1 cm below the top of the coal. Another coal layer crops out ~2 m below the 2380. Based on mapping and elevation, we do not believe this coal to be the 2330 coal and instead believe that Jack's Channel cut out the 2330 coal. Paleomagnetic samples were collected around the 2380 coal at this location and results presented in Sprain et al. (in review) show that the C29r/C29n reversal, dated at 65.726 ± 0.013/0.044 Ma, occurs right around the 2380 coal and significantly above the fossil locality.

The Coke's Clemmys fossil locality (CC) is located ~10.3 m above the top of the MCZ and lies directly on top of the 2330 coal (Fig. 3.2). Between the MCZ and the 2330 coal at this locality is ~10 m of alternating siltstone and mudstone layers with a 1.4 m-thick sandstone layer exposed ~1.5 m above the MCZ. The Coke's Clemmys fossil locality is within a ~6.5 m thick channel deposit which comprises mostly siltstone. The fossil-bearing horizon falls within a cross-bedded sandstone at the base of the channel deposit. The channel locally cuts down into the 2330 coal. The 2330 coal here is ~0.5 m thick and contains one tephra layer that was collected for $^{40}Ar/^{39}Ar$ analysis (sample name CC15-2; Fig. 3.3). The tephra layer occurs ~5 cm below the top of the

coal, and is 2 cm thick. The layer is red/brown (10 R 3/4) in color and is largely unconsolidated. Euhedral grains of feldspar are identifiable. The tephra is laterally discontinuous and is locally cut out by the Coke's Clemmys channel. Around 1 kg of tephra was collected for analysis. About 0.5 m above the top of the Coke's Clemmys channel is a larger channel deposit, ~14 m thick, that consists of fine-medium grained sandstone (litharenite). This larger channel has an erosive base, apparent cross bedding, and large indurated blocks. Eleven meters above the top of the large channel deposit, the 2440 coal crops out, ~32 m stratigraphically above the Coke's Clemmys fossil locality. Although the 2380 coal is not exposed here, mapping shows that it is cut out by the large channel fill above Coke's Clemmys, whose base is ~10 m above the 2330 coal in the NE 1/4, SW 1/4 section 3, T21n, R43e. This large channel fill can be observed to contact the 2380 coal and is overlain by strata that are capped by the 2440 coal. Thus, there is little doubt that the Coke's Clemmys channel was once capped by the 2380 coal.

In sum, all four localities studied here are in sandstone channel fill deposits of the basal Tullock Member. ZLQ and ZLE are the lowest stratigraphically and occur at approximately the same level; LOH and CC are stratigraphically higher than both ZLQ and ZLE, but their relative stratigraphic order remains unresolved.

Mammalian fossil collection

The mammalian fossil collection compiled for this study consists of specimens of isolated teeth and fragmentary jaws. Specimens were recovered from the four vertebrate microfossil localities described above (ZLQ, ZLE, LOH, and CC) via surface collection and underwater screenwashing of fossiliferous sediment over the course of several field seasons; first in the

1980s and early 1990s by UCMP and RAM crews, led by DLL, and later in the 2010s by UWBM field crews, led by GPW and SMS. Only specimens that are identifiable to the genus level or lower were included in our data set, with a few exceptions: four specimens referred to Metatheria, indeterminate; two specimens referred to the metatherian family Alphadontidae, and one specimen referred to the eutherian Periptychidae (a family of archaic ungulates). Although these specimens are not complete enough to identify to the genus level, we included them in our data set because they represent taxa that are unique in the sample (see 3.13 Appendix: Systematic Paleontology). The excluded specimens include small fragments of multituberculate teeth, single cusps of therian teeth, or specimens otherwise too worn to preserve genus-level diagnostic features.

Terminology

***Fauna* vs. *local fauna*.** We use the term "local fauna" *sensu* Woodburne, 2004 (p. xiii, after Tedford, 1970), as a group of fossil species that "have a limited distribution in time from a number of closely grouped localities in a limited geographic area." For example, we use "Z-Line local fauna" in reference to the mammalian species present at Z-Line Quarry and Z-Line East. We also use the term "fauna" *sensu* Woodburne, 2004 (p. xii; after Tedford, 1970): ". . . vertebrate fossils of similar taxonomic composition obtained from a small number of sites considered to have a limited temporal range . . . commonly composed of a number of local faunas." As used here, "fauna" has a greater spatiotemporal scope than "local fauna." For example, we use "Ferris Formation Pu1 fauna" to refer to the sample including all local faunas of Pu1 age in the Ferris Formation.

***Assemblage, sample* vs. *local fauna*.** We use the terms "assemblage" and "sample" interchangeably, to refer to the collection of fossil specimens recovered from a particular locality; whereas "local fauna" refers to the biological entities represented by those specimens (e.g., species).

Taxonomic diversity metrics, similarity, SQS, and rarefaction

All quantitative analyses were conducted in R version 3.3.2 (R Core Team, 2016; www.r-project.org).

***Relative abundances and taxonomic richness*.** We calculated relative abundance of individuals within mammalian taxa as the number of identifiable specimens for a taxon divided by the total number of specimens of all taxa in the sample (NISP); this is the most appropriate counting method for fluvially transported assemblages, such as those described here (Badgley, 1986). We assessed taxonomic richness in each mammalian local fauna via three metrics: raw richness, subsampled rarefied richness, and subsampled richness using shareholder quorum subsampling (SQS; Alroy, 2010). For each metric, we calculated taxonomic richness at the genus level as well as the species level. The genus-level calculation was used to account for the difficulties in assigning isolated teeth of *Mesodma* and *Mimatuta* to species (Novacek and Clemens, 1977; Van Valen, 1978; Lofgren, 1995; Smith and Wilson, 2017). See 3.13: Appendix for further information concerning these genera.

Two specimens in our samples (RAM 4045, Periptychidae indet., Fig. 3.13.15; RAM 4058, ?*Baioconodon* sp., Fig. 3.13.12) could not be confidently assigned to genus or species, but

because each represents a taxon distinct from all others in the sample, we included them in the genus- and species-level analyses. Six of the 17 metatherian specimens in the Z-Line assemblage could only be assigned to Metatheria indet. (four specimens) and Alphadontidae indet. (two specimens). Because it is unclear how many genera and species these specimens represent, we provisionally treated them as a single taxon ("Metatheria indet.") and represented them by a single specimen in our analyses. To include more than one specimen as "Metatheria indet." in the analyses would be to make the assumption that everything in that category belonged to a single taxon (genus or species); we do not have sufficient evidence to make such an assumption. Although it might artificially inflate the relative abundance of other taxa in the assemblage, this choice requires the fewest additional assumptions regarding taxonomic identity (i.e., there is no need to determine if what we count as one genus in our genus-level analyses includes more than one species), and still allows the taxon some representation in our analyses. We chose this approach as an intermediate between excluding all specimens of "Metatheria indet." and including all of them as distinct genera and species. This decision could artificially depress taxonomic richness in the ZL assemblage, but accurately reflects our understanding that there is at least one additional metatherian taxon present in the sample.

We conducted SQS at the genus and species level using the R script from John Alroy's website (SQS version 3.3; http://bio.mq.edu.au/~jalroy/SQS-3-3.R; Alroy, 2010). We ran 2,000 trials, both with and without correction for evenness (achieved by excluding the most common taxon; Alroy, 2010), and chose our quorum level (q) to accommodate the assemblage with the lowest value for Good's u (coverage; Good, 1953), which was LOH in every case. We also calculated rarefied richness using the function rarefy() from package vegan (version 2.4-2; Oksanen et al.,

2017), which follows the subsampling methodology of Hurlbert (1971). We estimated 95% confidence intervals for the rarefied richness values, using the formula 95% CI = mean value +/– 1.96*standard error. We ran rarefaction with sampling level N = (sample size of assemblage with the smallest sample) – 1. Additionally, we compared the ZL richness values to values for the similarly aged Worm Coulee 1 assemblage (WC1, UCMP V74111, UWBM C1369) from nearby Garfield County (data from Wilson, 2014). For those comparisons, the quorum level (q) was based on the coverage (u) at ZL, which was consistently lower than that of WC1.

Taxonomic diversity indices. We also calculated three other taxonomic diversity indices that incorporate richness and relative abundance data in various ways: Berger-Parker dominance index (1–*d*), Simpson's index (1–*D*), and Pielou's evenness (*J'*). These indices are relatively easy to interpret, are biologically meaningful, and emphasize different aspects of abundance structure (e.g., Berger-Parker index emphasizes the most common taxon, whereas Pielou's evenness places more emphasis on rarer taxa). Pielou's evenness (*J'*) is subject to many of the same biases as Shannon's *H'* (Magurran, 2004), but includes a correction for the number of species present in the assemblage: $J' = H'/H_{max} = H'/\ln S$, where *S* is raw taxonomic richness (Hammer and Harper, 2006). The Berger-Parker index was calculated as 1 – (proportion of the assemblage attributed to the most common genus or species). Simpson's 1–*D* was calculated with the function diversity() from the package vegan (index = "simpson"). *J'* was also calculated using diversity(), by first calculating *H'* (index = "shannon") and then dividing by ln *S*. The 95% confidence intervals were generated for each index using a custom bootstrapping function (1,000 replicates).

Faunal similarity analysis. We assessed similarity in faunal composition among McGuire Creek localities using two distance metrics that incorporate relative abundance data: the Bray-Curtis similarity metric (B-C; Bray and Curtis, 1957) and the Canberra distance metric (CM; Lance and Williams, 1967). These two distance metrics perform well at small sample sizes with low species richness (Krebs, 1989). Whereas B-C is strongly affected by abundant taxa, CM places greater emphasis on rare taxa (Krebs, 1989); thus, including both helps to balance our interpretations. To further balance the influence of common and rare taxa in these analyses, we i) square-root transformed our raw abundance data, and ii) standardized values for each species to equal maximum abundance (Faith et al., 1987; Krebs, 1989). Standardization was performed using the vegan function decostand(method = "max"). We calculated B-C and CM at both the genus and species level on the dataset (see data set in *Taxonomic richness*), using the vegan function vegdist(method = "bray" or "canberra").

To broaden our comparative context, we also conducted similarity analyses of earliest Paleocene (Puercan) mammalian faunas across the Western Interior of North America. We compiled genus-level presence-absence data for 16 faunas from Saskatchewan to New Mexico (Table 3.6). When a taxonomic occurrence listing was modified with "cf.", "?", or present only as a range-through occurrence, we alternately considered that taxon as absent (0) in one permutation of the data set and present (1) in a second permutation of the data set. We then performed similarity analyses on both permutations of the data set. We used the Sørensen-Dice index (S-D; Dice, 1945; Sørensen, 1948) as our measure of similarity. Because S-D normalizes to the average number of taxa, rather than the total number of taxa, in the two samples being compared, it has the advantage of being less sensitive to differences in sample size compared to the Jaccard index (Hammer and

Harper, 2006). We calculated S-D using vegdist(method = "bray", binary = T). Our dendrogram was constructed using the resulting distance matrix and the function hlclust(method = "average") (=UPGMA) from package ade4 (Dray and Dufour, 2007). We also conducted correspondence analysis (CA, which groups taxa [R-mode] and samples [Q-mode] via chi-square distance) using the function ca() from package ca (Nenadic and Greenacre, 2007). We included CA in addition to cluster analysis to visualize the association of both local faunas and the related taxa on the same plot, as well as to detect trends through the Puercan NALMA in faunal and taxonomic groupings.

$^{40}Ar/^{39}Ar$ Geochronology

Sample Prep. Feldspars for $^{40}Ar/^{39}Ar$ analysis were separated from a ~1 kg sample of the CC15-2 tephra, which is within the 2330 coal directly below the Coke's Clemmys locality. First the sample was disaggregated using water suspension, and was subsequently washed and sieved. To further concentrate feldspar, the sample underwent magnetic and density separations in addition to ultrasonic cleaning in 7% hydrofluoric acid. Because some of the feldspars showed evidence of alteration, the sample underwent further treatment with HF in order to remove the altered material. This sample also required a treatment of hydrogen peroxide to remove excess coal. Clear euhedral grains were picked preferentially.

Analysis. Analyses were performed at the Berkeley Geochronology Center (BGC; California). The sample was irradiated in a 50-hour irradiation in the Cadmium-Lined In-Core Irradiation Tube (CLICIT) facility of the Oregon State University Triga reactor. The sample was loaded into an Al disk figured in Renne et al. (2015, fig. S2) for irradiation. The fast neutron fluence,

monitored by the J parameter, was calculated by analyzing crystals of the standard Fish Canyon sanidine (FCs-EK; Morgan et al., 2014) by single crystal total fusion for each of the six positions that spanned the disk. The J value for all unknowns was determined by interpolation within a planar fit to J values determined from the FCs. The precision on J was better than 0.04%.

Methods for mass spectrometry and the facilities used are described in Renne et al. (2013). In summary, single sanidine crytsals were analyzed by total fusion with a CO_2 laser on an extraction line connected to a MAP 215-50 mass spectrometer with a Nier type ion source and analog electron multiplier detector. Argon isotopes (^{40}Ar, ^{39}Ar, ^{38}Ar, ^{37}Ar, and ^{36}Ar) were measured by peak-hopping, which was accomplished by magnetic field switching on a single detector. Each isotope was measured in 15 cycles. Blanks were determined every three unknowns and air pipets were measured throughout the run to properly determine mass discrimination.

The final age was determined from blank-, discrimination-, and decay-corrected Ar isotope data. Corrections for reactor interferences were determined from Fe-doped $KAlSiO_4$ glass (Renne et al., 2013) and from fluorite (Renne et al., 2015) for K and Ca, respectively. Age uncertainty is reported at 1 sigma and is stated as X/Y where X = analytical uncertainty and Y = systematic uncertainties arising from calibration (Fig. 3.3). Calibration from Renne et al. (2011) was used.

3.6 RESULTS

Mammalian relative abundances

In each assemblage, the most abundant genus is the multituberculate *Mesodma*, with *Mesodma thompsoni* being the most common species (Table 3.1). The only other multituberculate genus in our sample is *Cimexomys*, which was not recovered from either locality in the Z-Line assemblage (ZL). Two species of *Cimexomys* are present in both the Luck O Hutch (LOH) and Coke's Clemmys (CC) assemblages. Metatherians are relatively abundant in ZL, at 23% of specimens, but are absent from LOH and CC. Of the metatherians present in ZL, the majority are *Thylacodon montanensis*, but also present are specimens referable to ?*Leptalestes cooki* and Alphadontidae, as well as some metatherian dental fragments which are unique enough to be distinguished from the other three metatherian taxa, but not complete enough to be identified to family or genus level (see 3.13: Appendix). The ZL eutherian sample, which makes up 12% of specimens at ZL, is dominated by *Procerberus formicarum* and the periptychid archaic ungulate *Mimatuta*. Eutherians are more abundant in LOH (27%) and CC (24%), with archaic ungulates being the most common eutherians both in number of species and number of specimens represented. Both assemblages include 2–7% of each of the archaic ungulates *Oxyprimus erikseni, Protungulatum donnae*, and *Mimatuta* sp. LOH also includes one specimen each of two other archaic ungulate taxa: *Baioconodon* sp., and a large, fragmented upper molar of an unidentified periptychid. LOH includes one specimen of the leptictid *Prodiacodon crustulum*, and two specimens of *Procerberus* cf. *P. grandis,* a slightly larger congener of *P. formicarum*. CC is the only assemblage that includes purgatoriids, with three specimens (5%) of *Purgatorius* cf. *P. coracis.*

Raw and subsampled taxonomic richness

Overall, irrespective of the subsampling method used (rarefaction or SQS), LOH and CC have richness values closer to one another than either is to the richness value of ZL (Fig. 3.4; Tables 3.2–3.3); the similarity between richness in LOH and CC, and their separation from ZL, appears more distinct when richness is assessed at the species level (Fig. 3.4B). In all four richness measures, ZL has the lowest value for both generic and species richness. Raw generic richness values are similar across all three assemblages, but raw species richness in LOH is nearly twice that of ZL (12 species versus 7); CC is not far behind LOH, with 10 species. Genus-level rarefied richness is significantly different among all localities; species-level rarefied richness is significantly different between LOH and ZL, and CC and ZL, but not between LOH and CC (95% CIs, Fig. 3.4). Rarefaction curves with 95% confidence intervals for all McGuire Creek assemblages (Fig. 3.5) show that sampling of the local faunas is incomplete (not horizontal); although the ZL curve is nearly level, the LOH and CC curves are still strongly inclined. Thus, greater sampling of LOH and CC would likely increase the difference in taxonomic richness between ZL and the two younger localities.

Both rarefaction (Table 3.4; Fig. 3.6) and SQS (Table 3.4) indicate a slightly higher level of richness in WC1 than ZL, but the richness estimates for corrected SQS at the genus level are nearly identical (Table 3.4). Unlike in McGuire Creek comparisons, where corrected SQS gave consistently higher richness estimates than uncorrected SQS (Tables 3.2–3.3; Fig. 3.4), this set of analyses yielded a lower estimate from corrected SQS (with the exception of ZL at genus level; Table 3.4).

Taxonomic diversity indices

The differences in the taxonomic diversity indices across the three assemblages are not statistically significant (Fig. 3.7). However, LOH and CC consistently have slightly higher values than ZL for every index, with LOH having the highest values (corresponding to lower dominance and higher evenness) in genus-level analyses (Fig. 3.7A), and CC having the highest values in species-level analyses (Fig. 3.7B). It is important to note that the sample size at ZL is approximately twice that of both LOH and CC, and despite the selection of indices designed to minimize differences in sample size (Magurran 2004), such a large discrepancy in sample size is likely still affecting our results. To investigate this possibility, we conducted a second set of bootstrap analyses for all three indices at both genus and species level, in which we subsampled each locality to 55 specimens for the genus-level analyses and 40 specimens for the species-level analyses; these values corresponds to lowest sample size in each case. The dotted vertical lines in Figure 3.7 represent the 95% confidence intervals for this second set of bootstrap analyses. This second set of bootstrap CIs are lower than measured values of both Simpson's 1–*D* and Berger - Parker index at ZL, indicating that the large sample size at ZL may be artificially inflating its evenness relative to LOH and CC (Fig. 3.7).

Faunal similarity, cluster analysis, and correspondence analysis

LOH and CC are more similar to each other in taxonomic composition and relative abundance structure than either is to ZL, at both the genus and species level and regardless of distance metric used (BC, CM; Table 3.5). In all four configurations, CC is slightly more similar to ZL than LOH is to ZL.

The most basal split in our UPGMA dendrogram of North American faunas and local faunas (Fig. 3.8) is between Pu1 faunas and Pu2+Pu3 faunas. Within the cluster of Pu1 faunas, LOH and CC are most similar to one another, and together are most similar to the Worm Coulee 1 local fauna (wc1MT) from Garfield County, Montana (which has been estimated to occur between 66.049 ± 0.008/0.043 Ma and 66.032 ± 0.007/0.036 Ma; Sprain et al. in review). This cluster of three is sister to a cluster including Pu1 faunas from Colorado and Wyoming (dahlCO, fpu1WY). ZL falls at the base of the cluster including all other Pu1 faunas. On the other side of the primary split in the dendrogram, several southern faunas cluster together (alCO, pu2WY, fpu3WY, pu2NM and pu3NM). The other Colorado fauna (coblCO, Corral Bluffs; Pu2/Pu3) is most similar to the Utah Wagonroad local fauna (wagUT; Pu3). The Pu3 Garbani Channel local fauna (garMT) from northeastern Montana is most similar to the Saskatchewan Rav W-1 local fauna (ravSK); these form a "northern" cluster with the Pu2 Hiatt local fauna from southeastern Montana (seMT). In the cluster analysis of the dataset that treats questionable occurrences ("cf.", "?", and range-through) as absences instead of presences, the only difference in the resulting dendrogram topology is the placement of the Alexander Locality local fauna. Instead of grouping with the cluster that includes Wyoming and New Mexico Pu2 and Pu3 faunas, alCO falls at the base of the Pu1 cluster on the other side of the dendrogram.

The results of the correspondence analysis (CA, Fig. 3.9) mirror those from the cluster analyses. Pu1 faunas cluster in the upper-left quadrant; Pu2 and Pu3 faunas from New Mexico, Wyoming, Colorado, and Utah cluster in the upper-right quadrant; and Pu2 and Pu3 faunas from Montana and Saskatchewan in the lower-right quadrant. The Pu1 group is united by the presence of several common Pu1 taxa, including *Oxyprimus*, *Mimatuta*, *Mesodma*, and *Cimexomys*.

Periptychus and other archaic ungulates, such as *Conacodon*, unify the southern/central grouping of Pu2 and Pu3 faunas (upper-right quadrant), whereas the northern grouping of Pu2 and Pu3 faunas (lower-right quadrant) is united by *Carcinodon* and *Stygimys*. *Purgatorius*, which is present in the two northernmost Pu3 local faunas (garMT and ravSK), is also present in the Pu1 ccMT local fauna, but does not cause these three to group near one another in the CA. Taxa such as *Taeniolabis* and *Loxolophus* are shared across many local faunas on both the upper- and lower-right side of the plot (Pu2 and Pu3 faunas). The location of faunas relative to one another is largely unchanged when uncertain occurrences are treated as absences; the three main groupings mentioned above remain intact.

Geochronology of the 2330 coal

From sample CC15-2 of the 2330 coal from Coke's Clemmys, 72 grains were analyzed. A majority of the grains analyzed were xenocrysts (reworked grains with distinctly older ages), quartz, and plagioclase. Although many of the feldspars analyzed were xenocrystic, a clear younger mode exists around 65.8 Ma composed of seven single crystal analyses. Of these seven grains, all proved to be K-feldspar based on measured K/Ca ratios. From this population, a weighted mean age of 65.802 ± 0.116/0.125 Ma with an MSWD of 0.99 was determined (Fig. 3.3).

3.7 DISCUSSION

The main goal of this study is to examine post-KPg mammalian biotic recovery at high temporal resolution. Critical to this examination is a high-precision local chronological framework. In the following discussion, we establish what our geochronological results mean for this framework,

and what the results of our faunal dynamic analyses mean for the local pattern of mammalian biotic recovery.

Temporal framework of McGuire Creek localities

Both the Z-Line Quarry and Z-Line Quarry East localities (ZL local fauna) occur below the MCZ and above the carbonaceous shale that contains a negative carbon isotope excursion interpreted to mark the KPB (Fig. 3.2; Arens et al., 2014); the age of the KPB is based on the Nirvana bentonite in the IrZ coal found in Garfield County. Accordingly, the age of the ZL local fauna is bracketed between 66.049 ± 0.008/0.043 Ma (pooled IrZ age from Sprain et al., in review) and 66.024 ± 0.014/0.044 Ma (pooled Z coal age from Sprain et al., in review), at most 25 ± 16 ka after the KPB. Both the Luck O Hutch (LOH) and Coke's Clemmys (CC) localities occur stratigraphically above the MCZ, so they must be younger than 66.024 ± 0.014/0.044 Ma (Fig. 3.2). At Coke's Clemmys we have an additional constraint for the maximum age of the local fauna from our new date for the 2330 coal, which is 65.802 ± 0.116/0.125 Ma. Mapping of the 2330 coal by one of us (DLL) indicates that Jack's Channel, which contains the Luck O Hutch locality, cuts out the 2330 coal; accordingly, the channel incision is likewise younger than 65.802 ± 0.116/0.125 Ma. However, according to hypotheses that explain the accumulation of vertebrate microfossils by Rogers and Brady (2010) and Rogers et al. (2017), the Luck O Hutch fossils could have been liberated from any of the older strata cut by Jack's Channel; thus, the age of the MCZ, not the age of the 2330 coal, should be used as a maximum age of the LOH. Near the Luck O Hutch locality, Sprain et al. (in review) collected samples for paleomagnetic analysis from just below the 2380 coal to the 2440 coal. They found that the C29r/C29n reversal occurs ~20 cm above the 2380 coal, and ~5.5 m below the 2440 coal. At Luck O Hutch, the 2380 coal

crops out ~10 m above Jack's Channel, and at Coke's Clemmys the 2440 coal crops out ~20 m above the top of Coke's Clemmys channel (Fig. 3.2). Accordingly, we infer that both local faunas occur within the Paleogene portion of C29r, and are at best older than the C29r/C29n reversal which Sprain et al. (in review) calculated to be 65.726 ± 0.013/0.044 Ma. Therefore, the Coke's Clemmys local fauna is constrained to between 323 ± 15 ka and 247 ± 116 ka after the KPB; the Luck O Hutch local fauna is constrained to between 323 ± 15 ka and 25 ± 16 ka after the KPB. We are unable to further constrain relative age of LOH and CC; however, both are distinctly younger than ZL.

Biotic recovery

Because biotic recovery is a multi-faceted biological phenomenon, it is critical to discuss what we mean by "recovery" and "recovered" in the context of this study. One commonly agreed-upon aspect of the biotic recovery process is an increase in taxonomic richness after peak extinction, followed by stabilization of richness once the taxonomic group or ecosystem has "fully recovered"; alternatively, a "fully recovered" community or fauna may be defined as one that has returned to pre-extinction taxonomic richness (Erwin, 1998). The pattern of structural change during biotic recovery has been described as having three broad phases: the immediate post-extinction "disaster" or "survival" phase, when local faunas have highly uneven relative abundance structure and consist mostly of ecological generalists (eurytopic taxa), opportunists, and species from refugia (immigrants); a "recovery" phase, which coincides with increasing taxonomic richness, and often includes the appearance of more ecological specialists and a decrease in the relative abundance of generalists and opportunists; and the "fully recovered"

phase, when pre-extinction levels of evenness have been reached (Kauffman and Harries, 1996; Erwin, 1998).

Although empirical evidence shows that specific pattern and rate of biotic recovery depend on taxonomic group, ecology, environment, and extinction severity (e.g., Jablonski, 1998; Chen and Benton, 2012; Zhuravlev, 1996; Donovan et al., 2016; Sepúlveda et al., 2009), and the process is likely complicated by trophic interactions among recovering groups (Solé et al., 2010), investigations of taxonomic composition, richness and heterogeneity have been used by paleobiologists and neontologists alike to track recovery in a variety of taxonomic groups throughout evolutionary history (e.g., McMahon et al., 1989; Del Moral, 1998; Sepkoski, 1998; Sahney and Benton, 2008; Payne et al., 2011; Hull, 2015). In the following sections, we integrate our high-precision chronostratigraphic framework and faunal analyses to synthesize what we know about the post-K-Pg mammalian faunal recovery at local, regional, and continental scales.

Local and regional signals: McGuire Creek faunal change and recovery in the context of NE MT

McGuire Creek local faunas show a modest degree of recovery within the first ca. 320 ka of the Paleogene. Our results indicate two different types of local faunas: an older type (ZL) and a younger type (LOH and CC). The similarities among all three local faunas unite them as belonging to the Pu1 NALMA interval zone (Fig. 3.8–3.9); the abundance of such characteristic Pu1 taxa as *Mesodma*, *Mimatuta*, *Oxyprimus*, *Procerberus*, and *Protungulatum* ally them with other Pu1 faunas from around North America (Lofgren et al., 2004 and below, Continential Signal: North American mammals in the earliest Paleogene). Yet relative abundances of

particular taxa, as well as several unique taxonomic occurrences, also distinguish these three faunas from one another; this new sub-interval zone resolution informs our understanding of how faunal change was occurring within the first ca. 320 ka of the Paleogene.

The ZL assemblage, which is the oldest McGuire Creek local fauna (within about the first 25 ka of the Paleocene, Fig. 3.2), can be characterized as a disaster fauna, largely consistent with previously reported disaster assemblages from the study area in relative abundance structure and taxonomic composition (e.g., Worm Coulee 1 local fauna [WC1]; Archibald, 1982; Clemens, 2002; Wilson, 2014). ZL is taxonomically depauperate; highly uneven, with 74% of mammalian specimens representing a single genus (*Mesodma*, Table 3.1); and has high relative abundance of the bloom taxa *Thylacodon montanensis*, *Procerberus formicarum*, and *Mesodma thompsoni* (Wilson, 2014). It is interesting to note that all three of these bloom taxa were likely carnivorous to omnivorous (Wilson, 2013) and have been considered local survivors (Wilson, 2014). Eurytopic taxa are often cited as the most common post-extinction bloom taxa (Kauffmann and Harries, 1996; Erwin, 1998); whereas this pattern might hold with invertebrate assemblages (e.g., Peryt and Lamolda, 1996; Erwin, 1998 and references therein), it appears that in the earliest post-K-Pg mammalian faunas, some degree of dietary specialization remains, at least in the most common species. It may be that invertebrate and vertebrate bloom taxa resulted from different extinction selectivity regimes, or followed different patterns of ecological expansion following mass extinctions; indeed, the most notable disaster taxon from the end-Permian mass extinction, the dicynodont *Lystrosaurus*, with a relative abundance upwards of 90% (Benton, 1983; Chen and Benton, 2012), was adapted for high-fiber herbivory (King et al., 1989; Jasinoski et al., 2009). Because of the variation in recovery patterns resulting from variation in extinction

intensity, geographic region, and taxonomic group under study (Jablonski, 1998; Solé et al., 2010), it is unsurprising that there is also substantial variation in the ecological characteristics of bloom taxa. Nonetheless, the overall composition of the ZL local fauna (low taxonomic richness, high abundance of opportunistic taxa, uneven relative abundances of taxa; Table 3.1, Fig. 3.4–3.7) is similar to what has been documented in other disaster faunas (e.g., Payne et al., 2011; Chen and Benton, 2012; Ruta et al., 2013; Wilson, 2014).

A further relevant characteristic of the ZL local disaster fauna is the presence of two taxa that may represent "Dead Clades Walking" (DCW; Jablonski, 2002): two Lancian-aspect metatherians, *Leptalestes* and another species only referable to Alphadontidae. *Leptalestes* is represented by a single specimen, and the unidentified alphadontid by two specimens. The presence of these taxa in the assemblage may indicate i) a low level of local survival of these typically Lancian taxa into the Puercan, as is seen in palynological assemblages of the earliest Puercan (Bercovici et al., 2009); or ii) post-depositional reworking of latest Cretaceous fossils resulting from the Z-Line channel cutting into lower strata. If (ii) were correct, we might expect to find non-avian dinosaur fossils intermingled with Puercan taxa. At present, no such dinosaur fossils have been recovered from Z-Line, which distinguishes it from the mixed assemblages of Bug Creek Anthills and other mixed localities near McGuire Creek (Archibald and Lofgren, 1990; Lofgren, 1995). With these data, in conjunction with Arens et al.'s (2014) evidence for the KPB carbon isotope excursion stratigraphically below the Z-Line channel, we interpret the presence of these mammals as the first evidence of limited range extension of Lancian-aspect metatherian taxa into the earliest Puercan. Although two of the taxa identified here as bloom taxa (*Procerberus* and *Thylacodon*) have also previously been termed DCW due to their local decline

throughout the Puercan (Wilson, 2014), our two metatherian taxa (*Leptalestes*, Alphadontidae) are DCW on a more compressed time frame.

Other broadly contemporaneous local faunas in the Hell Creek region are similar to ZL in taxonomic composition, but with some key differences that should be considered when interpreting variability of local and regional recovery patterns. The Worm Coulee 1 local fauna (WC1; UCMP V74111/UWBM C1369) is less than 3 m above the IrZ (our proxy for the KPB, Fig. 3.2; 66.049 ± 0.008/0.043 Ma, Sprain et al., in review) in the Hell Hollow Channel sandstone, which is capped by the HFZ 11.9 m above the top of the channel (65.973 ± 0.020/0.047 Ma, Sprain et al., 2015). On the basis of a sedimentation accumulation rate, the upper bound of the Hell Hollow channel was estimated to be ca. 17 ka after the KPB in Sprain et al. (in review; an age of 66.032 ± 0.007/0.036 Ma). Wilson (2014) reported on a sample of 883 mammalian specimens from WC1 (Fig. 3.6). The three most common taxa in both the ZL and WC1 local faunas are *Procerberus formicarum*, *Mesodma thompsoni*, and *Thylacodon montanensis*; as noted above, these are considered to be bloom taxa and DCW. SQS analyses comparing the two assemblages (Table 3.4) indicate that when accounting for evenness, subsampled generic richness is nearly the same in both WC1 and ZL.

A notable difference between WC1 and ZL is the absence of the multituberculate *Stygimys* from ZL. Unlike the bloom multituberculate *Mesodma*, a resident survivor of the K-Pg extinction, *Stygimys* is a post-extinction immigrant to the Western Interior (Clemens, 2010). It is common in early Paleocene mammalian assemblages of the northern portions of the Western Interior of North America (e.g., Sloan and Van Valen, 1965; Archibald, 1982; Lofgren et al., 2005,

Clemens, 2010), including localities in McCone County, geographically close to ZL (UCMP localities V87072, V87037, V87038, etc.; Lofgren, 1995), but not in LOH or CC. Also present in WC1 but absent from ZL are the common Pu1 archaic ungulate immigrants *Baioconodon*, *Oxyprimus*, and *Protungulatum*. Such differences could be interpreted as WC1 being slightly more recovered due to its complete loss of Lancian-aspect taxa and its increase in number of immigrant taxa relative to ZL. However, an eastern Garfield County locality, Constenius (UCMP V96268/UWBM C1665) is, like ZL, situated stratigraphically between the KPB (as determined by the negative carbon isotope excursion of Arens et al., 2014) and the MCZ, and is very similar in composition to WC1. Although the assemblage has yet to be formally described, both *Stygimys* and the larger archaic ungulates are common in the Constenius local fauna. It is possible that these differences are due to preservational bias against larger, more fragile fossils at ZL; for example, the Constenius locality frequently produces well-preserved articulated jaws, whereas ZL produces almost exclusively small isolated teeth. In the case of ZL vs. WC1, it is possible that the large difference in sampling intensity is responsible for the difference between them; it is also possible that the difference is due to geographic separation or differences in habitat. Further sampling at ZL and more detailed information regarding the depositional environment at these localities will shed light on the potential biases affecting faunal composition at ZL. Whatever the cause, these slight compositional differences indicate that comparisons between ZL and other faunas of the Western Interior should be interpreted with careful consideration of the potential effects of geographic separation and depositional environment.

The LOH and CC assemblages, which are temporally constrained between ca. 25 ka and ca. 323 ka after the KPB, and ca. 247 ka and ca. 323 ka after the KPB, respectively (ages of 66.024 ± 0.014/0.044 Ma and 65.726 ± 0.013/0.044 Ma, and 65.802 ± 0.116/0.125 Ma and 65.726 ± 0.013/0.044 Ma, respectively, Fig. 3.2; Sprain et al., in review), represent local faunas that have undergone a modest degree of recovery from the K-Pg mass extinction. Although the increase in evenness between ZL and LOH/CC are both slight (Fig. 3.7), a comparison of faunal composition (Table 3.1) reveals striking differences between the older and younger local faunas. The Lancian-aspect DCW metatherians present in the ZL local fauna are absent in LOH and CC; in fact, no metatherians appear at either LOH or CC. The lack of metatherians and greater relative abundance of archaic ungulates in LOH and CC (*Mimatuta, Protungulatum*, *Oxyprimus*, Table 3.1), and the fact that *Protungulatum donnae* overtakes *Procerberus formicarum* for the second-most abundant taxon in LOH, both indicate a slight shift away from the dominance of bloom taxa. Moreover, several new taxa appear in the LOH and CC local faunas, including characteristic Pu1 taxa at both LOH and CC (e.g., *Protungulatum, Oxyprimus*); *Purgatorius* cf. *P. coracis* at CC; and ?*Prodiacodon crustulum*, *Procerberus* cf. *P. grandis*, and a large periptychid archaic ungulate (similar to *Hemithlaeus* and *Tinuviel*, see 3.13: Appendix) at LOH. *Purgatorius* and *Prodiacodon* are otherwise only known from Pu2 and Pu3 local faunas in the northern portion of western North America (Fig. 3.9; Johnston and Fox, 1984; Fox, 1990; Lofgren et al., 2004; Clemens, 2002, 2017; Fox and Scott, 2011; Wilson, 2014). Similarly, *Hemithlaeus* and *Tinuviel* are otherwise known only from the Pu2 and Pu3 of New Mexico and SE MT (Williamson, 1996; Hunter et al., 1997). The appearance of these mammals, and some specimens with affinities to these mammals, at LOH and CC shows that new, younger-aspect taxa (immigrants; Clemens, 2002, 2004, 2010, 2017; Wilson, 2014) began to appear before

McGuire Creek local faunas significantly increased in taxonomic richness (Fig. 3.7), and did not appear locally in a single appearance event corresponding to the beginning of a new NALMA interval zone. This series of immigration events early in the biotic recovery serves to highlight the key role immigrants played in the reshaping of mammalian faunas in the earliest Paleogene, as has been suggested previously (Clemens, 2002, 2010; Wilson, 2013, 2014).

Comparison with younger local faunas from the greater Hell Creek region reveals a major increase in regional taxonomic richness occurred between LOH/CC and the Garbani Channel local fauna (garMT, Fig. 3.8–3.9). The Garbani Channel local fauna has been estimated (via sediment accumulation rates) to occur between ca. 372 and 847 ka after the KPB (Sprain et al., in review; ages of 65.677 ± 0.041/0.059 Ma and 65.202 ± 0.057/0.104 Ma, respectively). Even with conservative estimates of the number of taxa in garMT (Wilson, 2014; Clemens, pers. comm.), there are more than twice as many species in garMT than any McGuire Creek local fauna. Although the Garbani Channel local fauna is still under study, preliminary work indicates a distinct uptick in the number of archaic ungulate, multituberculate, and plesiadapiform taxa present on the landscape between LOH/CC and garMT. As such, we infer that the new taxa appearing in LOH and CC are merely the beginning of a shift toward more taxonomically diverse, recovered faunas. The main wave of appearances seems to have occurred between ca. 323 ka and ca. 847 ka after the KPB (ages of 65.726 ± 0.013/0.044 Ma and 65.202 ± 0.057/0.104 Ma), a span of ca. 524 ka that we still know relatively little about.

To obtain finer stratigraphic resolution on the main phase of mammalian biotic recovery, it will be necessary to find a succession of localities within this poorly known time interval, because the

Garbani Channel deposit is large and cannot yet be subdivided into specific chronostratigraphic units.

Continental Signal: North American mammals in the earliest Paleocene

Results from our cluster analyses and correspondence analysis reveal the broader spatiotemporal context of the early phase of biotic recovery documented in McGuire Creek. Earliest Puercan (Pu1) faunas, including all McGuire Creek local faunas, have some compositional differences among them but are largely similar across Montana, Wyoming, and Colorado (Fig. 3.8–3.9); Pu1 faunas are not known from farther south, and faunas from Alberta and Saskatchewan that have sometimes been assigned to Pu1 (e.g., Long Fall Horizon and Frenchman 1) are poorly constrained temporally (Cifelli et al. 2004; Lofgren et al., 2004; Clemens 2017) and have therefore not been included here. In contrast, the Pu2 and Pu3 faunas are compositionally separated into northern and southern groups (Fig. 3.9). This implies that by the Pu2 interval at the latest, faunas began to differentiate into northern and southern faunal types; because of the lack of Pu1 faunas south of Colorado and Utah, we cannot rule out the possibility that Pu1 faunas were differentiated into northern and southern types earlier than Pu2. Eberle and Lillegraven (1998) similarly proposed that north-south differentiation of North American mammalian faunas began in Pu2, although they did not support this hypothesis with quantitative analysis. The same study noted a closer similarity in faunal composition between Pu2–Pu3 aged faunas of the Ferris Formation and other faunas to the south, as we find here. A north–south pattern of faunal differentiation in Pu2 and Pu3 has also been proposed by other workers (Williamson, 1996; Weil, 1999). This pattern could be driven by latitudinal effects or the appearance of discrete geographic barriers between the northern and southern portions of the Western Interior,

including a possible temporary western incursion of the Western Interior Seaway (Boyd and Lillegraven 2011).

Within this geographically broader context, it seems that based on CA, younger Pu1 faunas from McGuire Creek (LOH and CC local faunas) show greater similarity to the Pu2 and Pu3 faunas than do the older Pu1 faunas (e.g., ZL, WC1; Fig. 3.9). This pattern might indicate that the mammalian biotic recovery proceeded at a finer temporal scale than our current mammalian biochronology (NALMAs) allows us to express. Indeed, this has been previously observed in areas other than northeastern Montana. The Alexander Locality from the Denver Basin (alCO, Fig. 3.8–3.9), which has often been referred to Pu1 based on the presence of several classic Pu1 taxa, more closely resembles Pu2 faunas from the San Juan and Hanna Basins (Middleton, 1983; Eberle, 2003; Lofgren et al., 2004; Middleton and Dewar, 2004). In our CA (Fig. 3.9), alCO plots in a location intermediate to the main cluster of Pu1 faunas and the southern/central cluster of Pu2–3 faunas from Colorado, Wyoming, Utah, and New Mexico. These results support the hypothesis that alCO represents a transitional Pu1–2 fauna (Middleton, 1983; Eberle, 2003; Lofgren et al., 2004; Middleton and Dewar, 2004) that cannot be assigned to either Pu1 or Pu2 to the exclusion of the other. In combination with these results from alCO, our McGuire Creek results indicate that as temporal gaps in our sampling of the early Paleogene are filled, we will need more precise age constraints, such as those obtained from geochronology and paleomagnetism data, to understand and describe the nuances of the mammalian biotic recovery. In this study, although we increase the temporal resolution of our knowledge of the recovery process in a small geographic subsection of the greater Hell Creek region, the difficulties in determining relative faunal ages across large distances limit our comparisons with other faunas,

except on the relatively coarse scale of NALMA interval zones. A more precise continent-wide chronostratigraphic framework will be necessary to further increase the temporal resolution of our understanding of mammalian biotic recovery.

3.8 CONCLUSION

On a local scale within our McGuire Creek study area, mammalian biotic recovery is underway within the first ca. 323 ka after the KPB. Although the changes in taxonomic richness, evenness, dominance, and faunal composition between our oldest local fauna (ZL, minimum age of 66.024 ± 0.014/0.044 Ma) and our two younger local faunas (LOH and CC, maximum age of 65.802 ± 0.116/0.125 Ma, minimum age of 65.726 ± 0.013/0.044 Ma) are slight, they do reflect two distinct types of local faunas: the disaster local fauna at ZL, and the slightly more recovered local faunas at LOH and CC. The appearance of several new taxa, coupled with higher overall taxonomic richness and decreased relative abundance of bloom taxa distinguish LOH and CC from ZL. Yet all three McGuire Creek local faunas are still far removed from the higher levels of richness in the younger, nearby Garbani Channel local fauna, indicating that the very slight increase in taxonomic richness at McGuire Creek preceded the later, main wave of taxonomic appearances in the greater Hell Creek region.

The three McGuire Creek local faunas reported here broadly resemble other North American Pu1 faunas, which are relatively homogeneous throughout the Western Interior. Yet the presence of younger aspect taxa, such as *Purgatorius*, aligns the LOH and CC McGuire Creek local faunas with younger faunas in the northern half of the continent. These northern faunas begin to appear compositionally distinct from the southern faunas starting in Pu2. Future studies should strive to

capture more snapshots from the early and middle parts of the biotic recovery, from not only McGuire Creek and northeastern Montana, but from faunas elsewhere around the Western Interior.

Our findings here add to the increasing body of knowledge regarding the spatiotemporal variability of biotic recovery. Previous studies (e.g., Jablonski, 1998; Donovan et al., 2016) have shown striking geographic variation in patterns of biotic recovery across continents; with our more restricted geographic scale, we have shown spatial variation in recovery pattern even within the confines of North America. This finding highlights the importance of examining biotic recovery on a small spatial scale; yet we also find spatial variation in biotic recovery within a single region (the greater Hell Creek region) that may be due to incomplete sampling or taphonomic effects. Additionally, we find that commonly cited theoretical characteristics of the recovery process (e.g., eurytopic bloom taxa; Kauffman and Harries, 1996; Erwin, 1998) do not always correspond with empirical evidence. These results might reflect differences between biotic recovery in invertebrates, on which most theoretical models are based, and vertebrates. Further work comparing the biotic recovery process between terrestrial and aquatic faunas will help elucidate if these are true differences, or are an artifact of environment or sampling.

3.9 ACKNOWLEDGEMENTS

Funding for this research was provided by the University of Washington Department of Biology, and the Hell Creek Project III (N. Myhrvold). SMS received funding from the American Philosophical Society Lewis and Clark Fund for Exploration and Field Research, the American Society of Mammalogists, and the University of California Museum of Paleontology Welles Fund. CJS was funded by a National Science Foundation Graduate Research Fellowship for the duration of this work, and received additional funding from the Geological Society of America and the Paleontological Society. DLL was supported by the Annie M. Alexander Endowment of the University of California Museum of Paleontology, and National Science Foundation Grant BSR-85-13253 (to WAC). Geochronology work was funded by the Esper S. Larsen Fund and the Ann and Gordon Getty Foundation. Permits to collect vertebrate fossils were provided by the Charles M. Russell Wildlife Refuge, the U.S. Army Corps of Engineers, U.S. Department of Fish and Wildlife, and U.S. Department of the Interior. We are grateful to Isabel Fendley, Gabriella Quaresma, and Tom Tobin for their help with tephra collection; to previous McGuire Creek collection crews for their hard work and help acquiring specimens for this study, especially Don Hopkins for extensive matrix sorting; and to Alexandria Brannick, Jonathan Calede, David DeMar, Jr., Sarah Shelley, and Lucas Weaver for helpful comments regarding this research and manuscript.

3.10 REFERENCES CITED

Alroy, J., 1999, The fossil record of North American mammals: evidence for a Paleocene evolutionary radiation: Systematic Biology, v. 48, p. 107–118, doi: 10.1080/106351599260472.

Alroy, J., 2010, Fair Sampling of Taxonomic Richness and Unbiased Estimation of Origination and Extinction Rates: Quantitative methods in Paleobiology, v. 16, p. 55–80.

Alvarez, L.W., Alvarez, W., Asaro, F., and Michel, H.V., 1980, Extraterrestrial cause for the Cretaceous-Tertiary extinction: Science, v. 208, p. 1095–1108.

Archibald, J.D., 1982, A study of Mammalia and geology across the Cretaceous-Tertiary boundary in Garfield County, Montana: University of California Publications in Geological Sciences 122, 286 p.

Archibald, J.D., and Deutschman, D.H., 2001, Quantitative analysis of the timing of the origin and diversification of extant placental orders: Journal of Mammalian Evolution, v. 8, p. 107–124.

Archibald, J.D., and Lofgren, D.L., 1990, Mammalian zonation near the Cretaceous-Tertiary boundary: Geological Society of America Special Papers, v. 243, p. 31–50.

Archibald, J.D., Butler, R.F., Lindsay, E.H., Clemens, W.A., and Dingus, L., 1982, Upper Cretaceous–Paleocene biostratigraphy and magnetostratigraphy, Hell Creek and Tullock Formations, northeastern Montana: Geology, v. 10, p. 153–159.

Arens, N.C., Thompson, A., and Jahren, A.H., 2014, A preliminary test of the press-pulse extinction hypothesis: Palynological indicators of vegetation change preceding the Cretaceous-Paleogene boundary, McConeCounty, Montana, USA, *in* Wilson, G.P., Clemens, W.A., Horner, J.R., and Hartman, J.H., eds., Through the End of the Cretaceous in the Type Locality of the Hell Creek Formation in Montana and Adjacent Areas: Geological Society of America Special Paper, v. 503, p. 209–227.

Badgley, C., 1986, Counting individuals in mammalian fossil assemblages from fluvial environments: Palaios, p. 328–338.

Benton, M.J., 1983, Dinosaur success in the Triassic: a noncompetitive ecological model: The Quarterly Review of Biology, v. 58, p. 29–55.

Bercovici, A., Pearson, D., Nichols, D., and Wood, J., 2009, Biostratigraphy of selected K/T boundary sections in southwestern North Dakota, USA: toward a refinement of palynological identification criteria: Cretaceous Research, v. 30, p. 632–658, doi: 10.1016/j.cretres.2008.12.007.

Bohor, B.F., Foord, E.E., Modreski, P.J., and Triplehorn, D.M., 1984, Mineralogic evidence for an impact event at the Cretaceous-Tertiary boundary: Science, v. 224, p. 867–870.

Boyd, D.W., and Lillegraven, J.A., 2011, Persistence of the Western Interior Seaway: Historical background and significance of ichnogenus Rhizocorallium in Paleocene strata, south-central Wyoming: Rocky Mountain Geology, v. 46, p. 43–69.

Bray, J.R., and Curtis, J.T., 1957, An ordination of the upland forest communities of southern Wisconsin: Ecological monographs, v. 27, p. 325–349.

Brown, R.W., 1952, Tertiary strata in eastern Montana and western North and South Dakota, in Sonnenberg, F.P., ed., Billings Geological Society Guidebook, Third Annual Field Conference. Billings, Montana, Billings Geological Society, p. 89–92.

Calvert, W.R., 1912, Geology of certain lignite fields in eastern Montana. U.S. Geological Survey Bulletin 471, p. 187–201.

Chen, Z.-Q., and Benton, M.J., 2012, The timing and pattern of biotic recovery following the end-Permian mass extinction: Nature Geoscience, v. 5, p. 375–383, doi: 10.1038/ngeo1475.

Cherven, V.B., and Jacob, A.R., 1985, Evolution of Paleogene depositional systems, Williston Basin, in response to global sea level changes, in Flores, M.R., and Kaplan, S.S., eds., Cenozoic Paleogeography of the West-Central United States: Denver, Colorado, Society of Economic Paleontologists and Mineralogists, Rocky Mountain Section, p. 127–170.

Clemens, W.A., 2002, Evolution of the mammalian fauna across the Cretaceous-Tertiary boundary in northeastern Montana and other areas of the Western Interior: Geological Society of America Special Paper, v. 361, p. 217–245.

Clemens, W.A., 2004, Purgatorius (Plesiadapiformes, Primates?, Mammalia), a Paleocene Immigrant Into Northeastern Montana: Stratigraphic Occurrences and Incisor Proportions: Bulletin of Carnegie Museum of Natural History, v. 36, p. 3–13.

Clemens, W.A., 2010, Were immigrants a significant part of the earliest paleocene mammalian fauna of the north american western interior?: Vertebrata PalAsiatica, v. 48, p. 285–307.

Clemens, W.A., 2017, Procerberus (Cimolestidae, Mammalia) from the Latest Cretaceous and Earliest Paleocene of the Northern Western Interior, USA: PaleoBios, v. 34.

Clemens, W.A., and Hartman, J.H., 2014, From Tyrannosaurus rex to asteroid impact: Early studies (1901–1980) of the Hell Creek Formation in its type area: Geological Society of America Special Papers, v. 503, p. 1–87.

Clemens, W.A., and Williamson, T.E., 2005, A new species of Eoconodon (Triisodontidae, Mammalia) from the San Juan Basin, New Mexico: Journal of Vertebrate Paleontology, v. 25, p. 208–213.

Collier, A.J., and Knechtel, M., 1939, The coal resources of McCone County, Montana: U.S. Geological Survey Bulletin 905, 80 p.

Dahlberg, E.L., Eberle, J.J., Sertich, J.J.W., and Miller, I.M., 2016, A new earliest Paleocene (Puercan) mammalian fauna from Colorado's Denver Basin , U.S.A.: Rocky Mountain Geology, v. 51, p. 1–22, doi: 10.2113/gsrocky.51.1.1.

DeBey, L.B., and Wilson, G.P., 2014, Mammalian femora across the Cretaceous–Paleogene boundary in eastern Montana: Cretaceous Research, v. 51, p. 361–385.

Del Moral, R., 1998, Early succession on lahars spawned by Mount St. Helens.: American Journal of Botany, v. 85, p. 820–828.

Dice, L.R., 1945, Measures of the amount of ecologic association between species: Ecology, v. 26, p. 297–302.

Donovan, M.P., Iglesias, A., Wilf, P., Labandeira, C.C., and Cúneo, N.R., 2016, Rapid recovery of Patagonian plant–insect associations after the end-Cretaceous extinction: Nature Ecology & Evolution, v. 1, p. 12.

dos Reis, M., Donoghue, P.C.J., and Yang, Z., 2014, Neither phylogenomic nor palaeontological data support a Palaeogene origin of placental mammals: Biology Letters, v. 10, p. 20131003.

Dray, S., and Dufour, A.B., 2007, The ade4 package: implementing the duality diagram for ecologists: Journal of statistical software, v. 22, p. 1–20.

Eberle, J.J., 2003, Puercan mammalian systematics and biostratigraphy in the Denver Formation, Denver Basin, Colorado: Rocky Mountain Geology, v. 38, p. 143–169.

Eberle, J.J., and Lillegraven, J.A., 1998, A new important record of earliest Cenozoic mammalian history: Rocky Mountain Geology, v. 33, p. 49–117.

Erwin, D.H., 1998, The end and the beginning: Recoveries from mass extinctions: Trends in Ecology and Evolution, v. 13, p. 344–349, doi: 10.1016/S0169-5347(98)01436-0.

Faith, D.P., Minchin, P.R., and Belbin, L., 1987, Compositional dissimilarity as a robust measure of ecological distance: Vegetatio, v. 69, p. 57–68.

Fastovsky, D.E., 1987, Paleoenvironments of vertebrate-bearing strata during the Cretaceous-Paleogene transition, eastern Montana and western North Dakota: Palaios, p. 282–295.

Fastovsky, D.E., and Bercovici, A., 2016, The Hell Creek Formation and its contribution to the Cretaceous–Paleogene extinction: A short primer: Cretaceous Research, v. 57, p. 368–390.

Fox, R.C., 1990, The succession of Paleocene mammals in western Canada: Geological Society of America Special Papers, v. 243, p. 51–70.

Fox, R.C., and Youzwyshyn, G.P., 1994, New primitive carnivorans (Mammalia) from the Paleocene of western Canada, and their bearing on relationships of the order: Journal of Vertebrate Paleontology, v. 14, p. 382–404.

Fox, R.C., and Scott, C.S., 2011, A New, Early Puercan (Earliest Paleocene) Species of Purgatorius (Plesiadapiformes, Primates) from Saskatchewan, Canada: Journal of Paleontology, v. 85, p. 537–548, doi: 10.1666/10-059.1.

Gazin, C.L., 1941, The mammalian faunas of the Paleocene of central Utah, with notes on the geology: Smithsonian Inst., United States National Museum.

Gill, J.R., and Cobban, W.A., 1973, Stratigraphy and geologic history of the Montana Group and equivalent rocks, Montana, Wyoming, and North and South Dakota. U.S. Geological Survey Professional Paper 776, 36 p.

Good, I.J., 1953, The population frequencies of species and the estimation of population parameters: Biometrika, v. 40, p. 237–264.

Grossnickle, D.M., and Newham, E., 2016, Therian mammals experience an ecomorphological radiation during the Late Cretaceous and selective extinction at the K–Pg boundary, *in* Proc. R. Soc. B, The Royal Society, v. 283, p. 20160256.

Halliday, T.J.D., and Goswami, A., 2016, Eutherian morphological disparity across the end-Cretaceous mass extinction: Biological Journal of the Linnean Society, v. 118, p. 152–168, doi: 10.1111/bij.12731.

Hammer, O., and Harper, D.A.T., 2008, Paleontological data analysis: John Wiley & Sons.

Hartman, J.H., Butler, R.D., Weiler, M.W., and Schumaker, K.K., 2014, Context, naming, and formal designation of the Cretaceous Hell Creek Formation lectostratotype, Garfield County, Montana: Geological Society of America Special Paper, v. 503, p. 89–121.

Hotton, C.L., 2002, Palynology of the Cretaceous-Tertiary boundary in central Montana: evidence for extraterrestrial impact as a cause of the terminal Cretaceous extinctions: Geological Society of America Special Paper, v. 361, p. 473–502.

Hull, P., 2015, Life in the aftermath of mass extinctions: Current Biology, v. 25, p. R941–R952.

Hunter, J.P., Hartman, J.H., and Krause, D.W., 1997, Mammals and mollusks across the Cretaceous-Tertiary boundary from Makoshika State Park and vicinity (Williston Basin), Montana: Rocky Mountain Geology, v. 32, p. 61–114.

Hurlbert, S.H., 1971, The nonconcept of species diversity: a critique and alternative parameters: Ecology, v. 52, p. 577–586.

Ickert, R.B., Mulcahy, S.R., Sprain, C.J., Banaszak, J.F., and Renne, P.R., 2015, Chemical and Pb isotope composition of phenocrysts from bentonites constrains the chronostratigraphy around the Cretaceous-Paleogene boundary in the Hell Creek region, Montana: Geochemistry, Geophysics, Geosystems, v. 16, p. 2743–2761.

Jablonski, D., 1998, Geographic variation in the molluscan recovery from the end-Cretaceous extinction: Science, v. 279, p. 1327–1330.

Jablonski, D., 2002, Survival without recovery after mass extinctions: Proceedings of the National Academy of Sciences, v. 99, p. 8139–8144.

Jasinoski, S.C., Rayfield, E.J., and Chinsamy, A., 2009, Comparative feeding biomechanics of Lystrosaurus and the generalized dicynodont Oudenodon: The Anatomical Record, v. 292, p. 862–874.

Johnston, P.A., and Fox, R.C., 1984, Paleocene and late Cretaceous mammals from Saskatchewan, Canada: Palaeontographica Abteilung A, p. 163–222.

Kauffman, E.G., and Harries, P.J., 1996, The importance of crisis progenitors in recovery from mass extinction: Geological Society, London, Special Publications, v. 102, p. 15–39.

King, G.M., Oelofsen, B.W., and Rubidge, B.S., 1989, The evolution of the dicynodont feeding system: Zoological Journal of the Linnean Society, v. 96, p. 185–211.

Krebs, C.J., 1989, Ecological methodology: Harper & Row, New York.

Lance, G.N., and Williams, W.T., 1967, A general theory of classificatory sorting strategies: II. Clustering systems: The computer journal, v. 10, p. 271–277.

Lillegraven, J.A., 1972, Ordinal and familial diversity of Cenozoic mammals: Taxon, p. 261–274.

Lillegraven, J.A., and Eberle, J.J., 1999, Vertebrate faunal changes through Lancian and Puercan time in southern Wyoming: Journal of Paleontology, v. 73, p. 691–710.

Lofgren, D.L., 1995, The Bug Creek problem and the Cretaceous-Tertiary transition at McGuire Creek, Montana: Univ of California Press, v. 140.

Lofgren, D.L., Lillegraven, J.A., Clemens, W.A., Gingerich, P.D., and Williamson, T.E., 2004, Paleocene biochronology: the Puercan through Clarkforkian land mammal ages: Late Cretaceous and Cenozoic Mammals of North America: Biostratigraphy and Geochronology. Columbia University Press, New York, p. 43–105.

Lofgren, D.L., Scherer, B.E., Clark, C.K., and Standhardt, B., 2005, First record of Stygimys (Mammalia, Multituberculata, Eucosmodontidae) from the Paleocene (Puercan) part of the North Horn Formation, Utah, and a review of the genus: Journal of Mammalian Evolution, v. 12, p. 77–97.

Longrich, N.R., Scriberas, J., and Wills, M.A., 2016, Severe extinction and rapid recovery of mammals across the Cretaceous–Palaeogene boundary, and the effects of rarity on patterns of extinction and recovery: Journal of evolutionary biology, v. 29, p. 1495–1512.

Magurran, A.E., 2004, Measuring biological diversity: John Wiley & Sons.

MacMahon, J.A., Parmenter, R.R., Johnson, K.A., and Crisafulli, C.M., 1989, Small mammal recolonization on the Mount St. Helens volcano: 1980-1987: American Midland Naturalist, p. 365–387.

Meredith, R.W., Janecka, J.E., Gatesy, J., Ryder, O. a., Fisher, C. a., Teeling, E.C., Goodbla, a., Eizirik, E., Simao, T.L.L., Stadler, T., Rabosky, D.L., Honeycutt, R.L., Flynn, J.J., Ingram, C.M., et al., 2011, Impacts of the Cretaceous Terrestrial Revolution and KPg Extinction on Mammal Diversification: Science, v. 334, p. 521–524, doi: 10.1126/science.1211028.

Middleton, M. D., 1983, Early Paleocene Vertebrates of the Denver Basin, Colorado [Ph. D. thesis,]: Boulder, University of Colorado, 403 p.

Middleton, M.D., and Dewar, E.W., 2004, New mammals from the early Paleocene Littleton fauna (Denver Formation, Colorado): New Mexico Museum of Natural History and Science Bulletin, v. 26, p. 59–80.

Moore, J.R., Wilson, G.P., Sharma, M., Hallock, H.R., Braman, D.R., and Renne, P.R., 2014, Assessing the relationships of the Hell Creek–Fort Union contact, Cretaceous-Paleogene boundary, and Chicxulub impact ejecta horizon at the Hell Creek Formation lectostratotype, Montana, USA: Geological Society of America Special Papers, v. 503, p. 123–135.

Morgan, L.E., Mark, D.F., Imlach, J., Barfod, D., and Dymock, R., 2014, FCs-EK: a new sampling of the Fish Canyon Tuff $^{40}Ar/^{39}Ar$ neutron flux monitor: Geological Society, London, Special Publications, v. 378, p. 63 LP-67.

Nenadic, O., Greenacre, M., 2007, Correspondence Analysis in R, with two- and three-dimensional graphics: The ca package: Journal of Statistical Software v. 20, p.1-13.

Novacek, M., and Clemens, W.A., 1977, Aspects of intrageneric variation and evolution of Mesodma (Multituberculata, Mammalia): Journal of Paleontology, p. 701–717.

O'Leary, M. a., Bloch, J.I., Flynn, J.J., Gaudin, T.J., Giallombardo, a., Giannini, N.P., Goldberg, S.L., Kraatz, B.P., Luo, Z.-X., Meng, J., Ni, X., Novacek, M.J., Perini, F. a., Randall, Z.S., et al., 2013, The Placental Mammal Ancestor and the Post-K-Pg Radiation of Placentals: Science, v. 339, p. 662–667, doi: 10.1126/science.1229237.

Oksanen, J., Blanchet, F.G., Kindt, R., Legendre, P., Minchin, P.R., O'hara, R.B., Simpson, G.L., Solymos, P., Stevens, M.H.H., and Wagner, H., 2013, Package "vegan": Community ecology package, version 2.4-2, https://CRAN.R-project.org/package=vegan.

Payne, J.L., Summers, M., Rego, B.L., Altiner, D., Wei, J.Y., Yu, M.Y., and Lehrmann, D.J., 2011, Early and Middle Triassic trends in diversity, evenness, and size of foraminifers on a carbonate platform in south China: implications for tempo and mode of biotic recovery from the end-Permian mass extinction: Paleobiology, v. 37, p. 409–425, doi: 10.1666/08082.1.

Peryt, D., and Lamolda, M., 1996, Benthonic foraminiferal mass extinction and survival assemblages from the Cenomanian-Turonian Boundary Event in the Menoyo section, northern Spain: Geological Society, London, Special Publications, v. 102, p. 245–258.

R Core Team, 2017, R: A language and environment for statistical computing: R Foundation for Statistical Computing, Vienna, Austria: https://www.R-project.org/.

Renne, P.R., Balco, G., Ludwig, K.R., Mundil, R., and Min, K., 2011, Response to the comment by WH Schwarz et al. on "Joint determination of 40 K decay constants and 40 Ar∗/40 K for the Fish Canyon sanidine standard, and improved accuracy for 40 Ar/39 Ar geochronology" by PR Renne et al.(2010): Geochimica et Cosmochimica Acta, v. 75, p. 5097–5100.

Renne, P.R., Deino, A.L., Hilgen, F.J., Kuiper, K.F., Mark, D.F., Mitchell, W.S., Morgan, L.E., Mundil, R., and Smit, J., 2013, Time scales of critical events around the Cretaceous-Paleogene boundary: Science, v. 339, p. 684–7, doi: 10.1126/science.1230492.

Renne, P.R., Sprain, C.J., Richards, M.A., Self, S., Vanderkluysen, L., and Pande, K., 2015, State shift in Deccan volcanism at the Cretaceous-Paleogene boundary, possibly induced by impact: Science, v. 350, p. 76–78.

Robison, S.F., 1986, Paleocene (Puercan-Torrejonian) mammalian faunas of the North Horn Formation, central Utah: Brigham Young University Geology Studies, v. 30, p. 87–134.

Rogers, R.R., and Brady, M.E., 2010, Origins of microfossil bonebeds: insights from the Upper Cretaceous Judith River Formation of north-central Montana: Paleobiology, v. 36, p. 80–112.

Rogers, R.R., Carrano, M.T., Rogers, K.A.C., Perez, M., and Regan, A.K., 2017, Isotaphonomy in concept and practice: an exploration of vertebrate microfossil bonebeds in the Upper

Cretaceous (Campanian) Judith River Formation, north-central Montana: Paleobiology, v. 43, p. 248–273, doi: 10.1017/pab.2016.37.

Ruta, M., Angielczyk, K.D., Frobisch, J., and Benton, M.J., 2013, Decoupling of morphological disparity and taxic diversity during the adaptive radiation of anomodont therapsids: Proc Biol Sci, v. 280, p. 20131071, doi: 10.1098/rspb.2013.1071.

Sahney, S., and Benton, M.J., 2008, Recovery from the most profound mass extinction of all time: Proceedings of the Royal Society of London B: Biological Sciences, v. 275, p. 759–765.

Sepkoski, J.J., 1998, Rates of speciation in the fossil record.: Philosophical transactions of the Royal Society of London. Series B, Biological sciences, v. 353, p. 315–326, doi: 10.1098/rstb.1998.0212.

Sepúlveda, J., Wendler, J.E., Summons, R.E., and Hinrichs, K.-U., 2009, Rapid resurgence of marine productivity after the Cretaceous-Paleogene mass extinction: Science, v. 326, p. 129–132.

Sloan, R.E., 1981, Systematics of Paleocene multituberculates from the San Juan Basin, New Mexico: Advances in San Juan Basin Paleontology. University of New Mexico Press, Albuquerque, p. 127–160.

Sloan, R.E., and Van Valen, L., 1965, Cretaceous mammals from Montana: Science, v. 148, p. 220–227.

Smith, S.M., and Wilson, G.P., 2017, Species discrimination of co-occurring small fossil mammals: a case study of the Cretaceous-Paleogene Multituberculate genus Mesodma: Journal of Mammalian Evolution, v. 24, p. 147–157.

Smith, F.A., Boyer, A.G., Brown, J.H., Costa, D.P., Dayan, T., Ernest, S.K.M., Evans, A.R., Fortelius, M., Gittleman, J.L., and Hamilton, M.J., 2010, The evolution of maximum body size of terrestrial mammals: Science, v. 330, p. 1216–1219.

Solé, R. V., Saldaña, J., Montoya, J.M., and Erwin, D.H., 2010, Simple model of recovery dynamics after mass extinction: Journal of Theoretical Biology, v. 267, p. 193–200, doi: 10.1016/j.jtbi.2010.08.015.

Sørensen, T., 1948, A method of establishing groups of equal amplitude in plant sociology based on similarity of species and its application to analyses of the vegetation on Danish commons: Biol. Skr., v. 5, p. 1–34.

Sprain, C.J., Renne, P.R., Wilson, G.P., and Clemens, W.A., 2014, High-resolution chronostratigraphy of the terrestrial Cretaceous-Paleogene transition and recovery interval in the Hell Creek region, Montana: Geological Society of America Bulletin, v. 127, p. 393–409, doi: 10.1130/B31076.1.

Sprain, C.J., Renne, P.R., Wilson, G.P., and Clemens, W.A., Submitted, Calibration of Chron 29r: New high-precision geochronologic and paleomagnetic constraints from the Hell Creek region, Montana and their implications for the Cretaceous-Paleogene boundary mass extinction, in review Geological Society of American Bulletin.

Stucky, R.K., 1990, Evolution of land mammal diversity in North America during the Cenozoic: in H. H. Genoways, ed., Current mammalogy, Vol. 2., p. 375–432.

Swisher III, C.C., Dingus, L., and Butler, R.F., 1993, 40Ar/39Ar dating and magnetostratigraphic correlation of the terrestrial Cretaceous–Paleogene boundary and Puercan Mammal Age, Hell Creek–Tullock formations, eastern Montana: Canadian Journal of Earth Sciences, v. 30, p. 1981–1996.

Tedford, R.H., 1970, Principles and practices of mammalian geochronology in North America, *in* Proceedings of the North American Paleontological Convention, Allen Press Lawrence, Kans, v. 1, p. 666–703.

Van Valen, L., 1978, The beginning of the age of mammals: Evolutionary Theory, v. 4, p. 46–80.

Weil, A. 1999. Multituberculate phylogeny and mammalian biogeography in the Late Cretaceous and earliest Paleocene Western Interior of North America [Ph.D. thesis]: Berkeley, University of California, Berkeley, 243 p.

Williamson, T.E., 1996, The beginning of the age of mammals in the San Juan Basin, New Mexico; biostratigraphy and evolution of Paleocene mammals of the Nacimiento Formation: New Mexico Museum of Natural History and Science Bulletin, v. 8, p. 1–141.

Williamson, T.E., and Lucas, S.G., 1993, Paleocene vertebrate paleontology of the San Juan Basin, New Mexico: Bulletin, New Mexico Museum Of Natural History And Science, v. 2, p. 105–136.

Wilson, G.P., 2013, Mammals across the K/Pg boundary in northeastern Montana, U.S.A.: dental morphology and body-size patterns reveal extinction selectivity and immigrant-fueled ecospace filling: Paleobiology, v. 39, p. 429–469, doi: 10.1666/12041.

Wilson, G.P., 2014, Mammalian extinction, survival, and recovery dynamics across the Cretaceous-Paleogene boundary in northeastern Montana, USA: Geological Society of America Special Papers, v. 503, p. 365–392, doi: 10.1130/2014.2503(15).

Woodburne, M.O., 2004, Definitions, *in* Woodburne, M. O., ed., Late Cretaceous and Cenozoic mammals of North America: biostratigraphy and geochronology: Columbia University Press, p. xi–xvi.

Zhuravlev, A.Y., 1996, Reef ecosytem recovery after the Early Cambrian extinction: Geological Society, London, Special Publications, v. 102, p. 79–96.

3.11 FIGURES

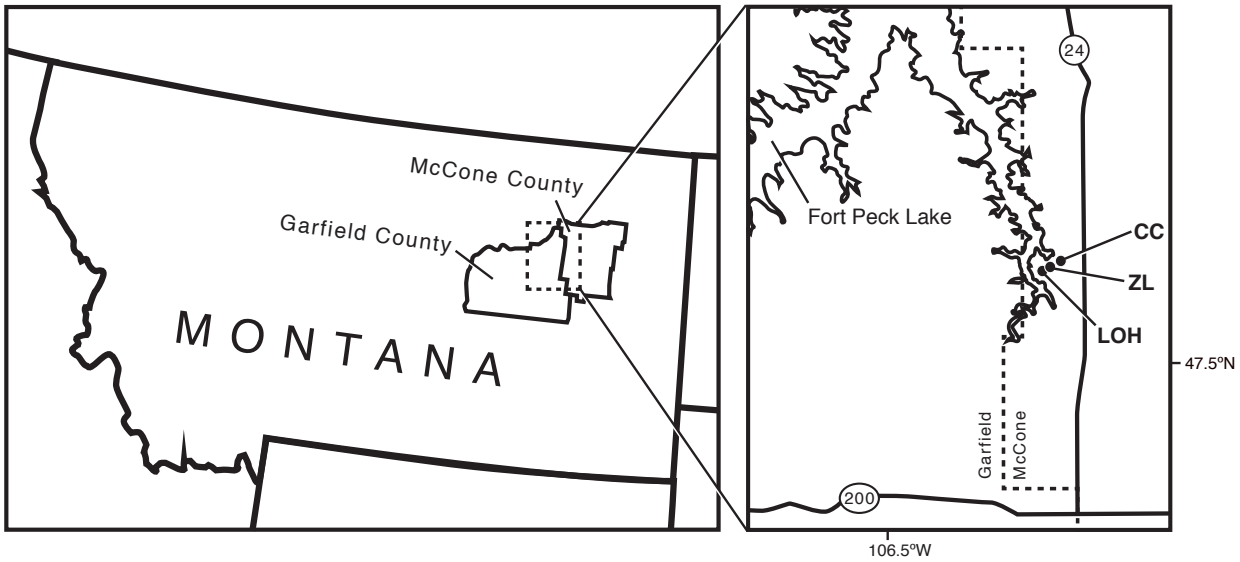

Figure 3.1 Map of vertebrate microfossil localities in the McGuire Creek area, northeastern Montana. Abbreviations: ZL = Z-Line; LOH = Luck O Hutch; CC = Coke's Clemmys.

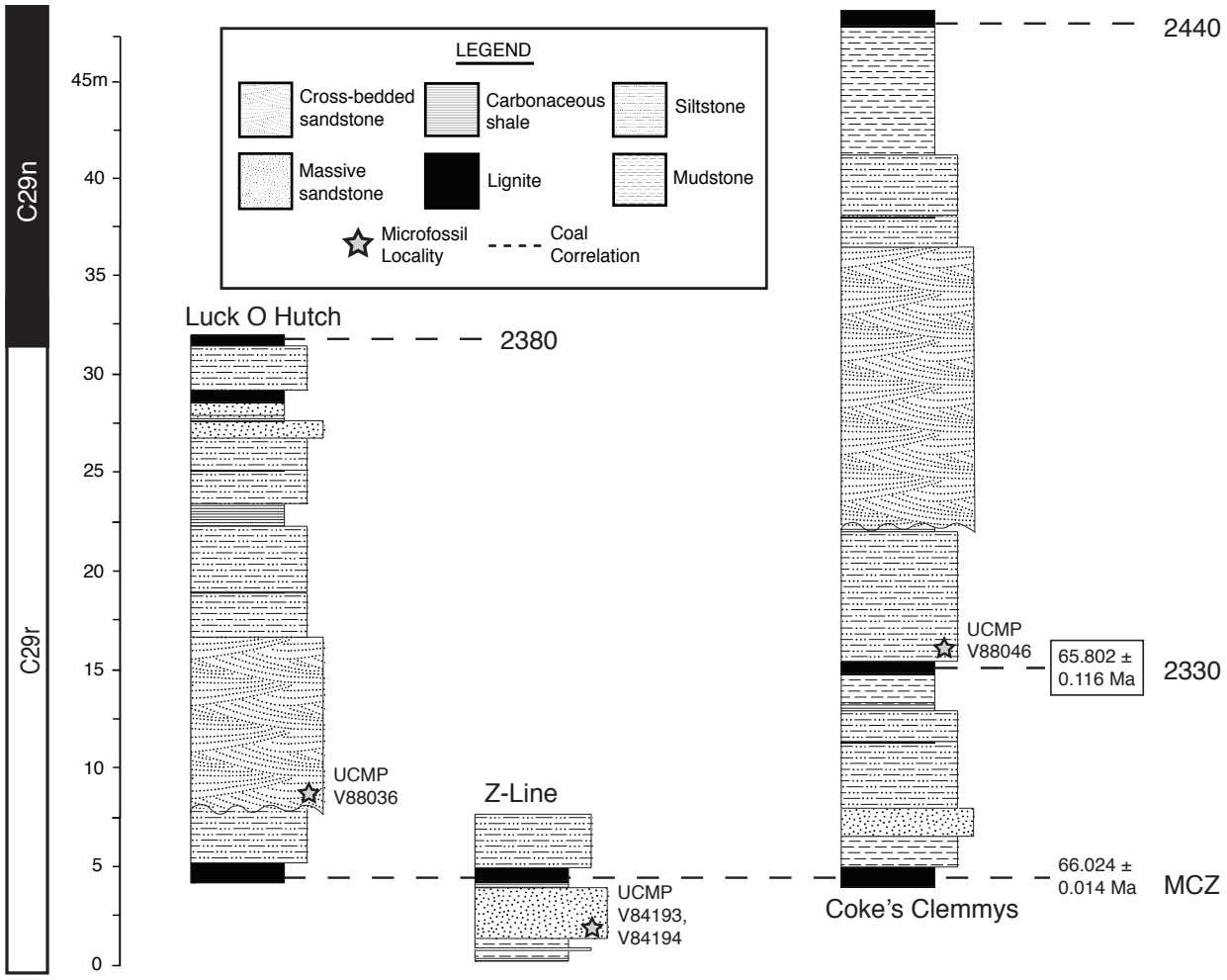

Figure 3.2 Composite stratigraphic section including vertebrate microfossil localities and coals used in this study. Localities are arranged according to longitude, with westernmost locality on the left, easternmost locality on the right. The age inside the rectangle indicates the date calculated in this study. The age not inside a rectangle is the previously published pooled age for the MCZ coal presented in Sprain et al. (in review).

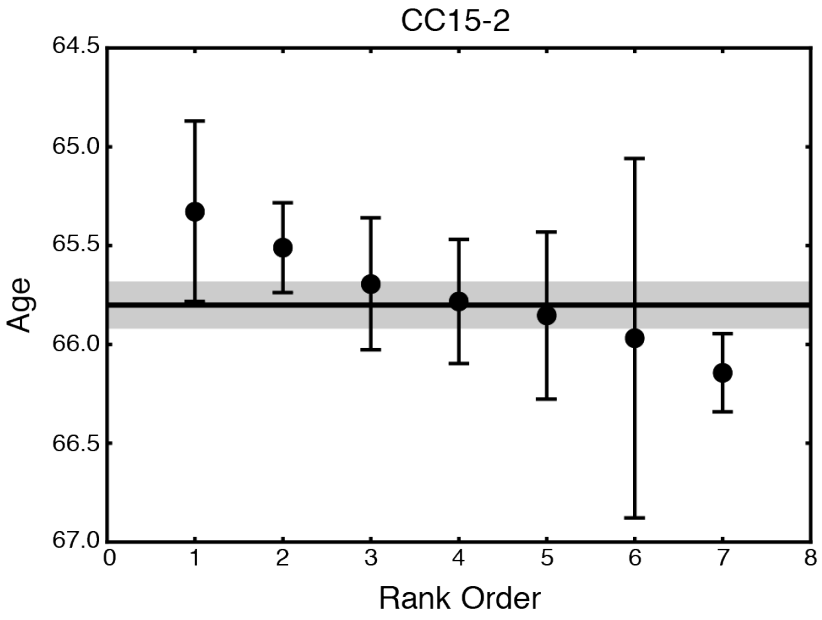

Figure 3.3 Single-crystal $^{40}Ar/^{39}Ar$ results for 2330 tephra [CC15-2]. Individual ages are shown in rank order with analytical uncertainty limits of 1σ. The thick horizontal line indicates the weighted mean age with the 1σ uncertainty shown by the grey box.

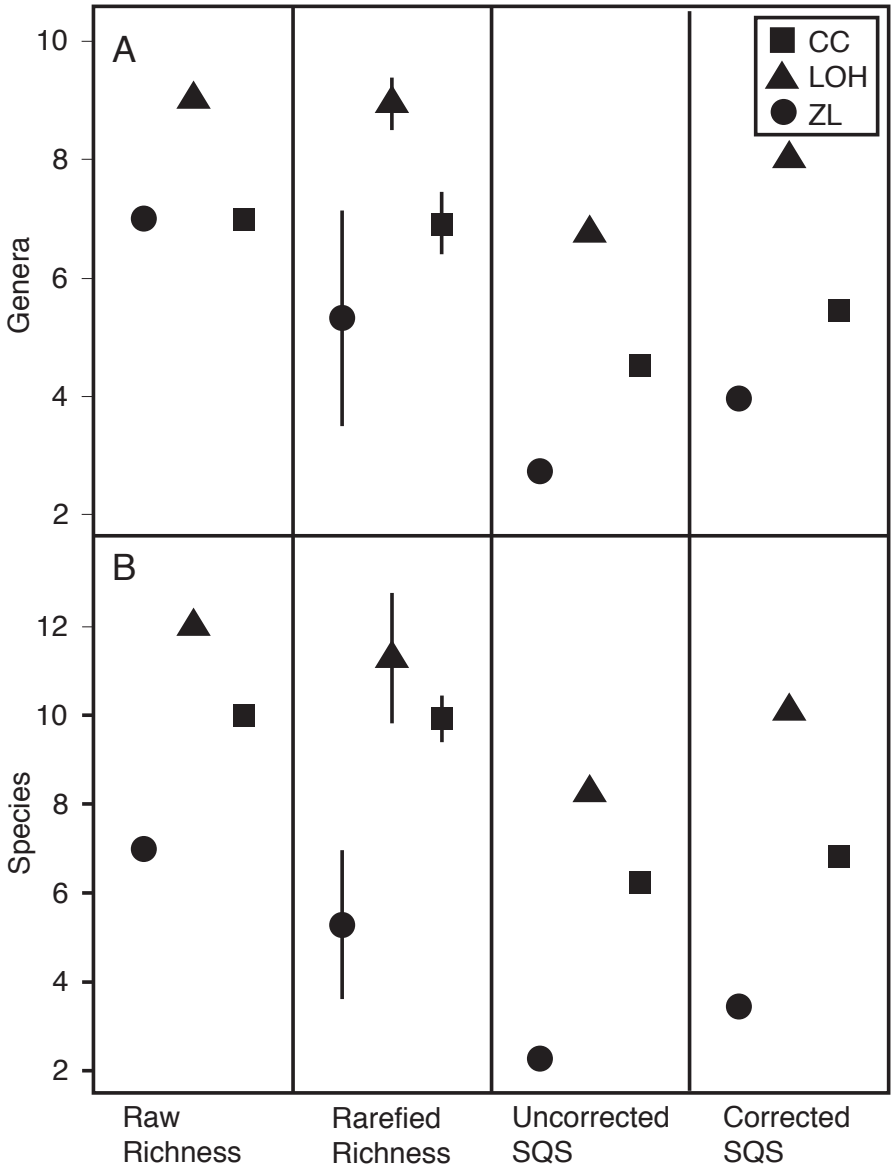

Figure 3.4 Raw, rarefied, and SQS richness for McGuire Creek mammalian assemblages, at genus level (A) and species level (B). Rarefied richness values are shown with 95% confidence intervals (calculated using standard error). Uncorrected SQS values were obtained by sampling the entire assemblage, whereas corrected SQS values were obtained using Alroy's (2010) evenness correction. Abbreviations: ZL = Z-Line; LOH = Luck O Hutch; CC = Coke's Clemmys.

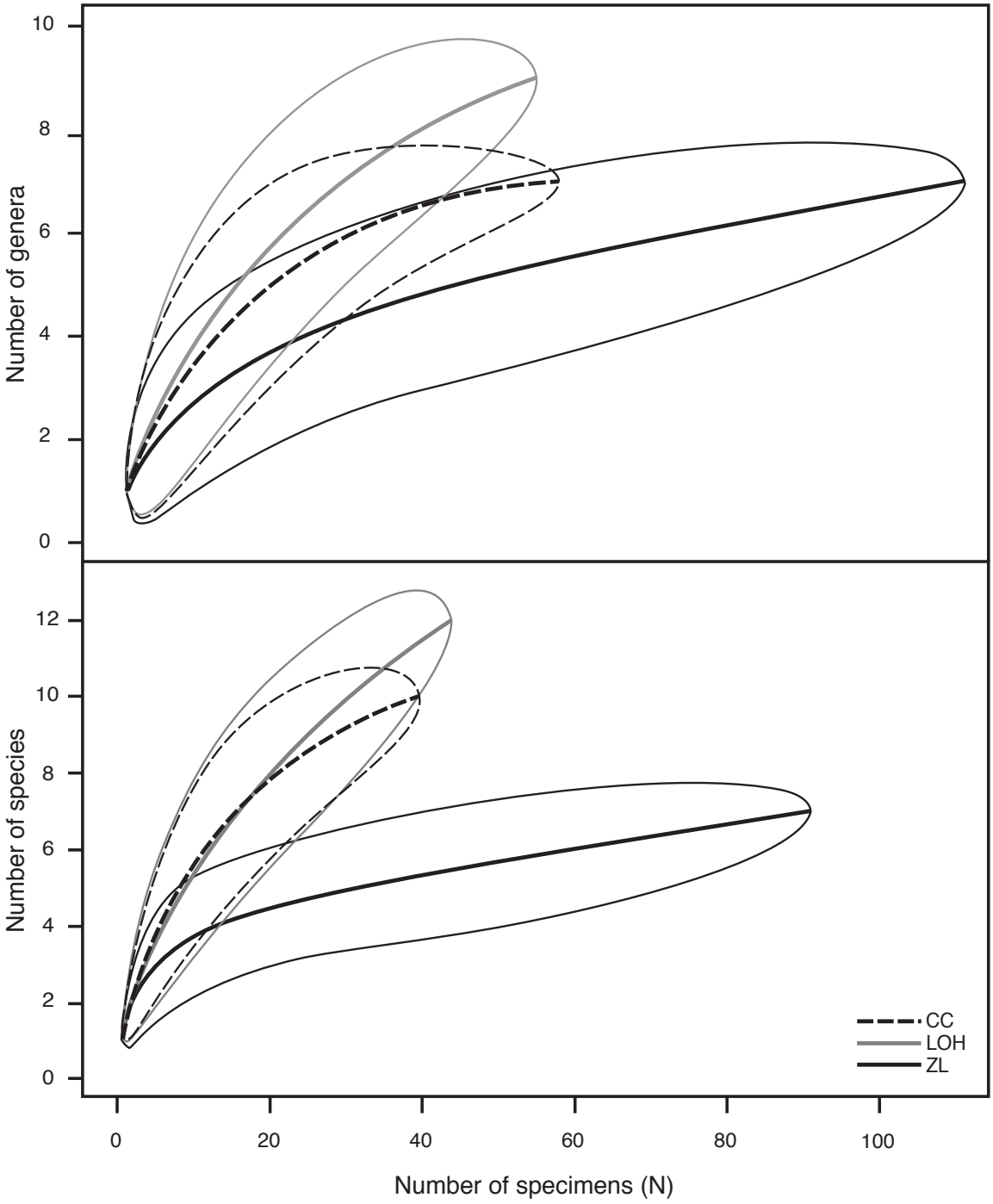

Figure 3.5 Rarefaction curves with 95% confidence intervals for McGuire Creek assemblages at genus-level (top) and species-level (bottom). Abbreviations: ZL = Z-Line; LOH = Luck O Hutch; CC = Coke's Clemmys.

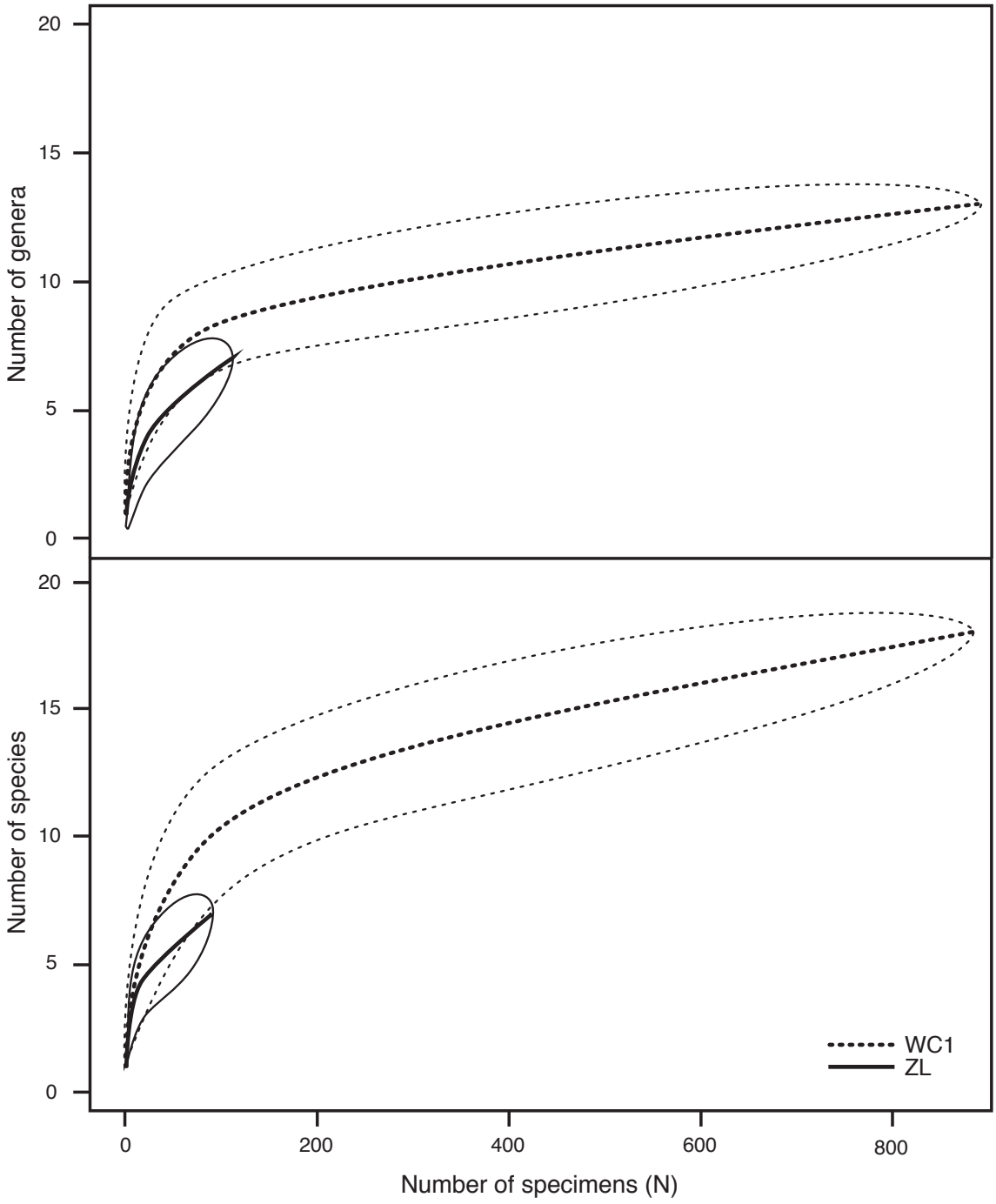

Figure 3.6 Rarefaction curves with 95% confidence intervals for Z-Line assemblage and Worm Coulee 1 assemblage, at genus-level (top) and species-level (bottom). Abbreviations: ZL = Z-Line; WC1 = Worm Coulee 1.

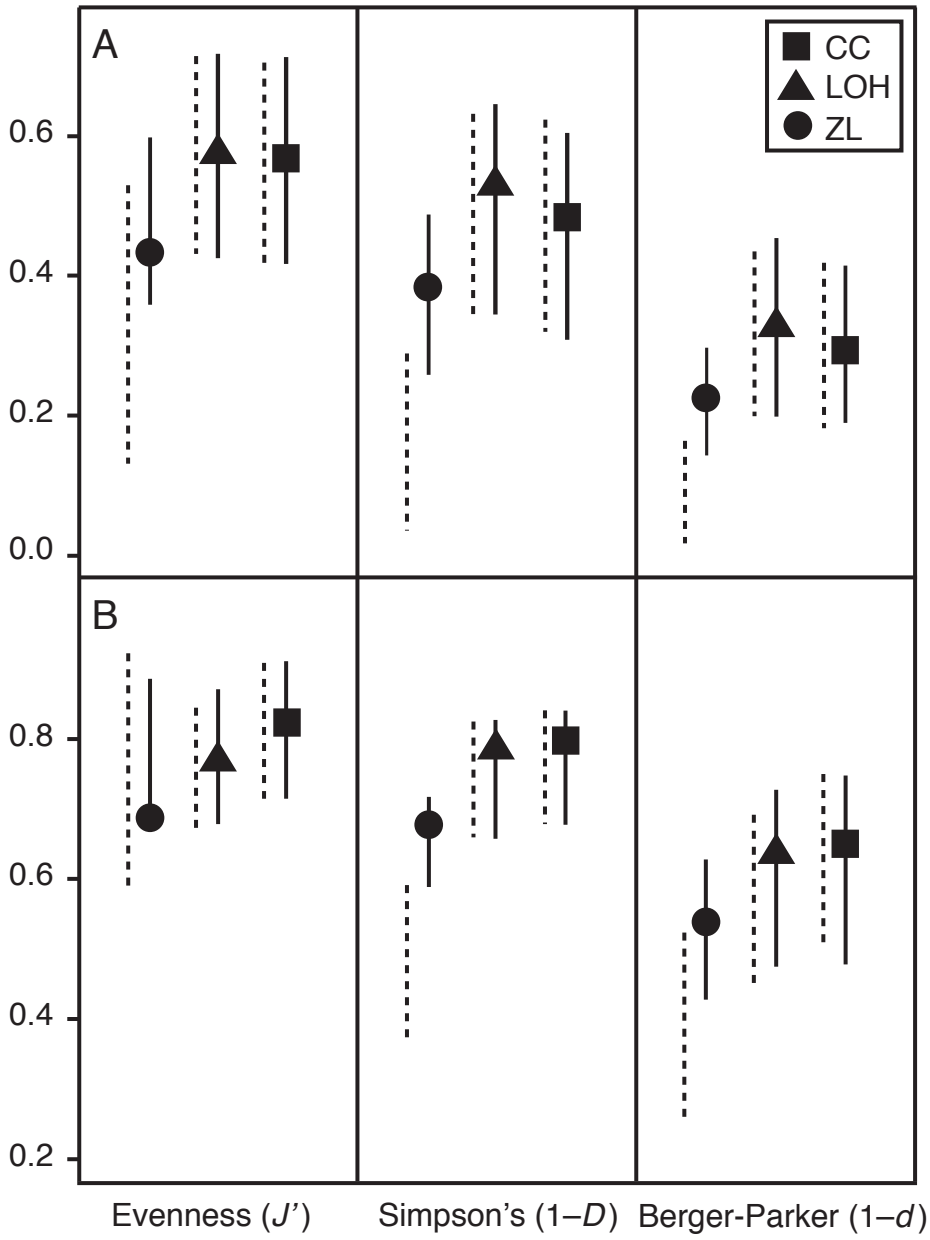

Figure 3.7 Evenness and dominance for McGuire Creek mammalian assemblages, at genus level (A) and species level (B). All values are shown with 95% confidence intervals obtained from 1000 bootstrap replicates. Dotted lines are bootstrap replicates conducted at sampling level for least well-sampled locality (N = 55 for A, N = 40 for B). Abbreviations: ZL = Z-Line; LOH = Luck O Hutch; CC = Coke's Clemmys.

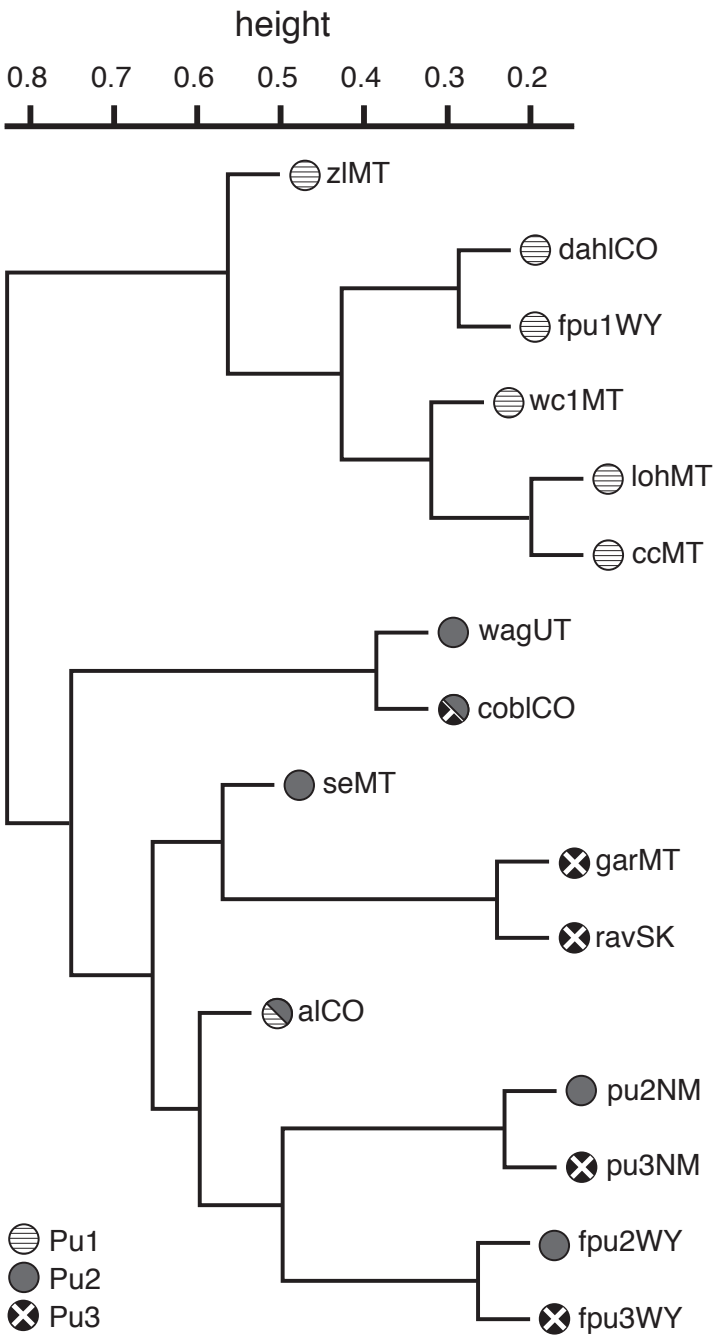

Figure 3.8 Dendrogram of North American mammalian faunas constructed using Sørensen-Dice (S-D) dissimilarity and UPGMA. Abbreviations for faunas are listed in Table 3.6. Filled circles next to the name of each fauna denote NALMA. Split circles indicate a transitional fauna (e.g., Pu2–3).

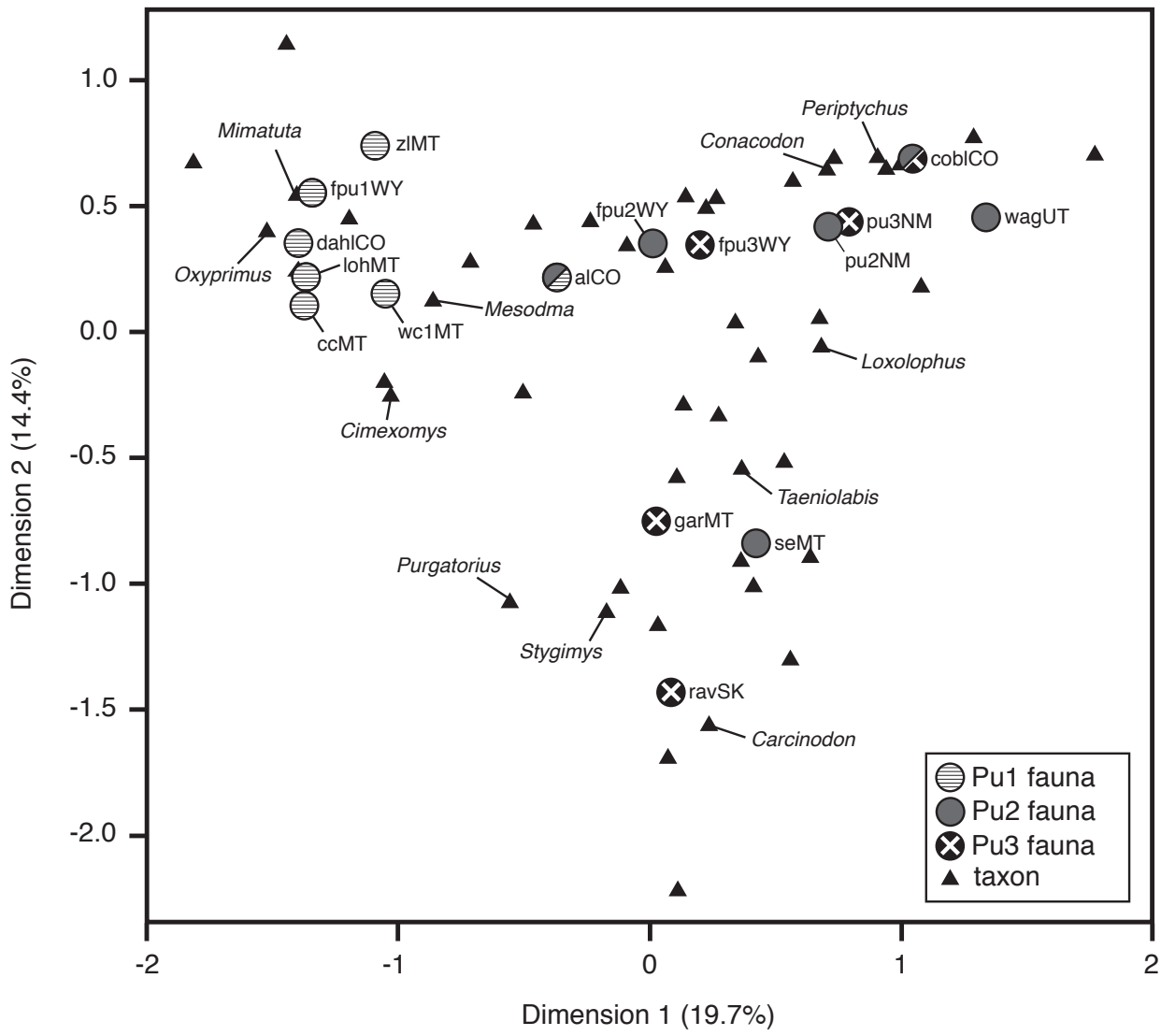

Figure 3.9 Correspondence analysis of North American mammalian faunas. Abbreviations for faunas are listed in Table 3.6. Filled circles next to the name of each fauna correspond to NALMA. Split circles indicate a transitional fauna (e.g., Pu2–3).

3.12 TABLES

Table 3.1 Relative abundance of mammals present at McGuire Creek fossil localities. Raw values are listed first, followed by relative abundance in parentheses. Also included for convenience are combined values for the complete Z Line assemblage (both ZLQ and ZLE).

Genus or family	species	V84193 (ZLQ)	V84194 (ZLE)	ZLQ + ZLE (ZL)	V88036 (LOH)	V88046 (CC)
Multituberculata						
Mesodma	*hensleighi*	-	-	-	1 (0.02)	3 (0.05)
Mesodma	*formosa*	11 (0.35)	16 (0.19)	27 (0.23)	11 (0.20)	9 (0.16)
Mesodma	*thompsoni*	12 (0.39)	30 (0.35)	42 (0.36)	16 (0.29)	14 (0.24)
Mesodma	sp.	3 (0.10)	14 (0.16)	17 (0.15)	9 (0.16)	15 (0.26)
Cimexomys	*minor*	-	-	-	1 (0.02)	2 (0.03)
Cimexomys	*gratus*	-	-	-	3 (0.05)	1 (0.02)
Metatheria						
Thylacodon	*montanensis*	-	10 (0.12)	10 (0.09)	-	-
?*Leptalestes*	*cooki*	-	1 (0.01)	1 (0.01)	-	-
Alphadontidae	indet.	-	2 (0.02)	2 (0.02)	-	-
Metatheria	indet.	-	4 (0.05)	4 (0.03)	-	-
Eutheria						
Procerberus	*formicarum*	3 (0.10)	6 (0.07)	9 (0.08)	1 (0.02)	4 (0.07)
Procerberus	cf. *grandis*	-	-	-	2 (0.04)	-
?*Ambilestes*	*cerberoides*	-	1 (0.01)	1 (0.01)	-	-
?*Prodiacodon*	*crustulum*	-	-	-	1 (0.02)	-
Protungulatum	*donnae*	-	-	-	4 (0.07)	1 (0.02)
Oxyprimus	*erikseni*	-	-	-	2 (0.04)	2 (0.03)
Baioconodon	sp.	-	-	-	1 (0.02)	-
Mimatuta	*morgoth*	-	-	-	1 (0.02)	-
Mimatuta	*minuial*	-	-	-	-	1 (0.02)
Mimatuta	sp.	2 (0.06)	1 (0.01)	3 (0.03)	1 (0.02)	3 (0.05)
Periptychidae	indet.	-	-	-	1 (0.02)	-
Purgatorius	cf. *coracis*	-	-	-	-	3 (0.05)
TOTAL N		31	85	116	55	58

Table 3.2 Genus-level richness for McGuire Creek localities. Richness estimated by SQS and rarefaction (see Methods for details). For uncorrected SQS, q = 0.9; for corrected SQS, q = 0.8; for rarefaction, N = 54 specimens. All specimens not identified to at least genus were excluded. Rarefaction curves are shown in Figure 4A.

Assemblage	N	Raw Richness	Good's u		Subsampled Richness		Rarefied Richness
			uncorrected	corrected	uncorrected	corrected	
ZLE + ZLQ	111	7	0.97	0.88	2.73	3.96	5.32
LOH	55	9	0.95	0.83	6.76	8.04	8.95
CC	58	7	0.98	0.94	4.53	5.43	6.93

Table 3.3 Species-level richness for McGuire Creek localities. Richness estimated by SQS and rarefaction (see Methods for details). For uncorrected SQS, q = 0.8; for corrected SQS, q = 0.75; for rarefaction, N = 39 specimens. All specimens not identified to species were excluded. Rarefaction curves are shown in Figure 4B.

Assemblage	N	Raw Richness	Good's u		Subsampled Richness		Rarefied Richness
			uncorrected	corrected	uncorrected	corrected	
ZLE + ZLQ	91	7	0.97	0.94	2.48	3.46	5.28
LOH	44	12	0.86	0.78	8.24	10.11	11.30
CC	40	10	0.93	0.88	6.25	6.85	9.93

Table 3.4 Genus- and species-level richness for Worm Coulee 1 and Z Line localities. Richness estimated by SQS and rarefaction (see Methods for details). For uncorrected SQS, q = 0.95; for corrected SQS, q = 0.85 for genus-level, q = 0.90 for species-level. For rarefaction, N = 110 specimens for genus-level, 90 specimens for species-level. Rarefaction curves are shown in Figure 5.

Assemblage	N	Raw Richness	Good's u		Subsampled Richness		Rarefied Richness
			uncorrected	corrected	uncorrected	corrected	
Genus-level							
ZLE + ZLQ	111	7	0.97	0.88	3.81	4.35	6.97
WC1	883	13	0.99	0.99	6.44	4.51	8.57
Species-level							
ZLE + ZLQ	91	7	0.96	0.97	4.12	3.52	6.97
WC1	883	18	0.99	0.99	8.33	7.08	10.00

Table 3.5 Dissimilarity among McGuire Creek localities. Upper triangle is Bray-Curtis Measure; lower triangle is Canberra Metric.

	Genus-level			Species-level		
	ZL	LOH	CC	ZL	LOH	CC
ZL	-	0.74	0.65	-	0.82	0.76
LOH	0.81	-	0.37	0.88	-	0.48
CC	0.77	0.47	-	0.84	0.56	-

Table 3.6 North American Puercan mammal faunas included in cluster analysis (Fig. 8) and correspondence analysis (Fig. 9).

Name	Abbrev.	Formation	State/ Province	References	NALMA
Alexander Locality	alCO	Denver (Denver Basin)	Colorado	Middleton 1983; Eberle 2003	Pu1/Pu2
Coke's Clemmys	ccMT	Tullock Mbr. (Williston Basin)	Montana	This study	Pu1
Corral Bluffs	coblCO	Denver (Denver Basin)	Colorado	Eberle 2003	Pu2/Pu3
DMNH 2560	dahlCO	Denver (Denver Basin)	Colorado	Dahlberg et al. 2016	Pu1
Ferris Pu1	fpu1WY	Ferris (Hanna Basin)	Wyoming	Eberle and Lillegraven 1998; Lillegraven and Eberle 1999	Pu1
Ferris Pu2	fpu2WY	Ferris (Hanna Basin)	Wyoming	Eberle and Lillegraven 1998; Lillegraven and Eberle 1999	Pu2
Ferris Pu3	fpu3WY	Ferris (Hanna Basin)	Wyoming	Eberle and Lillegraven 1998; Lillegraven and Eberle 1999	Pu3
Garbani Channel	garMT	Tullock Mbr. (Williston Basin)	Montana	Wilson 2014	Pu3
Harley's High Luck O Hutch	lohMT	Tullock Mbr. (Williston Basin)	Montana	This study	Pu1
Nacimiento Pu2	pu2NM	Nacimiento (San Juan Basin)	New Mexico	Sloan 1981; Williamson 1996; Clemens and Williamson 2005	Pu2
Nacimiento Pu3	pu3NM	Nacimiento (San Juan Basin)	New Mexico	Sloan 1981; Williamson and Lucas 1993; Williamson 1996	Pu3
Ravenscrag W-1	ravSK	Ravenscrag (Cypress Hills Plateau)	Saskatchewan	Johnston and Fox 1984; Fox 1990; Fox and Youzwyshyn 1994; Fox et al. 2010; Fox et al. 2011	Pu3
Hiatt Local	seMT	Fort Union (Williston Basin)	Montana	Hunter et al. 1997	Pu2
Wagonroad	wagUT	North Horn (Wasatch Plateau)	Utah	Gazin 1941; Robison 1986	Pu3
Worm Coulee 1	wc1MT	Tullock Mbr. (Williston Basin)	Montana	Wilson 2014	Pu1
Z-Line	zlMT	Hell Creek (Williston Basin)	Montana	This study	Pu1

3.13 APPENDIX: MAMMALIAN SYSTEMATICS

3.13.1 MATERIALS AND METHODS

Dental terminology, conventions, and measurements. Lower premolars and molars are denoted in the text, tables, and figures with lowercase letters (m1). Upper premolars and molars are denoted with uppercase letters (M1). General directional terms used are shown in Figure 3.13.1. We follow the multituberculate dental terminology of Kielan-Jaworowska et al. (2004). Although both Clemens (1963) and Kielan-Jaworowska et al. (2004) acknowledge the fact that cimolodontan multituberculates have four upper premolars that are probably homologous to P1–P3 and P5 of plagiaulacidans, we refer to the ultimate upper premolar as P4 for convenience in comparing with the majority of the systematic literature. Cusp numbers on premolars and molars are listed in order from labial to lingual rows, separated by colons (7:9:4). "R" denotes the presence of a continuous ridge instead of a row of separate cusps (3:3:R).

For therian dental terminology, we follow Bown and Kraus (1979), Van Valen (1994), and Salles (1996). Metatherian stylar cusps are designated A–E after Clemens (1966). O'Leary et al. (2013) proposed a new set of homologies for metatherian and eutherian molars. In their scheme, metatherians having three premolars (P/p1, P/p2, and P/p4, with P/p3 lost in more basal forms), a deciduous P/p5 in the place of what is traditionally termed an M/m1, and three molars (M/m1–M/m3); eutherians have P/p1, P/p2, P/p4, and P/p5, plus three molars (M/m1–M/m3). As with the multituberculate hypotheses above, we accept the dental homology hypotheses of O'Leary et al. (2013), but retain the traditional designations for metatherian (P/p1–P/p3, M/m1–M/m4) and eutherian (P/p1–P/p4, M/m1–M/m3) teeth in our systematics for convenience. Many descriptions

here incorporate comparative voucher specimens in publications or in the form of epoxy casts; these voucher specimens are listed in Table 3.13.1.

Dental measurement schemes are shown in Figure 3.13.1. Multituberculate P4 and p4 measurements follow Novacek and Clemens (1977); multituberculate molar measurements follow Lillegraven and Bieber (1986). Therian dental measurements follow Archibald (1982), with some slight terminology adjustments (see Fig. 3.13.2; Archibald, 1982: fig. 1). All measurements were taken using a Leica MZ9.5 binocular dissecting microscope, with a custom measuring stage precise to 0.001 mm. When taking measurements of therian and multituberculate teeth in occlusal view, specimens were oriented so that the occlusal plane was parallel to the microscope stage. Multituberculate p4 specimens were aligned such that the entire labial aspect of the crown was in the same focal plane.

Specimen photography. Prior to photographing, specimens were cleaned with water and a soft bristle brush, air dried, and dusted with magnesium to reduce glare and show details. In some cases, poor preservation has rendered a specimen exceedingly fragile; such specimens, especially very small specimens, were not cleaned or dusted, to prevent accidental breakage. Specimens were photographed using one of three setups: i) a Leica MZ9.5 binocular dissecting microscope and Clemex Vision Captiva version 7.0.7; ii) a Canon EOS 5DS DSLR camera body with Canon 100mm f2.8 Macro EF IS USM lens; or iii) a Canon EOS 7D Mark II DSLR camera body with attached Dun Inc. microscope body and 5X Mitutoyo microscope objective. In setups ii) and iii), the camera body was attached to a Dun Inc. P-51 Cam-Lift, and multiple-slice capture was executed with Phase One Capture One Pro 9.2; slices were stacked with Zerene Stacker

Professional, and scale bars added using camera- and lens-specific profiles in Adobe Photoshop CS6 Extended.

Institutional abbreviations

KU, University of Kansas Museum of Natural History; **LACM**, Natural History Museum of Los Angeles County; **RAM**, Raymond M. Alf Museum of Paleontology; **RSM**, Royal Saskatchewan Museum; **UA**, University of Alberta Paleontological Collections; **UM**, University of Michigan Museum of Paleontology; **UCMP**, University of California Museum of Paleontology; **USNM**, Smithsonian Institution National Museum of Natural History; **UWBM**, University of Washington Burke Museum of Natural History and Culture.

3.13.2 SYSTEMATIC PALEONTOLOGY

MAMMALIA Linnaeus, 1758

ALLOTHERIA Marsh, 1880

MULTITUBERCULATA Cope, 1884

PTILODONTOIDEA Sloan and Van Valen, 1965

NEOPLAGIAULACIDAE Ameghino, 1890

MESODMA Jepsen, 1940

MESODMA HENSLEIGHI Lillegraven, 1969

(Table 3.13.2)

Referred material—**V88036:** m2: RAM 6410. **V88046**: M2: RAM 4069; UWBM 106319, 106321.

Description and Discussion—In overall morphology, including cusp formulae and shape, these teeth match descriptions of *Mesodma* (Clemens, 1964; Novacek and Clemens, 1977; Archibald, 1982). We refer these teeth to *M. hensleighi* on the basis of their exceptionally small size, which is in the range reported by Lillegraven (1969).

MESODMA FORMOSA Marsh, 1889

(Tables 3.13.3, 3.13.4)

Referred material—**V84193:** p4: UCMP 132296; m1: UCMP 144280, 144281; m2: UCMP 144285; M2: UCMP 144286, 144287, 144289, 144290, 144292, 144293, 145217. **V84194:** p4: UCMP 134615, 239283, 239317, 239285; m2: UCMP 143659, 143663, 145158; M2: UCMP 143660, 143661, 143664, 143665, 145170, 239299, 239306, 239312, 239314. **V88036:** p4:

RAM 4044, 6408; m1: RAM 6384; m2: RAM 4033, 6403, UWBM 106216; P4: RAM 4034, 6398; M1: RAM 4060; M2: RAM 4021, 6392, 6404. **V88046:** p4: RAM 4112; m1: UWBM 105818; m2: RAM 4116, 4126, UWBM 105817, 105820; M2: UWBM 105821, 105870.

Description and Discussion—Like the listed specimens of *M. hensleighi*, these teeth match Clemens' (1964) descriptions of the morphology of *Mesodma* and are identified as *M. formosa* on the basis of size. Although previous studies (Clemens, 1964; Novacek and Clemens, 1977; Archibald, 1982) have attempted to differentiate *M. formosa* from congeners using the shape of the lower p4 (with *M. formosa* having a more "domed" appearance in labial view), Smith and Wilson (2016) showed that even when quantified, this characteristic does not allow for differentiation of *M. formosa* from other species. All teeth identified here are unambiguously within the size range of *M. formosa* to the exclusion of *M. thompsoni* and *M. hensleighi* based on published measurements (Clemens, 1964; Novacek and Clemens, 1977; Webb, 2001).

MESODMA THOMPSONI Clemens, 1964

Mesodma garfieldensis Archibald, 1982

(Tables 3.13.5, 3.13.6; Figure 3.13.2)

Referred material—**V84193:** p4: UCMP 132293, 132295; m1: UCMP 144282, 144283, 144284; P4: UCMP 132287, 132288, 132289, 132290; M1: UCMP 132292, 134611, 134613. **V84194:** p4: UCMP 132297, 132298, 134614, 145159, 239281, 239282, 239284, 239382, 239383; m1: UCMP 239307; dentary with p4–m1: UCMP 132304; P4: UCMP 134616, 145167, 239294, 239295, 239300, 239309, 239323, 239353, 239354, UWBM 106185, 106186; M1: UCMP 239279, 239280, 239291, 239292, 239308, 239315, 239324; M2: UCMP 145171. **V88036:** p4:

RAM 4025; m1: RAM 4041, 4043; P4: RAM 4026, 4032, 6377, 6406, 18581, 18582; m2: RAM 4061; M1: RAM 4063, 6400, 6402, 18577, 18586, UWBM, 105867. **V88046:** p4: RAM 4067, 4104, UWBM 106180; P4: RAM 4070, 4099, 4111, 4122; M1: RAM 4095, 4105, 4108, 4117, 4124, UWBM 106179, 106181.

Description and Discussion—As in *Mesodma hensleighi* and *M. formosa* specimens listed here, these teeth match previously described morphology of the genus *Mesodma* (Clemens 1964) and fall in the correct size range to be *M. thompsoni* (Clemens, 1964; Novacek and Clemens, 1977; Archibald, 1982; Smith and Wilson, 2016). It is important to note that the size range for teeth we recognize as *M. thompsoni* overlaps considerably with the size range of teeth previously attributed to *M. garfieldensis* (Archibald, 1982), now a junior synonym of *M. thompsoni* (Smith and Wilson 2016).

MESODMA SP.

Referred material—**V84193:** M1: UCMP 134612; M2: UCMP 144288; 144291. **V84194:** m1: UCMP 143662, 145161, 145162, 145163, 239287, 239288, UWBM 106183; P4: UCMP 239296, 239301, 239310, 239319; M1: UCMP 145168, 239293, UWBM 106182. **V88036:** p4: RAM 18584; m1: RAM 4051, 6395, 6407, 4113; M2: RAM 4052, 6409, 18579, UCMP 239391. **V88046**: p4: RAM 4068, 4076, UWBM 105824; m1: RAM 4098, 4100, 4093, UWBM 105822, 105827; P4: RAM 4109, 4121; M1: UWBM 105828; M2: RAM 4085, 4094, 4115, 4120.

Description and Discussion—We refer these specimens to *Mesodma* sp. because although they bear morphology that clearly affiliates them with the genus (Clemens, 1964), they are either 1) in

a range of size overlap between two species, or 2) broken or worn in such a way that it is impossible to obtain the necessary measurements to identify them to species level. The heavy reliance on size for species-level identification in this genus is problematic with samples including large numbers of incomplete teeth (see Lofgren, 1995; Webb, 2001).

INCERTAE SEDIS

CIMEXOMYS Sloan and Van Valen, 1965

CIMEXOMYS GRATUS Jepsen, 1930

Cimexomys hausoi Archibald, 1982

(Table 3.13.7, Figure 3.13.3)

Referred material—**V88036:** m1: RAM 6387; M1: RAM 18585; M1 distal fragment: RAM 4053. **V88046:** m1: UWBM 105826.

Description and Discussion—m1: RAM 6387 (Fig. 3.13.3A) has a cusp formula of 6:4. The crown is moderately worn, with a distinct wear facet on the labial side of the external cusp row. UWBM 105826 has a cusp formula of 6:3 but is broken at the distal end and may be missing cusps from both the lingual and labial rows. However, crown morphology, cusp morphology, and crown size for both m1s match those of *C. gratus* (Archibald, 1982; Lofgren, 1995; and casts, Table 3.13.1). Specific characters that ally these teeth with *C. gratus* include: cusps that are pyramidal in shape; closely appressed labial cusps that decrease in size towards the mesial end of the crown, and form a relatively continuous ridge that curves mesiolabially; and small grooves on the lingual side of the lingual cusps. RAM 6387 is slightly shorter than the observed range listed by Archibald (1982: table 16; L = 3.35–3.58 mm); both UWBM 105826 and RAM 6387 are well within the range of widths reported for *C. gratus* (Archibald, 1982: table 16).

Additionally, both specimens are too small to be representatives of *C. joyneri* or *C. foliatus* (Archibald, 1982: 71), but too large to be specimens of *Mesodma thompsoni* (Table 3.13.6) or *C. judithae* (Montellano et al., 2000: table 1).

M1: RAM 4053 (Fig. 3.13.3B) is a fragment of the distal end of the crown (W = 2.03 mm) that preserves three longitudinal rows of cusps: three in the labial row, six in the medial row, and a lingual ridge extending mesially from the distalmost end of the tooth for the length of the three distalmost medial cusps. RAM 18585 is a fully intact but heavily worn M1 with a cusp formula of 5:6:R. The morphology of these specimens matches the description for *C. gratus* by Lofgren (1995) and they are within the width and length ranges of specimens of *C. gratus* described therein. The presence of the lingual ridge on these teeth clearly separates them from similarly sized species of *Stygimys*, *Mesodma* and *Catopsalis.* Although there are morphological similarities between these M1s and those of *Cimexomys judithae*, RAM 4053 and 18585 are considerably larger than the size range for M1s of *C. judithae* (W = 1.12–1.20 mm; Montellano et al., 2000: table 1).

CIMEXOMYS MINOR, Sloan and Van Valen 1965

Referred material—**V88036:** P4: RAM 18588; M1: RAM 278. **V88046:** M1 distal fragment: UWBM 105819.

Description and Discussion—P4: RAM 18588 is a complete P4 (L = 2.20 mm; W = 1.20 mm) with cusp formula 3:5:2. Cusp number, as well as relative cusp size, location, and morphology in all three cusp rows matches Archibald's (1982: p. 103) description of P4s of *Cimexomys minor*, and the tooth closely resembles UCMP 116986 (Archibald, 1982: fig 35a–c). Although RAM

18588 is slightly smaller than Archibald's observed range for length and width of *C. minor* (1982: table 15), it is within the size range reported for *C. minor* P4s from McGuire Creek localities (Lofgren, 1995: table 19). RAM 18588 can be distinguished from similarly sized specimens of *Mesodma formosa* by its larger number of labial cusps, smaller number of cusps in the medial row, and the presence of a lingual cusp row, which is typically absent in *M. formosa* (Clemens, 1964; Archibald, 1982).

M1s: UWBM 105819 is a distal fragment of an upper M1 (W = 1.205 mm). It has three rows of cusps, with three visible in both the labial and medial rows, although there were likely more in both rows when the tooth was intact. The lingual "cusp row" is formed by a ridge, which extends mesially from the mesial end of the distalmost cusp in the medial row to the mesial edge of the third medial cusp from the distal end. There is a break on the distolabial side of the tooth that may have been the position of another external cusp (for a total of at least 4). RAM 278 is a complete M1 (L = 2.60 mm; W = 1.40 mm) with cusp formula 4–6:7:R. Labial row cusp numbers are not exact because the distalmost cusp is tiny and closely appressed to the cusp mesial to it, and the mesialmost cusp is mesiodistally elongate and ridgelike with two small bumps present, such that the row may be interpreted as having between 4 and 6 cusps. The lingual ridge has a similar mesiodistal extent to that of UWBM 105819. The cusps of the medial row, which increase in size from the mesial end of the tooth to the distal end, are closely appressed and separated by narrow slit-like gaps, forming a chisel-shaped ridge. UWBM 105819 and RAM 278 both resemble UCMP 73863, an upper M1 of *Cimexomys minor* from its type locality (Bug Creek Anthills; UCMP V65127), in shape and size of the crown, as well as relative size of the external and medial cusps and lingual ridge. Like *Cimexomys gratus*, M1s of *C. minor*

are distinct from similarly sized specimens of *Mesodma* via the lingual ridge and smaller number of cusps in the labial and medial rows (Sloan and Van Valen, 1965).

METATHERIA Huxley, 1880

MARSUPIALIFORMES Vullo et al., 2009

ALPHADONTIDAE Marshall et al., 1990

ALPHADONTIDAE GEN. ET. SP. INDET

(Figure 3.13.4)

Referred material—**V84194:** m1: UCMP 239334; MX labial fragment: UCMP 239349.

Description and Discussion—m1: UCMP 239334 (Fig. 3.13.4C–D) is a lower molar of a small metatherian (L = 1.82 mm; TriW = 1.11 mm; TalW = 1.18 mm). The trigonid is narrower than the talonid, with the paraconid and metaconid widely separated mesiodistally. This morphology indicates that the tooth is likely an m1. All three trigonid cusps are heavily worn such that it is impossible to tell what their relative heights would have been in an unworn state. The talonid is mesiodistally shorter than the trigonid, and preserves a tall, conical entoconid and a low, worn hypoconid. The distalmost portion of the talonid, which would bear the hypoconulid, is broken off, but the shape of the talonid indicates that the entoconid and hypoconulid were twinned. The cristid obliqua extends from the hypoconid, which is the lowest cusp of the talonid, to a point on the postvallid wall directly below the protocristid notch. This character state indicates that the tooth does not represent a member of the Pediomyidae or Glasbiidae, but is likely a member of Alphadontidae or the genus *Nortedelphys* (Clemens, 1966:83; Davis, 2007; Case et al., 2005; Williamson et al., 2012).

Alphadontids with m1s similar in size to UCMP 239344 include *Varalphadon wahweapensis*, *Protalphadon*, and *Alphadon.* UCMP 239344 shares several characters with *Protalphadon lulli*: it is within the size range reported by Clemens (1966: table 17) and shows the same widely separated paraconid and metaconid and shortened talonid as *P. lulli* (Clemens, 1966: fig. 58). This is in contrast to *V. wahweapensis,* which does not have as mesiodistally compressed a talonid (Cifelli, 1990: fig. 3G, H, I). UCMP 239344 further resembles *P. lulli* in the configuration of its cingula, of which there are two: one extending from the anterolabial face of the trigonid around to end on the labial face of the protoconid, and another extending from the distal side of the hypoconid towards the distal end of the talonid where the hypoconulid would have been. *Alphadon marshi* has cingulae in the same two locations; indeed, Clemens (1966) was unable to find any differences between the lowers of *A. marshi* and *P. lulli* other than size (1966:90; table 18). Because UCMP 239344 bears no characters that definitively associate it with a particular genus of alphadontids, we refer it to Alphadontidae, genus and species indeterminate.

MX labial fragment: UCMP 239349 (Fig. 3.13.4A–B) is the labial side of an upper molar, preserving the labial margin, stylar shelf, paracone, and metacone. The tooth is broken lingual to the paracone and metacone. The locations of all stylar cusps are preserved, although cusp B is broken off at the base. Despite being broken, cusp B is the tallest of the stylar cusps. Cusp A is small but distinct, and is connected to a mesial cingulum which likely extended to the paraconule. Cusp D is large and ridgelike. There are two small cusps of subequal size situated mesiodistally between cusps B and D. They are closely appressed and conjoined at the base to form a ridgelike structure; they form a straight line with the ridge formed by stylar cusp D.

UCMP 239349 (L = 2.45 mm) is larger than *Pediomys elegans*, *Leptalestes cooki,* and *L. krejcii* (Clemens, 1966; Lillegraven, 1969). It is similar in size and, to some extent, in shape, to *Nortedelphys jasoni*, *Alphadon marshi,* and *Thylacodon montanensis*. It differs from teeth of *Nortedelphys jasoni* in the shape of the centrocrista and the labial shape of the paracone and metacone. *N. jasoni* has a distinctly V-shaped centrocrista (Storer, 1991; Williamson et al., 2012), which is not present on UCMP 239349. UCMP 239349 also does not exhibit a paracone and metacone that are strongly concave on the labial side (Storer, 1991). UCMP 239349 more closely resembles M3s of of *Alphadon marshi* described by Clemens (1966); in this description, Clemens noted that on some M3s, "two small cusps are present in the D position" (1966:p7), which is similar to the configuration of cusps on UCMP 239349. Clemens also noted that on M3s, stylar cusp C was always larger than stylar cusp D (1966). However, that is not the case in UCMP 239349, and Lillegraven (1969) and Archibald (1982) found that this was not the case on any specimens of *A. marshi* in their respective samples. UCMP 239349 is distinct from *A. marshi* in the location of these two small cusps. In *A. marshi*, the cusp(s) in position C show a lingual shift; they are not located on the extreme labial margin of the stylar shelf like cusps B and D. The C cusps in UCMP 239349 are not shifted lingually, but are located on the labial margin of the stylar shelf. This configuration resembles that of *Thylacodon montanensis*. UCMP 239349 is within size ranges reported by Archibald (1982) for both M1s and M2s of *T. montanensis*, but also shows a more indented ectoflexus than most specimens of *T. montanensis*; indeed, an indented ectoflexus is more characteristic of species of *Alphadon*, and is one of the characters Archibald suggests as useful for distinguishing *Alphadon* and *Thylacodon* (1982:132).

We refer UCMP 239349 to Alphadontidae, genus and species indeterminate, because of the unusual configuration of stylar cusps, as well as the fact that the lingual portion of the tooth is

missing, which precludes measurement of the relative width of the tooth, a feature used to distinguish *A. marshi* from *A. wilsoni* (Lillegraven, 1969; Archibald, 1982).

HERPETOTHERIIDAE Trouessart, 1879

THYLACODON Matthew and Granger, 1921

THYLACODON MONTANENSIS, Williamson et al., 2012

Peradectes cf. *P. pusillus* Archibald, 1982

(Table 3.13.8, Figure 3.13.5)

Referred material—**V84194:** m2: UCMP 239305; m1 or 2 (fragmentary): UCMP 239337; m2 or 3 (fragmentary): UCMP 239304, 239340; m4: UCMP 239333; mx talonid: UCMP 239367; mx trigonid: UCMP 239336; M1: UCMP 132299; M2: UCMP 132300; M4: UCMP 239350.

Description and Discussion—This material is referred to *Thylacodon montanensis* on the basis of thorough morphological descriptions provided by Archibald (1982), Lofgren (1995), and Clemens (2006).

Lower molars: The two lower molars referred here, which fall within previously reported size ranges for *T. montanensis*, suffered considerable postmortem breakage on the trigonid. However, the talonid characteristics preserved on these specimens allows for differentiation from other possible small metatherians, particularly *Alphadon*. On both specimens, the cristid obliqua meets the distal face of the trigonid below the protoconid, in contrast to the location of this contact below the protocristid notch in *Alphadon*. Additionally, both teeth exhibit the distinct notch between the entoconid and hypoconulid noted in *T. montanensis* by Clemens (2006). The width of the trigonid and talonid are subequal in UCMP 239305, making it likely an m2 or m3, while

the talonid of UCMP 239333 is considerably narrower than the trigonid (Table 3.13.8), making it more likely an m4 (Archibald, 1982; Clemens, 2006). These two lowers closely match morphology of *T. montanensis* from Garfield County (UCMP locality V74111; Table 3.13.1).

Fragmentary lower molars: Several lower molars included here are missing the lingual side of the talonid basin, and therefore the entoconid and hypoconulid. These fragmentary teeth, as well as the isolated trigonid referred here, are similar to UCMP 239305 in length and width of the trigonid, as well as labial morphology of the talonid basin and contact point between the cristid obliqua and the postvallid wall, and we therefore also refer them to *T. montanensis.* The trigonid width of UCMP 239337 makes it more likely an m1 or 2, whereas UCMP 239304, 239340, and 239336 have slightly wider trigonids and are likely m2s or 3s. UCMP 239367, the isolated talonid, is relatively narrow and probably belongs to an m4.

Upper molars: UCMP 132299 and 132300, (M1 and M2, respectively) which may be associated teeth from a single fragment of maxilla, were included by Lofgren (1995) as *Peradectes* cf. *P. pusillus* and by Williamson et al. (2012) as *T. montanensis,* and will not be discussed further here. The M4 (UCMP 239350, Fig. 3.13.5) is missing a small sliver of the mesial margin of the paracone, a region which would ordinarily include the paraconule. The metacone is also broken. This tooth does not appear to have the small accessory cusp between metacone and metaconule as noted by Archibald (1982), but this may be a result of the breakage of the metacone. The metaconule is present but is ridgelike and hard to distinguish from the postmetaconular wing. Stylar cusp A is the tallest stylar cusp; Cusp B is very low and ridgelike in comparison. This tooth compares well in size and morphology with an epoxy cast of UCMP 117771 from locality V74111 (Archibald, 1982).

PEDIOMYIDAE Simpson, 1927

LEPTALESTES Davis, 2007

?LEPTALESTES COOKI Clemens, 1966

Pediomys cooki Clemens, 1966

(Figure 3.13.6)

Referred material—**V84194:** M1 or 2: UCMP 239344.

Description and Discussion—UCMP 239344 (Fig. 3.13.6) is intact except for the paracone, metacone, and stylar cusp D, all of which are broken at the base. All other occlusal morphology is well-preserved and shows minor wear. Stylar cusp D is the largest based on the cross-sectional area of the broken base, and in labial view is equal in height to stylar cusp B despite being broken. There are two minute, ridgelike cusps between cusps B and D, one each directly mesial and distal of the ectoflexus. It is unclear which of these, if either, should be designated as stylar cusp C.

UCMP 239344 is smaller in both length and width (L = 1.94 mm, MW = 2.1 mm, DW = 2.48 mm) than uppers of *Thylacodon montanensis* (Archibald, 1982:table 24) and has smaller, less trenchant stylar cusps. It differs from *T. montanensis* further in its relatively narrow stylar shelf, especially labial to the paracone. The narrow stylar shelf of UCMP 239344 resembles that of both *Pediomys elegans* and *?Leptalestes cooki*, but the stylar cusps are smaller and less trenchant than those of *P. elegans*, particularly cusp C, which is large and distinct in *P. elegans* but very small or absent in ?*L. cooki* (Clemens, 1966). In length, width, and occlusal shape, UCMP 239344 compares well to UCMP 47738 (?*L. cooki*), pictured by Clemens (1966). Based on

overall size and the width of the stylar shelf labial to the paracone, we designate this tooth an M1 or M2.

METATHERIA INDET.

(Figure 3.13.7)

Referred material—**V84194:** mx: UCMP 239330; MX: UCMP 239372, 239373; M4: UCMP 239368.

Description and Discussion—mx: UCMP 239330 preserves the paraconid, hypoconid, and hypoconulid with light apical wear; the shape of the talonid indicates that the tooth is from a metatherian. The labial margin of the tooth and postcingulid are also intact. However, the metaconid, entoconid, and protoconid are broken off completely, as is most of the mesial portion of the tooth basal to the paraconid. This tooth is close in size to, but slightly larger than, *Thylacodon pusillus* (Williamson et al., 2012: table 1). However, the occlusal morphology is too fragmentary to confidently identify this tooth to genus or species level.

MX: One upper molar (UCMP 239372, Fig. 3.13.7C–D) preserves the paracone, metacone, and distal portion of the stylar shelf, including two cusps which are likely stylar cusps C and D because the more mesial of the two is located at the furthest indentation of the ectoflexus. Because the anterior portion of the stylar shelf, as well as the entire lingual side of the tooth, are both missing, this tooth cannot be identified past Metatheria. We include it here because of its unusually large size. It is larger than molars of *Thylacodon montanensis*, *Leptalestes cooki*, and our specimens of Alphadontidae indet., indicating the possibility of a fourth species of metatherian present in V84194. The other upper molar (UCMP 239373) resembles *T.*

montanensis in occlusal outline shape and size, but the occlusal surface of the tooth is worn nearly flat, precluding the identification of the tooth to the genus or species level. Because of its indistinct morphology, we refer UCMP 239373 to Metatheria indeterminate.

M4: UCMP 239368 (L = 2.23 mm, MW = 3.12 mm, DW = 2.14 mm; Fig. 3.13.7A–B) is a well-preserved, complete M4.The paracone is broken. The protocone is taller than the metacone, which is the smallest cusp at its base. The metaconule is longer and more ridgelike than the paraconule, which is more round in cross-section; the metaconule projects slightly higher apically above the postprotocrista than the paraconule projects above the preprotocrista. The stylar shelf bears seven small cusps. In order from mesial to distal, the first, second, fifth, and sixth cusps are distinctly larger than the third, fourth, and seventh, and may represent stylar cusps A, B, C, and D; nevertheless, the fifth and sixth cusps are appressed and may represent a doubled cusp C. The stylar shelf extends from what is likely cusp A to the posterolabial side of the metacone. There are no lingual cingulae (contrast with *Leptalestes cooki*; Clemens, 1966) and no clear ectoflexus, but the labial margin of the tooth is slightly s-shaped.

UCMP 239368 has more stylar cusps and is larger than M4s of *Thylacodon montanensis* (Archibald, 1982: table 24), including UCMP 239350, which is from the same locality, V84194 (described above). It is also larger than M4s of *Nortedelphys jasoni, Leptalestes cooki* (Davis, 2007: fig. 19), *L. krejcii* (Davis 2007: fig 15), and *Pediomys elegans* (Clemens, 1966: table 7), although its occlusal morphology, particularly the large number of stylar cusps, is similar to that of *P. elegans* M4s described and illustrated by Clemens (1966: figs. 21, 23). The tooth is smaller than M4s of *Protolambda florencae* (Davis, 2007) and *P. hatcheri* (Zhang, 2009: table 16). M4s of *Alphadon marshi* are only slightly smaller than UCMP 239368, but the metacone in *A. marshi* is much smaller relative to the paracone than the metacone in UCMP 239368 (based on

comparison with epoxy cast of UWBM 55475/UA 2846; Lillegraven, 1969: fig. 15, 3a–c). UCMP 239368 also does not show the lingual position of cusp C on the stylar shelf (rather than the ectocingulum) that is observed in *A. marshi* (e.g. UA 3376, Lillegraven, 1969: fig. 15, 2a–c). Because of the unusual suite of characters on this tooth and the limited comparative sample of M4s, we refer this tooth to Metatheria only.

EUTHERIA Huxley, 1880

CIMOLESTA McKenna, 1975

CIMOLESTIDAE Marsh, 1889

PROCERBERUS Sloan and Van Valen, 1965

PROCERBERUS FORMICARUM Sloan and Van Valen, 1965

(Table 3.13.9, Figure 3.13.8)

Referred material—**V84193:** m3: UCMP 132285, 145218; MX fragment: UCMP 132284. **V84194:** p4: UCMP 239302; m1: UCMP 239325; m2: UCMP 145149; P3: UCMP 239318; MX: UCMP 132305; M1: UCMP 134617. **V88036:** p4: RAM 6390. **V88046:** p4: RAM 4106; m1: RAM 4083, 18539; P3: RAM 4071.

Description and Discussion—p4s: RAM 4106 (Fig. 3.13.8) is a complete lower fourth premolar with a laterally compressed, mesiodistally elongate crown. All the cusps show moderate apical wear. The metaconid and protoconid are approximately twice as tall as the paraconid, with the protoconid slightly taller than the metaconid. The paraconid is completely separate from the metaconid and protoconid, with its base located basal to those of the metaconid and protoconid, and the paracristid bears a distinct notch. The hypoconid is larger than the hypoconulid; it is difficult to assess the exact size of the entoconid because it is broken more basally than the other

two, but is likely similar in size to the hypoconid. The tooth is similar in length to dp4s of *Puercolestes simpsoni* (Williamson et al., 2011) and *Cimolestes incisus* (Clemens, 1973), and slightly smaller than *C. stirtoni* (Clemens, 1973; Archibald, 1982), but the trigonid is narrower and more mesodistally elongate than in those taxa. In size and morphology, the tooth most closely resembles p4s of *Procerberus formicarum* (Lillegraven, 1969: table 15, fig. 32, 1a-c; Archibald 1982: table 39; Clemens, 2017). RAM 4106 differs from the morphology described by Lillegraven (1969) in that the distal ridge of the protoconid is not continuous with the cristid obliqua, but otherwise agrees with the morphology described in his table 15 and the text (p. 67–68). The description of the p4 of *P. formicarum* in the original description of the taxon (Sloan and Van Valen, 1965) is less detailed than that of Lillegraven (1969), but matches the morphology of RAM 4106. RAM 6390 compares well with RAM 4106, although its entire surface has been smoothed slightly by post-depositional wear. Additionally, it has a slightly narrower talonid than RAM 4106, and may have only had two talonid cusps, or possibly two large (entoconid and hypoconid positions) and one small (hypoconulid position) talonid cusps. This variation in number of p4 talonid cusps in *P. formicarum* has been noted by Lillegraven (1969) and Clemens (2017). A third p4, UCMP 239302, is missing the paraconid but is otherwise well preserved and approximates morphology of RAM 6390 and 4106. UCMP 239302 has a narrow talonid similar to that of RAM 6390, but it has three talonid cusps like RAM 4106. The talonid cusps, metaconid, and protoconid show less apical wear than in the other two specimens, and they appear slightly taller as a result.

Lower molars: RAM 4083 and 18539 are most likely m1s based on the similarity in width of the trigonid and talonid, and mesiodistal length between the paraconid and metaconid. RAM 4083 shows slight wear on the cusp tips and along the cristid obliqua. A large portion of the hypoconid

is missing, and the enamel is chipped off the distal face of the talonid. The rest of the talonid is intact, with a wear facet visible on the anterolingual face of the basin. On RAM 18539, the trigonid is very worn and the enamel is chipped off the labial face of the protoconid. The talonid is less worn than the trigonid, but the hypoconid and hypoconulid are worn enough to expose dentine. In UCMP 239325, also an m1, only the paraconid and hypoconid are completely intact; the metaconid, protoconid, entoconid, and hypoconulid are all broken off at the base. However, the relative positions of all cusps are discernible. The cristid obliqua is intact in both RAM 18539 and UCMP 239325 and both exhibit the "distinct bump" (= mesoconid) noted by Lillegraven (1969, p. 68), which distinguishes them from *Ambilestes cerberoides*. UCMP 145149 (m2) and 145218 (m3) show considerable wear on both trigonid and talonid. UCMP 132285 (m3) has well-preserved cusps with only slight wear, except the entoconid, which is broken at the base, and also exhibits the bump (mesoconid) on the cristid obliqua.

P3: RAM 4071 is fully intact and preserves sharp cusps with only slight apical wear. UCMP 239318 has similar morphology but considerably more post-depositional wear, such that the crests on the tooth, as well as the height at which the paracone and metacone conjoin, are unclear. The crown morphology of both teeth resembles P3s pictured by Van Valen (1969:fig. 3) and Lillegraven (1969:fig 32, views 2a, b, and c).

Upper molars: UCMP 134617 (M1) is well preserved, with cusps exhibiting minimal apical wear. Like Lillegraven (1969), we find that in this unworn condition, the protocone is slightly higher than the metacone, in contrast to the original taxon description given by Sloan and Van Valen (1965). UCMP 132305 is a posterolabial fragment preserving parts of the labial margin,

metacone and paracone. It matches size and morphology of the posterolabial portion of UCMP 134617.

Like Lofgren (1995), we find that morphology of *P. formicarum* in the McGuire Creek area corresponds to detailed descriptions provided by Sloan and Van Valen (1965) and Lillegraven (1969). We can offer no novel morphologies to add to their descriptions.

PROCERBERUS cf. *P. GRANDIS* Middleton and Dewar, 2004

(Figure 3.13.9)

Referred material—**V88036:** m1: RAM 4042; M2: UCMP 134570.

Description and Discussion—m1: RAM 4042 (Fig. 3.13.9B–D) is most likely an m1 based on the similarity in width of the trigonid and talonid, as well as the width of the mesiodistal separation between the paraconid and metaconid. Only one lower molar of *Procerberus grandis* is known (UCM 34955; Middleton and Dewar, 2004), which means that the size range for lower molars of this taxon is not known. Although it is similar in size to some lower molars of *Protungulatum donnae* (appendix 5: Archibald, 1982), RAM 4042 exhibits a relatively higher trigonid and relatively longer talonid basin than *P. donnae*. Additionally, the paraconid is very distinct from both the metaconid and protoconid, with a deep notch between the paraconid and protoconid, which is not present in *P. donnae*.

The tooth is worn on the anterolabial face of the hypoconulid and entoconid. The hypoconulid is missing, but the remaining enameled perimeter indicates that the hypoconulid and entoconid likely formed a single slanted wear facet. Any small accessory cuspids that may have existed

between the hypoconid and hypoconulid, as were noted by Middleton and Dewar (2004), were lost with the hypoconulid. However, there are two distinct accessory cuspids preserved in the talonid notch, with the distal cuspid slightly larger than the mesial cuspid.

RAM 4042 (L = 4.49 mm, WTri = 2.63 mm, WTal = 2.56 mm) is smaller than UCM 34955 ((L = 5.60 mm, WTri = 3.5 mm, WTal = 3.60 mm; Middleton and Dewar 2004). However, the 0.7 mm difference in length between the M2s reported by Middleton and Dewar (2004) indicates the possibility for significant intraspecific size variation. Clemens (2017) noted the presence of two distinct size morphs for *Procerberus* in several North American faunas, with *P. grandis* being the larger morph in the Littleton local fauna, and *P. andesiticus* being the smaller morph. The smaller morph in the McGuire Creek fauna is *P. formicarum*, which differs from *P. andesiticus* in several key features, including size. It is possible, then, that the size difference between RAM 4042 and UCM 34955 is indicative of belonging to different species. Because more material is necessary from both locations to determine intraspecific variation among these larger morphs of *Procerberus*, we refer this specimen to *Procerberus* cf. *P. grandis.*

M2: UCMP 134570 (Fig. 3.13.9A) is a large upper molar with much of the enamel missing from the occlusal surface. Paracone, metacone, and protocone are all clearly visible, but the conules are completely worn away. The occlusal outline of the tooth is mesiodistally narrow and triangular in shape, with a shallow ectoflexus. The paracone is very narrow and the tooth bears a narrow precingulum on the mesial side of the protocone; the distal side of the protocone has no remaining enamel. The weakness of the precingulum on the tooth distinguishes it from similarly sized archaic ungulates (e.g., *Protungulatum donnae*), which tend to have much wider cingulae. The relatively steep lingual slope of the protocone on UCMP 134570 distinguishes it from

species of *Mimatuta* and other periptychids. It matches descriptions of *Procerberus* cf. *P. grandis* provided by Clemens (2017) and Middleton and Dewar (2004). Like RAM 4042, it is smaller (L = 3.72 mm , MW = 5.33 mm, DW = 5.19 mm) than upper molars reported by Middleton and Dewar (2004); however, the length of UCMP 134570 may be a slight underestimate because of the broken metastyle. Additionally, UCMP 134570 is smaller than UCMP 137189, *P.* cf. *P. grandis* from the Harley's Palate locality located in the Tullock of Garfield County, Montana, but slightly larger than *P.* cf. *P. grandis* recovered from the Mantua Lentil Quarry in the Polecat Bench of Wyoming (Clemens, 2017: tables 2 and 3). We refer UCMP 134570 to *Procerberus* cf. *P. grandis* because of its similarity in morphology and size to these published occurrences from around the Western Interior.

AMBILESTES Fox, 2015

?*AMBILESTES CERBEROIDES* Lillegraven, 1969

Cimolestes cerberoides Lilleraven, 1969

(Figure 3.13.10)

Referred material—**V84194:** maxillary fragment with P3: UCMP 145148.

Description and Discussion—UCMP 145148 (Fig. 3.13.10) is a small fragment of maxilla containing a P3. The maxillary fragment shows extreme post-depositional wear such that no diagnostic morphology can be discerned; however, a single alveolus is present mesial to the preserved tooth. The tooth itself shows little wear. It does not have a clear metacone, but does have a slight swelling in the location on the distal face of the paracone where a metacone might be expected. Additionally, the postparacrista is worn flat near the apex of the protocone; if an incipient metacone was present, it was likely worn off. UCMP 145148 is comparable in length

(L = 2.83 mm) to P3s of *Protungulatum donnae* (Sloan and Van Valen, 1965: fig. 7, S.P.S.M. 62-2061), but is less labiolingually transverse (also compare to Van Valen, 1969: fig. 4). The tooth size and morphology compare well with the P3 of *Ambilestes cerberoides* contained within the type, UA 2973 (Lillegraven, 1969; Fox, 2015). The morphology is distinct from that of *Procerberus formicarum*, which usually has a distinct metacone, and does not exhibit a distal accessory blade (Lillegraven, 1969), a feature that is easily visible in UCMP 145148. There is no obvious ridge connecting the protocone to the lingual base of the paracone, which is sometimes present on *A. cerberoides*, but in all other morphological aspects, UCMP 145148 matches the original taxonomic description of Lillegraven (1969). We refer this specimen to ?*Ambilestes cerberoides*, because of the lack of association with molars that might corroborate such a specific identification.

LEPTICTIDA McKenna, 1975

LEPTICTIDAE Gill, 1872

PRODIACODON Matthew, 1929

?*PRODIACODON CRUSTULUM* Novacek, 1977

(Figure 3.13.11)

Referred material—**V88036:** MX: RAM 6412.

Description and Discussion—Although RAM 4088 only preserves the lingual side of the tooth, RAM 6412 (Fig. 3.13.11) exhibits several characters that associate it with the genus *Prodiacodon*. It is a complete upper molar that shows considerable wear, especially in the trigon basin and on the lingual side of the tooth. The parastylar lobe of the tooth is also broken, but the paracone, metacone, and metastylar lobe, as well as most of the stylar shelf, are well preserved.

The mesiodistal length the trigon compares well with that of *Prodiacodon crustulum* specimens figured by Novacek (1977) and Clemens (2015), and is considerably smaller than that of *Prodiacodon puercensis* (Novacek, 1977). In occlusal view, the shape of the crown is similar to other upper molars of *Prodiacodon crustulum*, and the precingulum bears the crenulation noted by Novacek (1977). However, because the postcingulum is missing, it is impossible to determine its transverse length; because of the wear on the labial face of the protocone and in the trigon basin, it is difficult to tell the distance of the conules from the three primary cusps, or if the tooth exhibits the "double paraconule" noted by Clemens (2015) and Novacek (1977). Because the state of these characters has been obscured by wear, we refer RAM 6412 to ?*Prodiacodon crustulum*. Dimensions: MW = 3.31 mm, DW = 3.12 mm.

UNGULATA Linnaeus, 1766

ARCTOCYONIDAE Giebel, 1855

PROTUNGULATUM Sloan and Van Valen, 1965

PROTUNGULATUM DONNAE Sloan and Van Valen, 1965

(Table 3.13.10)

Referred material—**V88036:** mx trigonid: RAM 6389, 6396; m3: RAM 6376; M2: RAM 4056. **V88046:** m1 or 2: UWBM 105816.

Description and Discussion—Lower molars: RAM 6389, 6396, and 6376, and UWBM 105816 are referred to *Protungulatum donnae* on the basis of size (Table 3.13.10), trigonid morphology, and comparison with epoxy casts of *P. donnae* from its type locality (Bug Creek Anthills, McCone County) and other McCone County localities (see Table 3.13.1: voucher specimens).

These teeth can be distinguished from those of *Oxyprimus erikseni* (below) by their larger size and more closely appressed paraconid and metaconid (Luo, 1991); they can be distinguished from the similarly sized genus *Mimatuta* by the more lingual position of the paraconid relative to a mesiodistal line drawn along the groove between metaconid and protoconid (Luo, 1991; Lofgren, 1995).

Upper molars: RAM 4056 is a lingual fragment, likely an M2, preserving the lingual margin and cingula, protocone, and conules. In size, angle of incline and length of the lingual slope of the protocone, and relative position of the protocone and conules, RAM 4056 compares well with epoxy casts of M2s from Bug Creek Anthills (Table 3.13.1). It differs slightly from previously observed morphologies in that the pre- and post-cingulae join via a very weak cingulum on the lingual face of the protocone. However, because of the tendency of pre- and post-cingulae to be long, often close to joining, in *P. donnae* (Luo, 1991: table 1, fig. 8C), and the weakness of the cingulum connecting the two in RAM 4056, we interpret this morphology as being a result of intraspecific variation.

OXYPRIMUS Van Valen, 1978

OXYPRIMUS ERIKSENI Van Valen, 1978

Referred material—**V88036:** M3: RAM 4035, 6380. **V88046:** MX lingual fragment: RAM 4101; M3: RAM 4102.

Description and Discussion—M3: RAM 4035, 4102, and 6380 resemble M3s of both *Protungulatum donnae* and *Oxyprimus erikseni* from localities in McCone County (Table 3.13.1). RAM 6380 is fully intact and can be confidently assigned to *O. erikseni* based on length

and width measurements (L = 2.76 mm; MW = 4.48 mm; DW = 3.59 mm). RAM 4035 and 4102, however, are missing much of their labial sides; this breakage precludes accurate measurements of total length and width. Although Luo (1991) lists several morphological differences between upper molars of *P. donnae* and *O. erikseni* (Luo, 1991: table 1), he also mentions that the most practical method for differentiating the two is molar size. Similarly, Archibald (1982) referred an upper M3, UCMP 116514 (fig. 59D), to *O. erikseni* based on its small size, but noted that it might also belong to *Protungulatum* cf. *P. donnae.* On visual comparison of the remaining morphology of RAM 4035 and 4102 to UCMP 133245 (*O. erikseni*) and UCMP 105007 (*P. donnae*), they are closer in size to *O. erikseni*, and have a shorter lingual slope of the protocone than *P. donnae* (a feature shared by RAM 6380). As a result, we refer RAM 4035 and 4102 to *O. erikseni*.

MX lingual fragment: RAM 4101 compares well in size and morphology with UCMP 132347, an M2 of *O. erikseni* (Table 3.13.1). The small size, relatively small conules, and relatively short lingual slope of the paracone in RAM 4101 also affiliate it with *O. erikseni*.

BAIOCONODON Gazin, 1941

?*BAIOCONODON sp.*

(Figure 3.13.12)

Referred material—**V88036:** P3: RAM 4058.

Description and Discussion—RAM 4058 (Fig. 3.13.12) is an archaic ungulate upper premolar. The specimen preserves two roots, but breakage on the basal side indicates that there were likely three roots in the intact tooth. RAM 4058 is semimolariform, with a large, bulbous central

paracone and lingual protocone. A distinct crest extends along the distal face of the paracone and joins with a ridge forming the posterolabial margin of the metastylar lobe. There is no trace of a metacone but the metastylar lobe bears a small cuspule that is contiguous with the ridge. The parastylar lobe is smaller than the metastylar lobe, and exhibits a fresh break point that may have been the location of a small parastyle. The protocone is crescentic and about 50% the height of the paracone, and bears ridges extending from its apex in both antero- and posterolabial directions. There is a postcingulum present but the precingulum is very weak.

There are few published examples of upper third premolars of species of *Baioconodon*, but RAM 4058 resembles the P3 of *B. nordicum* described by Lofgren (1995), UCMP 134694, in both size and morphology. However, UCMP 134694 does not preserve a protoconal lobe, which precludes comparison with RAM 4058 in width or protocone morphology. Based on the description provided by Lofgren (1995), as well as the accompanying figure (1995:fig. 30D) and the overall size and inflated morphology of RAM 4058, we tentatively refer it to ?*Baioconodon sp.* until more complete comparative specimens are available. Dimensions: L = 3.85 mm, MW = 3.71 mm, DW = 3.71 mm.

PERIPTYCHIDAE Cope, 1882

MIMATUTA Van Valen, 1978

MIMATUTA MORGOTH Van Valen, 1978

(Figure 3.13.13, Table 3.13.11)

Referred material—**V88036:** portion of maxilla containing P4-M3: UCMP 134571.

Description and Discussion—UCMP 134571 is a piece of maxilla preserving P4 through M3 (Figure 3.13.13). Measurements of each tooth are provided in Table 3.13.11. All the teeth are well-preserved but have apical wear on the paracone, metacone, and protocone. None of the teeth preserve distinct conules, because of wear in the trigon basin; however, on all three molars, the preparaconule and postmetaconule cristae are still somewhat visible. The size of the teeth combined with the diagnostic lingual expansion of the protoconal slope, as well as the labial shift in the protocone on the molars, indicate that this specimen belongs to the family Periptychidae. For quantitative support of this identification, we took measurements of the ratio of length of the protoconal slope to total anterior buccolingual width of the tooth (A/W-A, here reported as A/MW; Archibald, 1982; Lofgren, 1995). Values for A/MW on the M1 and M3 of UCMP 134571 (Table 3.13.11) are outside the range for this value in the similarly-sized arctocyonid *Protungulatum donnae* reported by Lofgren (1995). Although the M2 has an A/MW value within the range of *P. donnae*, this may be due to the extensive wear in the trigon basin of the tooth (as indicated by the missing conules). It is likely that A/MW was higher for all three molars in their original unworn state; the fact that two of them retain a high A/MW ratio even after wear supports this possibility. As measured in their current worn state, the A/MW ratios of the M1 and M3 of UCMP 134571 fall within the range of species of *Mimatuta* (Lofgren, 1995).

Despite being derived in morphology and placement of the protocone, the molars of UCMP 134571 retain largely plesiomorphic characteristics relative to derived genera of periptychids. Although the M3 of UCMP 134571 has a distinct, slightly columnar hypocone, the hypocone of the M2 is weaker, and that of the M1 is either not present or has been worn away entirely. This is in distinct contrast to the molars of the more derived periptychid genera *Oxyacodon*, *Conacodon*, *Anisonchus*, and *Hemithlaeus*, which all have a buccolingually long, columnar hypocone on all

three molars (Archibald, 1982: table 55). Another feature of derived periptychids, the enlargement of the P4 relative to the M1, is also not exhibited by UCMP 134571; the P4 is slightly smaller than the M1 in all dimensions, a configuration that is closer to the more basal *Mimatuta* (Archibald, 1982: table 55).

UCMP 134571 compares well to LACM 112901, a specimen of *Mimatuta minuial* (Archibald, 1982:fig. 65), especially the M1, which is distinctly triangular in occlusal view in both specimens. The A/MW ratio for UCMP 134571 (Table 3.13.11) is closer to that of *M. morgoth* as reported by Lofgren (1995) than that of *M. minuial*, but it is impossible to tell to what extent that ratio is due to wear on the protocone and within the trigon basin on the M1 and M2 of UCMP 134571. The M3, which has the best-preserved protocone, has an A/MW ratio close to that of *M. morgoth*. In the absence of data for the other two molars, we refer this specimen to *Mimatuta morgoth*. The dorsal morphology of this specimen will be described elsewhere.

MIMATUTA MINUIAL Van Valen, 1978

(Figure 3.13.14, Table 3.13.12)

Referred material—**V88046:** left dentary with p3 alveolus, p4–m3: UWBM 99100.

Description and Discussion—UWBM 99100 is referable to *Mimatuta* based on size (Table 3.13.12) and the labial shift in its paraconids (Archibald, 1982), and is referable to *Mimatuta minuial* by its robust p4 metaconid (Figure 3.13.14) as compared to the smaller, "relatively weak" p4 metaconid of *Mimatuta morgoth* (Van Valen, 1978; Lofgren, 1995). Archibald (1982) and Lofgren (1995) have described the entire postcanine tooth row of *Mimatuta minuial* in detail, such that further comment is not necessary here.

MIMATUTA sp. Van Valen, 1978

(Table 3.13.13)

Referred material—**V84193:** m1: UCMP 132281; mx trigonid: UCMP 132282. **V84194:** dentary fragment with m2–3: UCMP 132301. **V88036:** P4: RAM 6397. **V88046:** mx trigonid: RAM 4087, 4074; m3 talonid: RAM 4082.

Description and Discussion—RAM 4074 and 4087 show diagnostic characteristics of *Mimatuta*, specifically a labial shift in the paraconid and the inflated appearance of the cusps (Archibald, 1982; Lofgren, 1995). RAM 4082 resembles species of *Mimatuta* in overall occlusal size (Table 3.13.13), shape, and closure of the talonid basin (relative to *Protungulatum donnae*). UCMP 132301 is a section of dentary containing the m2 talonid and fully intact m3. Both exhibit minimal wear and have distinct morphology matching published descriptions. Unfortunately, as noted in the original description of the genus (Van Valen, 1978) and subsequent discussions of morphology (Archibald, 1982; Lofgren, 1995), lower molars of *Mimatuta* can only be assigned to species if they are associated with a p4 (Van Valen, 1978). As such, these specimens can only be referred to *Mimatuta sp*. Similarly, RAM 6397 bears very close resemblance to the P4 of UCMP 134571, and has the enlarged protocone and low paracone present on P4s of *Mimatuta*, but because upper premolars of species of *Mimatuta* are not diagnostic (Eberle and Lillegraven, 1998), we refer RAM 6397 to *Mimatuta sp.*

PERIPTYCHIDAE GEN. ET. SP. INDET.

(Figure 3.13.15)

Referred material—**V88036:** MX lingual fragment: RAM 4045.

Description and Discussion—RAM 4045 is a lingual fragment of an upper molar. Although it preserves the protocone almost exclusively, it is still the largest tooth in the sample currently under study. The preserved portion of the tooth (Figure 3.13.15) includes the lingual slope and mesial and distal faces of the protocone. The mesial and distal faces of the protocone bear a precingulum (which may have had a pericone before wear) and postcingulum, respectively, both of which are worn. The enamel on the lingual slope of the protocone is crenulated, and the slope is inclined at an approximately 45 degree angle to the base of the crown.

The long lingual slope of the protocone, as well as the overall large size of the tooth indicates that RAM 4045 is likely a member of the Periptychidae. A/MW cannot be measured for this tooth because only the protocone is preserved. The slightly pointed (on the lingual margin), asymmetrical U-shape of the tooth in occlusal view, as well as the overall size of the specimen, resemble upper molars of the genus *Hemithlaeus*, specifically the M3 (Matthew, 1937: fig. 19; Kondrashov and Lucas, 2006: fig. 15a, b), as well as the M3 of *Tinuviel* (S. Shelley, pers.comm). Because RAM 4045 is relatively long mesiodistally, and does not have a strong hypocone, it is unlikely to belong to *Anisonchus*, *Haploconus*, or *Oxyacodon* (compared with Archibald et al., 1983: fig.1, and epoxy casts of USNM 15760, USNM 23279). It is larger and more bulbous than upper molars of *Mimatuta* (Archibald 1982: fig. 63). Due to the limited morphology preserved, we conservatively refer RAM 4045 to Periptychidae, genus and species indeterminate.

PRIMATES Linnaeus, 1758

PLESIADAPIFORMES Simons, 1972

PURGATORIIDAE Van Valen and Sloan, 1965

PURGATORIUS Van Valen and Sloan, 1965

PURGATORIUS cf. *P. CORACIS* Fox and Scott, 2011

(Figure 3.13.16, 3.13.17)

Referred material—**V88046:** m3: RAM 4078; M2: UWBM 106217; MX lingual fragment: RAM 4088.

Description and Discussion—m3: RAM 4078 (Figure 3.13.16) is a lower molar with the hypoconulid broken off. The remainder of the tooth is in good condition, with slight wear on the apices of the trigonid cusps and moderate wear on the hypoconid and entoconid. The talonid is narrower than the trigonid, and the talonid is relatively long even without accounting for the missing hypoconulid, indicating that the tooth is an m3. RAM 4078 is similar in size (L = 2.25 mm [approx.], WTri = 1.38 mm, WTal = 1.24 mm) to m3s of *Purgatorius unio* (Van Valen and Sloan, 1965: L = 2.20 mm, W = 1.40 mm; Clemens, 1974: mean L = 2.32 mm, N = 7), and slightly larger than mean sizes for *P. titusi* (Buckley, 1997: L = 2.10 mm, WTri = 1.23 mm, WTal =1.06 mm, N = 8). Although it is larger than the two reported m3s of *Purgatorius coracis* (Fox and Scott, 2011: L = 1.9–2.0 mm, WTri = 1.2–1.3 mm, WTal = 1.0–1.1 mm), it shares several characteristics with *P. coracis* that distinguish both from *P. unio.* Most notable among these characters are the smaller, lower, and more labial paraconid than *P. unio*; and a shallower talonid basin than *P. unio* (Fox and Scott, 2011). The cusps of RAM 4078 also appear slightly more bunodont than those of *P. unio*; it is probably more similar to the less insectivore-like, more primate-like specimens referred to *P. unio* (Clemens, 1974). Due to the broken hypoconulid, it is impossible to tell if there was "twinning" of that cusp, as sometimes observed in *P. unio*, but never observed in *P. titusi* (Buckley, 1997). Because RAM 4078 shares several important characters with *P. coracis*, but is larger than the currently observed range, we refer it

to *Purgatorius* cf. *P. coracis*. We are conservative with regard to the species designation especially because of the small known sample of *P. coracis* m3s (N = 2), and the fact that the hypoconulid of RAM 4078 is broken and the total tooth length is therefore approximate. A larger sample of *P. coracis* m3s will make the range of variation in size for that taxon more clear, and potentially clarify the affinity of RAM 4078.

M2: UWBM 106217 (Figure 3.13.17) is a complete M2 with light wear on the apices of the paracone, metacone, protocone, and conules. The stylar region is relatively narrow. The paracone is barely taller than the metacone, and canted slightly mesiolabially relative to the metacone. The lingual slope of the protocone makes up approximately ⅓ of the total labiolingual width of the tooth, and rises from the gumline at about a 45 degree angle. There are both pre- and post-cingulae, with the postcingulum being slightly wider mesiodistally than the precingulum. UWBM 106217 is larger than *Purgatorius pinecreeensis* (Table 3.13.14); however, it should be noted that only M1s have been recovered for *P. pinecreensis*, and its M2s, when recovered, are likely to be larger. UWBM 106217 is similar in size to *Purgatorius unio*, *P. titusi*, *P. janisae*, and *P. coracis*, but slightly larger than reported size ranges for any of those species except *P janisae* (Table 3.13.14); yet it is more transverse (L/DW = 0.62) than M2s of *P. janisae* (L/DW = 0.63–0.75; Clemens and Wilson, 2009: table 2). In occlusal shape, UWBM 106217 most closely resembles *P. coracis* (Fox and Scott, 2011: fig. 3.7–9). In comparison to *P. titusi* (Buckley, 1997: fig. 2.2), UWBM 106217 has a similarly shaped lingual margin, but is less mesiodistally constricted at the level of the conules, resulting in a squarer overall shape and less distinct "waist"; additionally, in *P. titusi*, the deepest indentation of the ectoflexus is at the same mesiodistal location as the notch in the centrocrista, where in UWBM 106217 the deepest indentation is positioned distal to the notch of the centrocrista. This character state in UWBM

106217 differs from *P. unio*, where the deepest indentation is similarly positioned to that in *P. titusi*; and from *P. pinecreeensis*, where the deepest indentation is slightly mesial to the centrocrista notch. The state in UWBM 106217 matches the state present in *P. coracis*. UWBM 106217 is further distinct from *P. unio* in its longer lingual extent of the postcingulum, a characteristic that also aligns it with *P. coracis* (Silcox, 2001; Fox and Scott, 2011).

Although the shape of the M2 lingual margin (in occlusal view) appears to be somewhat variable within a single species of *Purgatorius* (e.g., Van Valen and Sloan, 1965: fig. 1B, 1G), UWBM 106217 does not have a rounded lingual margin like M1s of *P. pinecreeensis* (Scott et al., 2016: fig. 2F, 2I), nor does it exhibit the indentation between the lingual edge of the protocone and the lingual edge of the postcingulum present in some specimens of *P. unio* (Van Valen and Sloan 1965: fig. 1G). Instead, the lingual margin of UWBM 106217 is flattened distal to the apex of the protocone, such that the margin is roughly parallel to the mesiodistal axis of the tooth, and mesial to the protocone is slanted labially at approximately a 50º angle to the mesiodistal axis. This matches the shape of the lingual margin in the holotype of *P. coracis*, UA 16070. Although the current existing sample of *P. coracis* M2s is small (N = 2), we find that there are sufficient similarities between *P. coracis* and UWBM 106217 to refer this specimen to *Purgatorius* cf. *P. coracis*.

MX lingual fragment: RAM 4088 is a lingual fragment of an upper molar preserving the paraconule, metaconule, and protocone with minimal wear on their apices. The tooth has relatively mesiodistally wide pre- and postcingulae, with the postcingulum being slightly wider and more lingually extensive than the precingulum. RAM 4088 is nearly identical in both size

and morphology to the lingual side of UWBM 106217, so we also refer it to *Purgatorius* cf. *P. coracis*.

3.13.3 REFERENCES CITED

Ameghino, F., 1890, Los Plagionlacídeos argentinos y sus relaciones zoológicas, geológicas y geográficaso: Boletin del Instituto Geográfico Argentino, v. 11, p. 143-208.

Archibald, J.D., 1982, A study of Mammalia and geology across the Cretaceous-Tertiary boundary in Garfield County, Montana: University of California Publications in Geological Sciences, v. 122, 286 p.

Archibald, J.D., Rigby Jr, J.K., and Robison, S.F., 1983, Systematic revision of *Oxyacodon* (Condylarthra, Periptychidae) and a description of *O. ferronensis* n. sp.: Journal of Paleontology, p. 53–72.

Bown, T.M., and Kraus, M.J., 1979, Origin of the tribosphenic molar and metatherian and eutherian dental formulae *in* Lillegraven, J.A., Kielan-Jaworowska, Z., and Clemens, W.A., eds., Mesozoic mammals: the first two-thirds of mammalian history: University of California Press, p. 172–181.

Buckley, G.A., 1997, A new species of Purgatorius (Mammalia; Primatomorpha) from the lower Paleocene Bear formation, Crazy Mountains basin, south-central Montana: Journal of Paleontology, v. 71, p. 149–155.

Case, J.A., Goin, F.J., and Woodburne, M.O., 2005, “South American” marsupials from the Late Cretaceous of North America and the origin of marsupial cohorts: Journal of Mammalian Evolution, v. 12, p. 461–494.

Cifelli, R.L., 1990, Cretaceous mammals of southern Utah. I. Marsupials from the Kaiparowits Formation (Judithian): Journal of Vertebrate Paleontology, v. 10, p. 295–319.

Clemens, W.A., 1964, Fossil mammals of the type Lance Formation,Wyoming. Part I. Introduction and Multituberculata: University of California Publications in Geological Sciences, v. 48, p. 1–105.

Clemens, W.A., 1966, Fossil mammals of the type Lance Formation, Wyoming. Part II. Marsupialia: University of California Publications in Geological Sciences, v. 62, p. 1–122.

Clemens, W.A., 1973, Fossil mammals of the type Lance Formation, Wyoming. Part III. Eutheria and summary: University of California Publications in Geological Sciences, v. 94, p. 1–102.

Clemens, W.A., 1974, *Purgatorius*, an early paromomyid primate (Mammalia): Science, v. 184, p. 903–905.

Clemens, W.A., 2006, Early Paleocene (Puercan) peradectid marsupials from northeastern Montana, North American Western Interior: Palaeontographica Abteilung A, v. 277, p. 19–31.

Clemens, W.A., 2015, *Prodiacodon crustulum* (Leptictidae, Mammalia) from the Tullock Member of the Fort Union Formation, Garfield and McCone Counties, Montana, USA: PaleoBios, v. 32.

Clemens, W.A., 2017, *Procerberus* (Cimolestidae, Mammalia) from the Latest Cretaceous and Earliest Paleocene of the Northern Western Interior, USA: PaleoBios, v. 34.

Clemens, W.A., and Wilson, G.P., 2009, Early Torrejonian mammalian local faunas from northeastern Montana, USA: Museum of Northern Arizona Bulletin, v. 65, p. 111–158.

Cope, E.D., 1882, The Periptychidae: The American Naturalist, v. 16, p. 832–833.

Cope, E.D., 1884, The Vertebrata of the Tertiary formations of the West: Book I. Report U.S. Geological Survey Territories, F. V. Hayden in charge, v. 3, p. 1–1009.

Davis, B.M., 2007, A revision of 'pediomyid' marsupials from the Late Cretaceous of North America: Acta Palaeontologica Polonica, v. 52.

Eberle, J.J., and Lillegraven, J.A., 1998, A new important record of earliest Cenozoic mammalian history: Rocky Mountain Geology, v. 33, p. 49–117.

Fox, R.C., 2015, A revision of the Late Cretaceous–Paleocene eutherian mammal *Cimolestes* Marsh, 1889: Canadian Journal of Earth Sciences, v. 52, p. 1137–1149.

Fox, R.C., and Scott, C.S., 2011, A new, early Puercan (earliest Paleocene) species of *Purgatorius* (Plesiadapiformes, Primates) from Saskatchewan, Canada: Journal of Paleontology, v. 85, p. 537–548.

Gazin, C.L., 1941, The mammalian faunas of the Paleocene of central Utah, with notes on the geology: Smithsonian Inst., United States National Museum.

Giebel, C.G., 1855, Die Säugetiere in zoologischer, anatomischer und palaeontologischer Beziehung umfassend dargestelt. Abel, Leipzig

Gill, T., 1872., Arrangement of the families of mammals and synoptical table of characters of the subdivisions of mammals: Smithsonian Miscellaneous Collections, v. 11, p. 1–98.

Huxley, T.H., 1880, On the application of the laws of evolution to the arrangement of the Vertebrata, and more particularly of the Mammalia: Proceedings of the Zoological Society of London, v. 43, p. 649–662.

Jepsen, G.L., 1930, Stratigraphy and paleontology of the Paleocene of northeastern Park County, Wyoming: Proceedings of the American Philosophical Society, v. 69, p. 463–528.

Jepsen, G.L., 1940, Paleocene faunas of the Polecat Bench Formation, Park County, Wyoming: Part I: Proceedings of the American Philosophical Society, v. 83, p. 217–340.

Johnston, P.A., and Fox, R.C., 1984, Paleocene and late Cretaceous mammals from Saskatchewan, Canada: Palaeontographica Abteilung A, p. 163–222.

Kielan-Jaworowska, Z., Cifelli, R.L., and Luo, Z.X., 2004, Mammals from the Age of Dinosaurs: Origins, evolution, and structure, New York, Columbia University Press, 630 p.

Kondrashov, P.E., and Lucas, S.G., 2006, Early Paleocene (Puercan and Torrejonian) archaic ungulates (Condylarthra, Procreodi and Acreodi) of the San Juan Basin, New Mexico: New Mexico Museum of Natural Historu and Science Bulletin, v. 34, p. 84–97.

Lillegraven, J.A., 1969, Latest Cretaceous mammals of upper part of Edmonton Formation of Alberta, Canada, and review of marsupial-placental dichotomy in mammalian evolution: The University of Kansas Paleontological Contributions, Article 50, 122 p.

Lillegraven, J.A., and Bieber, S.L., 1986, Repeatability of measurements of small mammalian fossils with an industrial measuring microscope: Journal of Vertebrate Paleontology, v. 6, p. 96–100.

Linnaeus, C., 1758, Systema naturae per regna triae naturae, secundum classis, ordines, genera, species cum characteribus, differentis, synonyms locus, Edito decima, Reformata, Laurentii Salvi, Stockholm, v. 1, 824 p.

Linnaeus, C., 1766, Systema naturae per regna triae naturae, secundum classis, ordines, genera, species cum characteribus, differentis, synonyms locus, Edito decima, Reformata, Laurentii Salvi, Stockholm, v. 7, 532 p.

Lofgren, D.L., 1995, The Bug Creek problem and the Cretaceous-Tertiary transition at McGuire Creek, Montana: University of California Press, v. 140, 185 p.

Luo, Z., 1991, Variability of Dental Morphology and the Relationships of the Earliest Arctocyonid Species: Journal of Vertebrate Paleontology, v. 11, p. 452–471.

Marsh, O. C., 1880, Notice of Jurassic mammals representing two new orders: American Journal of Science, v. 20, p. 235–239.

Marsh, O. C. 1889. Discovery of Cretaceous Mammalia, Part 1: American Journal of Science, v.

38, p. 81–92.

Marshall, L.G., 1990, Phylogenetic relationships of the families of marsupials: Current Mammalogy, v. 2, p. 433–505.

Matthew, W. D., 1929, Preoccupied names: Journal of Mammalogy, v. 10, p. 171.

Matthew, W.D., 1937, Paleocene faunas of the San Juan basin: Transactions of the American Philosophical Society, v. 30, p. 1-510.

Matthew, W.D., and Granger, W., 1921, New genera of Paleocene mammals: American Museum Novitates, v. 13, p. 1–7.

McKenna, M.C., 1975, Toward a phylogenetic classification of the Mammalia, *in* Luckett, W.P., and Szalay, F.S., eds., Phylogeny of the Primates: A Multidisciplinary Approach: Proceedings of the Wenner Gren Symposium, v. 61.

Middleton, M.D., and Dewar, E.W., 2004, New mammals from the early Paleocene Littleton fauna (Denver Formation, Colorado): New Mexico Museum of Natural History and Science Bulletin, v. 26, p. 59–80.

Montellano, M., Weil, A., and Clemens, W.A., 2000, An exceptional specimen of *Cimexomys judithae* (Mammalia: Multituberculata) from the Campanian Two Medicine Formation of Montana, and the phylogenetic status of Cimexomys: Journal of Vertebrate Paleontology, v. 20, p. 333–340.

Novacek, M., 1977, A review of Paleocene and Eocene Leptictidae (Eutheria: Mammalia) from

North America: PaleoBios, v. 24, p. 1–42.

Novacek, M., and Clemens, W.A., 1977, Aspects of intrageneric variation and evolution of *Mesodma* (Multituberculata, Mammalia): Journal of Paleontology, p. 701–717.

O'Leary, M. A., Bloch, J.I., Flynn, J.J., Gaudin, T.J., Giallombardo, a., Giannini, N.P., Goldberg, S.L., Kraatz, B.P., Luo, Z.-X., Meng, J., Ni, X., Novacek, M.J., Perini, F. a., Randall, Z.S., et al., 2013, The Placental Mammal Ancestor and the Post-K-Pg Radiation of Placentals: Science, v. 339, p. 662–667, doi: 10.1126/science.1229237.

Scott, C.S., Fox, R.C., and Redman, C.M., 2016, A new species of the basal plesiadapiform *Purgatorius* (Mammalia, Primates) from the early Paleocene Ravenscrag Formation, Cypress Hills, southwest Saskatchewan, Canada: further taxonomic and dietary diversity in the earliest primates: 1. Canadian Journal of Earth Sciences, v. 53, p. 343–354, doi: 10.1139/cjes-2015-0238.

Silcox, M. T., 2001, A phylogenetic analysis of Plesiadapiformes and their relationship to Euprimates and other archontans [Ph.D. thesis]: Baltimore, The Johns Hopkins University, 722 p.

Simons, E.L., 1972, Primate evolution: an introduction to man's place in nature: New York, The Macmillan Company, 322 p.

Simpson, G.G., 1927, Mesozoic Mammalia, VIII; Genera of Lance mammals other than multituberculates: American Journal of Science, p. 121–130.

Sloan, R.E., and Van Valen, L., 1965, Cretaceous mammals from Montana: Science, v. 148, p. 220–227.

Smith, S.M., and Wilson, G.P., 2017, Species Discrimination of Co-Occurring Small Fossil Mammals: A Case Study of the Cretaceous-Paleogene Multituberculate Genus *Mesodma*: Journal of Mammalian Evolution, v. 24, p. 147–157, doi: 10.1007/s10914-016-9332-2.

Storer, J.E., 1991, The mammals of the Gryde Local Fauna, Frenchman Formation (Maastrichtian: Lancian), Saskatchewan: Journal of Vertebrate Paleontology, v. 11, p. 350–369.

Trouessart, E.L., 1878, Catalogue des mammiferes vivant et fossils. Ordo III. Chiroptera: Revue et Magasin de Zoologie Pure et Appliqué, v. 6, p. 201–254.

Valen, L. Van, 1969, The multiple origins of the placental carnivores: Evolution, v. 23, p. 118–130.

Van Valen, L., 1978, The beginning of the age of mammals: Evolutionary Theory, v. 4, p. 46–80.

Van Valen, L.M., 1994, Serial homology : the crests and cusps of mammalian teeth: Acta Palaeontologica Polonica, v. 38, p. 145–158.

Van Valen, L., and Sloan, R.E., 1965, The earliest primates: Science, v. 150, p. 743–745.

Vullo, R., Gheerbrant, E., de Muizon, C., and Neraudeau, D., 2009, The oldest modern therian mammal from Europe and its bearing on stem marsupial paleobiogeography: Proceedings of the National Academy of Sciences, v. 106, p. 19910–19915.

Webb, M.W., 2001, Fluvial Architecture and Late Cretaceous mammals of the Lance Formation, southwestern Bighorn Basin, Wyoming [Ph.D. thesis]: University of Wyoming.

Williamson, T.E., Weil, A., and Standhardt, B., 2011, Cimolestids (Mammalia) from the early Paleocene (Puercan) of New Mexico: Journal of Vertebrate Paleontology, v. 31, p. 162–180, doi: 10.1080/02724634.2011.539649.

Williamson, T.E., Brusatte, S.L., Carr, T.D., Weil, A., and Standhardt, B.R., 2012, The phylogeny and evolution of Cretaceous–Palaeogene metatherians: cladistic analysis and description of new early Palaeocene specimens from the Nacimiento Formation, New Mexico: Journal of Systematic Palaeontology, v. 10, p. 625–651, doi: 10.1080/14772019.2011.631592.

Zhang, Y., 2015, Phylogenetics of Neoplagiaulacidae (Multituberculata, Mammalia), and Diet Reconstruction on Cimolodontan Multituberculates [Ph.D. thesis]: The Ohio State University.

3.13.4 FIGURES

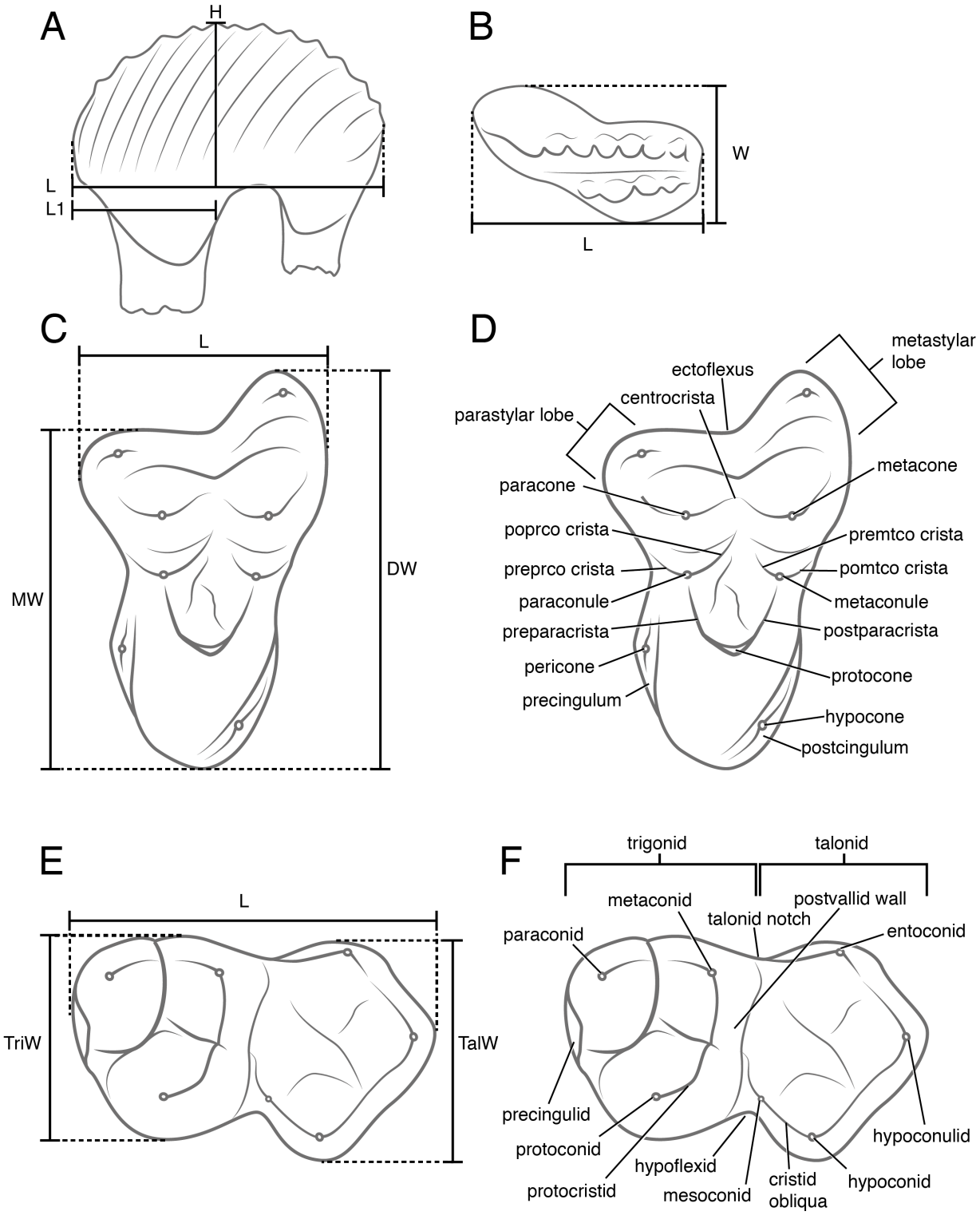

Figure 3.13.1 Tooth measurements and dental naming conventions used in this study. Multituberculate p4 (A) and P4 (B) measurements follow Novacek and Clemens (1977). C–F: upper (C–D) and lower (E–F) scematics of left therian teeth with measurements (C, E) and terminology (D, F) used in this study. Therian terminology is adapted from Bown and Kraus (1979), Van Valen (1994), and Salles (1996); therian measurements follow Archibald (1982). Abbreviations: **L** = length; **MW** = mesial width; **DW** = distal width; **TriW** = trigonid width; **TalW** = talonid width; **poprco** = postparaconule; **preprco** = preparaconule; **premtco** = premetaconule; **pomtco** = postmetaconule.

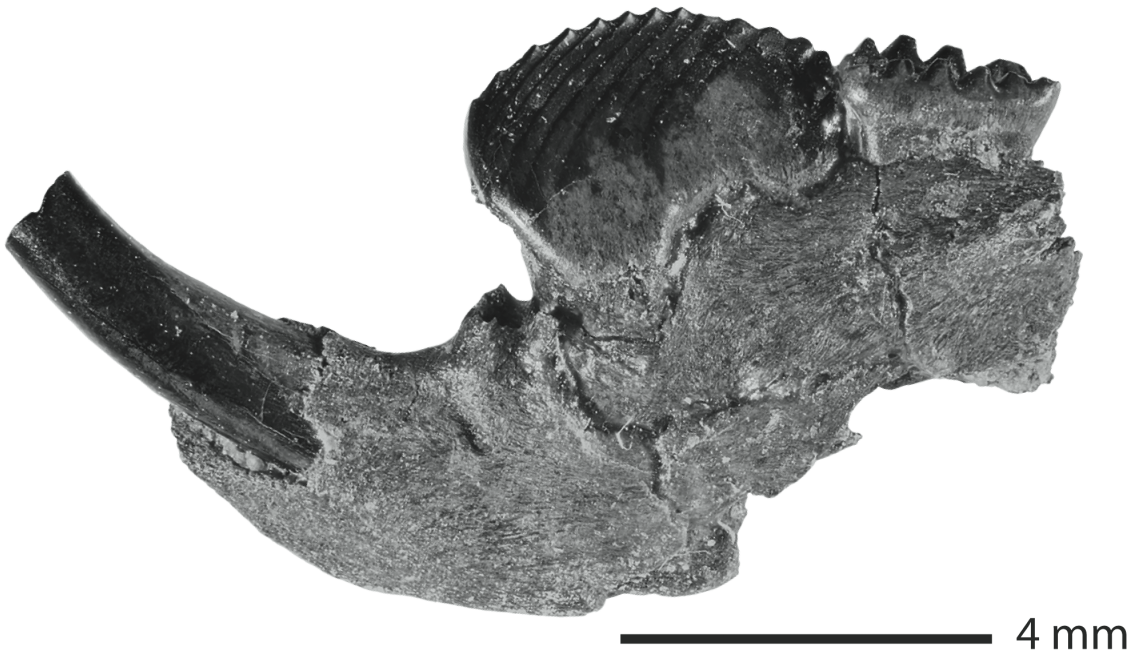

Figure 3.13.2 Mandible of *Mesodma thompsoni* with i–m2 (UCMP 132304) in labial view.

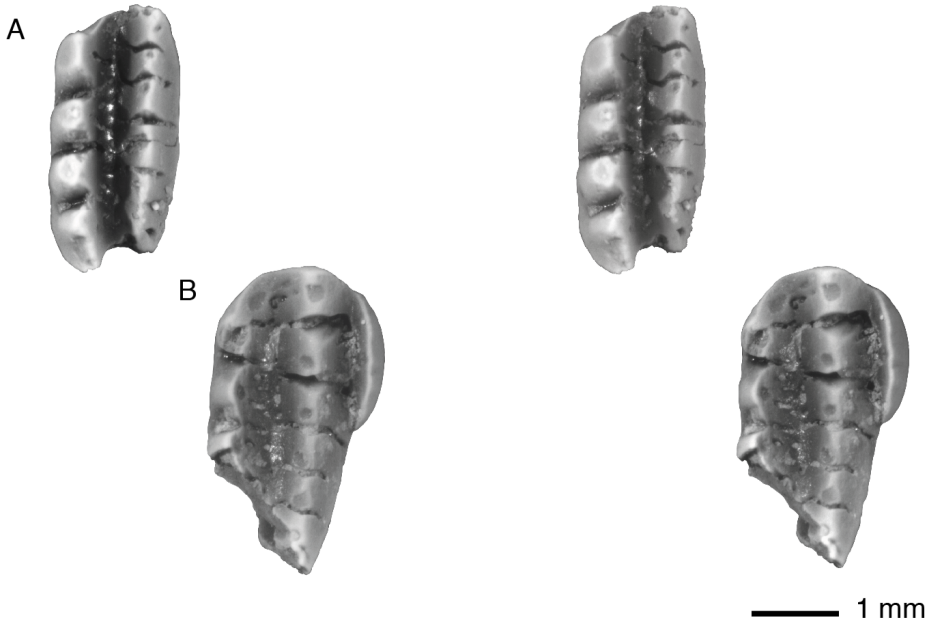

Figure 3.13.3 m1 (A, RAMP 6387) and M1 (B, RAMP 4053) of *Cimexomys gratus*, both in stereo occlusal view.

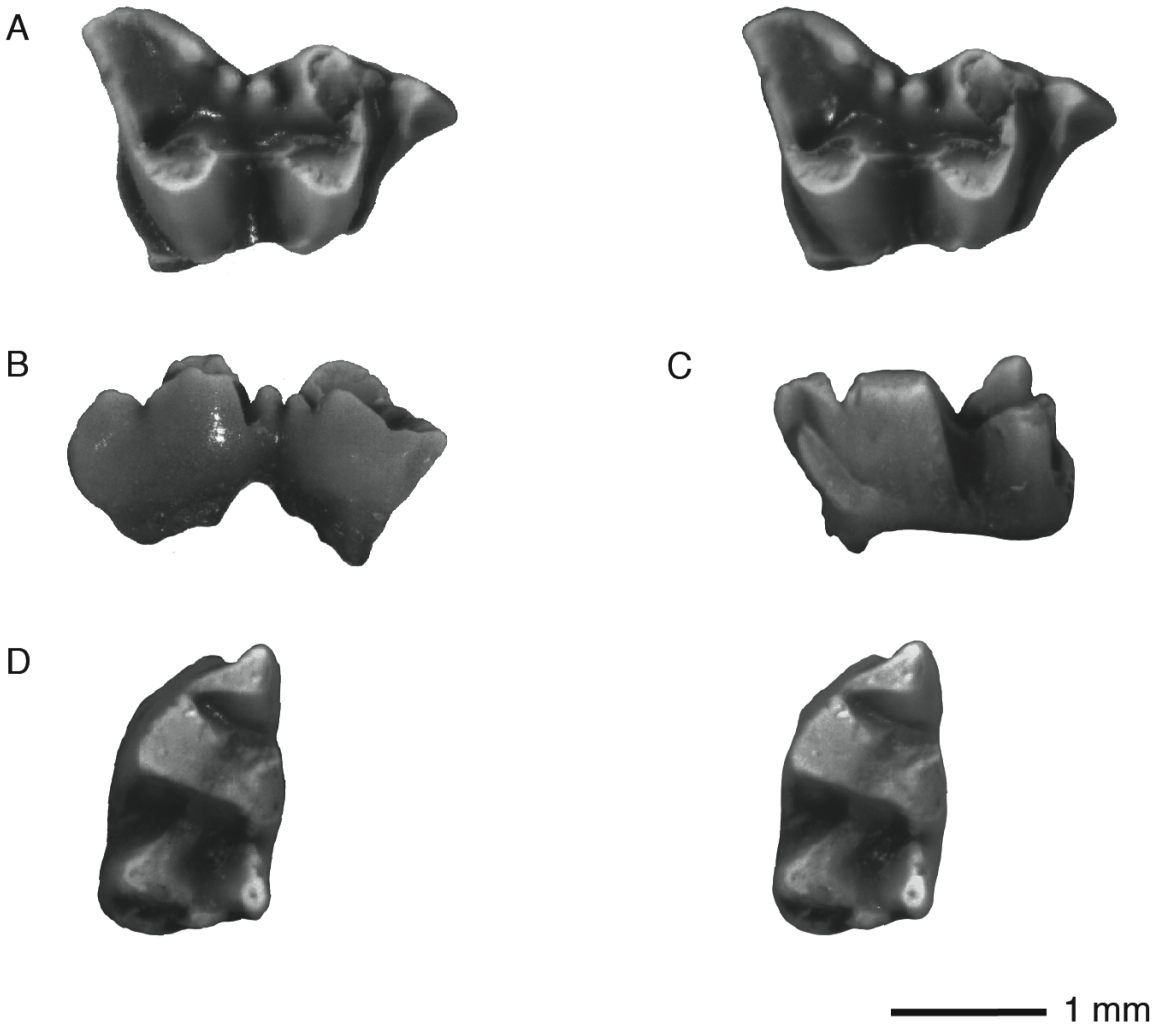

Figure 3.13.4 Alphadontidae genus and species indeterminate: labial MX fragment (UCMP 239349) in stereo occlusal (A) and labial (B) views; m1 (UCMP 239334) in labial (C) and stereo occlusal (D) views.

Figure 3.13.5 M4 of *Thylacodon montanensis* (UCMP 239350) in stereo occlusal view.

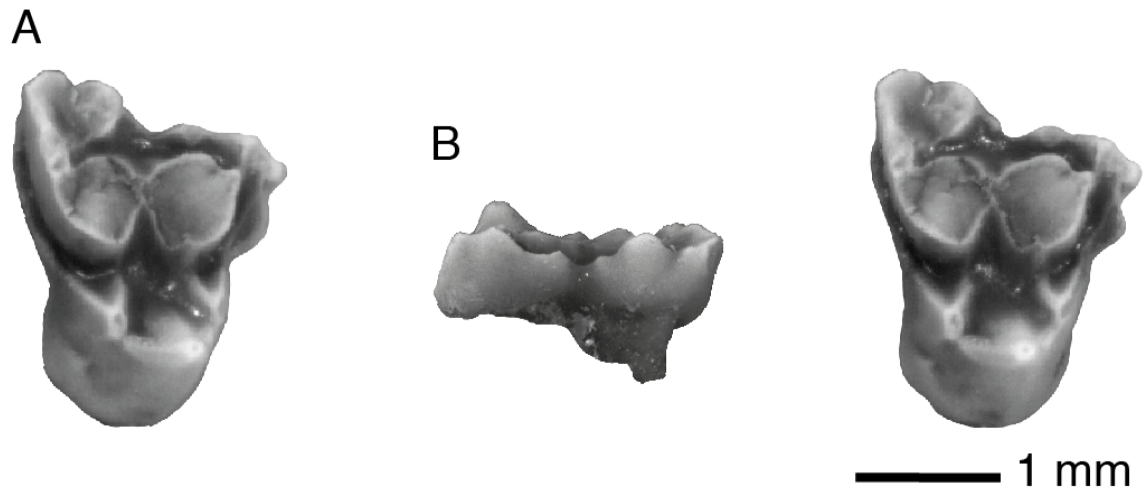

Figure 3.13.6 M1 or M2 of ?*Leptalestes cooki* (UCMP 239344) in stereo occlusal (A) and labial (B) views.

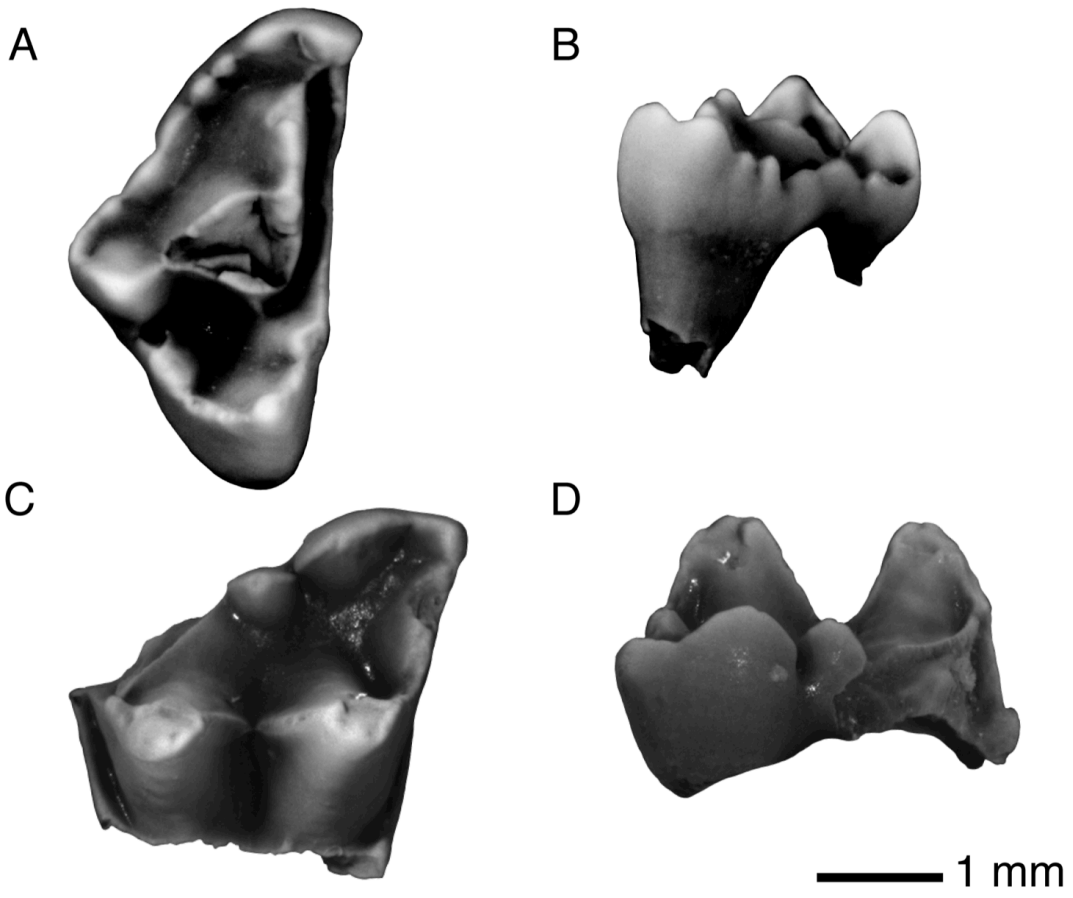

Figure 3.13.7 Metatheria indeterminate: M4 (UCMP 239368) in occlusal (A) and labial (B) views; MX fragment (UCMP 239372) in occlusal (C) and labial (D) views.

Figure 3.13.8 p4 of *Procerberus formicarum* (RAMP 4106) in stereo occlusal view.

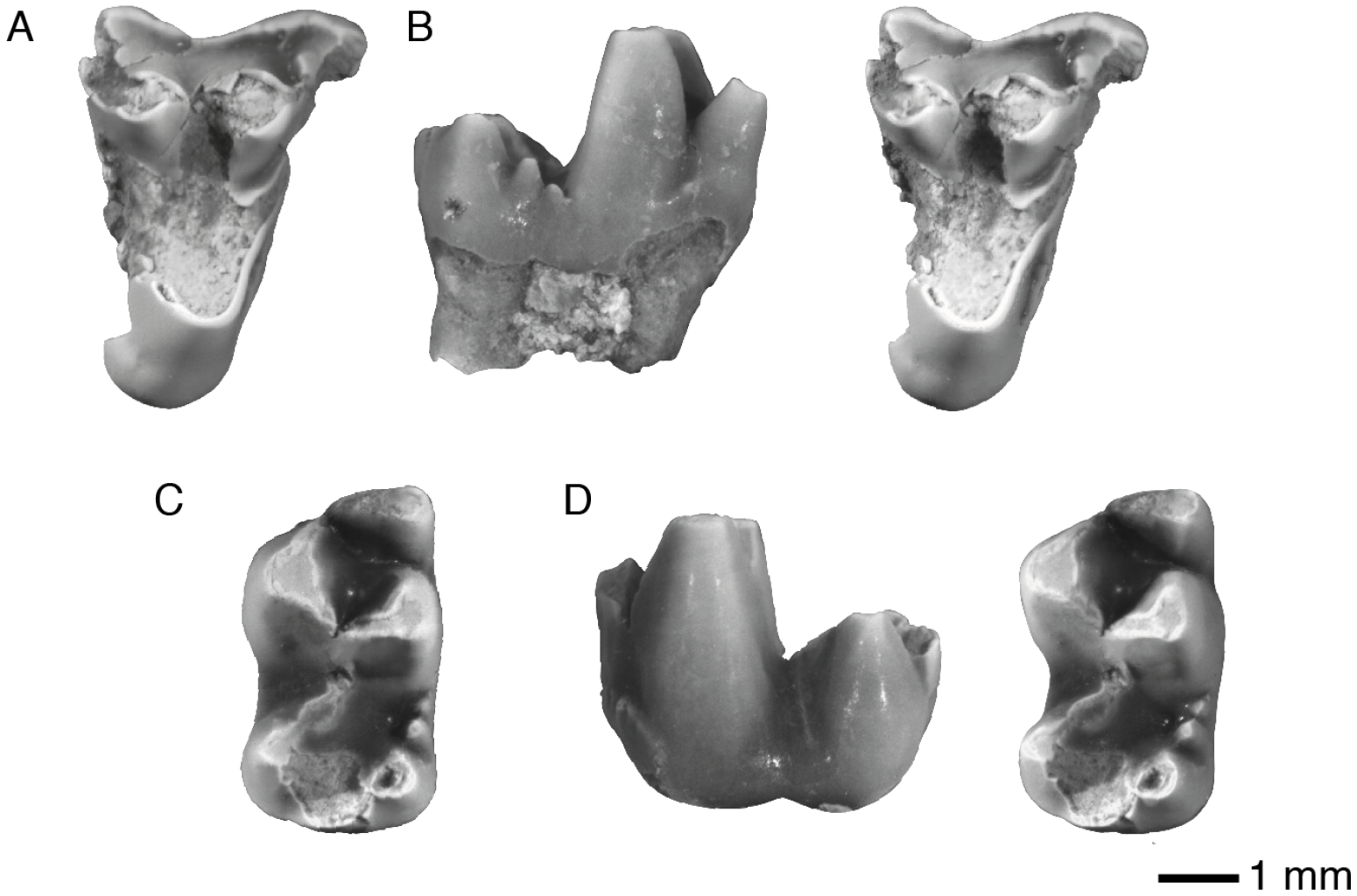

Figure 3.13.9 *Procerberus* cf. *P. grandis*: M2 (UCMP 134570) in stereo occlusal view (A); m1 (RAMP 4042) in lingual (B), stereo occlusal (C), and labial (D) views.

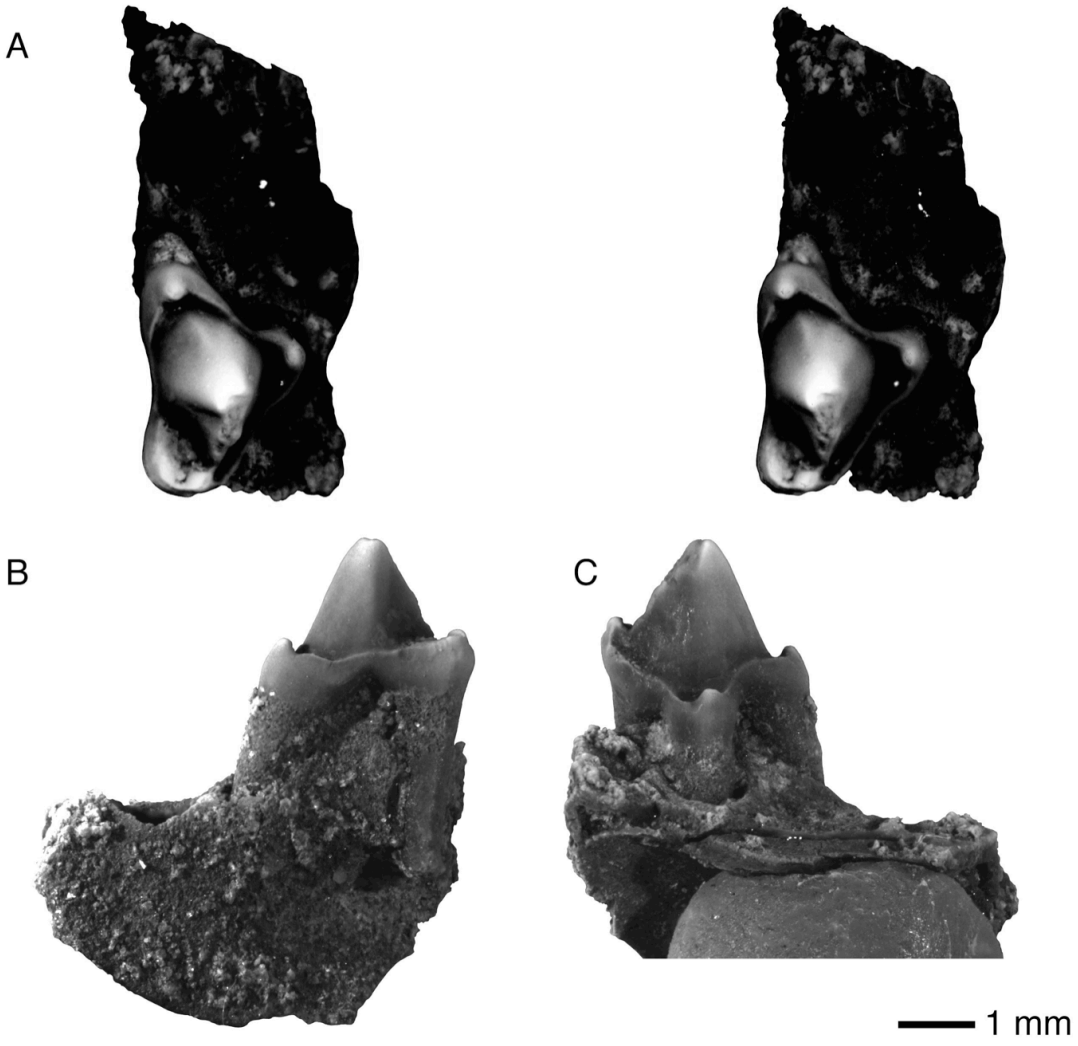

Figure 3.13.10 ?*Ambilestes cerberoides* maxillary fragment and P3 (UCMP 145148) in stereo occlusal (A), labial (B), and lingual (C) views.

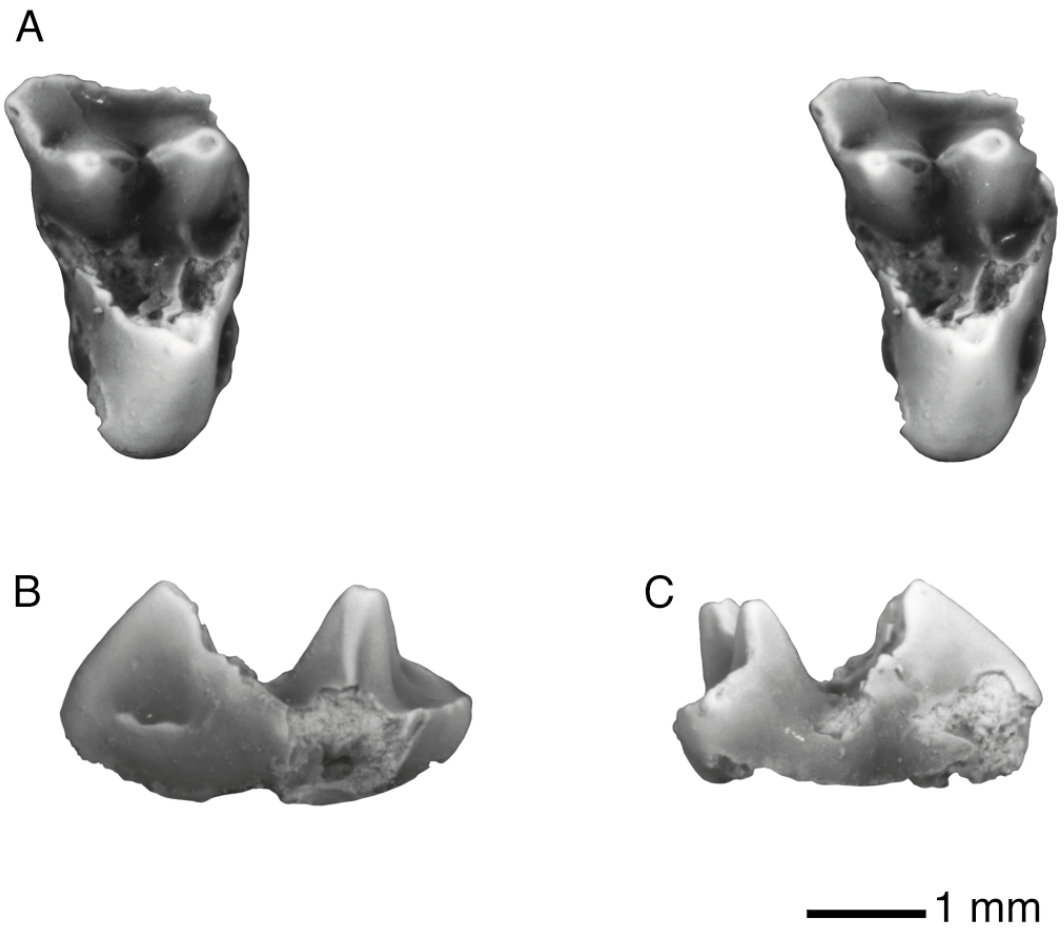

Figure 3.13.11 ?*Prodiacodon crustulum* (RAMP 6412) MX in stereo occlusal (A), mesial (B) and distal (C) views.

Figure 3.13.12 ?*Baioconodon* sp. P3 (RAMP 4058) in stereo occlusal view

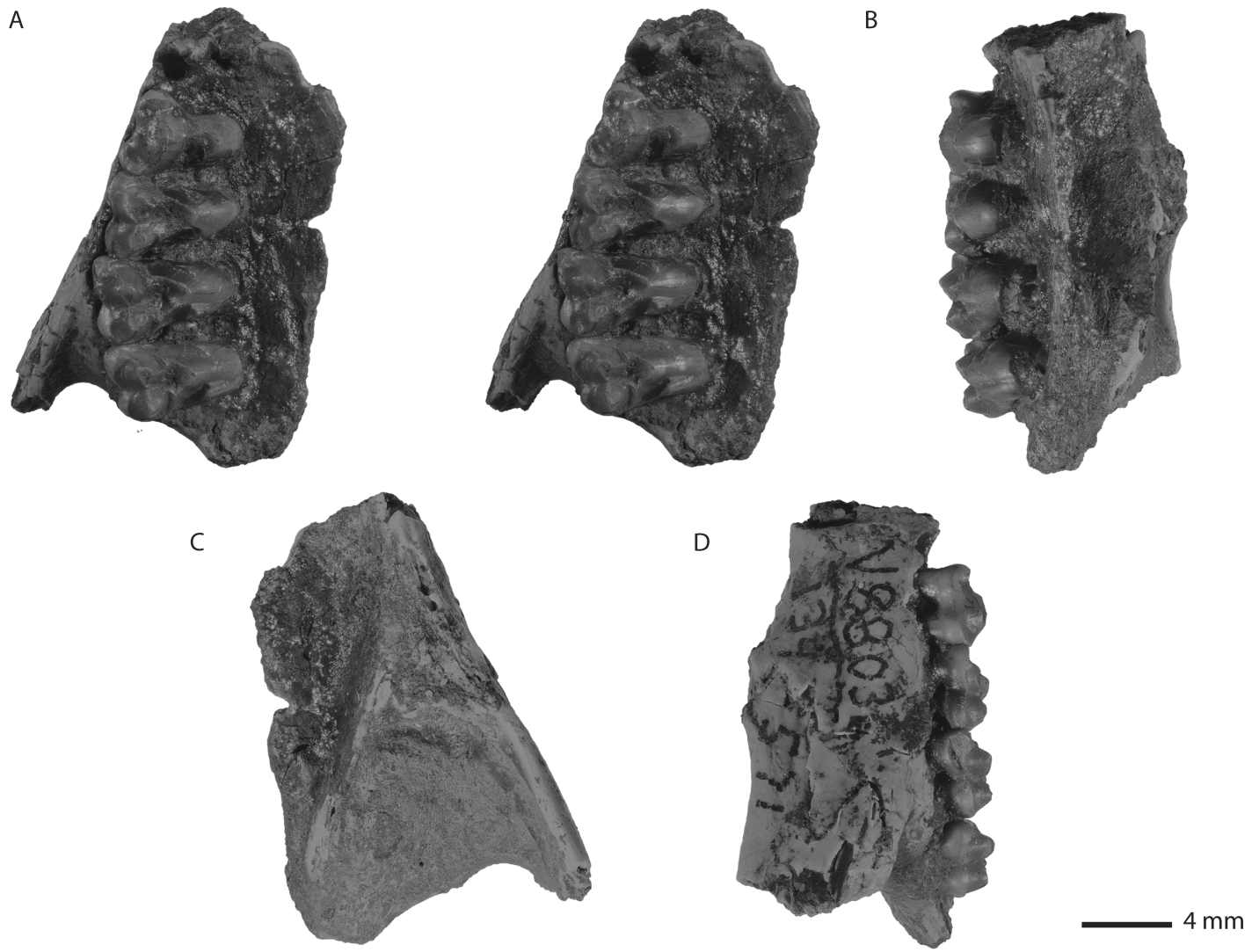

Figure 3.13.13 Maxillary fragment of *Mimatuta morgoth* with P4–M3 (UCMP 134571) in stereo occlusal (A), lingual (B), dorsal (C), and labial (D) views.

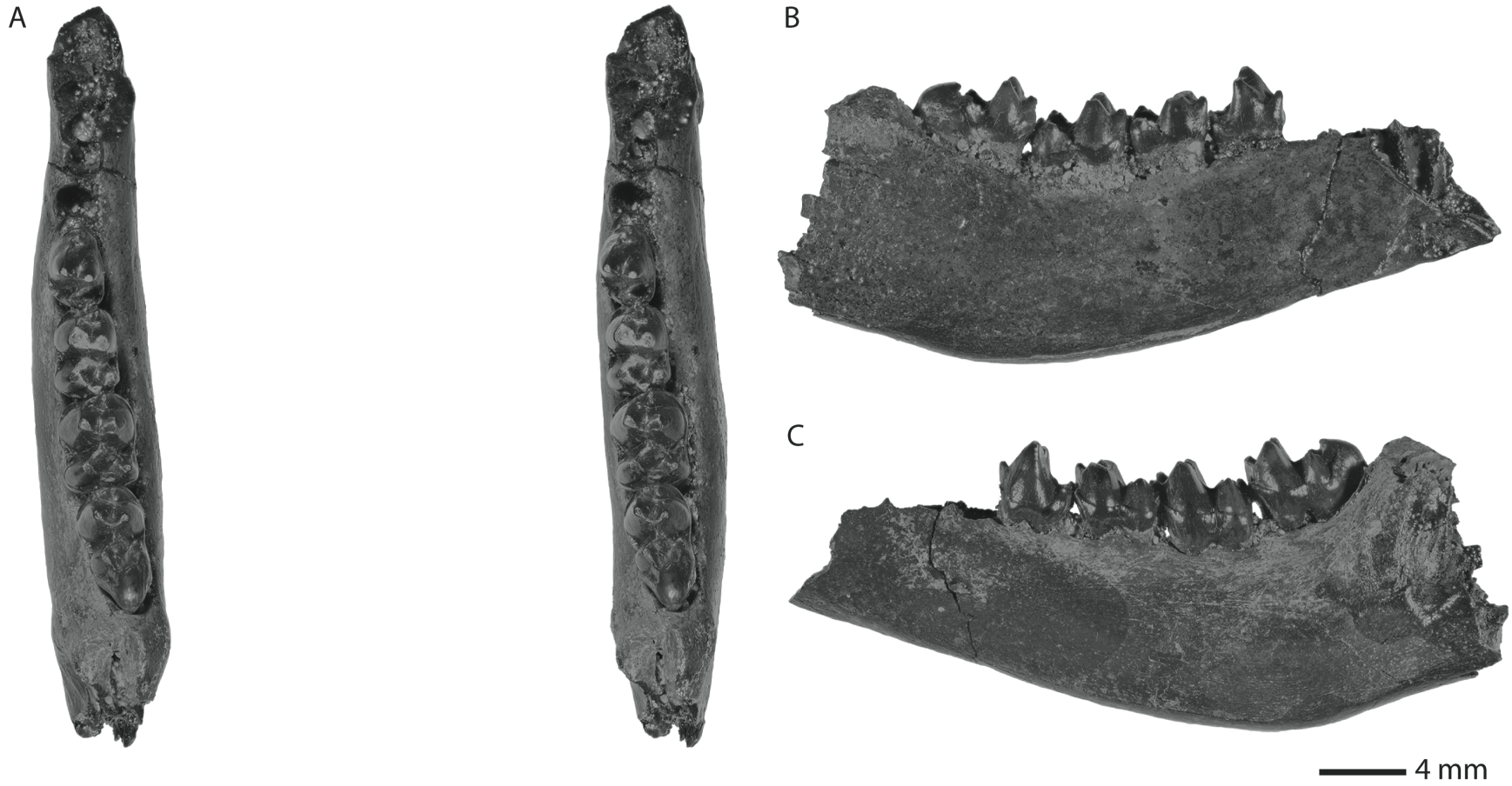

Figure 3.13.14 Mandible of *Mimatuta minuial* with p4–m3 (UWBM 99100) in stereo occlusal (A), lingual (B), and labial (C) views.

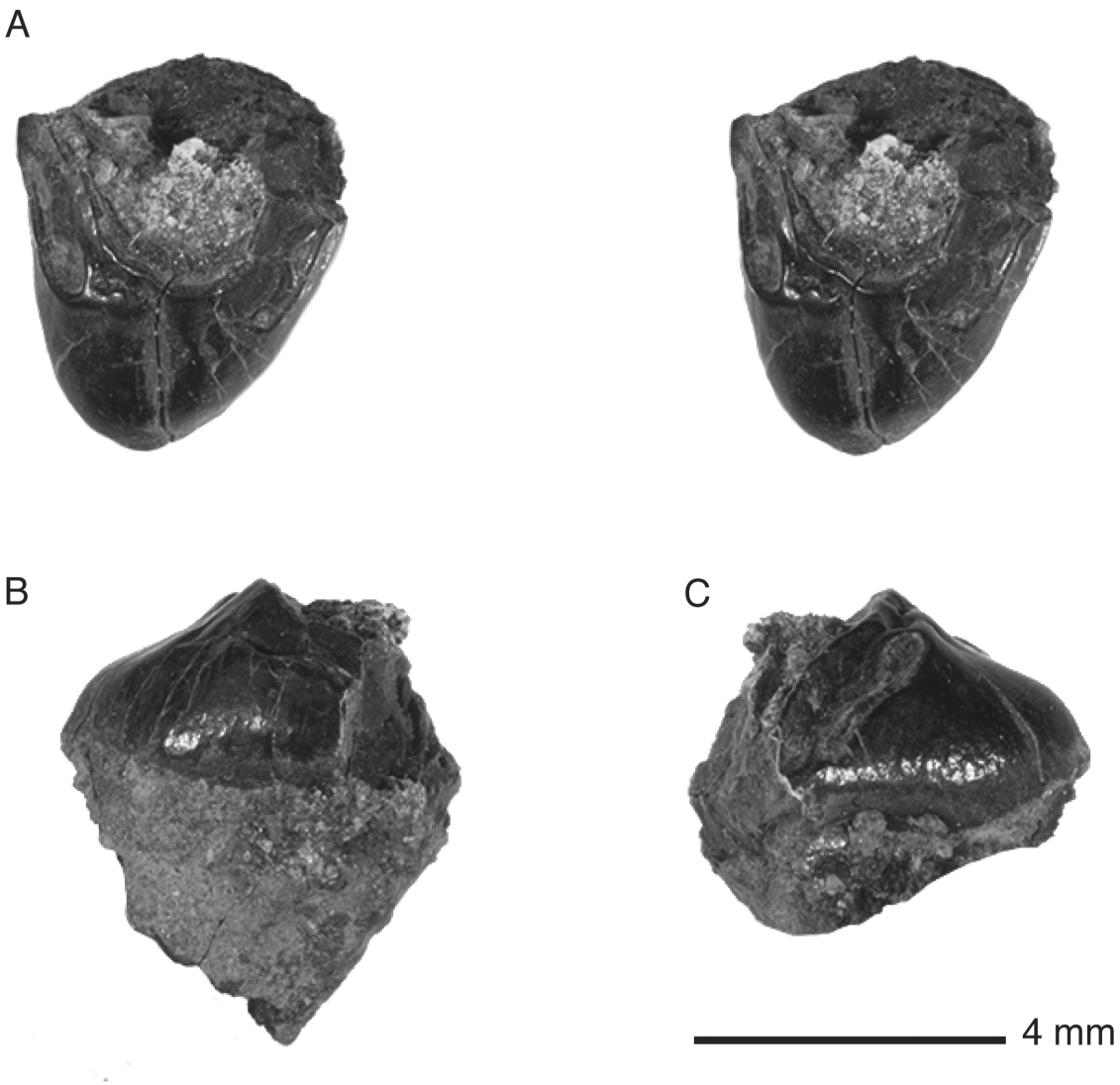

Figure 3.13.15 Lingual fragment of Periptychidae, genus and species indeterminate MX (RAMP 4045) in stereo occlusal (A), mesial (B), and distal (C) views.

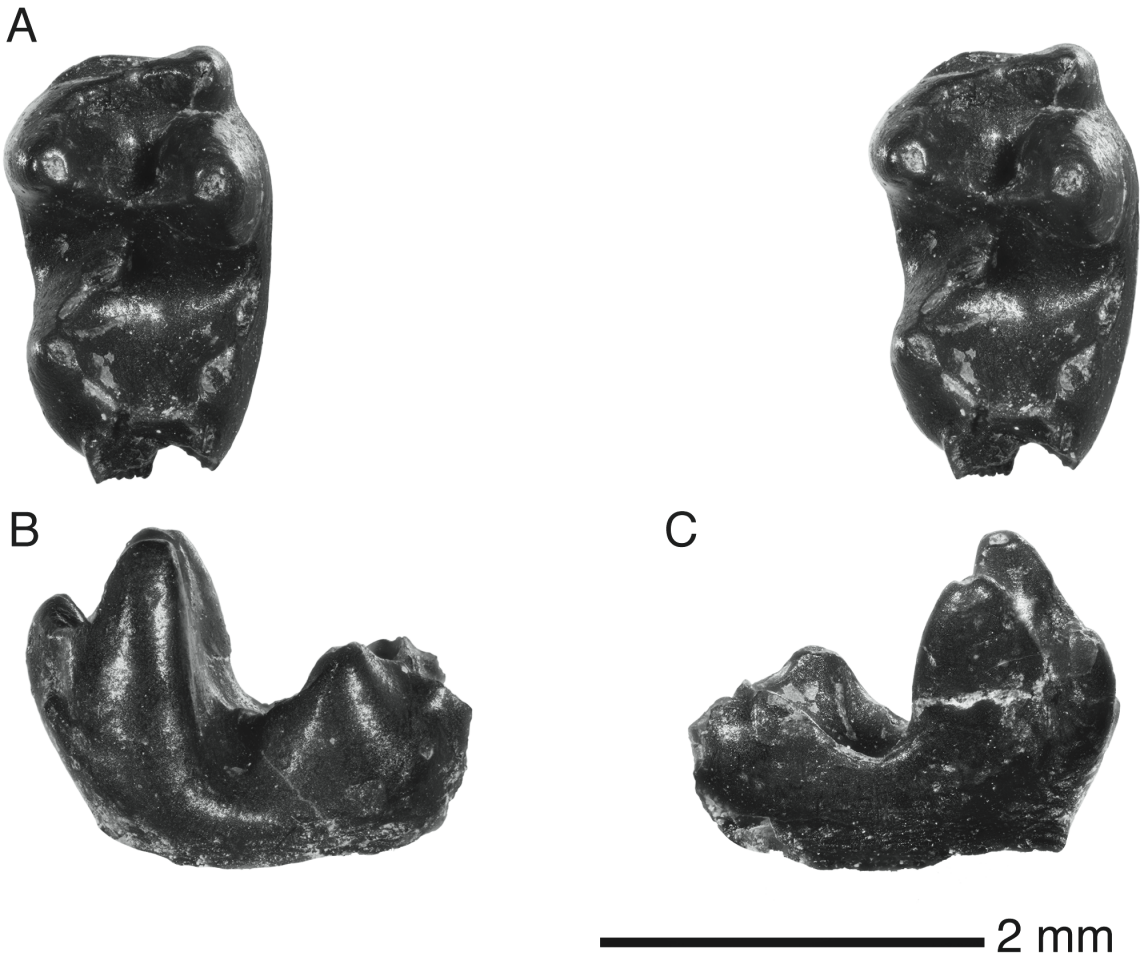

Figure 3.13.16 *Purgatorius* cf. *P. coracis* m3 (RAMP 4078) in stereo occlusal (A), labial (B), and lingual (C) views.

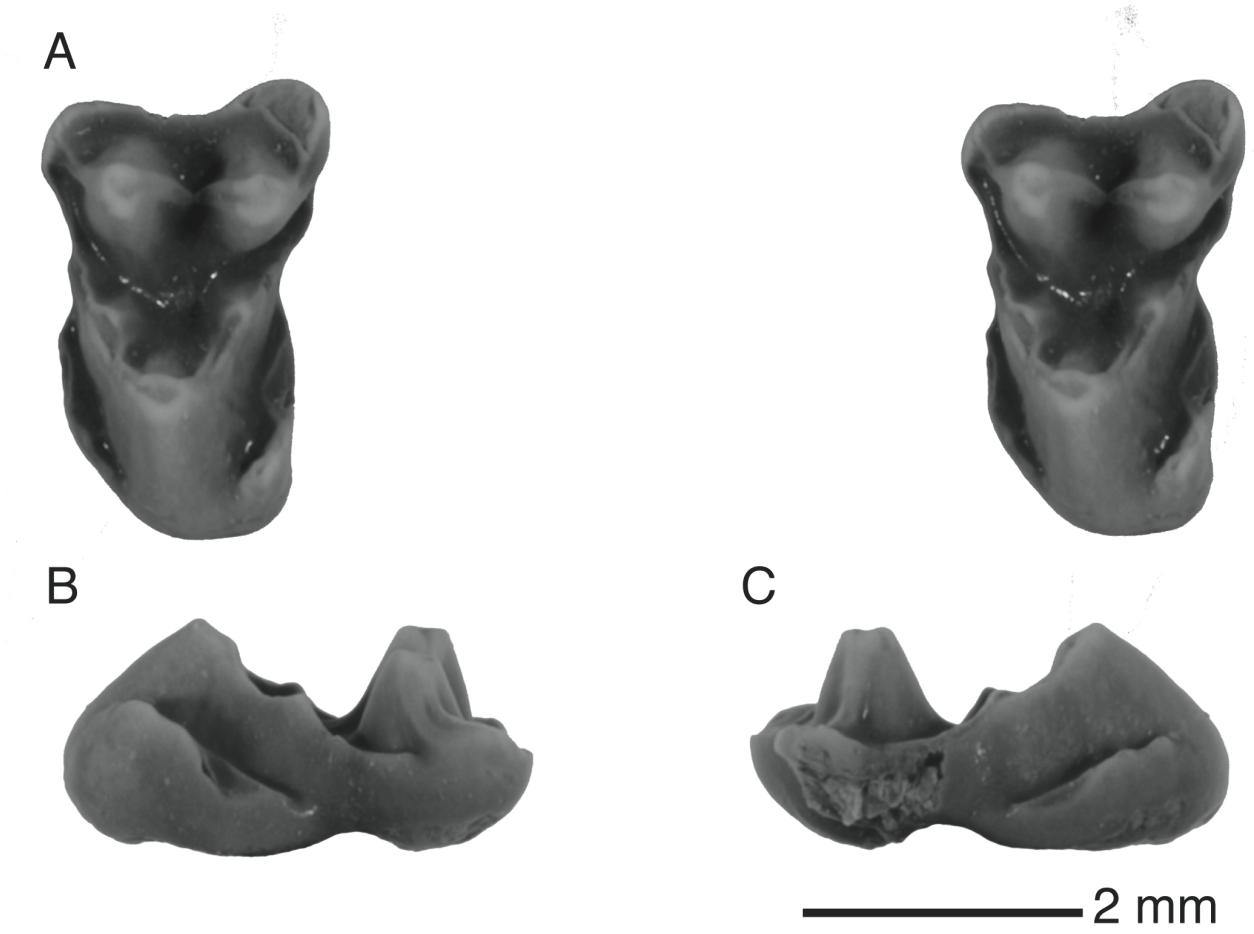

Figure 3.13.17 *Purgatorius* cf. *P. coracis* M2 (UWBM 106217) in stereo occlusal (A), distal (B), and mesial (C) views.

3.13.5 TABLES

All measurements in mm. Tables include only specimens where it was possible to take at least one measurement accurately.

Table 3.13.1 Voucher specimens used for systematic comparisons.

Institution	Number	Genus	Species	Position/material
UWBM/UA	71496/2846	*Alphadon*	*marshi*	Maxilla and dentary
UA	3376	*Alphadon*	*marshi*	M4
UA	2973	*Ambilestes*	*cerberoides*	Maxilla with P3–M1, M3
USNM	23297	*Anisonchus*	*athelas*	Maxilla with p4–m2
UCMP	134694	*Baioconodon*	*nordicum*	P3
UCMP	132711	*Cimexomys*	*gratus*	m1
UCMP	132712	*Cimexomys*	*gratus*	m1
UCMP	73863	*Cimexomys*	*gratus*	M1
UCMP	116986	*Cimexomys*	*minor*	P4
USNM	15760	*Haploconus*	*angustus*	Maxilla with M1–2
NMMNH	8680	*Hemithlaeus*	*kowalevskianus*	Maxilla with P4–M2
NMMNH	15044	*Hemithlaeus*	*kowalevskianus*	Dentary with p4–m3
UCMP	47738	*Leptalestes*	*cooki*	Maxilla with P3-M3
UCMP	52554	*Leptalestes*	*cooki*	M4
UCMP	168703	*Leptalestes*	*krejcii*	M4
LACM	112901	*Mimatuta*	*minuial*	Maxilla with P4–M2
UCMP	116518	*Mimatuta*	*morgoth*	M2
UCMP	116519	*Mimatuta*	*morgoth*	Maxilla with M2–3
UCMP	89690	*Oxyacodon*	*agapetillus*	Maxillae (L,R) with P3 fragments, P4–M3
UCMP	36640	*Oxyacodon*	*priscilla*	Maxilla with p4–m3
UNM	NP-319	*Oxyacodon*	*priscilla*	Maxilla with P3–M2
AMNH	3550	*Oxyacodon*	*apiculatus*	Maxilla with P4–M3
UCMP	133245	*Oxyprimus*	*erikseni*	M3
UCMP	132347	*Oxyprimus*	*erikseni*	M2
UCMP	116514	*Oxyprimus*	*erikseni*	M3

UCMP	53256	*Pediomys*	*elegans*	M4
KU	16079	*Procerberus*	*formicarum*	p4
KU	16078	*Procerberus*	*formicarum*	P3
UCMP	137189	*Procerberus*	cf. *P. Grandis*	Maxilla with P3-M3
UCM	34955	*Procerberus*	*grandis*	/mx
UCMP	46882	*Protalphadon*	*lulli*	Dentary with p2, m1–m3
SPSM	62-2061	*Protungulatum*	*donnae*	P3
UCMP	112002	*Protungulatum*	*donnae*	Dentary with p3–m1
UCMP	132610	*Protungulatum*	*donnae*	m1
UCMP	132595	*Protungulatum*	*donnae*	Dentary with p4–m1
UCMP	132499	*Protungulatum*	*donnae*	Dentary with m1–2
UCMP	132461	*Protungulatum*	*donnae*	Dentary with m2–3
UCMP	132497	*Protungulatum*	*donnae*	Dentary with m2
UCMP	132611	*Protungulatum*	*donnae*	m1
UCMP	105007	*Protungulatum*	*donnae*	Maxilla with M2–M3
UCMP	112111	*Protungulatum*	*donnae*	M1–M2
UCMP	112112	*Protungulatum*	*donnae*	M2–M3
UM	VP-1504	*Purgatorius*	*unio*	?m2
UM	VP-1506	*Purgatorius*	*unio*	m3
UCMP	117771	*Thylacodon*	*montanensis*	M4
OMNH	20536	*Varalphadon*	*wahweapensis*	m1–m3

Table 3.13.2 Measurements of isolated molars of *Mesodma hensleighi* from McGuire Creek localities.

Locality	Institution	Specimen	Tooth	Length	Width
V88036	RAM	6410	m2	1.08	1.10
V88046	RAM	4069	M2	1.14	1.16
V88046	UCMP	106319	M2	1.15	1.15
V88046	UCMP	106321	M2	1.14	1.22

Table 3.13.3 Measurements of isolated lower p4s of *Mesodma formosa* from McGuire Creek localities.

Locality	Institution	Specimen	Tooth	Length	L1	Height
V84193	UCMP	132296	p4	3.57	1.53	2.06
V84194	UCMP	134615	p4	3.87	1.72	2.02
V84194	UCMP	239283	p4	3.59	1.60	1.80
V84194	UCMP	239317	p4	3.79	1.75	1.95
V84194	UCMP	239285	p4	3.67	1.65	1.87
V88036	RAM	4044	p4	3.40	1.61	1.66
V88036	RAM	6408	p4	3.52	1.36	1.70

AVERAGES

Locality	Tooth		$\bar{x}$	OR	N
V84193	p4	L	3.57	-	1
		L1	1.53	-	1
		H	2.06	-	1
V84194	p4	L	3.73	3.59–3.87	4
		L1	1.68	1.60–1.75	4
		H	1.91	1.80–2.02	4
V88036	p4	L	3.46	3.40–3.52	2
		L1	1.49	1.36–1.61	2
		H	1.68	1.66–1.70	2

Table 3.13.4 Measurements of isolated teeth of *Mesodma formosa* from McGuire Creek localities.

Locality	Institution	Specimen	Tooth	Length	Width
V88036	RAM	4034	P4	2.14	1.18
V88036	RAM	6398	P4	-	0.98
V88036	RAM	4060	M1	2.88	1.35
V84193	UCMP	144286	M2	1.31	1.29
V84193	UCMP	144287	M2	1.37	1.34
V84193	UCMP	144289	M2	1.32	1.32
V84193	UCMP	144290	M2	1.36	1.45
V84193	UCMP	144292	M2	1.41	1.46
V84193	UCMP	144293	M2	1.31	1.27
V84193	UCMP	145217	M2	1.41	1.42
V84194	UCMP	143660	M2	1.45	1.44
V84194	UCMP	143661	M2	1.39	1.43
V84194	UCMP	143664	M2	1.36	1.36
V84194	UCMP	143665	M2	1.55	1.29
V84194	UCMP	145170	M2	1.36	1.32
V84194	UCMP	239299	M2	1.49	1.45
V84194	UCMP	239306	M2	1.47	1.42
V84194	UCMP	239312	M2	1.45	1.36
V84194	UCMP	239314	M2	1.46	1.44
V88036	RAM	4021	M2	-	1.32
V88036	RAM	6392	M2	1.49	1.27
V88036	RAM	6404	M2	1.49	1.43
V88046	UWBM	105821	M2	1.34	1.36
V88046	UWBM	105870	M2	1.47	1.49
V84193	UCMP	144280	m1	2.36	0.99
V84193	UCMP	144281	m1	2.35	1.00
V88036	RAM	6384	m1	2.47	1.05
V88046	UWBM	105818	m1	2.30	1.13
V84193	UCMP	144285	m2	1.48	1.21
V84194	UCMP	143659	m2	1.53	1.36
V84194	UCMP	143663	m2	1.43	1.24
V84194	UCMP	145158	m2	1.24	1.10
V88036	RAM	4033	m2	1.52	1.28
V88036	RAM	6403	m2	1.48	1.29
V88036	UCMP	106216	m2	1.39	1.10
V88046	RAM	4116	m2	1.48	1.31

V88046	RAM	4126	m2	1.32	1.22
V88046	UWBM	105820	m2	1.40	1.22
V88046	UWBM	105817	m2	1.43	1.19

AVERAGES

Locality	Tooth		$\bar{x}$	OR	N
V88036	P4	L	2.14	-	1
		W	1.08	0.98–1.18	2
V88036	M1	L	2.88	-	1
		W	1.35	-	1
V84193	M2	L	1.35	1.31–1.41	7
		W	1.36	1.27–1.46	7
V84194	M2	L	1.44	1.36–1.55	9
		W	1.39	1.29–1.45	9
V88036	M2	L	1.49	1.49	2
		W	1.34	1.27–1.43	3
V88046	M2	L	1.41	1.34–1.47	2
		W	1.43	1.36–1.49	2
V84193	m1	L	2.36	2.35–2.36	2
		W	1.00	0.99–1.00	2
V88036	m1	L	2.47	-	1
		W	1.05	-	1
V88046	m1	L	2.30	-	1
		W	1.13	-	1
V84193	m2	L	1.48	-	1
		W	1.21	-	1
V84194	m2	L	1.40	1.24–1.53	3
		W	1.23	1.10–1.36	3
V88036	m2	L	1.46	1.39–1.52	3
		W	1.22	1.10–1.29	3
V88046	m2	L	1.41	1.32–1.48	2
		W	1.24	1.19–1.31	2

Table 3.13.5 Measurements of lower p4s pf *Mesodma thompsoni* from McGuire Creek localities. Dagger (†) indicates a tooth from a dentary including other teeth, all of which have the same specimen number.

Locality	Institution	Specimen	Tooth	Length	L1	Height
V84193	UCMP	132293	p4	4.16	1.89	1.91
V84193	UCMP	132295	p4	4.03	1.80	2.06
V84194	UCMP	132297	p4	4.00	1.70	2.15
V84194	UCMP	132298	p4	4.34	1.86	2.09
V84194	UCMP	132304†	p4	4.01	1.82	1.98
V84194	UCMP	134614	p4	4.23	1.89	2.03
V84194	UCMP	145159	p4	4.01	1.79	1.91
V84194	UCMP	239281	p4	3.98	1.57	2.15
V84194	UCMP	239282	p4	4.12	1.90	1.84
V84194	UCMP	239284	p4	4.01	1.83	2.12
V84194	UCMP	239382	p4	4.23	-	-
V84194	UCMP	239383	p4	3.92	1.89	1.84
V88036	RAM	4025	p4	3.99	1.50	2.21
V88046	RAM	4067	p4	4.07	1.55	1.67
V88046	RAM	4104	p4	4.03	1.60	1.68
V88046	UWBM	106180	p4	3.95	1.42	2.00

AVERAGES

Locality	Tooth		$\bar{x}$	OR	N
V84193	p4	L	4.10	4.03–4.16	2
		L1	1.84	1.80–1.89	2
		H	1.98	1.91–2.06	2
V84194	p4	L	4.08	3.98–4.34	11
		L1	1.80	1.57–1.90	10
		H	2.01	1.84–2.15	10
V88036	p4	L	3.99	-	1
		L1	1.50	-	1
		H	2.21	-	1
V88046	p4	L	4.02	3.95–4.07	3
		L1	1.52	1.42–1.60	3
		H	1.78	1.67–2.00	3

Table 3.13.6 Measurements of teeth of *Mesodma thompsoni* from McGuire Creek localities. Dagger (†) indicates a tooth from a dentary including other teeth, all of which have the same specimen number. Asterisk indicates measurements are approximate due to breakage.

Locality	Institution	Specimen	Tooth	Length	Width
V84193	UCMP	132287	P4	2.93	1.65
V84193	UCMP	132288	P4	2.62	1.42
V84193	UCMP	132289	P4	2.71	1.32
V84193	UCMP	132290	P4	2.65	1.36
V84194	UCMP	134616	P4	3.15	1.54
V84194	UCMP	145167	P4	2.74	1.50
V84194	UCMP	239294	P4	2.98	1.52
V84194	UCMP	239295	P4	2.74	1.51
V84194	UCMP	239300	P4	2.96	1.40
V84194	UCMP	239309	P4	2.76	1.34
V84194	UCMP	239323	P4	3.00	1.41
V84194	UCMP	239353	P4	2.65	1.28
V84194	UCMP	239354	P4	3.12	1.55
V84194	UWBM	106185	P4	2.39*	1.26
V84194	UWBM	106186	P4	2.60	1.29
V88036	RAM	4026	P4	2.59	1.47
V88036	RAM	4032	P4	2.50	1.32
V88036	RAM	6377	P4	2.93	1.42
V88036	RAM	6406	P4	2.67	1.55
V88036	RAM	18581	P4	2.65	1.55
V88036	RAM	18582	P4	2.61	1.38
V88046	RAM	4070	P4	-	1.27
V88046	RAM	4099	P4	-	1.35
V88046	RAM	4111	P4	2.85	1.54
V88046	RAM	4122	P4	-	1.28
V84193	UCMP	132292	M1	3.34	1.48
V84193	UCMP	134611	M1	3.32	1.45
V84193	UCMP	134613	M1	3.25	1.47
V84194	UCMP	239280	M1	3.47	1.49
V84194	UCMP	239279	M1	3.45	1.48
V84194	UCMP	239291	M1	3.43	1.60
V84194	UCMP	239292	M1	3.23	1.47
V84194	UCMP	239308	M1	3.15	1.52
V84194	UCMP	239315	M1	3.38	1.50
V84194	UCMP	239324	M1	3.39	1.49
V88036	RAM	4063	M1	3.66	1.56

V88036	RAM	6400	M1	-	1.60
V88036	RAM	6402	M1	3.35	1.42
V88036	RAM	18577	M1	3.51	1.51
V88036	RAM	18586	M1	-	1.46
V88036	UWBM	105867	M1	3.29	1.50
V88046	RAM	4095	M1	-	1.45
V88046	RAM	4108	M1	-	1.64
V88046	RAM	4117	M1	-	1.46
V88046	RAM	4124	M1	3.27	1.53
V88046	UWBM	106181	M1	3.31	1.43
V88046	UWBM	106179	M1	-	1.45
V84194	UCMP	145171	M2	1.96	1.90
V84193	UCMP	144282	m1	2.66	1.20
V84193	UCMP	144283	m1	2.70	1.15
V84193	UCMP	144284	m1	2.68	1.03
V84194	UCMP	239307	m1	2.69	1.14
V84194	UCMP	132304†	m1	2.40	1.08
V88036	RAM	4041	m1	2.66	1.29
V88036	RAM	4043	m1	2.76	1.19
V88036	RAM	4061	m2	2.09	1.84

AVERAGES

Locality	Tooth		$\bar{x}$	OR	N
V84193	P4	L	2.73	2.62–2.93	4
		W	1.43	1.32–1.65	4
V84194	P4	L	2.28	2.39–3.15	11
		W	1.42	1.26–1.55	11
V88036	P4	L	2.66	2.50–2.93	6
		W	1.45	1.32–1.55	6
V88046	P4	L	2.85	-	1
		W	1.36	1.27–1.54	4
V84193	M1	L	3.30	3.25–3.34	3
		W	1.47	1.45–1.48	3
V84194	M1	L	3.36	3.15–3.47	7
		W	1.51	1.47–1.60	7
V88036	M1	L	3.45	3.29–3.66	4
		W	1.51	1.42–1.60	6
V88046	M1	L	3.29	3.27–3.31	2
		W	1.49	1.43–1.64	6
V84194	M2	L	1.96	-	1
		W	1.90	-	1
V84193	m1	L	2.68	2.66–2.70	3

		W	1.13	1.03–1.20	3
V84194	m1	L	2.54	2.40–2.69	2
		W	1.11	1.08–1.14	2
V88036	m1	L	2.71	2.66–2.76	2
		W	1.24	1.19–1.29	2

Table 3.13.7 Measurements of teeth of *Cimexomys gratus* from McGuire Creek localities.

Locality	Institution	Specimen	Tooth	Length	Width
V88036	RAM	4053	M1	-	2.03
V88036	RAM	18585	M1	3.28	1.63
V88036	RAM	6387	m1	3.28	1.57
V88046	UWBM	105826	m1	-	1.50

TABLE 3.13.8 Measurements of teeth of *Thylacodon montanensis* FROM UCMP V84194.

Locality	Institution	Specimen	Tooth	Length	MW or WTri	DW or WTal
V84194	UCMP	132299	M1	2.44	2.53	1.85
V84194	UCMP	132300	M2	2.41	2.84	2.51
V84194	UCMP	239350	M4	1.62	1.97	1.56
V84194	UCMP	239305	m2	2.19	1.36	1.34
V84194	UCMP	239337	m1 or 2	-	1.29	-
V84194	UCMP	239304	m2 or 3	-	1.50	-
V84194	UCMP	239340	m2 or 3	-	1.47	-
V84194	UCMP	239333	m4	2.10	1.40	1.12
V84194	UCMP	239336	mx trigonid	-	1.38	-
V84194	UCMP	239367	mx talonid	-	-	1.16

Table 3.13.9 Measurements of teeth of *Procerberus formicarum* from McGuire Creek localities. Asterisk indicates measurements are approximate due to breakage.

Locality	Institution	Specimen	Tooth	Length	MW or WTri	DW or WTal
V84194	UCMP	239318	P3	2.37	1.63	1.78
V88046	RAM	4071	P3	2.18	1.63	1.63
V84194	UCMP	134617	M1	2.45	3.07	3.27
V84194	UCMP	239302	p4	2.91	1.15	1.08
V88036	RAM	6390	p4	-	1.22	1.18
V88046	RAM	4106	p4	2.96	1.27	1.31
V84194	UCMP	239325	m1	2.69	1.71	1.54
V88046	RAM	4083	m1	2.58	1.56	1.51
V88046	RAM	18539	m1	2.54	1.46	1.44
V84194	UCMP	145149	m2	2.52	1.91	1.57
V84193	UCMP	132285	m3	3.05	1.98	1.53
V84193	UCMP	145218	m3	2.73*	1.58	1.28

Table 3.13.10 Measurements of lower molars of *Protungulatum donnae* from McGuire Creek localities. Asterisk indicates measurements are approximate due to breakage.

Locality	Institution	Specimen	Tooth	Length	MW or Tri W	DW or Tal W
V88036	RAM	6376	m3	4.44*	2.80	2.17
V88036	RAM	6389	mx trigonid	-	2.54	-
V88036	RAM	6396	mx trigonid	-	3.28	-
V88046	UWBM	105816	m1 or 2	4.10	2.80	2.83

TABLE 3.13.11 Measurements of teeth of UCMP 134571, *Mimatuta morgoth,* from UCMP V88036.

Tooth	Length	MW	DW	A/MW
P4	3.75	4.58	5.18	0.27
M1	3.8	5.53	5.88	0.39
M2	3.97	5.87	6.06	0.38
M3	3.63	5.64	5.53	0.40

Table 3.13.12 Measurements of teeth of UWBM 99100, *Mimatuta minuial*, from UCMP V88046.

Tooth	Length	WTri	WTal
p4	3.45	2.45	2.46
m1	3.81	2.69	2.76
m2	4.12	3.37	3.20
m3	5.40	2.95	2.64

TABLE 3.13.13 Measurements of lower molars of *Mimatuta* sp. from McGuire Creek localities.

Locality	Institution	Specimen	Tooth	Length	WTri	WTal
V84193	UCMP	132281	m1	3.86	2.68	2.82
V84194	UCMP	132301	m2 talonid	-	-	3.10
V84194	UCMP	132301	m3	4.67	2.89	2.47
V88046	RAM	4087	mx trigonid	-	2.92	-
V88046	RAM	4074	mx trigonid	-	2.93	-
V88046	RAM	4082	mx talonid	-	-	2.64

Table 3.13.14 Size comparisons between UWBM 106217 and upper molars of *Purgatorius* species. Some width measurements were reported simply as "width", without distinction between MW and DW; these measurements are labeled "W". No M2s have been reported for *P. pinecreeensis*; M1 measurements are provided for coarse size comparison.

Taxon	Tooth		$\bar{x}$	OR	N	Reference
Purgatorius cf. *P. coracis*	M2	L	1.98	-	1	This study: UWBM 106217
		MW	3.01	-	1	
		DW	3.21	-	1	
Purgatorius coracis	M2	L	1.85	1.7–1.9	4	Johnston and Fox, 1984; Fox and Scott, 2011
		W	2.78	2.7–2.8	4	
Purgatorius unio	M2	L	1.9	-	1	Van Valen, 1994
		W	2.85	2.8–2.9	2	
Purgatorius titusi	M2	L	1.98	1.90–2.00	4	Buckley, 1997
		MW	2.78	2.70–2.90	4	
		DW	2.83	2.80–2.90	4	
Purgatorius janisae	M2	L	1.95	1.77–2.18	24	Clemens and Wilson, 2009
		MW	2.71	2.46–3.04	25	
		DW	2.85	2.64–3.13	24	
Purgatorius pinecreeensis	M1	L	1.53	-	1	Scott et al., 2016
		W	2.14	2.08–2.20	2	

CHAPTER 4: MAMMALIAN DENTAL ECOMORPHOLOGY ACROSS THE CRETACEOUS-PALEOGENE BOUNDARY THROUGH THE FIRST 1.2 MILLION YEARS OF THE PALEOGENE

4.1 ABSTRACT

Understanding an animal's diet is critical to understanding the way in which it interacts with other organisms and its broader environment. Dietary ecology can be especially useful for piecing together ecosystems in the fossil record, where feeding behaviors cannot be directly observed but may be inferred from dental morphology. We use three-dimensional (3D) quantitative dental morphology to characterize dietary ecology of mammals following the Cretaceous-Paleogene (K-Pg) mass extinction, aiming to understand patterns of change in mammalian diets in the wake of a severe ecosystem perturbation. In previous studies of post-K-Pg mammalian ecological diversification, focus has been on patterns of change on a very large spatiotemporal scale, or only on the earliest aftermath of the mass extinction. We concentrate on the dietary ecology of mammals after the K-Pg mass extinction on a restricted spatiotemporal scale: the latest Cretaceous and first ca. 1.2 million years [Ma] of the Paleogene in northeastern Montana. To predict diet from dental morphology, we use three dental topographic metrics (orientation patch count rotated [OPCR], relief index [RFI], and Dirichlet normal energy [DNE]), which quantify surface features of teeth that can be correlated to the use of different food types. In therian mammals, we compare a single tooth position, the penultimate lower molar, across a sample of 24 extant mammals with known diets, and determine likely diet in

extinct taxa using discriminant function analysis based on the extant comparative sample. In multituberculate mammals, we determine likely diet via comparison of dental topographic metrics of full lower tooth rows from our study with those of previous studies on multituberculate dietary ecology. Our results indicate that i) in the first ca. 1.2 Ma of the Paleogene, mammalian diets shifted away from insectivory and toward omnivory and more plant-based diets, with early morphological disparity arising from immigrant taxa rather than local survivors of the extinction; and ii) the relationship between dietary ecology and dental topographic metrics of individual teeth needs to be further investigated, to better understand the relative contribution each individual tooth makes to overall tooth row shape descriptors.

4.2 INTRODUCTION

Understanding an animal's diet is critical to understanding the way in which it interacts with other organisms and its broader environment. Dietary ecology can be especially useful for piecing together ecosystems in the fossil record; if it is possible to infer dietary ecology from fossils, it is thereby possible to develop an understanding of the diversity and disparity of ecotypes in the environment at a given point in evolutionary history, and to track changes in niche occupation in various groups of organisms through evolutionary time. Further, in combination with other ecological data (e.g., locomotor habits of animals in a paleocommunity), environmental evidence, and precise dating techniques, it is possible to test hypotheses relating changes in organismal ecology to larger-scale environmental and biological phenomena. One such phenomenon is the Cretaceous-Paleogene (K-Pg) mass extinction event, which, in terrestrial ecosystems, most notably wiped out non-avian dinosaurs and signaled the beginning of the Age of Mammals.

The K-Pg mass extinction event was pivotal in the evolutionary history of mammals because of the rapid increases in mammalian taxonomic richness (Alroy 1999; Wilson 2014), body size (Alroy 1999; Smith et al 2010), and ecological disparity (Wilson 2013; Halliday and Goswami 2015; DeBey and Wilson 2014, 2017; Grossnickle and Newham 2016) that directly followed it. The K-Pg mass extinction and its causes, kill mechanisms, and selectivity as they relate to mammals have received considerable attention in the literature (e.g., Slater 2013; DeBey and Wilson 2014, 2017; Wilson et al. 2012, Wilson 2013, 2014; Longrich 2016); in contrast, mammalian ecological change following the mass extinction, although often considered briefly

in mass extinction studies, has received comparatively less attention and remains somewhat obscure.

Previous studies of post-K-Pg mammalian ecological diversification have largely focused on patterns of change on a very large spatiotemporal scale (e.g., using million-year time bins; Alroy 1999) or on only the immediate aftermath of the mass extinction (within 410 thousand years [ka] of the K-Pg boundary; Wilson 2013). In this study, we focus on the dietary ecology of mammals after the K-Pg mass extinction on a restricted spatiotemporal scale: the first ca. 1.2 million years [Ma] of the Paleogene in northeastern Montana, in the Hell Creek Formation and Tullock Member of the Fort Union Formation (Clemens and Wilson 2009; Sprain et al. 2015). Fossil-bearing strata in the Hell Creek area deposited during the Late Cretaceous through the early Paleocene are ideal for high-resolution studies of ecology in a variety of vertebrate groups, both pre- and post-mass-extinction (e.g., Estes and Berberian 1970; Archibald 1983;Wilson 2013; DeBey and Wilson 2014, 2017). Because the mammalian fossil record from this time period in North America is almost exclusively composed of isolated teeth and tooth-bearing elements, we apply dental topographic analysis (DTA, López-Torres et al. 2017) to 3D digital models of individual cheek teeth of extinct latest Cretaceous and early Paleogene mammals from our study area. DTA relies on several different metrics for summarizing the three-dimensional (3D) morphology of a tooth crown. Dietary inferences of extinct taxa are then based on comparisons with the DTA values of extant mammals of known diets.

With a few exceptions (e.g., Evans et al. 2007; Santana et al. 2011; Wilson and Self 2011; Wilson et al. 2012; Smits and Evans 2012; Pineda-Munoz et al. 2017), previous studies that use

DTA have been centered around primates and their extinct relatives (Boyer 2008; Bunn et al 2011; Evans 2013; Winchester et al. 2014; Pampush et al 2016; Spradley et al 2016; Prufrock et al 2016, 2016b; Lopez-Torres et al 2017; Thiery et al 2017). As a result, published comparative DTA data sets, especially those from individual teeth, tend to be phylogenetically biased toward primates. As such, the goals of this study are threefold: i) to build a comparative DTA data set of a phylogenetically broad sample of extant mammalian taxa with known diets; ii) to constrain dietary ecologies of K-Pg mammals via comparison with our extant DTA data set and other published DTA data sets, and iii) to quantify dental morphological disparity and dietary ecology of mammals across the K-Pg boundary and through the first ca. 1.2 Ma of the Paleogene, in order to shed light on the ecological dynamics of the post-K-Pg mammalian recovery.

Institutional Abbreviations

AMNH, American Museum of Natural History; **CCM,** Carter County Museum; **RAM,** Raymond M. Alf Museum of Paleontology; **UA**, University of Alberta Laboratory for Vertebrate Paleontology; **UCMP,** University of California Museum of Paleontology; **UM**, University of Michigan Museum of Paleontology; **USNM**, U.S. Smithsonian National Museum of Natural History; **UWBM,** University of Washington Burke Museum of Natural History and Culture.

4.3 MATERIALS AND METHODS

Extant mammalian sample choice and diet categories. For our comparative sample, we collected dental surface data from the lower molars of 24 species of extant mammals representing nine orders (Table 4.1). We selected these taxa because they are phylogenetically diverse, and include a wide variety of dietary ecologies and dental morphologies. Despite the fact

that the dental topographic metrics used here are homology-free, we limited our extant sample to taxa with clear dental positional homologies that use their teeth for oral food processing. We excluded mammals that are edentulous (e.g., echidnas), have homodont dentition (e.g., dolphins), or lack enamel on their teeth (e.g., aardvarks). Because our mammalian fossil sample (see below) includes both metatherians (members of the stem-based clade including modern marsupials; Rougier et al. 1998) and eutherians (members of the stem-based clade including modern placental mammals; O'Leary et al. 2013), we likewise included both metatherians and eutherians in our extant comparative sample. Dietary classification of extant mammals was based on the primary literature; we also assembled body mass for our extant sample using the primary literature and compendia (Table 4.1). Diet in mammals can be assessed via stomach contents, fecal contents, or the amount of time spent eating a particular food (Pineda-Munoz and Alroy 2014). It can also be quantified in a variety of ways (e.g., percentage of observed fecal pellets containing a particular resource; percent by volume of a resource in an animal's stomach contents). It is therefore difficult to obtain a homogeneous data set to quantitatively determine mammalian diet via numeric cutoffs in percent use of food resources. We nonetheless collected diet data from the literature and designated dietary categories using the following guidelines.

To reduce biases introduced by seasonal availability of food resources, we used data from studies with samples collected year-round or at several points during the year, whenever possible. We also preferred studies that reported sample size (e.g., number of fecal samples collected). We assigned species to one of eight dietary categories: folivory, frugivory, plant-dominated omnivory, animal-dominated omnivory, carnivory, insectivory, soft-insect insectivory, or hard-object invertivory. Species assigned to folivore, insectivore, or carnivore were reported to have

diets almost exclusively composed of one type of resource (leaves and shoots, insects, and vertebrates, respectively), regardless of the type of measurement (fecal, stomach contents, etc.). The coast mole (*Scapanus orarius*) was identified as a soft-insect specialist because of the high proportion of earthworms in its diet (70–95%; Moore 1933; Glendenning 1959) compared to the diets of other insectivores. Our strictest frugivore, the great fruit-eating bat *Artibeus lituratus*, has a diet consisting almost exclusively of fruits (Giannini and Kalko 2004); our other frugivore, *Pecari tajacu*, has a slightly more varied diet, which is nonetheless mainly composed of fruit (Desbiez et al. 2009). Two other taxa, classified here as plant-dominated omnivores (*Paradoxurus hermaphroditus* and *Nasua narica*) have diets rich in fruit as well (i.e., the most common item in their fecal samples, Table 4.1). The three other species identified as plant-dominated omnivores (*Caluromys derbianus*, *Sus scrofa*, and *Tamias townsendii*) ingest a more even distribution of plant matter types with less of a focus on fruit (Table 4.1 references). All five plant-dominated omnivores in our sample ingest a variety of food items, and occasionally eat animal matter, but mostly rely on plant parts, including leaves, roots, seeds, and fruits. The four animal-dominated omnivores in our sample also use a variety of food resources, but mostly rely on animal matter (insects and vertebrates, as well as carrion).

Specimen choice and 3D data collection. We selected dental specimens (both extant and fossil) with as little dental wear as possible; in all species except *Sus scrofa*, whose teeth function partially through secondary wear-induced morphology (Popowics et al. 2001, 2004), we excluded specimens with excessive wear (e.g., complete loss of cusps through breakage or attrition) to ensure that the majority of dental structures present on the teeth in life were sampled for our topographic analyses. For therian mammals (eutherians and metatherians), we conducted

our analyses on individual lower cheek teeth because isolated teeth are more common in the K-Pg mammalian fossil record than full tooth rows are. We decided against constructing and analyzing composites of lower molar rows from isolated teeth in part so that the results from our analysis of individual teeth could be more broadly compared to results in the existing literature and would allow for future comparisons with results from fossil taxa for which lower molar rows cannot be composited. We used the penultimate lower molar (i.e., the third molar [m3] in metatherians, and typically the second molar [m2] in eutherians) because it is likely functionally analogous across eutherians and metatherians due to its similar location along the tooth row relative to the fulcrum of the jaw (Janis 1990; Wilson 2013). In the hyena (*Crocuta crocuta*) and the tayra (*Eira barbara*), we analyzed the last lower molar (m1), rather than the penultimate lower molar; this tooth is the lower carnassial and is heavily involved in food processing via both slicing and crushing (Van Valkenburg 2007).

The multituberculates are an extinct group of mammals that are very common in K-Pg assemblages of the Western Interior of North America; they have been compared to rodents in terms of morphology and ecology. For their analysis, we used lower cheek teeth instead of individual teeth. Multituberculate dental morphology is very different from that of therian mammals, such that it is not clear which, if any, single tooth in multituberculates is the functional analog of the penultimate lower molar in therians. Because this precludes comparison between our multituberculate sample and our extant therian mammal sample, we made comparisons with the results of Evans et al. (2007) and Wilson et al. (2012; see below, Multituberculate OPCR Conversion).

Dental surface scans were collected from original tooth specimens (fossil and modern), epoxy casts of teeth, or molds of teeth. We also used several scans downloaded from MorphoSource (morphosource.org; see 4.10: Appendix 2 for specimen URLs). Epoxy casts were obtained from museum collections (Tables 4.2 and 4.3). Molds were made using Coltene President Plus polyvinylsiloxane (Type 2, medium consistency). We scanned specimens using one of three scanners: Bruker Skyscan 1172, Skyscan 1173, or NSI X5000. We determined appropriate scan resolution based on the size of the specimen; because the teeth in our sample vary in size (Tables 4.1–4.3), resolutions ranged from 4 μm to 71 μm; most specimens were scanned at resolutions between 6 and 20 μm. Scans were reconstructed in NRecon (Bruker microCT, Belguim), segmented in Materialise Mimics Research 18.0, cleaned and cropped to the base of the enamel crown, and oriented in Geomagic Studio (3DS Systems), resulting in a 3D model for DTA. Scan data from Morphosource were downloaded as image stacks where possible (either DICOM or .tif format) and segmented and processed in Mimics and Geomagic, respectively, following the same protocols as for other specimens. No image stack was available for *Purgatorius janisae* (UCMP 107406), so we used the uncropped .stl available on MorphoSource (4.10: Appendix 2).

Scans of multituberculate specimens were combined in Geomagic to form composite lower cheek tooth rows, and each tooth row was analyzed as a single unit. We chose specimens that were in similar wear stages, with minimal wear. Some multituberculate specimens include multiple teeth in a single jaw; because we could not replicate the exact in-jaw orientation of teeth for species whose models are composed of isolated teeth, and to account for error introduced by non-dental material linking individual teeth in scans of casts (i.e., any area of the mandible present between teeth), all multi-tooth specimens were separated using Geomagic and each tooth

was oriented individually. After Spradley et al. (2017), we downsampled clean models (individual lower molars in therians, full tooth rows in multituberculates) to 10,000 faces and smoothed with 25 iterations of the Smooth Surface function in Avizo 9 (ThermoFisher Scientific), with lambda = 0.6. Smooth models were saved as .ply files.

Therian and multituberculate fossil samples. We collected dental topographic data from single lower molars of 55 species of extinct therian mammals and from full lower cheek tooth rows of seven species of multituberculates from the latest Cretaceous and early Paleogene of northeastern Montana (Tables 4.2 and 4.3). This sample represents the majority of mammalian taxa known to occur in the Hell Creek Formation and Tullock Member of northeastern Montana from the Late Cretaceous Lancian (La) North American Land Mammal Age (NALMA) and the early Paleocene Puercan 1 (Pu1), Puercan 3 (Pu3), and Torrejonian 1 (To1) NALMA interval zones (Van Valen 1994; Clemens 2004, 2011; Clemens and Wilson 2009; Wilson 2013, 2014). Because the mammalian fossil assemblage from the Puercan 3 interval zone is still under study by W.A. Clemens, faunal lists for that interval zone are preliminary. We included as many species as possible from the preliminary list in Wilson (2014, table 1), as well as a number of unnamed morphotypes (e.g., "*Chriacus* species A") from the Pu3 collection of mammals at the University of California Museum of Paleontology. We included these morphotypes to sample the entire breadth of morphology present in that interval zone, despite the fact that not all species have been fully described. Brief descriptions of these morphotypes are included in 4.9: Appendix 1. Most fossil specimens represented in our analysis are from localities in the Hell Creek Formation or the Tullock Member of the Fort Union Formation.

For some species known from the Lancian, Puercan, or Torrejonian 1 NALMA interval zones of northeastern Montana, the appropriate tooth position is either not known from localities in northeastern Montana or the specimen was not available to us at the time of study. Thus, whenever possible, we substituted specimens of the same taxon from other parts of the Western Interior of North America (Table 4.2). We excluded therian taxa that are not known from m2s or m3s and multituberculate taxa for which composite lower cheek tooth rows could not be assembled.

Dental topographic analyses (DTA). All analyses were conducted in R version 3.3.3 (R Core Team 2017). Dental topographic analyses were conducted on each 3D tooth model using the molaR_Batch function from the package molaR, version 4.2 (Pampush et al. 2016). For analysis of Dirichlet normal energy (DNE), the boundary discard was set to "Vertex"; for relief index (RFI), the alpha was set to 0.15; for rotated orientation patch count (OPCR), the step number was set to eight and the minimum patch size to three pixels.

Multituberculate OPCR conversion. Our scanning, segmenting, and analysis protocols differ substantially from those of Wilson et al. (2012), which also examined multituberculate lower cheek tooth rows. To account for these differences and allow for comparisons across studies, we developed a predictive formula to convert our multituberculate OPCR values to values that are comparable to those of Wilson et al. (2012). We regressed mean OPCR values from six genera of multituberculates reported by Wilson et al. (2012) on mean OPCR values from the same six genera included in our analysis. We fit a least-squares linear model to the data, and used the resulting formula (see Results: Multituberculates: DTA, disparity, and diet categories through

time) to convert our OPCR values to values that correspond to those of Wilson et al. (2012). This conversion allowed us to make OPCR comparisons with a variety of other multituberculate taxa (Wilson et al. 2012) and extant taxa of known dietary preference (Evans et al. 2007).

Ordinations, morphological disparity, and discriminant function analysis. We natural-log-transformed our DTA data to reduce skew, and used these transformed data to construct a 3D scatterplot (OPCR vs. RFI vs DNE) and three bivariate scatterplots (OPCR vs. RFI, OPCR vs. DNE, and RFI vs. DNE). We tested for correlation among DTA metrics using least-squares linear regression and Spearman's rho. We examined morphospace occupation and clustering among diet categories in the 3D scatterplot. Using the function lda() from the package MASS (Venables and Ripley 2013), we conducted a discriminant function analysis (DFA), first on the extant DTA data to assess the accuracy of the discriminant function, and then on the fossil therian DTA data to predict dietary assignments of each taxon present in each NALMA interval zone that we sampled. We assessed morphological disparity through time using four different approaches applied to the sample from each NALMA interval zone. First, we calculated the variance of each DTA metric (OPCR, DNE, RFI). Second, we calculated mean pairwise 3D Euclidean distance between all taxon pairs; this metric is relatively robust even at small sample size (Ciampaglio et al. 2001). Third, we calculated the mean distance of each taxon from the sample centroid, with 95% confidence intervals estimated using a custom bootstrapping function with 1000 replicates. Fourth, using convhulln() from the package geometry (Habel et al. 2015), we calculated the volume of the 3D convex hull for the sample.

Phylogenetic signal. We tested our extant DTA results for phylogenetic signal using a tree downloaded from timetree.org (Fig. 4.1; Hedges et al. 2006, 2015; Kumar and Hedges 2011; Kumar et al. 2017). For log-transformed DNE, RFI, and OPCR, we calculated both Blomberg's K (Blomberg et al. 2003) and Pagel's lambda (Pagel 1992; Freckleton et al. 2002) using the function phylosig from the package phytools (Revell 2012). No published phylogeny currently exists that incorporates all of the taxa in our fossil sample; as such, we were unable to consider the effects of phylogeny across fossil taxa.

4.4 RESULTS

Phylogenetic signal. DNE and RFI contain a moderate amount of phylogenetic signal (Table 4.4). OPCR contains a more substantial phylogenetic signal. This moderate-to-high degree of phylogenetic signal is likely due in part to the fact that closely related species of mammals not only frequently have similar teeth, but also have similar diet. As such, the discovery of phylogenetic signal in our DTA metrics does not negate the findings of our ecomorphological investigations, but rather highlights the fact that dietary ecology may be phylogenetically conserved. However, the presence of phylogenetic signal also indicates that some degree of similarity in DTA metrics across our extant sample could potentially be due to phylogenetic relatedness rather than similarity of diet, and we therefore interpret our results carefully, especially with regard to diets that appear in only a single monophyletic clade (e.g., folivory in Euarchontans only) in our study (Fig. 4.1).

Extant sample: DTA and diet. Dental surface topography varies across diet categories in our extant sample, but in different ways depending on the DTA metric (Fig. 4.2; 4.11: Appendix 3).

We here exclude results from average slope measurements because average slope is tightly correlated with RFI (Table 4.5) and therefore provides no additional morphological information not provided by RFI. Although DNE and RFI are positively correlated (Table 4.5), their patterns differ slightly across dietary categories. Mean RFI is highest in insectivores and soft-insect specialists, followed by folivores, frugivores, and hard-object invertivores (Fig. 4.2). Mean DNE follows a similar pattern except that frugivores have the second-highest values. One specimen of *Sus scrofa* has an extremely low RFI as well, considerably outside the lower bound of the RFI range for frugivores. Carnivores and omnivores have mean RFI values that are similar to one another, with omnivores (both animal- and plant-dominated) showing the largest variation in RFI.

OPCR is positively correlated with DNE, but not significantly correlated with RFI (Table 4.5). OPCR is significantly higher in frugivores than it is in any other diet, except in both specimens of the plant-dominated omnivore *Sus scrofa* (Fig. 4.2). OPCR is lowest in hard-object invertivores, followed by folivores and carnivores, which both have similarly low mean OPCR values. Both types of omnivores and both types of insectivores all have similar mean OPCR values, which are lower than those of frugivores but higher than carnivores and folivores.

Extant sample: DTA morphospace occupation. In both bivariate scatterplots and a 3D scatterplot of log-transformed DTA values, there is separation of dietary groups in the morphospace (Fig. 4.3). Insectivores (both types) and hard-object invertivores cluster tightly and do not overlap with other dietary groups. Frugivores, with their unique combination of high DNE and OPCR but low RFI, are distinguished from all but two plant-dominated omnivores, both

specimens of *S. scrofa.* The remaining plant-dominated omnivores have medium-to-high values for OPCR, DNE, and RFI, placing them near the exact center of the morphospace. Animal-dominated omnivores occupy a very similar region of morphospace to plant-dominated omnivores, but with overall slightly higher RFI. Carnivores show tight clustering in the low-OPCR, medium-DNE and RFI region of morphospace. Folivores occur in the morphospace very close to carnivores, with some folivores (*Cynocephalus volans*, *Galeopterus variegatus*, and *Avahi laniger*) having slightly higher DNE, RFI, and OPCR than carnivores, and others (*Indri indri* and *Lepilemur mustelinus*) having slightly lower values than carnivores for all three DTA metrics. Notably, several areas of the morphospace are wholly unoccupied, including high OPCR/high RFI/low DNE, and low DNE/low OPCR/high RFI (Fig. 4.3).

Fossil sample: morphospace occupation. The fossil therians plot mostly near the center of the DTA morphospace, in the area occupied by extant carnivores, folivores, and both types of omnivores (Fig. 4.4). None of our fossil taxa plot among the hard-object invertivores, but several fossil taxa (*Chriacus* spp., *Glasbius twitchelli*, *Mimotricentes subtrigonus*, *Litaletes disjunctus*) fall near extant frugivores. A large number of fossil taxa, specifically some cimolestids [family Cimolestidae, late Cretaceous and early Paleogene eutherians; Fox 2015] and small metatherians, fall in the vicinity of extant insectivores. Several other fossil taxa fall well outside of the morphospace occupied by extant taxa. For example, the metatherians *Leptalestes cooki* and *Turgidodon rhaister*, and the archaic ungulate *Mimatuta morgoth*, have high RFI and high OPCR, placing them just outside the convex hulls encompassing modern animal-dominated omnivores (*M. morgoth* and *T. rhaister*) and insectivores (*L. cooki*). A number of cimolestids, as

well as the leptictid *Prodiacodon crustulum*, have similar RFI to modern insectivores but lower OPCR, and as such also fall just outside the insectivore convex hull (Fig. 4.4).

Extant and fossil samples: discriminant function analysis (DFA). The discriminant function analysis (DFA) correctly classified extant mammals into diet categories 82.2% of the time (Table 4.6). Most specimens (60.9%) were classified with a posterior probability greater than 0.60; however, some of those were not identified correctly. For example, both specimens of *Sus scrofa* were identified as frugivores rather than plant-dominated omnivores (at 0.99 posterior probability for UWBM 33170). Plant-dominated omnivores were the most commonly misidentified diet category: both specimens of *S. scrofa* were identified as frugivores, and *Caluromys derbianus* and *Tamias townsendii* were both identified as animal-dominated omnivores. Two folivores were misclassified: *Indri indri* was classified as a carnivore, and *Galeopterus variegatus* was classified as an insectivore. Lastly, the animal-dominated omnivore, *Eira barbara*, was classified as a plant-dominated omnivore.

A number of extant specimens were classified correctly, but with low posterior probabilities, often within 0.10 of the posterior probability of their second-most probable diet. *Sarcophilus harrisii* had a posterior probability of 0.49 for carnivore, but 0.41 for folivore; *Crocuta crocuta* (UWBM 33257) had a posterior probability of 0.49 for carnivore and 0.44 for animal-dominated omnivore; *Paradoxurus hermaphrodites* (UWBM 14711), had probabilities of 0.52 for plant-dominated omnivore, 0.46 for hard-object invertivore; and *Avahi laniger* had posterior probabilities nearly evenly split across folivore, animal-dominated omnivore, carnivore, and insectivore (Table 4.6).

Among fossil taxa (Table 4.7), DFA identified diet with more certainty than in extant taxa. 70.0% of specimens were classified with posterior probabilities of greater than 0.60 in the identified diet category. Further, 12.5% of specimens were classified with greater than 0.90 posterior probability; all of these were classified as insectivores or soft-insect specialists. In concordance with our observations from the scatterplots (Fig. 4.4), fossil taxa were most frequently identified as animal-dominated omnivores (23 taxa), followed by insectivores (14 taxa) and plant-dominated omnivores (8 taxa). Fossil taxa classified as animal-dominated omnivores include a large number of archaic ungulates such as *Oxyacodon*, *Oxyclaenus*, *Protungulatum gorgun* and *Baioconodon engdahli*, as well as both species of the "triisodontine" *Eoconodon*, the cimolestid *Procerberus formicarum*, metatherians including *Turgidodon rhaister* and *Peradectes minor*, and one of the earliest plesiadapiforms, *Purgatorius unio*. None of our fossil therian taxa were classified as carnivores or hard-object invertivores, although two classified as animal-dominated omnivores have relatively high posterior probabilities of being carnivores: *Oxytomodon perissum* (0.42), and *Purgatorius unio* (0.48).

Taxa classified as insectivores or soft-insect specialists include: all the cimolestids in the sample other than *Procerberus formicarum*; both species of *Gypsonictops*; metatherians such as *Protolambda florencae*, *Leptalestes krejcii*, and *Alphadon marshi*; the leptictid *Prodiacodon crustulum*; and an undescribed ?nyctithere. Only two taxa were classified as folivores: the metatherian *Protolambda hatcheri*, and the periptychid archaic ungulate *Mimatuta minuial.* Three taxa, all archaic ungulates, were classified as frugivores: *Mimotricentes subtrigonus*, *Chriacus baldwini*, and *Baioconodon nordicum*. Although they were classified instead as plant-

dominated omnivores, both *Glasbius twitchelli* and *Chriacus mediator* had relatively high posterior probabilities for frugivory. Other taxa identified as plant-dominated omnivores include the plesiadapiform *Pandemonium dis*, the primate *Paromomys farrandi*, and a variety of archaic ungulate taxa (e.g., *Litaletes disjunctus, Chriacus* species A) (Table 4.7). As in our extant sample, posterior probabilities of diet category were nearly evenly split across three or more diets in several fossil taxa. These notably include *Didelphodon vorax*, the largest therian mammal present in the Late Cretaceous of North America (Wilson et al. 2016), and *Protungulatum donnae*, an archaic ungulate whose appearance on the landscape marks the beginning of the Puercan 1 NALMA interval zone (Lofgren et al. 2004). Several taxa also had probabilities split nearly evenly between only two diet categories (Table 4.7, denoted by asterisks).

Fossil sample: disparity and diet categories through time. The representation of diet categories among our mammalian faunas changes through the K-Pg interval in our study area (Table 4.8). Although our sample sizes are small and we therefore cannot determine statistical significance of these changes, overall, there is a decrease in the relative number of insectivore or soft-insect specialist taxa, from 11 (68.8% of taxa) in the Lancian, to 3 (30.0%) in the Pu1, 8 (33.4%) in the Pu3, and finally 2 (20.0%) in the To1. Animal-dominated omnivores are rare in the Lancian (18.8% of taxa), but become much more abundant in the Puercan (50.0% in both interval zones), with a slight decrease in the To1 (30.0%). There is an increase in taxa with plant-based diets (plant-dominated omnivore, frugivore, folivore) between the Lancian (12.6%) and Pu1 (20.0%), a slight decrease between Pu1 and Pu3 (16.7%), and a distinct increase into To1 (50.0%).

Morphological disparity within each NALMA and interval zone, as represented by mean pairwise distance between taxa in the DTA morphospace, is lower in the La and Pu3, and higher in Pu1 and To1 (Table 4.9). Mean distance to centroid shows a similar pattern. However, convex hull volume reveals a different pattern. Although Pu3 has the largest number of taxa, La taxa cover the largest 3D volume of morphospace (Table 4.9).

Multituberculates: DTA, disparity, and diet categories through time. Dental topographic metrics covary differently in multituberculates than they do in therian mammals (Table 4.10, Fig. 4.5). In multituberculates, DNE and OPCR have a very strong positive correlation (Spearman's rho = 0.89) compared to in extant therians (Spearman's rho = 0.65). Across taxa, multituberculates with high DNE also have high OPCR. There are also correlations between OPCR and slope, as well as RFI and slope. There is not a strong correlation between DNE and RFI; multituberculates in our sample may have high or low DNE paired with high or low RFI. In fact, RFI appears to split multituberculate taxa into two groups: one comprising *Mesodma* and *Cimolodon*, which have relatively larger /p4s with large buccal lobes, and one comprising *Stygimys, Catopsalis, Meniscoessus,* and *Taeniolabis*, with relatively smaller, lower /p4s.

OPCR in our study covaries linearly with OPCR from Wilson et al. (2012) (Fig. 4.6). Using a least-squares linear regression, we converted our OPCR values to correspond to those of Wilson et al. (2012) and use them to determine likely diet category (Table 4.11). Based on those estimates, multituberculate diet categories do not vary as much through the NALMA interval zones included here as therian diet categories do. All three interval zones include carnivores,

animal-dominated omnivores, and plant-dominated omnivores; the Lancian and Pu3 interval zones also each include one herbivore (Table 4.11). Disparity patterns in multituberculates also differ from those of therians; mean pairwise distance and mean distance to centroid are highest in the Pu3, but convex hull volume is highest in the Pu1.

4.5 DISCUSSION

In this study, we conducted 3D quantitative topographic analyses of mammalian fossil teeth and teeth of extant mammals of known dietary ecology in order to infer changes in dietary ecology from the latest Cretaceous through the earliest Paleogene of northeastern Montana. Our main goal is to use our results to better understand the succession of mammalian ecospace occupation during biotic recovery from the Cretaceous-Paleogene mass extinction. Below we discuss i) new findings regarding DTA metrics from our extant mammalian comparative sample, including potential limitations of the methods used here and areas for further study; ii) dietary inferences of Late Cretaceous and early Paleocene mammals; and iii) changes in ecomorphospace occupation and dietary diversity and disparity through time, and how our results add to the growing body of knowledge regarding tempo and mode of the mammalian recovery from the K-Pg mass extinction.

Extant mammals: material properties of food and predicting diet from a single tooth. DTA results for our extant mammals are largely concordant with those of other similar 3D ecomorphological studies. For example, insectivores (e.g., *Sorex vagrans*, *Eptesicus fuscus,* and *Scapanus orarius*; Table 4.1; Fig. 4.3) and soft-insect specialists had high RFI and high DNE, as in previous studies (Boyer 2008; Bunn et al. 2011; Winchester et al. 2014). These results are

consistent with the typical molar crown morphology of insectivores, which is characterized by tall pointy cusps for puncturing tough carapaces and high shearing crest length to process soft insects (Strait 1993, 1997). The durophagous mammals in our data set (sea otters, *Enhydra lutris*) have low DNE, low OPCR, and low RFI. This result is expected considering that these taxa tend to have low molar crowns with rounded cusps, a morphology which can efficiently fracture hard, brittle food objects while avoiding catastrophic failure (Crofts and Summers 2014; Crofts 2015).

In contrast, DTA values for frugivores in our study differ from those in other studies. Frugivores tend to have low teeth with rugose basins for processing fruit pulp. We found these teeth to have low RFI and high DNE and OPCR (Figs. 4.2–4.3); whereas Bunn et al. (2011, fig. 4) found that frugivore teeth are more likely to have low values for RFI, DNE, and OPCR. Our higher OPCR and DNE values likely reflect the rugosities on the teeth, which may provide high-stress points for oral food processing (Norconk et al. 1998; Santana et al. 2011). Lopez-Torres et al. (2017), who followed the dietary classification guidelines for RFI and DNE put forth by Bunn et al. (2011), found one taxon (*Arcius lapparenti*, a European paromomyid primate) to be classified as a frugivore by its low RFI, and an omnivore-insectivore by its relatively high DNE (Lopez-Torres et al. 2017, table 2). That combination of values is more concordant with our overall pattern for frugivores (Fig. 4.2). However, this discrepancy among studies indicates that the morphological adaptations associated with frugivory should be studied further. It is possible that the difference in morphology of frugivorous taxa between our sample and that of Bunn et al. (2011) is due to phylogenetic sampling. The frugivore sample of Bunn et al. (2011) comprised primates only, and all of our extant frugivores are non-primates.

Omnivores in our sample fall primarily in the center of the DTA morphospace, with intermediate values for all three DTA metrics. One exception to this is the wild boar (*Sus scrofa*), which is consistently more similar to frugivores than it is to most other plant-dominated omnivores. This is perhaps related to a high percentage of both leaves and fruit in its diet (Ballari et al. 2015); its high OPCR and DNE correspond to a large number of tools for oral food processing, which are advantageous for soft, tough foods such as leaves (Strait 1997; Evans et al. 2007). However, if the teeth of *Sus scrofa* are at least somewhat adapted to process leaves efficiently, they do not resemble the teeth of folivores in our sample (Fig. 4.3), which tend to have much lower OPCR and DNE values. One potential explanation for this is insufficient sampling of folivore dental structures (discussed below). However, it is also important to note that the enamel of *Sus scrofa* functions differently than that of other mammals. The tendency of *Sus scrofa* enamel to fracture or crumble under stress means that through the life of the animal, new sharp points appear at the sites of breakage, and can increase efficiency of oral processing in plant matter while still being able to withstand loads during hard-object feeding (Popowics et al. 2001, 2004). Primates and dermopterans, the strict folivores in our sample, do not exhibit the crumbling enamel of *Sus scrofa*, and instead have molar teeth with sharp cusps and lophs. This suggests that teeth adapted for plant-dominated omnivory and folivory do not exist on a smooth morphofunctional continuum, but show unique combinations of morphological characters for addressing particular functional demands.

Extant folivores in our dataset unexpectedly plot alongside the carnivores in the DTA ecomorphospace (Figs. 4.2–4.3). There are no significant differences between carnivores and

folivores in any DTA metric (KS test, $p>0.1$), and animal-dominated omnivores also occupy an area of morphospace that overlaps considerably with both folivores and carnivores (Fig. 4.3). It has been previously observed that soft, tough foods, including both leaves and meat, require sharp blades for oral processing, as cracks do not self-propagate in soft, tough materials (Strait 1997; Evans and Sanson 2003). It is therefore not completely unexpected that our extant folivores and carnivores occupy similar areas of the DTA ecomorphospace (Figs. 4.2– 4.3). However, it is also true that meat is more easily digested and therefore requires less oral mechanical processing than leaves (Lucas 2004; Evans et al. 2007), which has led to the hypothesis that folivores will tend to have a greater number of processing tools on their teeth (Evans et al. 2007).

The high degree of similarity between teeth in these mammals with very different dietary ecologies may be due to the relative percentage of dental features sampled when considering a single tooth. Carnivores and herbivores have significantly different OPCR when considering full tooth rows (Evans et al. 2007; Pineda-Munoz et al. 2017). In our extant carnivorans, we sampled carnassials (m1s), which have a tendency to make up a large percentage of the total length of carnivoran tooth rows (both due to their increased size and the loss of posterior molars in carnivorans). We may therefore be inadvertently inflating the apparent oral processing capabilities of carnivoran teeth. This problem has not been previously detected because most single-tooth DTA studies up to this point have focused on primates and included only insectivores to represent animal-based diets. In these studies (Boyer et al. 2008; Bunn et al 2011), the similarity between folivore and insectivore teeth has been dealt with according to Kay's (1984) threshold, which predicts that, due to physiological metabolic constraints, animals

under 350 g cannot survive on a diet exclusively composed of leaves. This threshold cannot be used for our extant carnivores and folivores, because there is no significant difference in mean body mass between these two groups.

Thus, our study suggests that using a single tooth position restricts the potential for accurately distinguishing between carnivores and folivores. We suggest that additional studies should be undertaken to investigate how DTA values vary with tooth position sampled across phylogeny. Although the single-tooth method effectively distinguishes among insectivores, frugivores, plant-dominated omnivores, and hard-object invertivores, and can therefore be used effectively to infer diet in certain fossil taxa considered here, the distinction among animal-dominated omnivores, carnivores, and folivores remains unclear. Hereafter, we discuss the likely dietary ecologies of Late Cretaceous and early Paleogene mammals as determined by the single-tooth method, but we recognize that, especially among species classified as folivores, carnivores, or animal-dominated omnivores, this method is problematic. The single-tooth method needs to be refined before we can use it to distinguish among the full complement of dietary ecologies present, and test several important paleoecological hypotheses, including the hypothesis that carnivores were selectively culled by the K-Pg mass extinction (Wilson 2014), and the hypothesis that true folivory did not become common in mammals until after the Paleocene (Janis 1993, 2000).

Before the K-Pg mass extinction: Dietary ecology in the Lancian NALMA. Latest Cretaceous therian mammals had mostly animal-based diets (Table 4.7, Figs. 4.4, 4.7). The greatest concentration of Lancian taxa in the ecomorphospace is in the medium-high RFI/DNE, medium OPCR area. Animals falling in this region of the morphospace have teeth with tall

pointy cusps and long shearing crests that generally resemble those of extant insectivores (*Eptesicus fuscus, Sorex vagrans*). Within this area of morphospace, eutherians (cimolestids, e.g. *Cimolestes magnus* and *C. propalaeoryctes*, and gypsonictopids, e.g. *Gypsonictops illuminatus* and *G. hypoconus*, Fig. 4.4) have higher RFI than metatherians (e.g., *Turgidodon rhaister, Protolambda hatcheri*). In his 2D geometric morphometric analysis of La therian mammal taxa, Wilson (2013) found a separation between faunivorous eutherians and metatherians as well; however, that separation was partially due to the elongation of different shearing crests in the two groups, resulting in a similar overall shape but dissimilar relative sizes of homologous dental structures. Because our analyses are homology-free, it is less likely that this separation is due to phylogenetic effects, and is more likely that eutherians, particularly cimolestids, overall had slightly more trenchant molar cusps than metatherians. Based on their very high RFI, cimolestids have been filling a niche similar to the modern coast mole (*Scapanus orarius*, soft-insect specialist; Fig. 4.3).

Although relatively small-bodied insectivores were the most common mammalian ecotype present in in northeastern Montana in the La NALMA, they were not the only ecotype present. The largest recorded Cretaceous therian, *Didelphodon vorax*, has often been reconstructed as a hard-object feeder based on its unusually inflated premolar morphology and high estimated bite force (Clemens 1966, 1968; Fox and Naylor 2006; Wilson et al. 2016). However, single-tooth methodologies might not represent all ecologically relevant features on the tooth row (Wilson 2013). In this case, our analysis did not incorporate the inflated premolar morphology of *D. vorax*, which strongly reflects the hard-object-feeding capabilities of this taxon; whereas its molar morphology does not differ significantly from several other metatherians (*Turgidodon*

rhaister, *Protolambda hatcheri*; Fig. 4.4). Indeed, it has been suggested that in addition to the hard-object feeding implied by its premolar morphology and bite force, *Didelphodon* supplemented its diet with a wide variety of other food resources (Wilson et al. 2016). This generalist strategy and the related molar morphology may be part of the reason why our DFA was unable to classify *Didelphodon* with much confidence (Table 4.7). The nearby taxon *Protolambda hatcheri*, which is reconstructed as a folivore, is much too small to have the appropriate metabolic capabilities to subsist on leaves (Kay 1984); as such, we propose that it was more likely an animal-dominated omnivore or carnivore.

The most unique La taxon in terms of molar morphology is the metatherian *Glasbius twitchelli*, which is reconstructed as a plant-dominated omnivore (Table 4.7; Fig. 4.4). *Glasbius* has low, broad, complex molars that ally it with modern frugivores and plant-dominated omnivores (low RFI, high OPC and DNE) and distinguish it from all other La taxa. This finding corresponds to results of a previous study (Wilson 2013), which reconstructed *Glasbius* with a plant-based diet, in a distinct area of the morphospace from all other La therian taxa. Nonetheless, *Glasbius* was most likely not the only mammal with a plant-based diet present in the La; among multituberculates, there were plant-dominated omnivores and strict herbivores (*Meniscoessus robustus* and *Cimolodon nitidus*, Table 4.11). Both of these multituberculates are relatively large (Table 4.3), and could therefore likely subsist entirely on high-fiber plant matter; *Meniscoessus robustus*, in particular, is well within the herbivorous category (OPCR = 224.16) of Wilson et al. (2012). Geometric morphometric analysis of multituberculate p4s also suggested that *Meniscoessus* had a more plant-based diet than other La multituberculates, e.g., the neoplagiaulacid *Mesodma* (Wilson 2013, fig. 7). Thus, plant-based dietary niches (folivory) that

were probably not filled by therian mammals in the Lancian were at least partially occupied by larger herbivorous multituberculates (Table 4.11).

Disaster: Dietary ecology in the Puercan 1 NALMA interval zone. Immediately across the K-Pg boundary, mammalian taxonomic richness in northeastern Montana declined sharply, with up to 75% of lineages going extinct, and selective extinction of taxa with larger body sizes (Wilson 2014). In the earliest Paleogene Pu1 interval zone, mammals in northeastern Montana can be placed in one of two broad categories of biogeographic history. The "local survivors" category consists of (i) species that were locally present during both the Lancian and the Pu1 and (ii) species that were locally present in the Pu1 and had a probable ancestor locally present in the Lancian (Clemens 2002, 2010; see Wilson 2013 for a discussion of the caveats related to assumption of ancestor-descendant relationships). The "local immigrants" category consists of species with no likely ancestral lineages locally present in the La NALMA. Because those taxa are found almost immediately after the K-Pg boundary (within ca. 70 Ka), the interpretation is that they did not evolve in situ but that they survived the mass extinction event elsewhere (see Clemens 2010; Wilson 2014) and then immigrated into the local area.

Only a single metatherian lineage is hypothesized to have locally survived into the Paleocene (but see Williamson et al. 2012): *Thylacodon montanensis*, which we were unable to sample but which likely had an animal-based diet (Wilson 2013, 2014). We were able to sample *Procerberus formicarum*, the only survivor from the La cimolestid lineage, which is reconstructed in our DFA as an animal-dominated omnivore. Our only other sampled survivors, two species within the multituberculate genus *Mesodma*, are also faunivorous (Table 4.11). This

corresponds to previous analyses that suggest that the extinction was selective against animals, such as *Glasbius twitchelli* (Wilson 2014), that had plant-based diets.

Procerberus formicarum occupies similar morphospace to that of most La cimolestids (Fig. 4.4). However, that morphospace, which in the La was populated with cimolestids and gypsonictopids, are empty in the Pu1 other than *P. formicarum*. It has also been suggested that the extinction was selective against strict carnivores, including *Cimolestes magnus* (Wilson 2014). Because of the limitations of our single-tooth DTA (discussed above), it is unclear how many of the high-RFI, high-DNE, mid-OPC animals present in the La were likely carnivores rather than insectivores, and it is therefore not possible to assess preferential extinction of carnivores using our current data.

Having sampled only a single local therian survivor of the K-Pg mass extinction, it is also not possible to quantitatively compare morphospace occupation between local survivors and immigrants. Yet, it is clear that therian Pu1 immigrants occupy a broader range of dietary preferences relative to the La therians, even immediately after the mass extinction. Immigrants define the extremes of all three DTA metrics except maximum RFI, defined by the local resident *Procerberus formicarum* (Fig. 4.4). Further, the variance for all three DTA metrics is higher in the Pu1 sample than in the La sample (Table 4.9). This result differs slightly from results of 2D geometric morphometrics (Wilson 2013), which indicate a slight decline in morphological disparity in therian mammals across the K-Pg boundary. We find that, according to some measures, there may have been a slight, but not statistically significant, increase in morphological disparity (Table 4.9). Importantly, however, we did not sample the highly

derived, likely carnivorous taxon *Nanocuris improvida* (Fox et al. 2007; Wilson and Riedel 2010) which, along with *Glasbius*, defined the major morphofunctional axis of variation in Wilson's (2013) geometric morphometric analyses of lower molars. Had we been able to obtain a complete specimen of *N. improvida* to sample, it is likely that we would also have found a decrease in therian disparity across the K-Pg boundary. Morphological disparity does decrease in multituberculates between La and Pu1 (Table 4.12); however, multituberculate immigrants in Pu1, particularly the plant-dominated omnivore *Catopsalis joyneri*, also lend some morphological disparity to replace that lost via the extinctions of *Meniscoessus robustus* and *Cimolodon nitidus* (Fig. 4.5, Tables 4.11 and 4.12).

All immigrant therians that we sampled in the Pu1 are archaic ungulates, a taxonomically diverse group of early Paleogene placental mammals that likely includes the ancestor of modern ungulate taxa (Archibald 1998). Even from their first appearance in the fossil record in the Pu1, archaic ungulates exhibit a variety of likely dietary ecologies. *Baioconodon nordicum* (Fig. 4.3) is classified as a plant-dominated omnivore by DFA; *Protungulatum gorgun*, although classified as an animal-dominated omnivore by DFA, has some affinity with hard-object invertivores (*Enhydra lutris*). In addition to archaic ungulates, Pu1 has the earliest occurrence of the immigrant plesiadapiform genus *Purgatorius,* specifically *P. coracis* (Clemens and Wilsom 2012; Smith et al. in review). We were unable to sample *P. coracis* for this study; however, based on the morphological similarity between the molars of *P. coracis* and *P. unio* (Fox and Scott 2011), it is likely that *P. coracis* would be classified as an insectivore or animal-dominated omnivore (see below). Overall, the surge of eutherian and multituberculate immigrants appearing in the Pu1 (Clemens 2002, 2008, 2010; Wilson 2013, 2014) contributed most to the dietary

disparity present, and fueled a shift in overall morphospace occupation from a concentration around insectivore ecomorphospace to a concentration around omnivory (Fig. 4.4, 4.8).

Recovery: Dietary ecology in the Puercan 3 and Torrejonian 1 NALMA interval zones. The Pu3 sample has the largest range of therian body size of any NALMA interval zone discussed so far (Fig. 4.7), but ecomorphological disparity is not distinctly higher in Pu3 than Pu1 (Table 4.9). Aside from 3D morphospace volume, all other therian disparity measures drop between Pu1 and Pu3. In contrast, four of six morphological disparity measures in multituberculates increase between Pu1 and Pu3 (Table 4.12). The appearance of the very large multituberculate *Taeniolabis lamberti* (Table 4.3, 4.11) also contributes to an increase in mean multituberculate body size, and re-expands multituberculate ecological diversity to include herbivores. Thus, from Pu1 to Pu3, multituberculates increase in both morphological disparity and body size range, whereas therians are primarily increasing in body size range. A change in body size range with no associated change in dental morphological disparity does not necessarily indicate stagnation in ecological space occupation; instead, therians might be invading new ecospace through the exploitation of a variety of sizes of resources (Hutchinson 1959; Wilson 1975). Nonetheless, this therian pattern of rapid increase in morphological disparity early in the post-K-Pg radiation corresponds to the pattern found in a variety of metazoan groups, with disparity increasing quickly in the early history of a clade or direct aftermath of an extinction event (Foote 1997 and references therein). Multituberculates seem to be following a slightly different trajectory, with incremental increases in disparity rather than immediate expansion into available ecospace; multituberculates might also be continuing the trajectory of radiation that began in the Late Cretaceous (Wilson et al. 2012). Despite the stasis in therian morphological

disparity, other dental properties reveal the potential for an increase in dietary diversity without distinct changes in gross dental morphology.

The triisodontine genus *Eoconodon* appears on the edge of animal-dominated omnivory space, adjacent to folivores and carnivores (Fig. 4.4). *Eoconodon* also shares some characteristics with plant-dominated omnivores (posterior probability = 0.233–0.292, Table 4.7) and has low RFI values. The relatively low, rounded tooth morphology of *Eoconodon* in combination with the presence of Hunter-Schreger bands in its enamel (Clemens 2011) suggests adaptation for processing hard-food objects (Tseng 2012; Berthaume et al. 2013; Berthaume 2016; Crofts 2015), potentially bone-cracking in the style of *Crocuta*, which is nearby in the ecomorphospace. If this is correct, *Eoconodon* represents a new type of dietary ecology that has not been sampled earlier in the Paleogene, further expanding the diversity of diets present in Pu3 without producing an increase in DTA disparity. Three new plesiadapiforms appear in Pu3: two of them (*Purgatorius janisae* and *P. unio*) are both reconstructed as having animal-based diets, but *Pandemonium dis* is reconstructed as a plant-dominated omnivore, indicating relatively fast within-group ecomorphological diversification occurring early in the history of this important clade (Van Valen 1994). In sum, a number of new taxonomic groups appear in Pu3 and begin to diversify ecomorphologically, and therian body size range shows a marked increase. Multituberculate ecomorphological disparity also increases. Although therian dental morphology does not show an increase in disparity overall, the potential for bone-cracking capabilities in *Eoconodon*, as well as the increase in body size range, suggests a continuing increase in mammalian ecotypes present.

The following NALMA interval zone, the Torrejonian 1, is still under study (Clemens and Wilson 2009; Hovatter and Wilson 2015, 2016) and as such has a small sample of therian taxa (N = 8) relative to Pu3 (N = 24) and no multituberculate sample in the current study. Therefore, interpretations from the To1 should be considered preliminary. Although we hesitate to make inferences about quantitative disparity measures with such a small sample of the total taxa likely present in the To1, we nonetheless note that there is an increase in range of OPCR values present in To1 (Fig. 4.7), which is related to the appearance of the first mammals classified by our DFA as true frugivores: *Mimotricentes subtrigonus* and *Chriacus baldwini*. These taxa have the highest OPCR of any fossil in our data set, and their first occurrences in the To1 suggest that mammals continued to diversify into plant-based niches after the Pu3. This trend in the Pu and To1 towards frugivory may be related to increasing average angiosperm fruit size during the early Paleogene (Eriksson et al. 2000). After the extinction of non-avian dinosaurs, vegetation structure may have become more closed, due in part to lack of consistent disturbance by large herbivorous organisms (Wing and Tiffney 1987). It has been argued that the increase in angiosperm fruit size in the early Paleogene was selectively advantageous in more closed canopy environments, and larger fruits resulted in greater selective advantage for animal dispersal rather than wind dispersal (Eriksson et al. 2000). This increase in fruit size, and therefore overall increase in available food volume for frugivores, provided a new food source, and likely allowed mammalian frugivores to become more specialized and diversify. If, as suggested in previous studies (Janis 1993, 2000), folivory did not become common in mammals until the Eocene, but generalist herbivores were on the rise in the Paleocene, it is possible that increasing mammalian body size in the Paleogene (Alroy 1999; Smith et al. 2010) may have played a role in the invasion of folivore ecospace. Because most therian mammals in the early Paleogene were

relatively small-bodied (e.g., Table 4.2), they may not have been capable of maintaining their high metabolism with a diet composed only of hard-to-digest leaves (Kay 1984). On the other hand, the carbohydrates in fruit require less digestion to be usable in metabolic processes, and fruit can therefore be the primary nutrient source for small mammals (Kay 1984). As average mammalian body size increased through the Paleogene, folivory became feasible for a greater number of mammals. However, large multituberculates (e.g., *Taeniolabis lamberti,* Pu3) appearing in the early-to-mid Paleocene were herbivorous (Wilson et al. 2012, this study) and could potentially have been strictly folivorous. Future study should expand the comparative sample of full tooth rows from extant mammalian frugivores and folivores to attempt to tease apart morphological correlates of different types of herbivory (folivory, frugivory) in multituberculates.

Most therian taxa present in To1 occupy areas of morphospace that were also occupied in Pu3, suggesting that other than the appearance of the two frugivores, there were no new invasions of ecomorphospace in the To1. This trend is supported by the placement of the paromomyid primate *Paromomys farrandi,* which is reconstructed as a plant-dominated omnivore (Table 4.7) and is highly abundant in the localities where it appears (Clemens and Wilson 2009; Hovatter and Wilson 2015, 2016). Lopez-Torres et al. (2017) reconstruct *Paromomys* as an omnivore-frugivore. Although we agree with this classification, we find that *Paromomys* lacks some characteristics of frugivory that we found in our non-primate extant comparative sample, and feel that more study of phylogenetic signal in characteristics of frugivores is necessary. Irrespective of exact dietary preference, the very high relative abundance of *Paromomys* in To1 faunas (Clemens and Wilson 2009; Hovatter and Wilson 2015, 2016) reflects a slightly uneven

mammalian assemblage, somewhat like Pu1 assemblages from around northeastern Montana (Wilson 2014, Smith et al. in review). Further investigation of the locally high relative abundance of *Paromomys* is critical to understanding the later progression of the mammalian faunal recovery in northeastern Montana following the K-Pg. Because faunal heterogeneity is used as a barometer of ecological stability (Magurran 2004; Cadotte et al. 2012), highly uneven To1 faunas could mean that i) mammalian faunas were still actively recovering, and not nearing ecological stability, within the first ca. 1.2 Ma of the Paleogene, or ii) a new biotic or environmental change caused faunal disruption in the To1.

Synthesis: Implications for the K-Pg mammalian biotic recovery

In this study, we found that directly following the K-Pg mass extinction, the local appearance of therian immigrants caused an overall shift in the occupied mammalian dietary ecomorphospace, from a high concentration of insectivorous therian taxa in the Lancian to a greater variety of omnivores in the early Puercan; multituberculate Pu1 immigrants filled niches of pre-extinction multituberculates with plant-based diets. During the main wave of taxonomic origination in the area, which took place leading into Pu3 (Wilson 2014; Smith et al. in review), new therian and multituberculate immigrants further increased the ecomorphotypes present on the landscape, and surviving lineages (e.g., cimolestids) began repopulating once-packed ecospace that had been significantly thinned by the mass extinction event. The Torrejonian 1 interval zone saw the advent of the first true frugivores, but an otherwise relatively static ecomorphospace, suggesting that the ecosystem had not completely settled into stasis but could be approaching equilibrium.

Future work on the trends presented here will require exhaustive sampling of taxa present on the landscape in each NALMA interval zone to more completely determine the extremes of morphology present in each; for example, this study did not sample a number of multituberculate species, including the very small *Microcosmodon harleyi* (Weil 1998), which would likely have an impact on the ecomorphological disparity of the sample if included. Additionally, collection of relative abundance data for Pu3 and To1 faunas will allow for integration of ecological information about diet, locomotion (DeBey and Wilson 2014, 2017), and heterogeneity for a more holistic picture of mammalian communities through time. Lastly, full tooth rows should be incorporated in ecomorphological studies of fossil mammals wherever possible, and the morphological correlates of diet in extant mammals more specifically studied, to make models on which we base our inferences in the fossil record as robust as possible.

4.6 REFERENCES CITED

Alroy, J., 1999, The fossil record of North American mammals: evidence for a Paleocene evolutionary radiation: Systematic biology, v. 48, p. 107–118, doi: 10.1080/106351599260472.

Archibald, J.D., 1983, Structure of the KT mammal radiation in North America: speculations on turnover rates and trophic structure: Acta Palaeontologica Polonica, v. 28, p. 7–17.

Archibald, J.D., 1998, 20 Archaic ungulates (“ Condylarthra”): Evolution of Tertiary Mammals of North America: Volume 1, Terrestrial Carnivores, Ungulates, and Ungulate Like Mammals, v. 1, p. 292–331.

Archibald, J.D., Rigby Jr, J.K., and Robison, S.F., 1983, Systematic revision of Oxyacodon (Condylarthra, Periptychidae) and a description of O. ferronensis n. sp.: Journal of Paleontology, p. 53–72.

Baker, R.H., and Baker, M.W., 1975, Montane Habitat Used by the Spotted Skunk (Spilogale putorius) in Mexico: Journal of Mammalogy, v. 56, p. 671–673.

Ballari, S.A., Cuevas, M.F., Ojeda, R.A., and Navarro, J.L., 2015, Diet of wild boar (Sus scrofa) in a protected area of Argentina: the importance of baiting: Mammal Research, v. 60, p. 81–87, doi: 10.1007/s13364-014-0202-0.

Barclay, R.M.R., and Brigham, R.M., 1991, Prey detection, dietary niche breadth, and body size in bats: why are aerial insectivorous bats so small? The American Naturalist, v. 137, p. 693–703.

Bartoszewicz, M., Okarma, H., Zalewski, A., and Szczęsna, J., 2008, Ecology of the raccoon (Procyon lotor) from western Poland: Annales Zoologici Fennici, v. 45, p. 291–298.

Berthaume, M.A., 2016, On the Relationship Between Tooth Shape and Masticatory Efficiency: A Finite Element Study: Anatomical Record, v. 299, p. 679–687, doi: 10.1002/ar.23328.

Berthaume, M.A., Dumont, E.R., Godfrey, L.R., Grosse, I.R., Wood, B., Schroer, K., Ungar, P., Sponheimer, M., Strait, D., Kay, R., Simons, E., Kay, R., Kay, R., Boyer, D., et al., 2013, How does tooth cusp radius of curvature affect brittle food item processing? Journal of the Royal Society, Interface, v. 10, p. 20130240, doi: 10.1098/rsif.2013.0240.

Bisbal, E.F.J., 1986, Food habits of some neotropical carnivores in Venezuela (Mammalia, Carnivora): Mammalia, v. 50, p. 329–339.

Bloch, J.I., Rose, K.D., and Gingerich, P.D., 1998, New Species of Batodonoides (Lipotyphla, Geolabididae) from the Early Eocene of Wyoming: Smallest Known Mammal? Journal of Mammalogy, v. 79, p. 804–827.

Blomberg, S.P., Garland Jr, T., and Ives, A.R., 2003, Testing for phylogenetic signal in comparative data: behavioral traits are more labile: Evolution, v. 57, p. 717–745.

Boyer, D.M., 2008, Relief index of second mandibular molars is a correlate of diet among prosimian primates and other euarchontan mammals: Journal of Human Evolution, v. 55, p. 1118–1137, doi: 10.1016/j.jhevol.2008.08.002.

Britt, A., Randriamandratonirina, N.J., Glasscock, K.D., and Iambana, B.R., 2002, Diet and feeding behaviour of Indri indri in a low-altitude rain forest: Folia Primatologica, v. 73, p. 225–239.

Bucher, B.J.E., and Hoffmann, R.S., Caluromys derbianus: Mammalian Species, no.140, p. 1–4.

Bunn, J.M., Boyer, D.M., Lipman, Y., St. Clair, E.M., Jernvall, J., and Daubechies, I., 2011, Comparing Dirichlet normal surface energy of tooth crowns, a new technique of molar shape quantification for dietary inference, with previous methods in isolation and in combination: American Journal of Physical Anthropology, v. 145, p. 247–261, doi: 10.1002/ajpa.21489.

Cadotte, M.W., Dinnage, R., and Tilman, D., 2012, Phylogenetic diversity promotes ecosystem stability: Ecology, v. 93.

Ciampaglio, C.N., Kemp, M., and McShea, D.W., 2001, Detecting changes in morphospace occupation patterns in the fossil record: characterization and analysis of measures of disparity: Paleobiology, v. 27, p. 695–715.

Clemens, W.A., 1966, Fossil mammals of the type Lance Formation, Wyoming. Part II. Marsupialia: University of California Publications in Geological Sciences, v. 62, p. 1–105.

Clemens, W.A., 1968, A mandible of Didelphodon vorax (Marsupialia, Mammalia): Los Angeles County Museum of Natural History Contributions in Science, p.1–11.

Clemens, W.A., 1974, Purgatorius, an early paromomyid primate (Mammalia): Science, v. 184, p. 903–905.

Clemens, W. A., 2002, Evolution of the mammalian fauna across the Cretaceous-Tertiary boundary in northeastern Montana and other areas of the Western Interior: Geological Society of America, Special Paper, v. 361, p. 217–245.

Clemens, W. A., 2004, Purgatorius (Plesiadapiformes, Primates?, Mammalia), a Paleocene Immigrant Into Northeastern Montana: Stratigraphic Occurrences and Incisor Proportions: Bulletin of Carnegie Museum of Natural History, v. 36, p. 3–13, doi: 10.2992/0145-9058(2004)36[3:PPPMAP]2.0.CO;2.

Clemens, W., 2006, Early Paleocene (Puercan) peradectid marsupials from northeastern Montana, North American Western Interior: Palaeontographica Abteilung A, v. 277, p. 19–31.

Clemens, W. A., 2008, Patterns of mammalian evolution across the Cretaceous-Tertiary boundary: Zoosystematics and Evolution, v. 77, p. 175–191, doi: 10.1002/mmnz.20010770204.

Clemens, W. A., 2010, Were immigrants a significant part of the earliest Paleocene mammalian fauna of the North American Western Interior? Vertebrata PalAsiatica, v. 48, p. 285–307.

Clemens, W. A., 2011, Eoconodon (“Triisodontidae,” Mammalia) from the Early Paleocene (Puercan) of northeastern Montana, USA: Palaeontologia Electronica, v. 14, p. 1–22.

Clemens, W. A., and Wilson, G.P., 2009, Early Torrejonian mammalian local faunas from northeastern Montana, USA: Museum of Northern Arizona Bulletin, v. 65, p. 111–158.

Clemens, W.A., and Wilson, G.P., 2012, Pattern of immigration of purgatoriids and other eutherians into the northern North American Western Interior: Supplement to the Journal of Vertebrate Paleontology, p. 80.

Clothier, R.R., 1955, Contribution to the life history of Sorex vagrans in Montana: Journal of Mammalogy, v. 36, p. 214–221.

Cooper, S.M., Holekamp, K.E., and Smale, L., 1999, A seasonal feast: long-term analysis of feeding behaviour in the spotted hyaena (Crocuta crocuta): African Journal of Ecology, v. 37, p. 149–160.

Crofts, S., 2015, Finite element modeling of occlusal variation in durophagous tooth systems: Journal of Experimental Biology, no. 281, p. 2705–2711, doi: 10.1242/jeb.120097.

Crofts, S.B., and Summers, A.P., 2014, How to best smash a snail: the effect of tooth shape on crushing load.: Journal of the Royal Society, Interface / the Royal Society, v. 11, p. 20131053, doi: 10.1098/rsif.2013.1053.

De Bast, E., and Smith, T., 2013, Reassessment of the small “arctocyonid”Prolatidens waudruae from the early Paleocene of Belgium, and its phylogenetic relationships with ungulate-like mammals: Journal of Vertebrate Paleontology, v. 33, p. 964–976.

Debey, L.B., and Wilson, G.P., 2014, Mammalian femora across the Cretaceous-Paleogene boundary in eastern Montana: Cretaceous Research, v. 51, p. 361–385, doi: 10.1016/j.cretres.2014.06.001.

DeBey, L.B., and Wilson, G.P., 2017, Mammalian distal humerus fossils from eastern Montana, USA with implications for the Cretaceous-Paleogene mass extinction and the adaptive radiation of placentals: Palaeontologia Electronica, v. 20, p. 1–93.

Desbiez, A.L.J., Santos, S.A., Keuroghlian, A., and Bodmer, R.E., 2009, Niche partitioning among white-lipped peccaries (Tayassu pecari), collared peccaries (Pecari tajacu), and feral pigs (Sus scrofa): Journal of Mammalogy, v. 90, p. 119–128.

Dewar, E.W., 2003, Functional diversity within the Littleton fauna (early Paleocene), Colorado : evidence from body mass, tooth structure, and tooth wear: PaleoBios, v. 23, p. 1–19.

Dzulhelmi, M.N., and Abdullah, M.T., 2009, Foraging ecology of the Sunda colugo (Galeopterus variegatus) in Bako National Park, Sarawak, Malaysia: Malayan Nature Journal, v. 61, p. 285–294.

Eisenberg, J.F., and Wilson, D.E., 1981, Relative brain size and demographic strategies in didelphid marsupials: The American Naturalist, v. 118, p. 1–15.

Eriksson, O., Friis, E.M., and Löfgren, P., 2000, Seed size, fruit size and dispersal spectra in angiosperms from the Early Cretaceous to the Late Tertiary: The American Naturalist, v. 156, p. 47–58.

Estes, R, and Berberian, P, 1970, Paleoecology of a Late Cretaceous Vertebrate Community from Montana: Breviora, v. 343, p. 1–35.

Evans, A.R., 2013, Shape descriptors as ecometrics in dental ecology: Hystrix, v. 24, p. 133–140, doi: 10.4404/hystrix-24.1-6363.

Evans, A.R., and Sanson, G.D., 2003, The tooth of perfection: Functional and spatial constraints on mammalian tooth shape: Biological Journal of the Linnean Society, v. 78, p. 173–191, doi: 10.1046/j.1095-8312.2003.00146.x.

Evans, A.R., Wilson, G.P., Fortelius, M., and Jernvall, J., 2007, High-level similarity of dentitions in carnivorans and rodents: Nature, v. 445, p. 78–81, doi: 10.1038/nature05433.

Foote, M., 1997, The Evolution of Morphological Diversity: Annual Review of Ecology and Systematics, v. 28, p. 129–152, doi: 10.1146/annurev.ecolsys.28.1.129.

Fox, B.J., and Archer, E., 1984, The Diets of Sminthopsis Murina and Antechinus Stuartii (Marsupialia: Dasyuridae) in Sympatry.: Wildlife Research, v. 11, p. 235–248.

Fox, R.C., 2015, A revision of the Late Cretaceous–Paleocene eutherian mammal Cimolestes Marsh, 1889: Canadian Journal of Earth Sciences, v. 52, p. 1137–1149.

Fox, R.C., and Naylor, B.G., 2006, Stagodontid marsupials from the Late Cretaceous of Canada and their systematic and functional implications: v. 51, p. 13–36.

Fox, R.C., and Scott, C.S., 2011, A New, Early Puercan (Earliest Paleocene) Species of Purgatorius (Plesiadapiformes, Primates) from Saskatchewan, Canada: Journal of Paleontology, v. 85, p. 537–548, doi: 10.1666/10-059.1.

Fox, R. C., Scott, C.S., and Bryant, H.N., 2007, A new, unusual therian mammal from the Upper Cretaceous of Saskatchewan, Canada: Cretaceous Research, v. 28, p.821–829.

Freckleton, R.P., Harvey, P.H., and Pagel, M., 2002, Phylogenetic analysis and comparative data: a test and review of evidence: The American Naturalist, v. 160, p. 712–726.

Gardner, A.L., 1982, Virginia opossum *in* Chapman, J., and Feldhamer, G., Wild mammals of North America: biology, management, and economics: John Hopkins University Press, Baltimore, Maryland, p. 3–36.

Giannini, N.P., and Kalko, E.K. V, 2004, Trophic structure in a large assemblage of phyllostomid bats in Panama: Oikos, v. 105, p. 209–220.

Gittleman, J.L., 1985, Carnivore body size: ecological and taxonomic correlates: Oecologia, v. 67, p. 540–554.

Glen, A.S., and Dickman, C.R., 2006, Diet of the spotted-tailed quoll (Dasyurus maculatus) in eastern Australia: effects of season, sex and size: v. 269, p. 241–248, doi: 10.1111/j.1469-7998.2006.00046.x.

Glendenning, R., 1959, Biology and control of the coast mole, Scapanus orarius orarius True, in British Columbia: Canadian Journal of Animal Science, v. 39, p. 34–44.

Grossnickle, D.M., and Newham, E., 2016, Therian mammals experience an ecomorphological radiation during the Late Cretaceous and selective extinction at the K–Pg boundary: Proceedings of the Royal Society B: Biological Sciences, v. 283, p. 20160256, doi: 10.1098/rspb.2016.0256.

Habel, K., Grasman, R., Gramacy, R.B., Stahel, A., and Sterratt, D.C., 2015, geometry: mesh generation and surface tessellation, v. 0.3-6.

Halliday, T.J.D., and Goswami, A., 2016, Eutherian morphological disparity across the end-Cretaceous mass extinction: Biological Journal of the Linnean Society, v. 118, p. 152–168, doi: 10.1111/bij.12731.

Harcourt, C., 1991, Diet and behaviour of a nocturnal lemur, Avahi laniger, in the wild: Journal of Zoology, v. 223, p. 667–674.

Harestad, A.S., and Bunnel, F.L., 1979, Home Range and Body Weight--A Reevaluation: Ecology, v. 60, p. 389–402.

Hayssen, V., 2008, Patterns of body and tail length and body mass in Sciuridae: Journal of Mammalogy, v. 89, p. 852–873.

Hedges, S.B., Dudley, J., and Kumar, S., 2006, TimeTree: a public knowledge-base of divergence times among organisms: Bioinformatics, v. 22, p. 2971–2972.

Hedges, S.B., Marin, J., Suleski, M., Paymer, M., and Kumar, S., 2015, Tree of life reveals clock-like speciation and diversification: Molecular biology and evolution, v. 32, p. 835–845.

Hladik, C.M., and Charles-Dominique, P., 1974, The behaviour and ecology of the sportive lemur (Lepilemur mustelinus) in relation to its dietary peculiarities, *in* Martin, R.D., Doyle, G.A., and Walker, A.C., eds., Prosimian biology: Duckworth, London, p. 25-37.

Holleley, C.E., Dickman, C.R., Crowther, M.S., and Oldroyd, B.P., 2006, Size breeds success: multiple paternity, multivariate selection and male semelparity in a small marsupial, Antechinus stuartii: Molecular Ecology, v. 15, p. 3439–3448.

Hovatter, B.T., and Wilson, G.P., 2015, Faunal analysis of earliest Torrejonian (To1) mammals from northeastern Montana, USA: Supplement to the Journal of Vertebrate Paleontology, p. 142.

Hovatter, B. T. and Wilson, G. P., 2016, The early Paleogene rise of placentals and decline of multituberculates: Insights from analysis of dental disparity, morphospace occupation, and body size of earliest Torrejonian (To1) mammals from northeastern Montana, USA: Supplement to the Journal of Vertebrate Paleontology, p. 158.

Hutchinson, G.E., 1959, Homage to Santa Rosalia or why are there so many kinds of animals?: The American Naturalist, v. 93, p. 145–159.

Janis, C.M., 1990, Correlation of cranial and dental variables with dietary preferences in mammals: a comparison of macropodoids and ungulates: Memoirs of the Queensland Museum, v. 28, p. 349–366.

Janis, C.M., 1993, Tertiary mammal evolution in the context of changing climates, vegetation, and tectonic events: Annual Review of Ecology and Systematics, v. 24, p. 467–500.

Janis, C.M., 2000, Patterns in the evolution of herbivory in large terrestrial mammals: the Paleogene of North America: Evolution of herbivory in terrestrial vertebrates. Cambridge University Press, Cambridge, p. 168–222.

Johnston, P.A., and Fox, R.C., 1984, Paleocene and late Cretaceous mammals from Saskatchewan, Canada: Palaeontographica Abteilung A, p. 163–222.

Jones, M.E., Rose, R.K., and Burnett, S., 2001, Dasyurus maculatus: Mammalian Species, no. 676, p. 1–9.

Kay, R.F., 1984, On the use of anatomical features to infer foraging behavior in extinct primates *in* Rodman, P.S., Cant, J.G.H., eds., Adaptations for foraging in Nonhuman Primates: contributions to an organismal biology of prosimians, monkeys and apes: New York, Columbia University Press, p. 21–53.

Kinlaw, A., 1995, Spilogale putorius: Mammalian species, no. 511, p. 1–7.

Kondrashov, P.E., and Lucas, S.G., 2004, Oxyclaenus from the early Paleocene of New Mexico and the status of the Oxyclaeninae (Mammalia, Arctocyonidae), *in* Lucas, S.G., Zeigler, K.E. and Kondrashov, P.E., eds.,Paleogene Mammals: New Mexico Museum of Natural History and Science Bulletin No. 26, p. 21–31.

Kondrashov, P.E., and Lucas, S.G., 2015, Paleocene vertebrate faunas of the San Juan Basin, New Mexico, *in* Lucas, S. G. and Sullivan, R. M., eds. Fossil Vertebrates in New Mexico: New Mexico Museum in Natural History and Science Bulletin No. 68, p. 131–148.

Kumar, S., and Hedges, S.B., 2011, TimeTree2: species divergence times on the iPhone: Bioinformatics, v. 27, p. 2023–2024.

Kumar, S., Stecher, G., Suleski, M., and Hedges, S.B., 2017, TimeTree: a resource for timelines, timetrees, and divergence times: Molecular Biology and Evolution, v. 34, p. 1812–1819.

Lofgren, D.L., Lillegraven, J.A., Clemens, W.A., Gingerich, P.D., and Williamson, T.E., 2004, Paleocene biochronology: the Puercan through Clarkforkian land mammal ages: Late

Cretaceous and Cenozoic Mammals of North America: Biostratigraphy and Geochronology. Columbia University Press, New York, p. 43–105.

Longrich, N.R., Scriberas, J., and Wills, M.A., 2016, Severe extinction and rapid recovery of mammals across the Cretaceous–Palaeogene boundary, and the effects of rarity on patterns of extinction and recovery: Journal of Evolutionary Biology, v. 29, p. 1495–1512, doi: 10.1111/jeb.12882.

López-Torres, S., Selig, K.R., Prufrock, K.A., Lin, D., and Silcox, M.T., 2017, Dental topographic analysis of paromomyid (Plesiadapiformes, Primates) cheek teeth: more than 15 million years of changing surfaces and shifting ecologies: Historical Biology, p. 1–13.

Lotze, J.-H., and Anderson, S., 1979, Procyon lotor: Mammalian Species, no. 119, p. 1–8.

Lucas, P.W., 2004, Dental functional morphology: how teeth work: Cambridge University Press.

Magurran, A.E., 2004, Measuring biological diversity: John Wiley & Sons.

McKenna, M.C., 1968, Leptacodon, an American Paleocene nyctithere (Mammalia, Insectivora). American Museum novitates; no. 2317, p. 1–12.

Middleton, M.D., and Dewar, E.W., 2004, New mammals from the early Paleocene Littleton fauna (Denver Formation, Colorado) *in* Lucas, S.G., Zeigler, K.E. and Kondrashov, P.E., eds., Paleogene Mammals: New Mexico Museum of Natural History and Science Bulletin, v. 26, p. 59–80.

Moore, A.W., 1933, Food habits of Townsend and coast moles: Journal of Mammalogy, v. 14, p. 36–40.

Nakashima, Y., Nakabayashi, M., and Sukor, J.A., 2013, Space use, habitat selection, and day-beds of the common palm civet (Paradoxurus hermaphroditus) in human-modified habitats in Sabah, Borneo: Journal of Mammalogy, v. 94, p. 1169–1178.

Norconk, M.A., Grafton, B.W., and Conklin-Brittain, N.L., 1998, Seed dispersal by neotropical seed predators: American Journal of Primatology, v. 45, p. 103–126.

O'Leary, M. a., Bloch, J.I., Flynn, J.J., Gaudin, T.J., Giallombardo, a., Giannini, N.P., Goldberg, S.L., Kraatz, B.P., Luo, Z.-X., Meng, J., Ni, X., Novacek, M.J., Perini, F. a., Randall, Z.S., et al., 2013, The Placental Mammal Ancestor and the Post-K-Pg Radiation of Placentals: Science, v. 339, p. 662–667, doi: 10.1126/science.1229237.

Pagel, M.D., 1992, A method for the analysis of comparative data: Journal of Theoretical Biology, v. 156, p. 431–442, doi: 10.1016/S0022-5193(05)80637-X.

Pampush, J.D., Winchester, J.M., Morse, P.E., Vining, A.Q., Boyer, D.M., and Kay, R.F., 2016, Introducing molaR : a New R Package for Quantitative Topographic Analysis of Teeth (and Other Topographic Surfaces): Journal of Mammalian Evolution, doi: 10.1007/s10914-016-9326-0.

Pemberton, D., Gales, S., Bauer, B., Gales, R., Lazenby, B., and Medlock, K., 2008, The diet of the Tasmanian Devil, Sarcophilusharrisii, as determined from analysis of scat and stomach contents: Papers and Proceedings of the Royal Society of Tasmania, v. 142, p. 13–22.

Pineda-Munoz, S., and Alroy, J., 2014, Dietary characterization of terrestrial mammals: Proceedings of the Royal Society B: Biological Sciences, v. 281.

Pineda-Munoz, S., Lazagabaster, I.A., Alroy, J., and Evans, A.R., 2017, Inferring diet from dental morphology in terrestrial mammals: Methods in Ecology and Evolution, v. 8, p. 481–491.

Popowics, T.E., Rensberger, J.M., and Herring, S.W., 2001, The fracture behaviour of human and pig molar cusps: Archives of Oral Biology, v. 46, p. 1–12.

Popowics, T.E., Rensberger, J.M., and Herring, S.W., 2004, Enamel microstructure and microstrain in the fracture of human and pig molar cusps: Archives of Oral Biology, v. 49, p. 595–605, doi: 10.1016/j.archoralbio.2004.01.016.

Prufrock, K.A., Boyer, D.M., and Silcox, M.T., 2016a, The First Major Primate Extinction : An Evaluation of Paleoecological Dynamics of North American Stem Primates Using a Homology Free Measure of Tooth Shape: American Journal of Physical Anthropology, doi: 10.1002/ajpa.22927.

Prufrock, K.A., López-torres, S., Silcox, M.T., and Boyer, D.M., 2016b, Surfaces and spaces : troubleshooting the study of dietary niche space overlap between North American stem primates and rodents: Surface Topography: Metrology and Properties, v. 4, p. 24005, doi: 10.1088/2051-672X/4/2/024005.

R Core Team, 2017, R: A language and environment for statistical computing: R Foundation for Statistical Computing, Vienna, Austria: https://www.R-project.org/.

Revell, L.J., 2012, phytools: an R package for phylogenetic comparative biology (and other things): Methods in Ecology and Evolution, v. 3, p. 217–223.

Riedman, M.L., and Estes, J. A., 1990, The Sea Otter (Enhydra lutris): Behavior, Ecology, and Natural History: Biological Report, v. 90, p. 1–136.

Rigby Jr, J.K., 1981, A skeleton of Gillisonchus gillianus (Mammalia; Condylarthra) from the early Paleocene (Puercan) Ojo Alamo Sandstone, San Juan Basin, New Mexico, with comments on the local stratigraphy of Betonnie Tsosie Wash, *in* Advances in San Juan Basin Paleontology: University of New Mexico Press, Albuquerque, p. 89–126.

Robinson, J.G., and Redford, K.H., 1986, Body size, diet, and population density of Neotropical forest mammals: The American Naturalist, v. 128, p. 665–680.

Rougier, G.W., Wible, J.R., and Novacek, M.J., 1998, Implications of Deltatheridium specimens for early marsupial history: Nature, v. 396, p. 459–463.

Santana, S.E., Strait, S., and Dumont, E.R., 2011, The better to eat you with: functional correlates of tooth structure in bats: Functional Ecology, v. 25, p. 839–847, doi: 10.1111/j.1365-2435.2011.01832.x.

Saunders, G., and McLeod, S., 1999, Predicting home range size from the body mass or population densities of feral pigs, Sus scrofa (Artiodactyla: Suidae): Austral Ecology, v. 24, p. 538–543.

Schoonover, L.J., and Marshall, W.H., 1951, Food habits of the raccoon (Procyon lotor hirtus) in north-central Minnesota: Journal of Mammalogy, v. 32, p. 422–428.

Silcox, M.T., and Teaford, M.F., 2002, The diet of worms: An analysis of mole dental microwear: Journal of Mammalogy, v. 83, p. 804–814, doi: 10.1644/1545-1542(2002)083<0804:TDOWAA>2.0.CO;2.

Slater, G.J., 2013, Phylogenetic evidence for a shift in the mode of mammalian body size evolution at the Cretaceous-Palaeogene boundary: Methods in Ecology and Evolution, v. 4, p. 734–744, doi: 10.1111/2041-210X.12084.

Smith, F.A., Boyer, A.G., Brown, J.H., Costa, D.P., Dayan, T., Ernest, S.K.M., Evans, A.R., Fortelius, M., Gittleman, J.L., and Hamilton, M.J., 2010, The evolution of maximum body size of terrestrial mammals: Science, v. 330, p. 1216–1219.

Smith, S.M., Sprain, C.S., Clemens, W.A., Lofgren, D.L., Renne, P.R., and Wilson, G.P, in review, Mammalian recovery following the end-Cretaceous mass extinction: A high-resolution view from McGuire Creek, Montana, USA.

Smits, P.D., and Evans, A.R., 2012, Functional constraints on tooth morphology in carnivorous mammals: BMC evolutionary biology, v. 12, p. 146.

Smits, P., and Wilson, G.P., 2011, Estimates and trends in body size of Laurasian Cretaceous mammals: Thirteenth Conference on Australasian Vertebrate Evolution, Paleontology and Systematics, Geological Survey of Western Australia, Perth, Record 2011/9:76.

Spradley, J.P., Pampush, J.D., Morse, P.E., and Kay, R.F., 2017, Smooth operator: The effects of different 3D mesh retriangulation protocols on the computation of Dirichlet normal energy: American Journal of Physical Anthropology, doi: 10.1002/ajpa.23188.

Sprain, C.J., Renne, P.R., Wilson, G.P., and Clemens, W. A., 2015, High-resolution chronostratigraphy of the terrestrial Cretaceous-Paleogene transition and recovery interval in the Hell Creek region, Montana: Geological Society of America Bulletin, v. 127, p. 393–409, doi: 10.1130/B31076.1.

Strait, S.G., 1993, Molar morphology and food texture among small-bodied insectivorous mammals: Journal of Mammalogy, v. 74, p. 391–402.

Strait, S.G., 1997, Tooth use and the physical properties of food: Evolutionary Anthropology: Issues, News, and Reviews, v. 5, p. 199–211, doi: 10.1002/(SICI)1520-6505(1997)5:6<199::AID-EVAN2>3.0.CO;2-8.

Thiery, G., Gillet, G., Lazzari, V., Merceron, G., and Guy, F., 2017, Was Mesopithecus a seed eating colobine? Assessment of cracking, grinding and shearing ability using dental topography: Journal of Human Evolution, v. 112, p. 79–92.

Trombulak, S.C., 1985, The influence of interspecific competition on home range size in chipmunks (Eutamias): Journal of Mammalogy, v. 66, p. 329–337.

Tseng, Z.J., 2012, Connecting Hunter − Schreger Band microstructure to enamel microwear features : New insights from durophagous carnivores: Acta Palaeontologica Polonica, v. 54, p. 473–484.

Valenzuela, D. Natural history of the white-nosed coati, Nasua narica, in a tropical dry forest of western Mexico: Revista Mexicana de Mastozoología, v. 3, p. 26–44.

Van Valen, L.M., 1994, The Origin of the Plesiadapid Primates and the Nature of 'Purgatorius': Evolutionary Monographs, v. 15, p. 1–79.

Van Valkenburgh, B., 1990, Skeletal and dental predictors of body mass in carnivores, *in* Damuth, J., and MacFadden, B.J., Body size in mammalian paleobiology: estimation and biological implications: Cambridge, Cambridge University Press, p. 181–205.

Van Valkenburgh, B., 2007, Déjà vu: the evolution of feeding morphologies in the Carnivora: Integrative and Comparative Biology, v. 47, p. 147–163.

Venables, W.N., and Ripley, B.D., 2013, Modern applied statistics with S-PLUS: Springer Science & Business Media.

Weil, A., 1998, A new species of Microcosmodon (Mammalia: Multituberculata) from the Paleocene Tullock Formation of Montana, and an argument for the Microcosmodontinae: PaleoBios, v. 18, p. 1–15.

Whitaker Jr, J.O., and Barnard, S.M., 2005, Food of big brown bats (Eptesicus fuscus) from a colony at Morrow, Georgia: Southeastern Naturalist, v. 4, p. 111–118.

Williamson, T.E., Brusatte, S.L., Carr, T.D., Weil, A., and Standhardt, B.R., 2012, The phylogeny and evolution of Cretaceous–Palaeogene metatherians: cladistic analysis and description of new early Palaeocene specimens from the Nacimiento Formation, New Mexico: Journal of Systematic Palaeontology, v. 10, p. 625–651, doi: 10.1080/14772019.2011.631592.

Wilson, D.S., 1975, The adequacy of body size as a niche difference: The American Naturalist, v. 109, p. 769–784.

Wilson, G.P., 2013, Mammals across the K/Pg boundary in northeastern Montana, U.S.A.: dental morphology and body-size patterns reveal extinction selectivity and immigrant-fueled ecospace filling: Paleobiology, v. 39, p. 429–469, doi: 10.1666/12041.

Wilson, G.P., 2014, Mammalian extinction, survival, and recovery dynamics across the Cretaceous-Paleogene boundary in northeastern Montana, USA: Geological Society of America Special Papers, v. 503, p. 365–392, doi: 10.1130/2014.2503(15).

Wilson, G.P., Evans, A. R., Corfe, I.J., Smits, P.D., Fortelius, M., and Jernvall, J., 2012, Adaptive radiation of multituberculate mammals before the extinction of dinosaurs: Nature, v. 483, p. 457–460, doi: 10.1038/nature10880.

Wilson, G.P., Ekdale, E.G., Hoganson, J.W., Calede, J.J., and Vander Linden, A., 2016, A large carnivorous mammal from the Late Cretaceous and the North American origin of marsupials: Nature Communications, v. 7, p. 13734, doi: 10.1038/ncomms13734.

Wilson, G.P., and Riedel, J.A., 2010, New Specimen Reveals Deltatheroidan Affinities of the North American Late Cretaceous Mammal Nanocuris: Journal of Vertebrate Paleontology, v. 30, p. 872–884, doi: 10.1080/02724631003762948.

Wilson, G. P., and Self, C., 2011, Mammalian dental complexity across the Cretaceous-Paleogene boundary with implications for ecological recovery and expansion: Supplement to the Journal of Vertebrate Paleontology p. 215.

Winchester, J.M., Boyer, D.M., St. Clair, E.M., Gosselin-Ildari, A.D., Cooke, S.B., and Ledogar, J.A., 2014, Dental topography of platyrrhines and prosimians: Convergence and contrasts: American Journal of Physical Anthropology, v. 153, p. 29–44, doi: 10.1002/ajpa.22398.

Wing, S.L., and Tiffney, B.H., 1987, The reciprocal interaction of angiosperm evolution and tetrapod herbivory: Review of Palaeobotany and Palynology, v. 50, p. 179–210.

Wischusen, E.W., and Richmond, M.E., 1998, Foraging ecology of the Philippine flying lemur (Cynocephalus volans): Journal of Mammalogy, v. 79, p. 1288–1295.

4.7 FIGURES

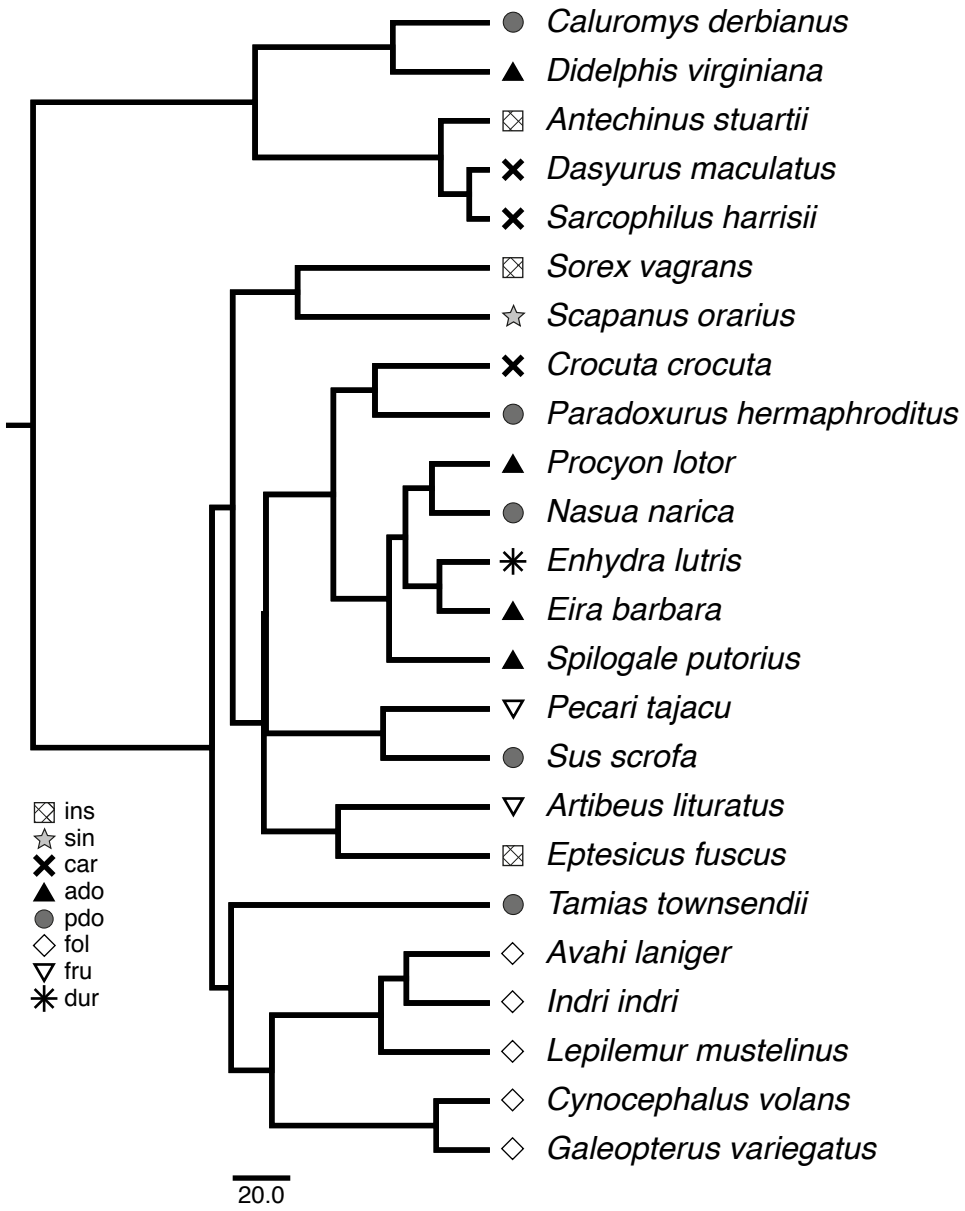

Figure 4.1 Tree of extant mammals included in our comparative sample (from timetree.org). Abbreviations – **ins** = insectivore; **sin** = soft insect specialist; **car** = carnivore; **fol** = folivore; **fru** = frugivore; **dur** = hard-object invertivore; **ado** = animal dominated omnivore; **pdo** = plant dominated omnivore.

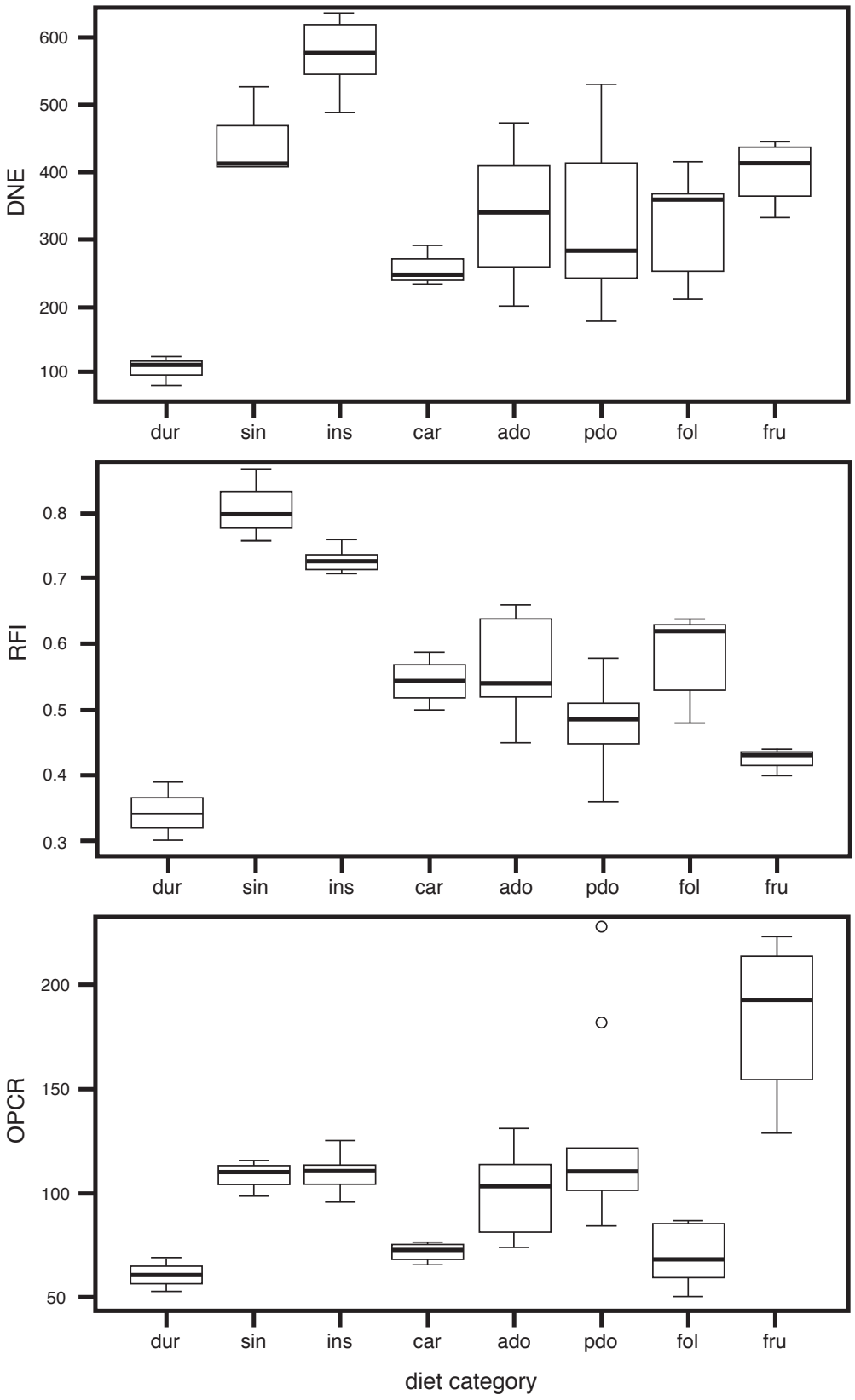
DNE
600
500
400
300
200
100
dur
sin
ins
car
ado
pdo
fol
fru
RFI
0.8
0.7
0.6
0.5
0.4
0.3
dur
sin
ins
car
ado
pdo
fol
fru
OPCR
200
150
100
50
dur
sin
ins
car
ado
pdo
fol
fru
diet category

Figure 4.2 Boxplots of orientation patch count (OPCR), Dirichlet normal energy (DNE), and relief index (RFI) across extant dietary groups. Abbreviations – **ins** = insectivore; **sin** = soft insect specialist; **car** = carnivore; **fol** = folivore; **fru** = frugivore; **dur** = hard-object invertivore; **ado** = animal dominated omnivore; **pdo** = plant dominated omnivore.

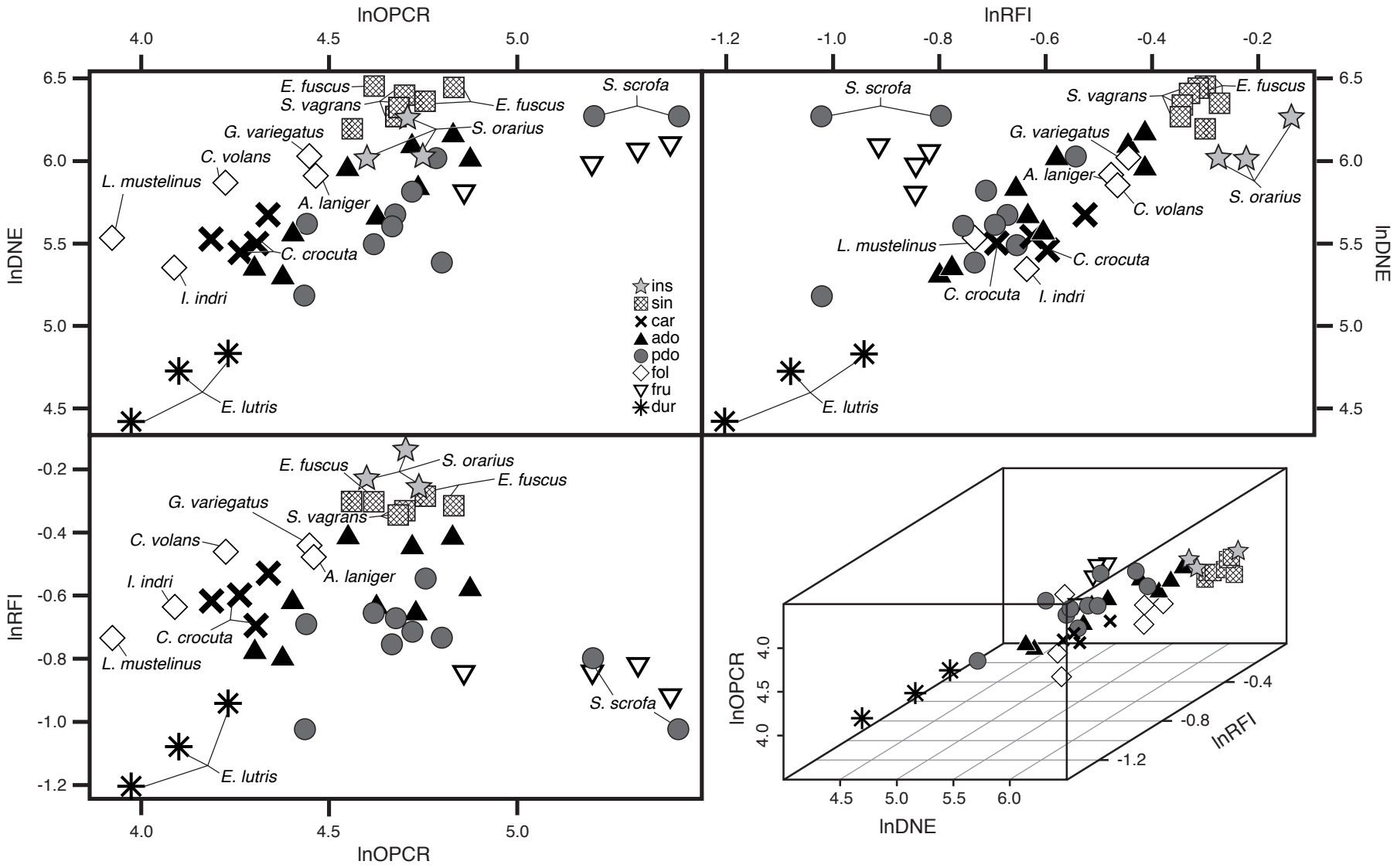
lnOPCR
lnRFI
lnDNE
E. fuscus
S. vagrans
S. orarius
G. variegatus
C. volans
L. mustelinus
A. laniger
C. crocuta
I. indri
E. lutris
S. scrofa
ins
sin
car
ado
pdo
fol
fru
dur

Figure 4.3 Bivariate scatter plots of orientation patch count rotated (OPCR), Dirichlet normal energy (DNE), and relief index (RFI), and 3D scatter plot of all three DTA metrics for extant comparative sample. Shapes correspond to true dietary category as determined from the literature. See Table 4.1 for full taxonomic names. Abbreviations – **ins** = insectivore; **sin** = soft insect specialist; **car** = carnivore; **fol** = folivore; **fru** = frugivore; **dur** = hard-object invertivore; **ado** = animal dominated omnivore; **pdo** = plant dominated omnivore.

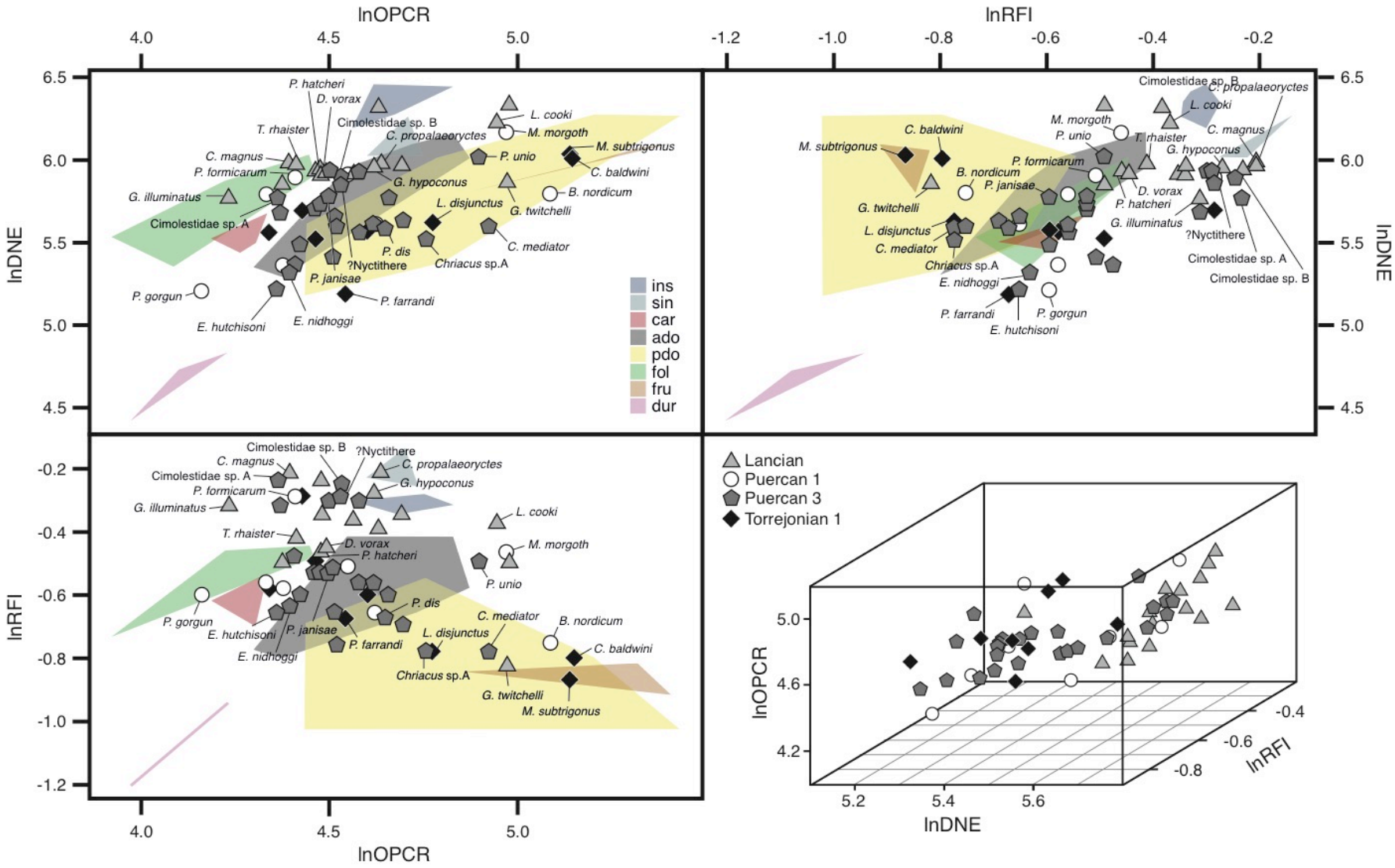
lnOPCR
lnRFI
lnDNE
ins
sin
car
ado
pdo
fol
fru
dur
Lancian
Puercan 1
Puercan 3
Torrejonian 1
P. hatcheri
D. vorax
Cimolestidae sp. B
T. rhaister
C. propalaeoryctes
L. cooki
M. morgoth
M. subtrigonus
C. magnus
P. formicarum
P. unio
C. baldwini
G. hypoconus
G. illuminatus
B. nordicum
L. disjunctus
G. twitchelli
Cimolestidae sp. A
C. mediator
P. dis
?Nyctithere
Chriacus sp.A
P. janisae
P. gorgun
P. farrandi
E. hutchisoni
E. nidhoggi

Figure 4.4 Bivariate scatter plots of orientation patch count rotated (OPCR), Dirichlet normal energy (DNE), and relief index (RFI), and 3D scatter plot of all three DTA metrics for fossil therian taxa. Colored polygons are regions of the morphospace covered by extant dietary groups. Shapes correspond to NALMA interval. See Table 4.2 for full taxonomic names. Abbreviations – **ins** = insectivore; **sin** = soft insect specialist; **car** = carnivore; **fol** = folivore; **fru** = frugivore; **dur** = hard-object invertivore; **ado** = animal dominated omnivore; **pdo** = plant dominated omnivore.

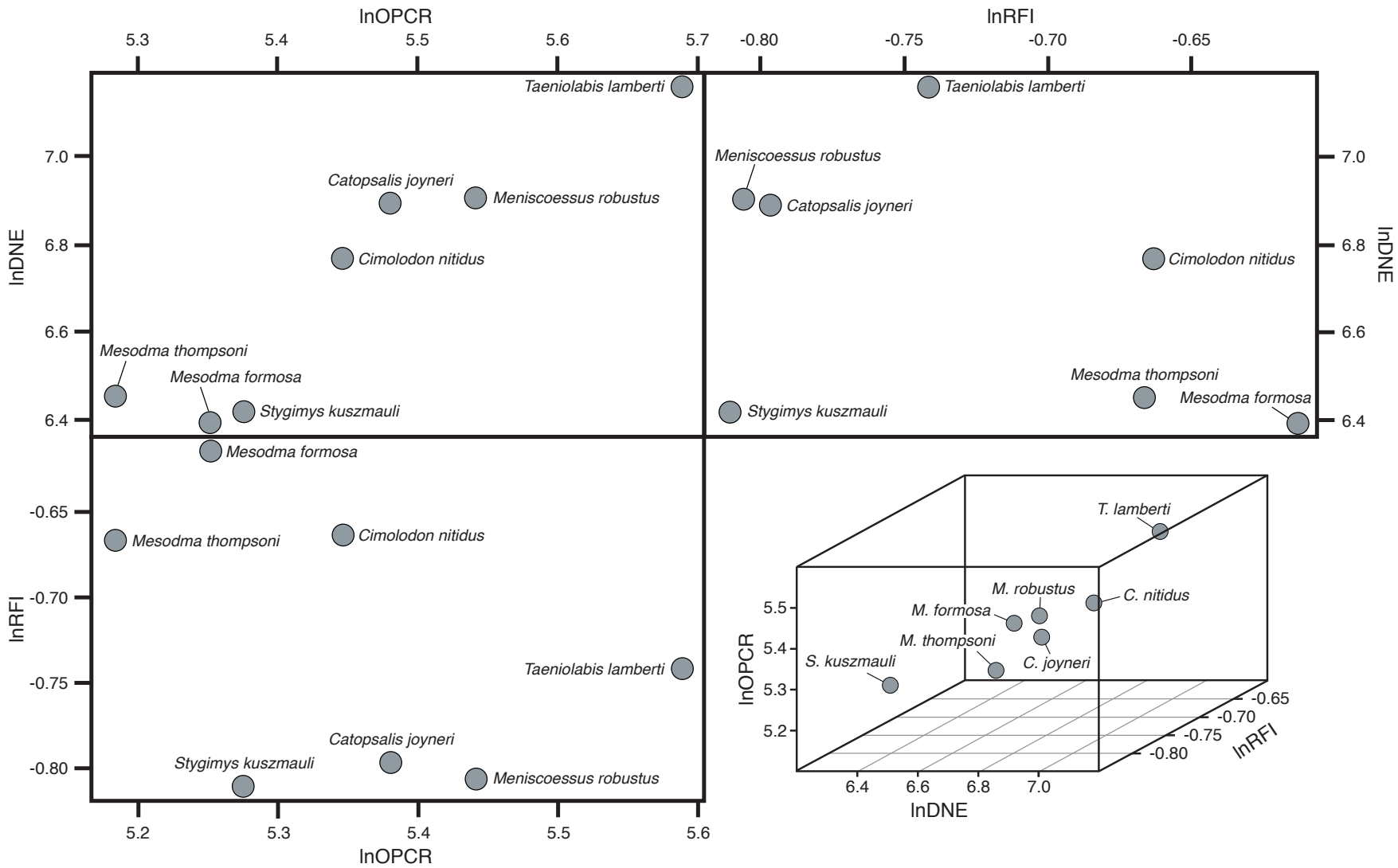
lnOPCR
lnRFI
lnDNE
Taeniolabis lamberti
Catopsalis joyneri
Meniscoessus robustus
Cimolodon nitidus
Mesodma thompsoni
Mesodma formosa
Stygimys kuszmauli
T. lamberti
M. robustus
C. nitidus
M. formosa
M. thompsoni
C. joyneri
S. kuszmauli

Figure 4.5 Bivariate scatter plots of orientation patch count rotated (OPCR), Dirichlet normal energy (DNE), and relief index (RFI), and 3D scatter plot of all three DTA metrics for multituberculate taxa. Taxa are labeled by name because many of them are present in more than one NALMA interval zone, so shapes could not be used to represent interval zone. See Table 4.3 for interval zones in which each taxon appears.

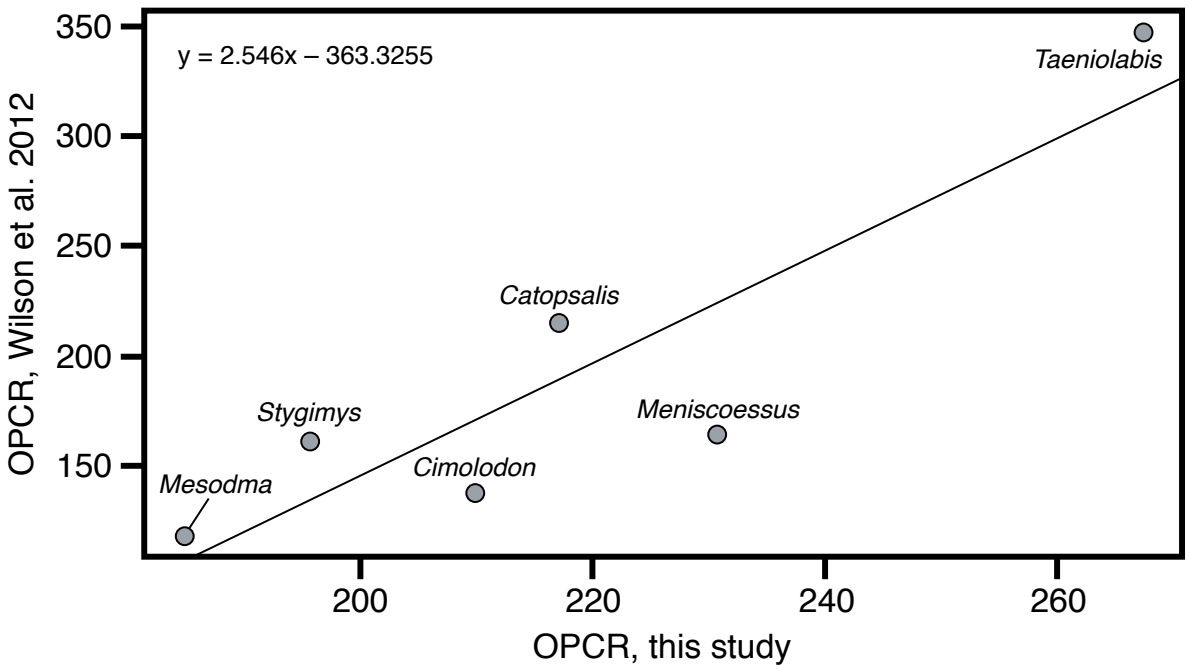

Figure 4.6 Least-squares linear regression of OPCR from Wilson et al. (2012, x-axis) on OPCR from this study (y-axis). Regression equation in upper left of plot.

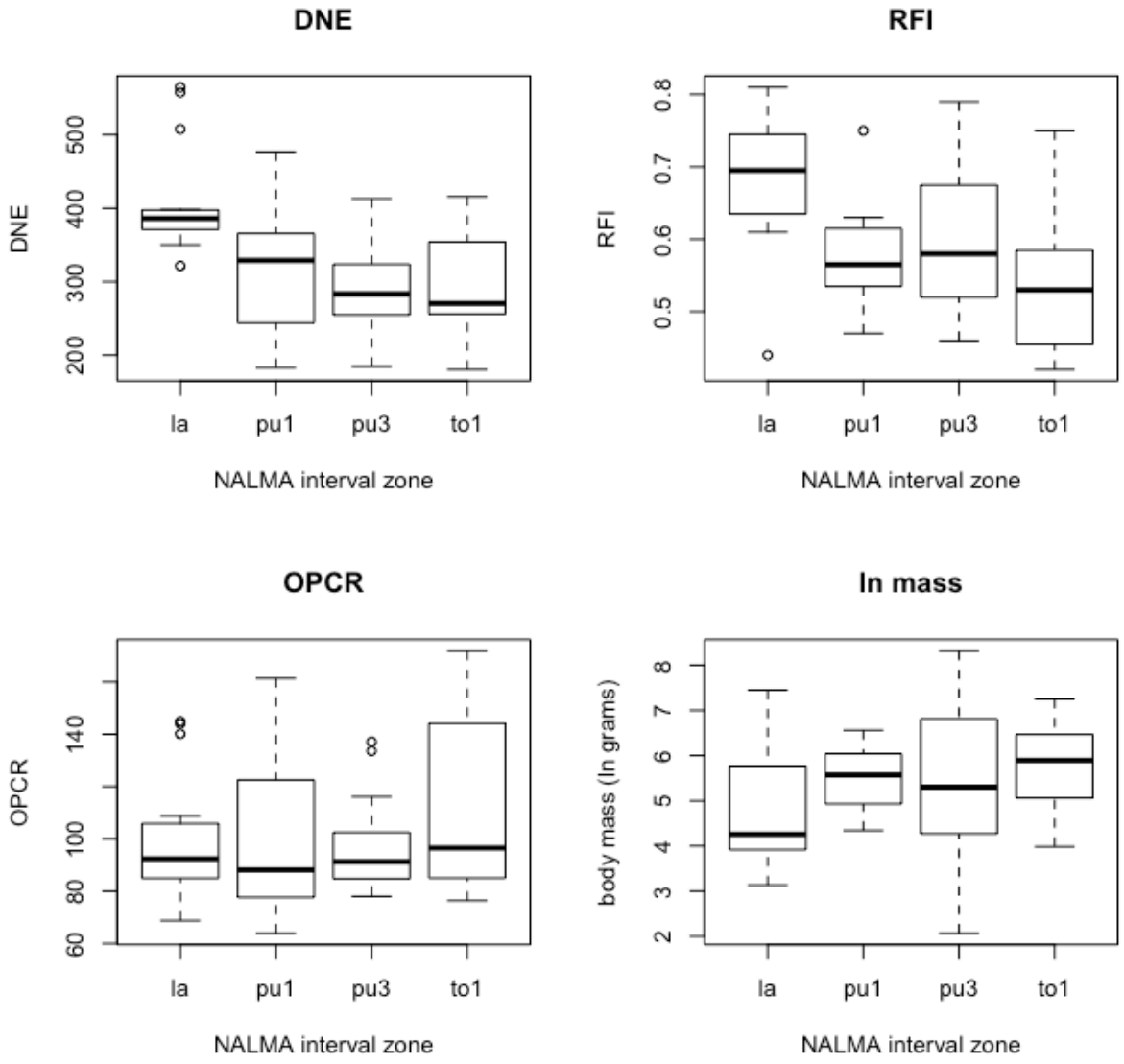

Figure 4.7 Boxplots of raw DTA metrics, and ln body mass, through NALMA interval zones included here. Abbreviations – **La** = Lancian; **Pu1** = Puercan 1; **Pu3** = Puercan 3; **To1** = Torrejonian 1; **OPCR** = orientation patch count rotated; **DNE** = Dirichlet normal energy; **RFI** = relief index.

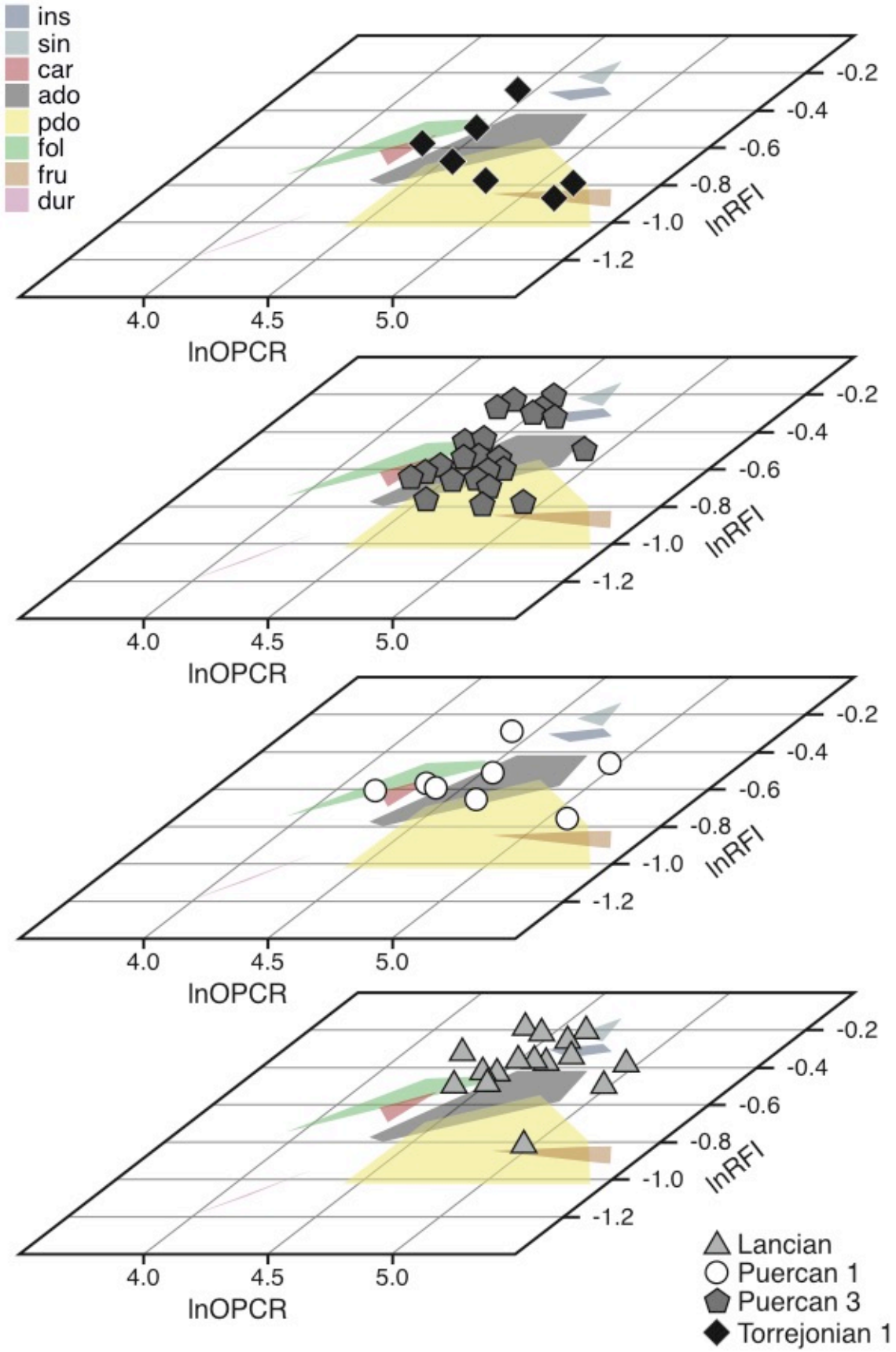
ins
sin
car
ado
pdo
fol
fru
dur
-0.2
-0.4
-0.6
-0.8
-1.0
-1.2
lnRFI
4.0
4.5
5.0
lnOPCR
Lancian
Puercan 1
Puercan 3
Torrejonian 1

Figure 4.8 Scatterplots of lnOPCR versus lnRFI through time. Time proceeds upward on the chart, with the oldest NALMA interval zone (Lancian) at the bottom, and the youngest (Torrejonian 1) at the top. Abbreviations – **La** = Lancian; **Pu1** = Puercan 1; **Pu3** = Puercan 3; **To1** = Torrejonian 1; **ins** = insectivore; **sin** = soft insect specialist; **car** = carnivore; **fol** = folivore; **fru** = frugivore; **dur** = hard-object invertivore; **ado** = animal dominated omnivore; **pdo** = plant dominated omnivore.

4.8 TABLES

Table 4.1 Extant mammalian comparative sample used in this study. Mean body mass is listed as ln(grams). When two body mass values are listed, one is the female mean and one is the male mean, and our sample included at least one male and one female.

Species	Order	N	Tooth	Diet	Diet source(s)	Body mass	Mass source
Antechinus stuartii	Dasyuromorphia	1	m3	ins	Fox and Archer 1984	3.30	Holleley et al. 2006
Artibeus lituratus	Chiroptera	3	m1	fru	Giannini and Kalko 2004	4.16	Barclay and Brigham 1991
Avahi laniger	Primates	1	m2	fol	Harcourt 1991	7.07	Boyer 2008
Caluromys derbianus	Didelphimorphia	1	m3	pdo	Bucher and Hoffmann 1980	7.17	Robinson and Redford 1986
Crocuta crocuta	Carnivora	2	m1	car	Cooper et al. 1999	10.86	Van Valkenburgh 1990
Cynocephalus volans	Dermoptera	1	m2	fol	Wischusen and Richmond 1998	7.14	Boyer 2008
Dasyurus maculatus	Dasyuromorphia	1	m3	car	Glen and Dickman 2006	8.16	Jones et al. 2001
Didelphis virginiana	Didelphimorphia	3	m3	ado	Gardner 1982	7.61	Eisenberg and Wilson 1981
Eira barbara	Carnivora	1	m1	ado	Bisbal 1986	8.34	Van Valkenburgh 1990
Enhydra lutris	Carnivora	3	m1	dur	Riedman and Estes 1990	10.37	Van Valkenburgh 1990
Eptesicus fuscus	Chiroptera	3	m2	ins	Whitaker and Barnard 2005	2.88	Barclay and Brigham 1991
Galeopterus variegatus	Dermoptera	1	m2	fol	Dzulhelmi and Abdullah 2009	7.29	Boyer 2008
Indri indri	Primates	1	m2	fol	Britt et al. 2002	8.75	Boyer 2008
Lepilemur mustelinus	Primates	1	m2	fol	Hladik and Charles-Dominique 1974	6.41	Boyer 2008
Nasua narica	Carnivora	2	m1	pdo	Valenzuela 1998	8.52	Gittleman 1985
Paradoxurus hermaphroditus	Carnivora	2	m1	pdo	Nakashima et al. 2013	8.01	Gittleman 1985
Pecari tajacu	Artiodactyla	1	m2	fru	Desbiez et al. 2009	10.08	Harestad and Bunnel 1979
Procyon lotor	Carnivora	3	m1	ado	Bartoszewicz et al. 2008, Schoonover and Marshall 1951, Lotze and Anderson	9.16	Van Valkenburgh 1990

					1979		
Sarcophilus harrisii	Dasyuromorphia	1	m3	car	Pemberton et al. 2008	8.95	Van Valkenburgh 1990
Scapanus orarius	Eulipotyphla	3	m2	sin	Moore 1933; Silcox and Teaford 2002	(m) 4.31 (f) 4.25	Glendenning 1959
Sorex vagrans	Eulipotyphla	3	m2	ins	Clothier 1955	1.50	Harestad and Bunnel 1979
Spilogale putorius	Carnivora	2	m1	ado	Baker and Baker 1975	5.99	Kinlaw 1995
Sus scrofa	Artiodactyla	2	m2	pdo	Ballari et al. 2014	10.84	Saunders and McCleod 1999
Tamias townsendii	Rodentia	3	m2	pdo	Trombulak 1985	(m) 4.25 (f) 4.33	Hayssen 2008

Table 4.2 Fossil therian mammals included in this study. All fossil taxa are N=1 except where noted. Asterisk (*) denotes a locality located somewhere other than NE Montana; state or province is indicated in parentheses. Body mass listed as ln(grams). ln body masses were taken directly from Wilson (2013); all other citations are sources for /m1 linear measurements, which were used to calculate body mass in ln(grams) using the regression in Bloch et al. (1998) (eutherians) or Smits and Wilson 2011 (metatherians). Specimens with mass sources listed as "this study, /m1" are specimens that preserve an m1, which we used to estimate body mass using the regression in Bloch et al. (1998). Specimens with "this study, /m2" listed as the source do not preserve an m1, and/or are not a named taxon; as such, no m1 measurements could be taken from the literature, and m2 measurements were used with the Bloch et al. (1998) regression, or Smits and Wilson (2011) regression, to estimate body mass. Body mass listed for Cimolestidae sp. B is mean calculated from the two specimens.

Species	Tooth position	Specimen	Locality	NALMA	Body mass	Mass source
Alphadon marshi	m3	UCMP 191126	UCMP V99227	La	4.47	Wilson 2013
Arctocyonidae sp. A	m2	UCMP 145686	UCMP V73080	Pu3	5.12	this study, m2
Arctocyonidae sp. B	m2	UCMP 185970	UCMP V73080	Pu3	5.41	this study, m2
Arctocyonidae sp. C	m2	UCMP 281300	UCMP V72134	Pu3	7.95	this study, m2
Arctocyonidae sp. D	m2	UCMP 281302	UCMP V75195	Pu3	4.06	this study, m2
Baioconodon engdahli	m2	UCMP 116542	UCMP V74110	Pu1	6.27	Wilson 2013
Baioconodon nordicum	m2	UCMP 134592	UCMP V88044	Pu1	6.56	Wilson 2013
?*Carcinodon* sp.	m2	UCMP 218957	UCMP V73080	Pu3	6.08	this study, /m2
Chriacus baldwini	m2	USNM 9278	Sweetgrass Co. (MT)*	To1	6.72	this study, /m1
Chriacus mediator	m2	UCMP 110446	UCMP V73080	Pu3	6.68	this study, /m1
Chriacus sp. A	m2	UCMP 281296	UCMP V73082	Pu3	7.10	this study, /m2
Cimolestes magnus	m2	UA 3791	KUA-1 (AB)*	La	6.34	Wilson 2013

Cimolestes propalaeoryctes	m2	UA 3756	KUA-1 (AB)*	La	3.89	Wilson 2013
Cimolestes stirtoni	m2	UCMP 117659	UCMP V73087	La	5.74	Wilson 2013
Cimolestidae sp. A	m2	UCMP 281295	UCMP V74122	Pu3	3.18	this study, /m2
Cimolestidae sp. B (N=2)	m2	UCMP 258019, UCMP 258046	UCMP V73080, UCMP V72134	Pu3	5.16	this study, /m2
Condylarthra sp. A	m2	UCMP 281303	UCMP V99438	Pu3	7.82	this study, /m2
Didelphodon vorax	m3	UCMP 55290	UCMP V5620 (WY)*	La	7.45	Wilson 2013
Eoconodon hutchisoni	m2	UCMP 156117	UCMP V75196	Pu3	8.31	Clemens 2011
Eoconodon nidhoggi	m2	UCMP 170848	UCMP V73080	Pu3	7.59	Clemens 2011
Glasbius twitchelli	m3	UCMP 134781	UCMP V87072	La	3.98	Wilson 2013
Gypsonictops hypoconus	m2	UWBM 92455	UWBM C1121	La	3.48	Wilson 2013
Gypsonictops illuminatus	m2	UCMP 170870	UCMP V77130	La	4.12	Wilson 2013
Leptalestes cooki	m3	UCMP 153629	UCMP V80092	La	4.39	Wilson 2013
Leptalestes krejcii	m3	UCMP 51347	UCMP V5620 (WY)*	La	3.13	Wilson 2013
Litaletes disjunctus	m2	USNM 9323	Sweetgrass Co. (MT)*	To1	5.92	this study, m1
Mimatuta minuial	m2	UCMP 192402	UCMP V77087	Pu1	5.81	Wilson 2013
Mimatuta morgoth	m2	UCMP 132454	UCMP V86031	Pu1	5.72	Wilson 2013
Mimotricentes subtrigonus	m2	USNM 15273	Gazin Loc. 149-36 (NM)*	To1	7.25	this study, m1
Nortedelphys jasoni	m3	UWBM 91426	UWBM C1112	La	3.99	Wilson 2013
?Nyctithere sp.	m2	UCMP 224190	UCMP V74122	Pu3	2.42	this study, m2
Oxyacodon sp.	m2	UCMP 186029	UCMP V73080	Pu3	5.14	this study, m2
Oxyclaenus simplex	m2	UWBM 59320	UWBM C0192 (NM)*	Pu3	6.22	Kondrashov and Lucas 2004
Oxyclaenus sp. A	m2	UCMP 186021	UCMP V73080	Pu3	5.73	this study, m2
Oxyclaenus sp. B	m2	UCMP 186000	UCMP V73080	Pu3	5.92	this study, m2
Oxyclaenus subbituminus	m2	UCMP 148328	UCMP V73095	To1	5.86	this study, m2
?*Oxyclaenus* sp.	m2	UCMP 186157	UCMP V73080	Pu3	6.94	this study, m2
Oxyprimus erikseni	m2	UCMP 132315	UCMP V87095	Pu1	4.86	Wilson 2013
Oxytomodon perissum	m2	USNM 16183	Dragon Paleocene (UT)*	To1	5.42	this study, m2
Pandemonium dis	m2	UM 1631	UCMP V71202	Pu3	4.47	Van Valen 1994
Paromomys farrandi	m2	UWBM 99692	UWBM C1418	To1	3.98	Clemens and Wilson 2009
Pediomys elegans	m3	UCMP 191138	UCMP V99370	La	3.94	Wilson 2013

Peradectes minor	m3	UCMP 115392	UCMP V74122	Pu3	2.06	Clemens 2006
Periptychidae sp.	m2	UCMP 189503	UCMP V73082	Pu3	5.96	this study, m2
Procerberus formicarum	m2	UCMP 117903	UCMP V74111	Pu1	4.34	Wilson 2013
Prodiacodon crustulum	m2	UCMP 192104	UCMP V99438	Pu3	4.50	Clemens and Wilson 2009
Prodiacodon cf. *P. crustulum*	m2	UCMP 189532	UCMP V76171	To1	4.70	Clemens and Wilson 2009
Protalphadon foxi	m3	UWBM 97291	UWBM C1153	La	3.42	Wilson 2013
Protolambda florencae	m3	UCMP 117617	UCMP V75178	La	5.8	Wilson 2013
Protolambda hatcheri	m3	UCMP 46326	UCMP V5620 (WY)*	La	5.46	Wilson 2013
Protungulatum donnae	m2	UWBM 98161	UWBM C1688	Pu1	5.42	Wilson 2013
Protungulatum gorgun	m2	UCMP 133837	UCMP V87115	Pu1	5.00	Wilson 2013
Purgatorius janisae	m2	UCMP 107406	UCMP V72130	Pu3	3.40	Clemens 1974
Purgatorius unio	m2	UCMP 107409	UCMP V72130	Pu3	3.14	this study, m1
Turgidodon rhaister	m3	UCMP 174524	UCMP V75178	La	5.82	Wilson 2013

Table 4.3 Multituberculate specimens included in this study. Body mass for *T. lamberti* was estimated using m1 dimensions from this study and the methods described in Wilson et al. (2012). Body mass listed as ln(grams).

Species	Tooth position	Specimen	Locality	NALMA(s)	Body mass	Mass source
Catopsalis joyneri	p4	UCMP 73828	UCMP V65127			
	m1	UCMP 105532	UCMP V65127	Pu1, Pu3	7.80	Wilson 2013
	m2	UCMP 105501	UCMP V65127			
Cimolodon nitidus	p4	UCMP 168716	UCMP V77130			
	m1	UWBM 91418	UWBM C116	La	5.19	Wilson 2013
	m2	UCMP 212329	UCMP V77130			
Meniscoessus robustus	p4–m2	UCMP 107405	UCMP V73051	La	7.10	Wilson 2013
Mesodma formosa	p4	UCMP 239283	UCMP V84194			
	m1	UCMP 144281	UCMP V84193	La, Pu1, Pu3	3.55	Wilson 2013
	m2	UCMP 144285	UCMP V84193			
Mesodma thompsoni	p4, m1	UCMP 132304	UCMP V84194	La, Pu1, Pu3	3.98	Wilson 2013
	m2	UWBM 107220	UWBM C1912			
Stygimys kuszmauli	p4	UWBM 104326	UWBM C1665			
	m1	UWBM 107222	UWBM C1665	Pu1	5.35	Wilson 2013
	m2	UWBM 107221	UWBM C1665			
Taeniolabis lamberti	p4–m2	CCM 71-110	UCMP V76175	Pu3	9.42	This study; Wilson et al. 2012

Table 4.4 Phylogenetic correlation in DTA metrics for our extant sample: Pagel's lambda (λ) and Blomberg's K.

	λ	K
DNE	0.66	0.58
RFI	0.72	0.64
OPCR	0.98	0.70

Table 4.5 Correlations among dental topographic metrics in extant therian mammals. Upper right triangle of table is linear R^2; lower left triangle of table is Spearman's rho, with associated p-values in parentheses. Bolded p-values are significant ($p < 0.05$).

	DNE	RFI	OPCR	Slope
DNE	-	0.42	0.41	0.37
RFI	0.56 **(4e-5)**	-	0.0020	0.94
OPCR	0.65 (0.65)	-0.031 (0.83)	-	0.002
Slope	-0.55 **(6e-5)**	-0.97 (**2e-16**)	0.013 (0.93)	-

Table 4.6 Posterior probabilities of dietary group membership resulting from discriminant function analysis (DFA) for extant mammalian sample. Highest posterior probability for each specimen (= diet identified by DFA) is in bold. Other posteriors for each specimen that are close to the highest posterior (within 0.10) are marked with an asterisk (*). Posteriors less than 0.001 are not reported (" - "). Listed specimen numbers are UWBM numbers, except where noted (AMNH). A bullet (•) next to a taxon's diet indicates that it was classified incorrectly by DFA.

Species	Specimen	true diet	ado	car	dur	fol	fru	pdo	ins	sin
Antechinus stuartii	68916	ins	0.011	0.007	0.000	0.035	0.000	0.000	**0.925**	0.021
Artibeus lituratus	62023	fru	-	-	-	-	**0.950**	0.050	-	-
Artibeus lituratus	62030	fru	-	-	-	-	**0.989**	0.011	-	-
Artibeus lituratus	62034	fru •	0.042	0.001	-	-	0.092	**0.865**	-	-
Avahi laniger (AMNH)	100635	fol	0.258*	0.229*	-	**0.276**	-	0.003	0.229*	0.005
Caluromys derbianus	32255	pdo •	**0.781**	0.043	-	0.007	-	0.137	0.029	0.003
Crocuta crocuta	26583	car	0.335	**0.518**	-	0.102	-	0.044*	0.001	-
Crocuta crocuta	33257	car	0.444*	**0.490**	-	0.043	-	0.021	0.001	0.001
Galeopterus variegatus (AMNH)	102703	fol •	0.033	0.068	-	0.444*	-	-	**0.454**	0.001
Cynocephalus volans (AMNH)	120449	fol	0.002	0.039	-	**0.867**	-	-	0.091	-
Dasyurus maculatus	68901	car	0.330	**0.446**	-	0.190	-	0.006	0.026	0.002
Didelphis virginiana	35526	ado	**0.453**	0.133	-	0.059	-	0.005	0.283	0.067
Didelphis virginiana	39355	ado	**0.664**	0.019	-	0.003	-	0.034	0.166	0.114
Didelphis virginiana	6640	ado	**0.617**	0.055	-	0.019	-	0.022	0.251	0.036
Eira barbara	39436	ado •	0.338	0.086	0.015	0.001	0.001	**0.559**	-	-
Enhydra lutris	34554	dur	-	-	**1.000**	-	-	-	-	-
Enhydra lutris	34559	dur	-	-	**0.999**	-	-	0.001	-	-
Enhydra lutris	81970	dur	0.001	-	**0.980**	-	-	0.018	-	-
Eptesicus fuscus	66977	ins	-	-	-	0.028	-	-	**0.972**	-

Eptesicus fuscus	66980	ins	0.012	0.002	-	0.004	-	-	**0.925**	0.057
Eptesicus fuscus	79331	ins	0.010	0.001	-	0.004	-	-	**0.971**	0.013
Indri indri (AMNH)	100503	fol •	0.090	**0.666**	-	0.241	-	0.002	0.001	-
Lepilemur mustelinus (AMNH)	170578	fol	-	0.012	-	**0.988**	-	-	-	-
Nasua narica	41688	pdo	0.411	0.008	-	-	0.003	**0.577**	-	-
Nasua narica	41687	pdo	0.037	-	0.003	-	0.137	**0.823**	-	-
Paradoxurus hermaphroditus	14711	pdo	0.013	0.002	0.457*	-	0.007	**0.522**	-	-
Paradoxurus hermaphroditus	82651	pdo	0.209	0.007	-	-	0.009	**0.775**	-	-
Pecari tajacu	20670	fru	0.001	-	-	-	**0.848**	0.151	-	-
Procyon lotor	32812	ado	**0.508**	0.019	-	0.001	0.003	0.469*	0.001	-
Procyon lotor	32814	ado	**0.577**	0.008	-	-	0.005	0.407	0.002	0.001
Procyon lotor	39563	ado	**0.597**	0.027	-	-	0.001	0.374	-	-
Sarcophilus harrisii	20671	car	0.088	**0.493**	-	0.413	-	0.002	0.004	-
Scapanus orarius	64808	sin	0.002	-	-	-	-	-	0.134	**0.864**
Scapanus orarius	64811	sin	0.051	0.001	-	-	-	0.001	0.007	**0.941**
Scapanus orarius	64820	sin	0.017	0.002	-	-	-	-	0.034	**0.947**
Sorex vagrans	58638	ins	0.003	0.001	-	0.019	-	-	**0.976**	0.001
Sorex vagrans	58645	ins	0.008	0.003	-	0.025	-	-	**0.959**	0.004
Sorex vagrans	60637	ins	0.025	0.007	-	0.022	-	-	**0.929**	0.016
Spilogale putorius	20192	ado	**0.647**	0.260	-	0.016	-	0.076	0.001	0.001
Spilogale putorius	76080	ado	**0.406**	0.344*	0.003	0.015	-	0.232	-	-
Sus scrofa	31576	pdo •	0.012	-	-	-	**0.544**	0.444*	-	-
Sus scrofa	33170	pdo •	-	-	-	-	**0.990**	0.010	-	-
Tamias townsendii	20077	pdo	0.370	0.019	-	0.001	0.004	**0.606**	-	-
Tamias townsendii	43787	pdo	0.424	0.013	-	-	0.003	**0.560**	-	-
Tamias townsendii	44335	pdo •	**0.536**	0.279	-	0.039	-	0.145	0.001	-

Table 4.7 Posterior probabilities of dietary group membership resulting from discriminant function analysis (DFA) for fossil therian mammalian sample. Highest posterior probability for each specimen (= diet identified by DFA) is in bold. Other posteriors for each specimen that are close to the highest posterior (within 0.10) are marked with an asterisk (*). Posteriors less than 0.001 are not reported (" - ").

Species	Specimen	ado	car	dur	fol	fru	pdo	ins	sin
Alphadon marshi	UCMP 191126	0.378*	0.058	-	0.009	-	0.003	0.129	**0.423**
Arctocyonidae sp. A	UCMP 145686	**0.751**	0.026	-	-	-	0.217	-	0.006
Arctocyonidae sp. B	UCMP 185970	**0.694**	0.232	-	0.027	-	0.029	0.012	0.006
Arctocyonidae sp. C	UCMP 281300	0.309	0.007	-	-	0.007	**0.678**	-	-
Arctocyonidae sp. D	UCMP 281302	**0.790**	0.048	-	-	-	0.051	-	0.111
Baioconodon engdahli	UCMP 116542	0.**530**	0.022	-	-	0.001	0.446*	-	-
Baioconodon nordicum	UCMP 134592	0.007	-	-	-	**0.601**	0.392	-	-
?*Carcinodon* sp.	UCMP 218957	**0.791**	0.020	-	-	-	0.141	-	0.048
Chriacus baldwini	USNM 9278	0.006	-	-	-	**0.632**	0.362	-	-
Chriacus mediator	UCMP 110446	0.016	-	-	-	0.303	**0.680**	-	-
Chriacus sp. A	UCMP 281296	0.064	-	0.001	-	0.055	**0.880**	-	-
Cimolestes magnus	UA 3791	0.011	0.012	-	0.020	-	-	**0.494**	0.464*
Cimolestes propalaeoryctes	UA 3756	0.009	-	-	-	-	-	0.006	**0.984**
Cimolestes stirtoni	UCMP 117659	0.027	0.009	-	0.003	-	-	0.122	**0.840**
Cimolestidae sp. A	UCMP 281295	0.022	0.010	-	0.002	-	-	0.026	**0.940**
Cimolestidae sp. B	UCMP 258019	0.145	0.053	-	0.004	-	-	0.021	**0.778**
Cimolestidae sp. B	UCMP 258046	0.030	0.004	-	-	-	-	0.020	**0.946**
Condylarthra sp. A	UCMP 281303	0.437*	0.098	-	0.005	0.001	**0.460**	-	-
Didelphodon vorax	UCMP 55290	**0.337**	0.203	-	0.163	-	0.003	0.276*	0.018
Eoconodon hutchisoni	UCMP 156117	**0.636**	0.063	0.007	-	-	0.292	-	0.001
Eoconodon nidhoggi	UCMP 170848	**0.689**	0.076	0.001	-	-	0.233	-	0.001
Glasbius twitchelli	UCMP 134781	0.023	-	-	-	0.238	**0.739**	-	-

Gypsonictops hypoconus	UWBM 94255	0.062	0.004	-	-	-	-	0.027	**0.906**
Gypsonictops illuminatus	UCMP 170870	0.046	0.174	-	0.296*	-	-	**0.377**	0.107
Leptalestes cooki	UCMP 153629	**0.498**	0.004	-	-	-	0.032	0.078	0.387
Leptalestes krejcii	UCMP 51347	0.004	0.004	-	0.081	-	-	**0.911**	0.001
Litaletes disjunctus	USNM 9323	0.086	0.001	-	-	0.041	**0.872**	-	-
Mimatuta minuial	UCMP 192402	0.061	0.226	-	**0.669**	-	0.001	0.044	-
Mimatuta morgoth	UCMP 132454	**0.740**	0.004	-	-	0.002	0.191	0.015	0.048
Mimotricentes subtrigonus	USNM 15273	0.003	-	-	-	**0.680**	0.317	-	-
Nortedelphys jasoni	UWBM 91426	0.297	0.011	-	0.001	-	0.005	0.033	**0.654**
?Nyctithere sp.	UCMP 224190	0.082	0.010	-	0.001	-	-	0.023	**0.885**
Oxyacodon sp.	UCMP 186029	**0.683**	0.233	-	0.034	-	0.028	0.017	0.006
Oxyclaenus simplex	UWBM 59320	**0.828**	0.073	-	0.001	-	0.053	0.001	0.045
Oxyclaenus sp. A	UCMP 186021	**0.734**	0.021	-	-	-	0.239	-	0.006
Oxyclaenus sp. B	UCMP 186000	**0.713**	0.040	-	0.001	-	0.244	0.001	0.001
Oxyclaenus subbituminus	UCMP 148328	**0.656**	0.020	-	-	0.001	0.321	-	0.002
?*Oxyclaenus* sp.	UCMP 186157	**0.656**	0.148	-	0.010	-	0.184	0.001	-
Oxyprimus erikseni	UCMP 132315	**0.566**	0.205	-	0.099	-	0.019	0.107	0.005
Oxytomodon perissum	USNM 16183	**0.494**	0.423*	-	0.056	-	0.022	0.004	0.001
Pandemonium dis	UM 1631	0.404	0.011	-	-	0.003	**0.582**	-	-
Paromomys farrandi	UWBM 99692	0.246	0.002	0.026	-	0.005	**0.720**	-	-
Pediomys elegans	UCMP 191138	0.011	0.005	-	0.037	-	-	**0.943**	0.004
Peradectes minor	UCMP 115392	**0.617**	0.012	-	0.004	0.001	0.117	0.242	0.008
Periptychidae sp.	UCMP 189503	0.128	0.014	-	0.002	-	0.001	0.056	**0.800**
Procerberus formicarum	UCMP 117903	**0.744**	0.141	-	0.002	-	0.111	-	0.002
Prodiacodon crustulum	UCMP 192104	0.063	0.010	-	-	-	-	0.004	**0.923**
Prodiacodon cf. *P. crustulum*	UCMP 189532	0.080	0.057	-	0.036	-	-	0.342	**0.485**
Protalphadon foxi	UWBM 97291	0.126	0.039	-	0.013	-	-	0.230	**0.591**
Protolambda florencae	UCMP 117617	0.228	0.095	-	0.042	-	0.001	**0.335**	0.298*
Protolambda hatcheri	UCMP 46326	0.093	0.217	-	**0.542**	-	0.001	0.148	0.001
Protungulatum donnae	UWBM 98161	0.197	0.183	-	0.289*	-	0.002	**0.324**	0.005
Protungulatum gorgun	UCMP 133837	**0.776**	0.111	-	0.001	-	0.108	-	0.004

Purgatorius janisae	UCMP 107406	0.036	0.082	-	0.404*	-	-	**0.476**	0.003
Purgatorius unio	UCMP 107409	**0.487**	0.480*	0.001	0.007	-	0.024	-	0.001
Turgidodon rhaister	UCMP 174524	**0.719**	0.005	-	-	0.002	0.247	0.003	0.024

Table 4.8 Diet types present in each NALMA interval zone as determined by DFA. Values are numbers of taxa assigned to that diet type; numbers in parentheses are percent of total taxa assigned to that diet type in that interval zone. Because of rounding, percentages do not add to 100% in every case.

Diet	La	Pu1	Pu3	To1
ado	3 (18.8)	5 (62.5)	12 (50.0)	3 (37.5)
car	-	-	-	-
dur	-	-	-	-
fol	1 (6.3)	1 (12.5)	-	-
fru	-	1 (12.5)	-	2 (25.0)
pdo	1 (6.3)	-	4 (16.7)	2 (25.0)
ins	5 (31.3)	1 (12.5)	1(4.2)	-
sin	6 (37.5)	-	7 (29.2)	1 (12.5)

Table 4.9 Disparity and morphospace occupation measures for therian mammals within each NALMA interval zone. Abbrevations: MPD = mean pairwise Euclidean distance between pairs of taxa in 3D morphospace; MDC = mean distance to centroid, with lower and upper 95% confidence intervals in parentheses. Confidence intervals were obtained via 1000 boostrap replicates with replacement. Volume is total volume in 3D space of a convex hull enclosing all taxa in a particular interval zone (see methods).

	N	MPD	MDC	Volume	Variance		
					DNE	RFI	OPCR
La	16	0.38	0.26 (0.18, 0.34)	0.0456	0.026	0.022	0.049
Pu1	8	0.61	0.40 (0.26, 0.53)	0.0347	0.097	0.029	0.10
Pu3	24	0.39	0.27 (0.22, 0.32)	0.0424	0.042	0.028	0.023
To1	8	0.58	0.39 (0.26, 0.52)	0.0286	0.074	0.035	0.099

Table 4.10 Correlation of dental topographic metrics in multituberculates included in this study. Upper right triangle of table is linear R^2; lower right triangle of table is Spearman's rho.

	DNE	RFI	OPCR	Slope
DNE	-	0.17	0.89	0.57
RFI	-0.32	-	0.19	0.64
OPCR	0.89	-0.39	-	0.61
Slope	0.57	-0.61	0.75	-

Table 4.11 OPCR values and dietary classifications of multituberculates in this study based on linear regression with the same genera from Wilson et al. (2012). See Fig. 6 for regression.

Species	OPCR (this study)	OPCR (Wilson et al. 2012)	Diet category (Wilson et al 2012)
Catopsalis joyneri	217.12	189.46	plant-dominated omnivore
Cimolodon nitidus	209.88	171.03	plant-dominated omnivore
Meniscoessus robustus	230.75	224.16	herbivore
Mesodma formosa	191.00	122.96	animal-dominated omnivore
Mesodma thompsoni	178.38	90.83	carnivore
Stygimys kuszmauli	195.62	134.72	animal-dominated omnivore
Taeniolabis lamberti	267.50	317.73	herbivore

Table 4.12 Disparity and morphospace occupation measures for multituberculate mammals within each NALMA interval zone. Abbrevations: MPD = mean pairwise Euclidean distance in 3D morphospace; MDC = mean distance to centroid, with lower and upper 95% confidence intervals in parentheses. Confidence intervals were obtained via 1000 boostrap replicates with replacement. Volume is total volume in 3D space of a convex hull enclosing all taxa in a particular interval zone (see methods).

	N	MPD	MDC	Volume	Variance		
					DNE	RFI	OPCR
La	4	0.37	0.24 (0.17, 0.30)	8.2e-4	0.061	0.0068	0.013
Pu1	4	0.33	0.21 (0.14, 0.31)	1.3e-3	0.056	0.0094	0.0066
Pu3	4	0.53	0.34 (0.24, 0.46)	7.1e-4	0.13	0.0065	0.032

4.9 APPENDIX 1: DESCRIPTIONS OF UNATTRIBUTED MAMMALIAN MORPHOTYPES

Because the Puercan 3 (Pu3) mammalian fauna from northeastern Montana is still under study (W. A. Clemens, pers. comm. 2017), several specimens present in the Pu3 interval zone have not been assigned to known species. However, we chose to include them in our study in the interest of sampling the complete range of mammalian dental morphologies present on the landscape at the time. As such we have assigned them to morphotypes as described here; full taxonomic descriptions and diagnoses will be published separately. All localities of origin listed are in the upper Tullock Member of Garfield County, Montana.

"Arctocyonidae", genus and species indeterminate (Species A–D). The following four specimens, identified as "Arctocyonidae" species A–D, are all similar in morphology, but with slight distinctions that made us inclined to include all of them as potentially separate taxa. All are referred to "Arctocyonidae", a plesiomorphic grouping of archaic ungulates that has been referred to in the past as a family (Archibald 1998), but is more likely a polyphyletic wastebasket taxon (DeBast and Smith 2013). None of these were referred to the Periptychidae, which includes members of similar size and overall morphology, because none of them bear the labial shift in the protoconid that is characteristic of periptychids.

"Arctocyonidae" species A — A right dentary with m2–m3, UCMP 145686, from UCMP locality V73080. This specimen is relatively small and gracile, with a broken m2 paraconid and light wear on the other cusp tips. It is similar in size (m2 length = 3.105 mm) to other small

archaic ungulates (e.g., *Oxyprimus*), and its molars are rectangular with trigonid and talonid subequal in width and a very weak labial cingulid present.

"Arctocyonidae" species B — A left dentary with m2–m3, UCMP 185970, from UCMP locality V73080. This specimen is slightly larger than "Arctocyonidae" sp. A (m2 length = 3.375 mm), and has more gracile trigonid cusps. UCMP 185970 also has a more trenchant mesial cingulid than UCMP 145686, and less difference in height between trigonid and talonid cusps.

"Arctocyonidae" species C — A right m2, UCMP 281300, from UCMP locality V72134. This specimen is the largest of the four "Arcotocyonidae" morphotypes (length = 7.81). It is similar in size and morphology to *Baioconodon cannoni* (Middleton and Dewar 2004) but has a less robust/inflated appearance. Comparisons are also favorable with *Loxolophus* (Kondrashov and Lucas 2015) but it differs from m2s of *L. priscus* in that its talonid and trigonid are subequal in width.

"Arctocyonidae" species D — A right m2, UCMP 281302, from UCMP locality V75195. This specimen is considerably smaller (length = 2.200 mm) than the other arctocyonid morphotypes discussed above, but is similar in having trigonid and talonid of subequal width and overall rectangular shape in occlusal view. Compared to "Arctocyonidae" sp. A–C, the paraconid of UCMP 281302 is relatively larger and less appressed to the metaconid.

Condylarthra sp. A — A left m2, UCMP 281303, from UCMP locality V99438. This specimen is similar to UCMP 281300 but is slightly smaller (length = 7.255), with a narrower trigonid width relative to talonid. UCMP 281303 also has a number of unusual additional cuspules on the trigonid. Though this could represent a pathology, it is also possible that it is a new taxon. Until further material with this morphology has been recovered, we refer this specimen to Condylarthra sp. A.

?Carcinodon sp. — A left m2, UCMP 218957, from UCMP locality V73090. This specimen is a medium sized archaic ungulate (length = 4.500 mm), and compares favorably in size and morphology to specimens of *Carcinodon aquilonius* (Johnston and Fox 1984), particularly in relative size and placement of the paraconid. Although this specimen is similar in size to species of *Oxyclaenus*, it is slightly longer relative to width that *Oxyclaenus* (maximum width = 3.220 mm, for a ratio of l/w = 1.40; *O. subbituminus* l/w = 1.36, Middleton and Dewar 2004).

Chriacus species A — A right dentary with m2–m3, UCMP 281296, from UCMP locality V73082. This specimen compares favorably with *Chriacus mediator* (UCMP 110446, this study) but differs in having a more mesiodistally compressed m3 trigonid and labiolingually expanded m3 talonid. As such we tentatively refer this specimen to *Chriacus* species A.

Cimolestidae, genus and species indeterminate. The two morphotypes of cimolestids described here represent the two common cimolestid size morphs present in the Garbani Channel local fauna of Garfield County, Montana (W.A. Clemens, pers. comm. 2017).

Cimolestidae species A — A right m2, UCMP 281295, from UCMP locality V74122. This small cimolestid morphotype (length = 1.84 mm) is smaller than *Scollardius propalaeoryctes* (length m2 = 2.480 mm, UA 3756), making it the smallest cimolestid in our sample. It bears morphology typical of cimolestids, including tall, trenchant trigonid cusps and a wide trigonid relative to talonid. In comparison to *Scollardius propalaeoryctes*, *Altacreodus magnus*, and *Cimolestes stirtoni*, UCMP 281295 has a narrower trigonid relative to talonid width. Until further study of the entire sample of this taxon, we tentatively refer it to Cimolestidae sp. A.

Cimolestidae species B — Two right m2s, UCMP 258019 and 258046, from UCMP localities V73080 and V72134, respectively. These teeth (mean length = 3.395) are distinctly larger than specimens of Cimolestidae sp. A. They are similar in size to *Cimolestes incisus*, but have a less wide trigonid relative to talonid width than other cimolestids, and a paraconid that is lower relative to the full trigonid height than other species. We therefore refer these teeth to Cimolestidae sp. B.

?Nyctitheriidae — A left m2, UCMP 224190, from UCMP locality V74122. This specimen represents a collection of specimens, all of the same morphotype, from the Garbani Channel local fauna of Garfield County, Montana. It is the smallest taxon in our sample (length = 1.405 mm). UCMP 224190 has a sharp anteriorly projecting paraconid, and trigonid cusps approximately twice as tall as the talonid. Trigonid and talonid are subequal in width. Comparisons with *Leptacodon* (McKenna 1968) are favorable, in both size and shape; we tentatively assign this specimen to ?Nyctitheriidae.

Oxyacodon sp. — A right m2, 186029, from UCMP locality V73080. This specimen bears the mesiodistally short talonid and strongly inflated trigonid cusps of species of *Oxyacodon* (Archibald et al. 1983), and is similar in size to *O. ferronensis* (UCMP 120381, Archibald et al. 1983, fig. 7). However, dimensional ratios among teeth are important to distinguishing the several species of *Oxyacodon* (Archibald et al. 1983), and we therefore refer this specimen to *Oxyacodon* sp.

***Oxyclaenus* species indeterminate.** We refer the following three morphotypes tentatively to the genus *Oxyclaenus* on the basis of favorable comparisons with published specimens of the genus (e.g., Dewar 2003, fig. 4; Kondrashov and Lucas 2004). All three morphotypes exhibit the reduced paraconid that is slightly appressed to the metaconid, and bulbous cusps of the Oxyclaeninae (Kondrashov and Lucas 2004). Slight differences distinguish these three morphotypes. *Oxyclaenus* species A and B are differentiated primarily based on the strength of the extocingulid, and as such might not be separate species but polymorphs of a single species. More study is required to determine the nature of their relationship.

?Oxyclaenus sp. — A left m2, UCMP 186157, from UCMP V73080. This specimen is a medium-sized (length = 5.28 mm) oxyclaenid that compares well with *O. simplex* but has a more prominent labial cingulid.

Oxyclaenus species A — A left m2, UCMP 186021, from UCMP locality V73080. This specimen resembles *Oxyclaenus* in overall morphology, and similar in size to *O. simplex* and *O*

subbituminus. It has a relatively weak ectocingulid, potentially affiliating it with *Oxyclaenus subbituminus* (Middleton and Dewar 2004).

Oxyclaenus species B — A left m2, UCMP 186000, from UCMP locality V73080. This specimen resembles *Oxyclaenus* in overall morphology, and similar in size to *O. simplex* and *O subbituminus*. It has a relatively prominent ectocingulid compared to *Oxyclaenus* sp. A.

Periptychidae sp. — A left dentary with m2–m3, UCMP 189503, from UCMP locality V73082. This specimen is referred to the Periptychidae because of the relative labial shift in its paraconid and its strongly inflated trigonid cusps and mesiodistally short talonid. Comparisons with *Mithrandir gillianus* are somewhat favorable (Rigby 1981), but UCMP 189503 is slightly smaller (m2 length = 4.015 mm).

4.10 APPENDIX 2: MORPHOSOURCE SPECIMENS

Table 4.10.1 Specimens included in this study downloaded from MorphoSource.org.

Specimen number	Genus	species	Tooth	MorphoSource media number	URL (no DOI available)	Citation
AMNH M 100635	*Avahi*	*laniger*	m2	M119-55	www.morphosource.org/Detail/MediaDetail/Show/media_id/119	Boyer 2008
AMNH M 102703	*Cynocephalus (Galeopterus)*	*variegatus*	m2	M144-79	www.morphosource.org/Detail/MediaDetail/Show/media_id/144	Boyer 2008
AMNH M 120449	*Cynocephalus*	*volans*	m2	M156-91	www.morphosource.org/Detail/MediaDetail/Show/media_id/156	Boyer 2008
AMNH M 100503	*Indri*	*indri*	m2	M281-212	/www.morphosource.org/Detail/MediaDetail/Show/media_id/281	Boyer 2008
AMNH M 170578	*Lepilemur*	*mustelinus*	m2	M337-262	www.morphosource.org/Detail/MediaDetail/Show/media_id/337	Boyer 2008
UCMP 107406	*Purgatorius*	*janisae*	m2	M14929-27216	www.morphosource.org/Detail/MediaDetail/Show/media_id/14929	López-Torres et al. 2017

4.11 APPENDIX 3: RAW DENTAL TOPOGRAPHIC ANALYSIS (DTA) DATA

Table 4.11.1 Raw dental topographic analysis (DTA) results for extant comparative sample. All specimen numbers are UWBM numbers except those denoted by an asterisk (*), which are AMNH numbers. OPCR patch size is 3.

Species	Specimen Number	Sex	Tooth	Specimen type	RFI	DNE	OPCR	Average slope
Antechinus stuartii	68916	f	m3	original	0.74	491.67	95.88	8.10
Artibeus lituratus	62023	m	m1	mold	0.44	428.31	204.75	21.22
Artibeus lituratus	62030	f	m1	mold	0.40	445.85	223.25	24.90
Artibeus lituratus	62034	m	m1	mold	0.43	332.93	129.12	21.23
Avahi laniger	100635*	m	m2	MorphoSource	0.62	368.38	87.00	15.43
Caluromys derbianus	32255	?	m3	mold	0.58	414.11	116.62	13.42
Crocuta crocuta	26583	?	m1	original	0.50	244.48	73.62	17.64
Crocuta crocuta	33257	?	m1	original	0.55	234.96	71.62	16.91
Cynocephalus volans	120449*	f	m2	MorphoSource	0.63	358.31	68.38	12.64
Dasyurus maculatus	68901	m	m3	mold	0.59	291.94	76.50	15.87
Didelphis virginiana	35526	f	m3	mold	0.66	385.05	94.62	12.67
Didelphis virginiana	39355	m	m3	mold	0.66	474.15	125.25	12.84
Didelphis virginiana	6640	m	m3	mold	0.64	443.18	112.25	13.38
Eira barbara	39436	?	m1	mold	0.45	200.75	79.62	24.80
Enhydra lutris	34554	f	m1	mold	0.30	82.90	53.25	34.93
Enhydra lutris	34559	m	m1	mold	0.34	112.75	60.38	30.26
Enhydra lutris	81970	?	m1	mold	0.39	125.41	68.88	23.76
Eptesicus fuscus	66977	m	m2	original	0.74	637.24	101.50	9.64
Eptesicus fuscus	66980	m	m2	original	0.76	578.50	116.25	8.16
Eptesicus fuscus	79331	f	m2	original	0.73	632.42	125.38	9.52
Galeopterus variegatus	102703*	f	m2	MorphoSource	0.63	358.31	68.38	12.64
Indri indri	100503*	f	m2	MorphoSource	0.53	211.70	59.62	19.42
Lepilemur mustelinus	170578*	f	m2	MorphoSource	0.48	253.57	50.62	18.12
Nasua narica	41688	f	m1	mold	0.48	219.01	121.50	18.88
Nasua narica	41687	?	m1	mold	0.52	243.62	101.50	18.15

Paradoxurus hermaphroditus	14711	?	m1	mold	0.36	178.41	84.38	28.47
Paradoxurus hermaphroditus	82651	?	m1	mold	0.47	272.10	106.50	17.90
Pecari tajacu	20670	f	m2	mold	0.43	396.52	181.38	25.15
Procyon lotor	32812	f	m1	mold	0.52	340.81	113.50	16.72
Procyon lotor	32814	f	m1	original	0.56	409.55	131.00	15.06
Procyon lotor	39563	m	m1	original	0.53	287.56	102.25	17.32
Sarcophilus harrisii	20671	m	m3	mold	0.54	251.74	65.88	18.99
Scapanus orarius	64808	m	m2	original	0.87	527.12	110.12	6.92
Scapanus orarius	64811	m	m2	original	0.76	412.57	115.62	7.93
Scapanus orarius	64820	f	m2	original	0.80	410.31	99.62	6.82
Sorex vagrans	58638	m	m2	original	0.72	607.67	110.12	9.78
Sorex vagrans	58645	f	m2	original	0.71	562.70	108.25	10.29
Sorex vagrans	60637	m	m2	original	0.71	530.52	108.38	9.93
Spilogale putorius	20192	m	m1	mold	0.54	259.48	81.75	18.18
Spilogale putorius	76080	m	m1	mold	0.46	211.04	73.88	23.21
Sus scrofa	31576	f	m2	mold	0.45	531.50	182.38	26.39
Sus scrofa	33170	f	m2	mold	0.36	529.92	228.50	31.69
Tamias townsendii	20077	m	m2	original	0.49	336.44	112.50	20.20
Tamias townsendii	43787	m	m2	original	0.51	291.69	107.38	17.19
Tamias townsendii	44335	f	m2	original	0.50	275.78	84.88	16.52

Table 4.11.2 Raw dental topographic analysis (DTA) results for extinct therian mammal sample. OPCR patch size is 3.

Species	Specimen Number	Tooth	Specimen type	RFI	DNE	OPCR	Average slope
Alphadon marshi	UCMP 191126	m3	original	0.70	371.62	95.62	10.39
Arctocyonidae sp. A	UCMP 145686	m2	original	0.57	260.43	97.00	13.50
Arctocyonidae sp. B	UCMP 185970	m2	original	0.59	300.88	86.38	14.26
Arctocyonidae sp. C	UCMP 281300	m2	original	0.50	279.55	109.12	19.58
Arctocyonidae sp. D	UCMP 281302	m2	original	0.62	214.75	81.88	11.71
Baioconodon engdahli	UCMP 116542	m2	cast	0.52	274.53	101.25	19.38
Baioconodon nordicum	UCMP 134592	m2	cast	0.47	330.13	161.38	23.07
?*Carcinodon* sp.	UCMP 218957	m2	original	0.60	224.18	90.62	13.85
Chriacus baldwini	USNM 9278	m2	cast	0.45	410.60	171.88	23.54
Chriacus mediator	UCMP 110446	m2	original	0.46	269.54	137.12	20.32
Chriacus sp. A	UCMP 281296	m2	original	0.46	249.08	116.12	22.82
Cimolestes magnus	UA 3791	m2	cast	0.81	398.23	80.75	9.29
Cimolestes propalaeoryctes	UA 3756	m2	cast	0.81	396.85	103.00	8.26
Cimolestes stirtoni	UCMP 117659	m2	original	0.79	382.88	87.75	8.70
Cimolestidae sp. A	UCMP 281295	m2	original	0.79	321.41	78.25	7.34
Cimolestidae sp. B	UCMP 258019	m2	original	0.73	294.59	78.75	9.09
Cimolestidae sp. B	UCMP 258046	m2	original	0.78	364.88	92.75	7.70
Condylarthra sp. A	UCMP 281303	m2	original	0.47	269.48	91.50	22.03
Didelphodon vorax	UCMP 55290	m3	cast	0.64	371.87	89.00	13.84
Eoconodon hutchisoni	UCMP 156117	m2	original	0.52	184.63	78.00	19.62
Eoconodon nidhoggi	UCMP 170848	m2	original	0.53	204.24	80.75	18.86
Glasbius twitchelli	UCMP 134781	m3	original	0.44	354.76	144.00	21.40
Gypsonictops hypoconus	UWBM 92455	m2	original	0.76	389.19	101.12	8.63
Gypsonictops illuminatus	UCMP 170870	m2	cast	0.73	321.50	68.75	9.38
Leptalestes cooki	UCMP 153629	m3	cast	0.69	507.61	140.12	8.92
Leptalestes krejcii	UCMP 51347	m3	cast	0.68	557.63	102.25	11.76
Litaletes disjunctus	USNM 9323	m2	cast	0.46	278.24	118.00	23.30
Mimatuta minuial	UCMP 192402	m2	cast	0.57	327.87	75.88	15.98
Mimatuta morgoth	UCMP 132454	m2	cast	0.63	476.75	143.75	13.21

Mimotricentes subtrigonus	USNM 15273	m2	cast	0.42	415.71	170.38	25.92
Nortedelphys jasoni	UWBM 91426	m3	original	0.71	392.65	108.75	9.53
?Nyctithere sp.	UCMP 224190	m2	original	0.75	350.61	92.38	6.24
Oxyacodon sp.	UCMP 186029	m2	original	0.59	310.63	87.62	14.84
Oxyclaenus simplex	UWBM 59320	m2	original	0.61	251.06	86.50	16.88
Oxyclaenus sp. A	UCMP 186021	m2	original	0.57	274.64	100.88	15.31
Oxyclaenus sp. B	UCMP 186000	m2	original	0.55	321.89	105.00	15.36
Oxyclaenus subbituminus	UCMP 148328	m2	original	0.55	262.76	99.38	17.71
?*Oxyclaenus* sp.	UCMP 186157	m2	original	0.52	287.27	91.00	18.03
Oxyprimus erikseni	UCMP 132315	m2	cast	0.60	368.33	94.25	14.27
Oxytomodon perissum	USNM 16183	m2	original	0.56	260.91	76.38	15.51
Pandemonium dis	UM 1631	m2	cast	0.51	267.13	104.00	21.19
Paromomys farrandi	UWBM 99692	m2	original	0.51	180.40	93.62	17.60
Pediomys elegans	UCMP 191138	m3	original	0.61	564.66	144.88	10.57
Peradectes minor	UCMP 115392	m3	original	0.74	377.31	97.12	6.84
Periptychidae sp.	UCMP 189503	m2	original	0.55	241.90	83.12	18.12
Procerberus formicarum	UCMP 117903	m2	cast	0.75	363.01	82.00	9.62
Prodiacodon crustulum	UCMP 192104	m2	original	0.74	377.61	89.62	8.04
Prodiacodon cf. *P. crustulum*	UCMP 189532	m2	original	0.75	297.74	83.50	8.14
Protalphadon foxi	UWBM 97291	m3	original	0.71	371.07	88.12	10.24
Protolambda florencae	UCMP 117617	m3	cast	0.61	350.16	79.25	13.75
Protolambda hatcheri	UCMP 46326	m3	cast	0.63	382.12	87.75	12.73
Protungulatum donnae	UWBM 98161	m2	original	0.56	213.75	79.38	17.66
Protungulatum gorgun	UCMP 133837	m2	cast	0.55	182.87	63.88	18.70
Purgatorius janisae	UCMP 107406	m2	MorphoSource	0.59	325.59	89.50	15.89
Purgatorius unio	UCMP 107409	m2	cast	0.61	412.88	133.62	14.18
Turgidodon rhaister	UCMP 174524	m3	cast	0.66	396.97	82.12	12.65

Table 4.11.3 Raw dental topographic analysis (DTA) results for extinct multituberculate mammal sample. OPCR patch size is 3. See Table 4.3 for specimen numbers.

Species	Specimen type(s)	RFI	DNE	OPCR	Average slope
Catopsalis joyneri	cast	0.45	983.00	217.12	20.02
Cimolodon nitidus	cast, original	0.52	869.07	209.88	15.97
Meniscoessus robustus	cast	0.45	996.15	230.75	17.67
Mesodma formosa	original	0.54	596.23	191.00	14.00
Mesodma thompsoni	original	0.51	632.89	178.38	13.40
Stygimys kuszmauli	original	0.44	613.55	195.62	17.70
Taeniolabis lamberti	cast	0.48	1286.70	267.50	19.65

CHAPTER 5: CONCLUDING REMARKS

In light of the studies presented in the preceding chapters, several important conclusions can be drawn regarding the specific problems discussed in this dissertation and the broader context of mammalian recovery following the Cretaceous-Paleogene (K-Pg) mass extinction.

1. **Quantitative taxonomic diagnoses, and the repeatability of accurate identification of mammalian fossils, are critical to understanding and interpreting faunal change in the mammalian fossil record.**

   Difficulties related to taxonomic identification of mammalian dental fossils, though extremely common, can sometimes be mitigated by using quantitative techniques to delineate the exact nature of morphological differences among taxa, as I have done here within the multituberculate genus *Mesodma*. Determining how biologically meaningful those diagnoses are is particularly challenging, but continuing study of mammalian dental development and intraspecific variation will help future workers make more biologically relevant decisions regarding the importance of particular morphological features.

2. **Anagenetic change in the fossil record complicates taxonomic identification, especially in high-resolution studies with dense fossil sampling through time.**

   As mammalian fossil samples become larger and stratigraphic sampling more complete, the likelihood of sampling intermediate morphological forms increases, making it more

difficult to determine where one species ends and another begins, morphologically speaking. I was able to recognize size change in *Mesodma formosa* across the K-Pg extinction boundary, but with less complete sampling, *M. formosa* could have been interpreted as two distinct species. Although this problem is far from solved, the combination of linear measurements, geometric morphometrics, and coefficient of variation in my case study of *Mesodma* provides one feasible approach to dealing with it.

3. **Post K-Pg mammalian faunal recovery began slowly: in the first ca. 323 thousand years (ka) of the Paleogene, mammalian local faunas in the McGuire Creek area of northeastern Montana showed slight increases in richness and heterogeneity, but the main wave of taxonomic originations in the area did not take place until slightly later, within 300–600 ka of the extinction boundary.**

Although there are only two time slices represented in my sample of mammals from McGuire Creek, the younger faunas show a few signs of recovery relative to the older fauna, including not only slight increases in taxonomic richness and heterogeneity, but also the appearance of taxa such as the plesiadapiform *Purgatorius*. *Purgatorius* is usually associated with even younger faunas, including fully recovered local faunas in northeastern Montana. Yet the two younger McGuire Creek faunas still have less than half of the taxonomic richness of fully recovered faunas in the larger Hell Creek region of northesastern Montana, indicating that later in-situ diversification of immigrant taxa, new waves of immigrants, or both, occurring 300–600 ka after the extinction, were the main source of taxonomic richness contributing to local recovery.

4. **In the middle to late Puercan North American Land Mammal Age (NALMA), mammalian faunas in the Western Interior began to differentiate into northern and southern faunal types.**

   The emergence of distinct northern (Montana, Saskatchewan) and southern (Wyoming, Utah, Colorado, New Mexico) faunal types in the middle to late Puercan suggests a potential geographic vicariance event in the middle Puercan, perhaps cutting off faunal exchange among basins of the Western Interior. Nonetheless, without early Puercan faunas from New Mexico, it cannot be determined if the characteristic southern taxa present in Puercan 2 and 3 originated from southern Puercan 1 faunas that have yet to be sampled. This biogeographic pattern also highlights the challenges of using biochronology to correlate timing of biological events across large geographic distances: when precise geochronological data are not available, it is sometimes unclear to what degree differences in faunal composition are due to separation in space versus separation in time.

5. **In the first ca. 1.2 million years of the Paleogene, mammalian diets shifted away from insectivory and toward omnivory and more plant-based diets, with early morphological disparity arising from immigrant taxa rather than local survivors of the extinction.**

Directly following the K-Pg mass extinction, the majority of taxonomic richness as well as dental morphological disparity, in mammals of northeastern Montana, is due to an influx of immigrants. In contrast to the preponderance of insectivores in the Cretaceous, these earliest Paleogene (Puercan 1) group of mammals includes a greater proportion of animal- and plant-dominated omnivores. Subsequent interval zones (Puercan 3, Torrejonian 1) see a continuing tendency towards plant-based diets. Several taxa in Torrejonian 1 are reconstructed as being strictly friugivorous, a trend which may be connected to the growing role of mammalian seed dispersal in the evolution of angiosperms.

6. **The relationship between dietary ecology and dental surface metrics of single teeth needs to be further investigated, to better understand the relative contribution each individual tooth makes to overall tooth row shape descriptors.**

The single-tooth dental surface metrics I use to predict dietary ecology in the fossil record do not differ significantly between strict carnivores and strict folivores in my phylogenetically broad comparative sample. This problem has not been previously detected because single-tooth metrics have until now been used mostly in a phylogenetically narrow (and therefore morphologically conserved) group of mammals (Primates). To more effectively use single teeth to predict diet in the mammalian fossil record, it will be necessary to develop a deeper understanding of how derived teeth such as carnassials change the distribution of dental complexity across individual tooth positions in a tooth row. An alternative solution, though one that is not always available

in the fossil record, is to examine dental surface metrics of entire tooth rows. This may be preferable simply because a full tooth row includes more complete dietary information than a single tooth alone, and is less sensitive to differences among specific tooth positions in the derived dentitions of modern mammalian groups.